AD-A107 169   TEXAS UNIV AT AUSTIN APPLIED RESEARCH LABS   F/G 20/1
               COVARIANCE FUNCTIONS AND RELATED STATISTICAL PROPERTIES OF ACOU--ETC(U)
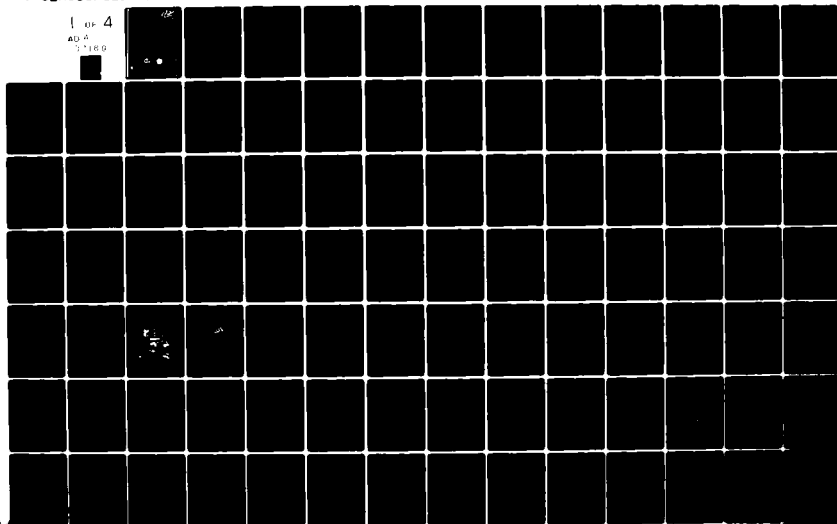   JUN 81   G R WILSON   N00014-80-C-0490
UNCLASSIFIED   ARL-TR-81-23   NL

1 OF 4
AD A
107169

ARL-TR-81-23

COVARIANCE FUNCTIONS AND RELATED STATISTICAL PROPERTIES OF ACOUSTIC BACKSCATTERING FROM A RANDOMLY ROUGH AIR-WATER INTERFACE

Gary R. Wilson

APPLIED RESEARCH LABORATORIES
THE UNIVERSITY OF TEXAS AT AUSTIN
POST OFFICE BOX 8029, AUSTIN, TEXAS 78712

19 June 1981

Technical Report

APPROVED FOR PUBLIC RELEASE;
DISTRIBUTION UNLIMITED.

Prepared for:

OFFICE OF NAVAL RESEARCH
DEPARTMENT OF THE NAVY
ARLINGTON, VA 22217

SECURITY CLASSIFICATION OF THIS PAGE *(When Data Entered)*

REPORT DOCUMENTATION PAGE	READ INSTRUCTIONS BEFORE COMPLETING FORM

1. REPORT NUMBER	2. GOVT ACCESSION NO. AD-A107 169	3. RECIPIENT'S CATALOG NUMBER

4. TITLE *(and Subtitle)* COVARIANCE FUNCTIONS AND RELATED STATISTICAL PROPERTIES OF ACOUSTIC BACKSCATTERING FROM A RANDOMLY ROUGH AIR-WATER INTERFACE .	5. TYPE OF REPORT & PERIOD COVERED technical report.
	6. PERFORMING ORG. REPORT NUMBER ARL-TR-81-23

7. AUTHOR(s) Gary R. Wilson	8. CONTRACT OR GRANT NUMBER(s) N00014-80-C-0490

9. PERFORMING ORGANIZATION NAME AND ADDRESS Applied Research Laboratories The University of Texas at Austin Austin, Texas 78712	10. PROGRAM ELEMENT, PROJECT, TASK AREA & WORK UNIT NUMBERS Task 0003

11. CONTROLLING OFFICE NAME AND ADDRESS Office of Naval Research Department of the Navy Arlington, VA 22217	12. REPORT DATE 19 June 1981
	13. NUMBER OF PAGES 267 298

14. MONITORING AGENCY NAME & ADDRESS*(if different from Controlling Office)*	15. SECURITY CLASS. *(of this report)* UNCLASSIFIED
	15a. DECLASSIFICATION DOWNGRADING SCHEDULE

16. DISTRIBUTION STATEMENT *(of this Report)*

Approved for public release; distribution unlimited.

17. DISTRIBUTION STATEMENT *(of the abstract entered in Block 20, if different from Report)*

18. SUPPLEMENTARY NOTES

19. KEY WORDS *(Continue on reverse side if necessary and identify by block number)*

20. ABSTRACT *(Continue on reverse side if necessary and identify by block number)*

An experimental and theoretical study of the scattering of sound from the surface of a freshwater lake was performed. The study was limited to back-scattered sound (reverberation) from a pulsed sound source. The experimental study employed nine vertically separated receivers and four horizontally separated receivers in order to examine the spatial and temporal covariance of the backscattered sound for both orientations simultaneously. Approximately 1000 narrowband reverberation returns were generated by repetitively projecting

DD ₁ FORM 73 1473 EDITION OF 1 NOV 65 IS OBSOLETE

20. (Cont'd)

a 100 μsec CW pulse centered at 80 kHz at the wind-roughened surface of a freshwater lake at a 10.5 degree grazing angle. The returns were sampled digitally for a 10 msec interval during which surface reverberation was predominant, and were formed into ensembles at each sample time. Various univariate moments and the time-difference component of the covariance were computed experimentally, utilizing ensemble averages. The statistical validity of the ensembles was determined by testing each ensemble for randomness and homogeneity. The ensembles were also tested for normality and found to be non-Gaussian, in contrast to previous studies.

The experimental results were compared to a theoretical model developed by D. Middleton and others, based on point scattering and Poisson statistics. The reverberation is modeled as weak scattering from random point sources representing inhomogeneities at the air-water interface of an otherwise homogeneous medium. In the present study the point source was assumed to be a perfect point reflector distributed uniformly over the surface. The implementation of the model took into account most of the relevant geometrical parameters (spatial distribution of sensors, grazing angle, range) and acoustic parameters (frequency, pulse length, directionality, aperture response, bandwidth, signal spectrum) but did not take into account environmental parameters (surface wave height, wave spectrum, wind direction).

Significant differences were observed between the covariances of the vertical and horizontal arrays. The envelope of the covariance between the vertical receivers maintained a significant level at much larger separations than the horizontal receivers. The phase of the vertical covariance was found to change linearly with time, resulting in a slow oscillation of the covariance with time, while the phase of the horizontal covariance was constant (and non-zero). The vertical covariance was also shown to depend on the location of the elements on the array.

The theory, which had been applied previously only to horizontal arrays, was extended to a vertical array. The theory correctly predicted the dependence of the horizontal and vertical covariance on the time of observation and on the time-difference of the observations. In addition, it predicted the dependence of the envelope of the covariance on horizontal separation of the receivers. The change of the phase of the vertical covariance with time was also predicted by theory. However, the theory failed to predict the dependence of the envelope of the covariance on vertical separation and the non-zero phase of the horizontal covariance. The two failures of the theory were shown to most likely be the result of the failure to include the environmental parameters into the implementation of the model. Ways to include these environmental parameters were suggested.

TABLE OF CONTENTS

iii

iv

vi

LIST OF FIGURES

vii

viii

ix

xiv

LIST OF TABLES

LIST OF SYMBOLS

$A_R(\widehat{R}_R)$ — Directivity function of receiver R in the direction $\widehat{R}_R$.

$A_T(\widehat{R}_T)$ — Directivity function of the projector T in the direction $\widehat{R}_T$.

$a_R(\vec{\eta})$ — Aperture response of receiver R at the point $\vec{\eta}$ on the receiver. The spatial Fourier transform of A_R.

$a_T(\vec{\xi})$ — Aperture response of projector T at the point $\vec{\xi}$ on the projector. The spatial Fourier transform of A_T.

b_2 — Sample estimate of the kurtosis.

$\sqrt{b_1}$ — Sample estimate of the skew

$B(k;n,p)$ — Binomial probability function.

c — Speed of sound in water.

D — Test statistic for D'Agostino's test for normality.

D_N — Test statistic for the Kolmogorov-Smirnov one-sample test for normality for an ensemble of size N.

D_{mn} — Test statistic for the Kolmogorov-Smirnov two-sample test for homogeneity between two ensembles of size m and n.

$E_{ij}(t,\tau)$ — Theoretical estimate of the envelope of the narrowband covariance between receiver i at time t and receiver j at time t+τ.

xx

$e_{ij}(t,\tau)$ — Sample estimate of the envelope of the narrowband covariance between receiver i at time t and receiver j at time $t+\tau$.

$\tilde{e}_{ij}(t,\tau)$ — Sample estimate of the envelope of the normalized narrowband covariance between receiver i at time t and receiver j at time $t+\tau$.

$F_{X^{(1)}X^{(2)}}$ — Joint characteristic function of two reverberation processes $X^{(1)}(t_1,t')$ and $X^{(2)}(t_2,t')$ resulting from scattering at time t'.

$F_n(i\xi_1,t_1;\ldots;i\xi_n,t_n|t',\Lambda)$ — Joint characteristic function of a reverberation process at the times $t_1,\ldots,t_n$ due to a scatter density at the time t' in a scattering region Λ.

$F_2(i\xi_1,t_1,i\xi_2,t_2|t',\Lambda)$ — Joint characteristic function of a reverberation process at the times t_1 and t_2.

$F_1(i\xi_1,t_1|t',\Lambda)$ — Characteristic function of a reverberation process at the time t_1.

$F_Z(z)$ — Distribution function of a test statistic Z.

$G_T(t,\vec{\xi})$ — Pressure density on the surface of the projector T at the point $\vec{\xi}$ at time t.

$G_{scat}(t,\vec{R}|\vec{R}_T)$ — Scattered pressure density on the surface $\vec{R}$ of a scatterer at the location $\vec{R}_T$.

xxi

H_0 — Null hypothesis of a statistical test.

H_1 — Alternative hypothesis of a statistical test.

$h(\tau, t, \vec{R}_T)$ — Response function of a point scatter.

h — Depth of the center of the transducer array.

$K_X(t_1, t_2 | t')$ — Theoretical covariance between the reverberation process $X(t_1, t')$ at time t_1 and $X(t_2, t')$ at time t_2 due to a scatter density at the time t'.

$K^{(12)}(t_1, t_2 | t')$ — Theoretical covariance between random processes $X^{(1)}(t_1, t')$ and $X^{(2)}(t_2, t')$.

$K_{12}(t_1, \tau)$ — Narrowband approximation of the theoretical covariance between receiver 1 at time t_1 and receiver 2 at time $t_1 + \tau$.

k — Number of hypothesis test outcomes below the significance level.

$k_{ij}(t, \tau)$ — Narrowband approximation of the sample estimate of the covariance between receiver i at time t and receiver j at time $t + \tau$.

$\tilde{k}_{ij}(t, \tau)$ — Narrowband approximation of the sample estimate of the normalized covariance between receiver i at time t and receiver j at time $t + \tau$.

xxii

$K_{ij}(t,\tau)$	Narrowband approximation of the theoretical covariance between receiver i at time t and receiver j at time t+τ.
ℓ_{RiV}	Vertical length of receiver i.
ℓ_{RiH}	Horizontal length of receiver i.
ℓ_{TV}	Vertical length of projector.
ℓ_{TH}	Horizontal length of projector.
m	Sample mean of an ensemble.
m_r	r^{th} centralized sample moment.
$m_r(t_n,i)$	Sample estimate of $\mu_r(t,i)$. The rth centralized sample moment at time t_n for the ith channel.
$M(t')$	Number of contributing scatterers at time t'.
n	Number of independent test outcomes used in the binomial probability law.
N	Size of an ensemble.
N(0,1)	Normal distribution with a mean of 0 and a variance of 1.
p	Probability that the value of α for an hypothesis test would be below the level of significance.
$P(N|t',\Lambda)$	Probability of N scatterers occurring at time t' in the region Λ.

$P_{inc.}$ Incident pressure at a point $\vec{R}_p$ from the projector.

$P_{scat}(t,\vec{r}')$ Scattered pressure at time t and position $\vec{r}'$ from scatterer.

$\vec{R}_R$ Vector from receiver R to scatterer at a point λ.

$\hat{R}_R$ Unit vector in the direction $\vec{R}_R$.

R_R Magnitude of $\vec{R}_R$.

$R_{Rix}, R_{Riy}, R_{Riz}$ Cartesian coordinates of the vector $\vec{R}_{Ri}$ from receiver Ri to scatterer at Λ.

$\vec{R}_T$ Vector from projector T to scatterer at a point λ.

$\hat{R}_T$ Unit vector in the direction $\vec{R}_T$.

R_T Magnitude of $\vec{R}_T$.

R_{Tx}, R_{Ty}, R_{Tz} Cartesian coordinates of $\vec{R}_T$.

ΔR Travel time difference between a scatterer at point λ and receivers R1 and R2:

$$\frac{R_{R2}-R_{R1}}{c}$$

$\vec{r}$ $\vec{R}_T - \vec{\xi}$

$\vec{r}'$ $\vec{R}_R - \vec{\eta}$

$\vec{R}$ Vector to a point on a scatterer.

r Number of runs in the runs up and down test.

$S_{in}(f)$ Frequency spectrum of the input electrical signal to the projector.

S Matrix representing the rotation of the transducer array through an angle ψ.

s_w^2	Variance of the Wilcoxon rank-sum statistic W.
s^2	Sample variance of an ensemble.
$T_R(f)$	Frequency response of receiver R.
$T_T(f)$	Frequency response of projector T.
T	Transmitted pulse length.
$t_1, t_2, \ldots, t_n$	Discrete observation times of the reverberation process.
t_T	Time of occurrence of a scattering event. Retarded time $t - \frac{R_R + R_T}{c}$
t_{r1}	Retarded time from time t_1 and receiver R1.
t_{r2}	Retarded time from time t_2 and receiver R2.
t_U	Upper limit of the t_T integration.
t_L	Lower limit of the t_T integration.
t_{iL}	Minimum time t_T at which scatterers can contribute to receiver i at time t.
t_{iU}	Maximum time t_T at which scatterers can contribute to receiver i at time t.
t'	Temporal parameter of the scatter density $\rho(\lambda; t')$.
$U_1(t_1, \lambda)$	Elementary scattered waveform at receiver 1 at time t_1 due to a scatter density at the point λ.
$U_2(t_2, \lambda)$	Elementary scattered waveform at receiver 2 at time t_2 due to a scatter density at the point λ.

$\vec{u}$	Vector from coordinate origin on surface to center of array.
$V_i(t_r)$	Distorted waveform of the input electrical signal at the time t_r on receiver i.
V_T	Volume of the projector.
$v_i(t,\omega)$	Experimental sample of the reverberation process from receiver i at time t and ping ω.
$\vec{v}_T$	Vector from center of array to projector.
$\vec{v}_{Ri}$	Vector from center of array to receiver i.
W	Wilcoxon rank-sum statistic
$\overline{W}$	Mean of W.
$W(X_1,t_1,X_2,t_2,N\mid t',\Lambda)$	Joint density function of $X(t_1)$, $X(t_2)$, and number of contributing scatterers N in spatial interval Λ at time t'.
$W(X_1,t_1,X_2,t_2\mid t',\Lambda)$	Joint density function of $X(t_1)$ and $X(t_2)$ in the spatial interval Λ at time t'.
X_i	i^{th} sample of an ensemble.
$X(t,t')$	Reverberation process at time t due to a scatter density at the time t'.
$X^{(1)}(t_1,t')$	Reverberation process from receiver 1 at time t_1.
$X^{(2)}(t_2,t')$	Reverberation process from receiver 2 at time t_2.

$X_{12}(t_1, t_2), Y_{12}(t_1, t_2)$ — In-phase and quadrature components, respectively, of the theoretical covariance between receiver 1 at time t_1 and 2 at time t_2.

$X_i(t_r), Y_i(t_r)$ — In-phase and quadrature components, respectively, of the distorted waveform $V_i(t_r)$ of the input electrical signal from receiver i at time t_r.

X, Y — In-phase and quadrature components, respectively, of the product of $V_1(t_{r1})$ and $V_2(t_{r2})$, the distorted waveforms of the input electrical signal from receivers 1 and 2 at times t_{r1} and t_{r2}.

$X_i(t), Y_i(t)$ — In-phase and quadrature components, respectively, of the measured reverberation process $v_i(t)$ from the ith receiver at time t.

$X_i(t, \omega), Y_i(t, \omega)$ — In-phase and quadrature components, respectively, of the individual realizations ω of the measured reverberation process $v_i(t)$ from the ith receiver at time t.

$x_{ij}(t, \tau), y_{ij}(t, \tau)$ — In-phase and quadrature components, respectively, of the difference term of the covariance between receiver i at time t and receiver j at time t+τ.

xxvii

Y_i	Response function of a perfect point reflector scatterer to receiver i.
Z	Transformed or standardized test statistic of a hypothesis test.
z	Calculated value of the test statistic Z. Also used to denote the random variable associated with surface waveheight.
α_{Ri}	Spherical angular coordinate from the ith receiver to a point scatterer.
α_T	Spherical angular coordinate from the projector to a point scatterer.
α	Probability of a Type I error; also called level of significance.
β_{Ri}	Spherical angular coordinate from the ith receiver to a point scatterer.
β_T	Spherical angular coordinate from the projector to a point scatterer.
β	Probability of a Type II error.
Λ	Scattering region.
Λ_{12}	Region of scatterers contributing to receivers 1 and 2.
$\vec{\eta}$	A point on a receiver.
θ	Set of random parameters associated with the scattering process.
$\kappa_{ij}(t,t+\tau)$	Sample estimate of the covariance between $v_i(t)$ and $v_j(t+\tau)$.

$\vec{\lambda}$	Vector to a scatterer from the origin in the surface coordinate system.
$\hat{\lambda}$	Unit vector in the direction $\vec{\lambda}$.
λ	Coordinate of a scatterer. Also used as wavelength of sound.
$\bar{\lambda}$	Coordinate of a scatterer in the mean surface level.
$\mu_r(t,i)$	r^{th} population moment about the mean of $v_i(t)$, the reverberation process from receiver i at time t.
μ_{rs}	Joint population moment between two random processes.
μ	Mean of the number of runs r in the runs up and down test.
ρ	Density of scatterers at point λ at time t'.
ρ_v	Volume scatter density.
σ, σ_s	Uniform surface scatter density.
σ^2	Variance of the test statistic r in the runs up and down test.
τ	Time difference between t_2 and t_1: $t_2 - t_1$.
$\phi_{ij}(t,\tau)$	Theoretical estimate of the phase of the narrowband covariance between receiver i at time t and receiver j at time t + τ.

$\phi_{ij}(t,\tau)$ Sample estimate of the phase of the narrow-
band covariance between receiver i at
time t and receiver j at time t + τ.

$\phi(t_r)$ Narrowband phase of the distorted waveform
$V(t_r)$.

ϕ Azimuthal angle to a point scatterer from
a surface coordinate system. It is one
of the two variables of integration in
the theoretical model.

ϕ_L Lower limit in the ϕ integration.

ϕ_U Upper limit in the ϕ integration.

Ω Parent population of all possible reali-
zations of a reverberation process.

ω, ω_o Angular frequency of sound; $2\pi f$.

ω_{ij} Rate of change of $\phi_{ij}(t,\tau)$ with t.

I. INTRODUCTION

The scattering of waves, either electromagnetic or acoustic, from a boundary or a volume has been the subject of study in many varied fields. The communications field studies scattering of electromagnetic waves from the ionosphere to provide over-the-horizon communications. Acoustics has recently provided improved diagnostic capabilities to the medical community by considering the scattering of ultrasound from organs and tissues of the body. Sound scattered from volume scatterers can provide information on the number of pollution particles in the atmosphere or the number of fish in a school. Other diverse fields such as seismic exploration, non-destructive testing, and architectural engineering all claim interest in the scattering of waves.

The present study is most directly related to the field of sonar. Techniques have been developed in this field to enable active sonars to better detect signals in the presence of noise due to surface backscattering (reverberation). However many of these techniques require a knowledge of the statistical properties of surface reverberation, in particular the coherence of the reverberation. This requirement has led to interest in the fundamental problem of the scattering of sound from the surface. The present study is one response to this interest. The focus of this study is on the coherence of the scattered sound.

I.1 Previous Experimental Studies

Much of the previous experimental work which has been performed in this area has investigated the coherence of forward-scattered sound.

1

The sound source was usually either continuous[1-3] or explosive;[4-7] in some cases a pulsed source was used.[8-11] In almost every case the received signal was assumed to be stationary and ergodic. Thus the coherence was calculated using time averages.

Other experimental work has dealt with the coherence of back-scattered sound, or reverberation. As opposed to the experiments with forward-scattered sound, the source was pulsed[12-19] or explosive[20-22] rather than continuous. In addition, the coherence was almost always computed using ensemble averages rather than time averages. Thus the results were not constrained by the assumptions of stationarity and ergodicity. The present study is limited to the coherence of back-scattered sound from a pulsed sound source. Ensemble averages are used to experimentally estimate the reverberation coherence.

Most of the previous experimental studies of the coherence of reverberation from a pulsed sound source utilize a single receiver and so only consider temporal coherence.[12-16,18] Two studies used a multi-sensor array and examined the dependence of the coherence on the spatial separation of the observation points, as well as the time of observation.[17,19] However, these studies considered the spatial dependence of the coherence only for a linear horizontal array. The present study employs both a horizontal and a vertical array to examine the spatial dependence of the coherence for both orientations simultaneously.

The spatial coherence of forward-scattered sound has been examined for both horizontal and vertical arrays. However, since forward-scattered sound is predominantly specular, significant differences in

the spatial coherence of forward-scattered sound and back-scattered

sound are to be expected. In fact, a comparison of forward-scattered

data by Wille[5] and back-scattered data by Urick,[22] both using explosive

sources, indicates that the back-scattered coherence is significantly

less. Thus it is to be expected that the present study of back-scattered

sound from a pulsed source will demonstrate results which differ signi-

ficantly from similar forward-scattered data.

The spatial coherence of back-scattered sound has also

been examined for both horizontal and vertical arrays utilizing an

explosive sound source and performing time averages to estimate the

coherence.[21,22] The results indicated significant differences between

the coherence of horizontal and vertical arrays. Thus it is to be

expected that the present study will also demonstrate significant

differences between the coherence of horizontal and vertical arrays.

I.2   Theoretical Studies in Surface Scattering

Theoretical models of underwater acoustic scattering at an

air-water interface can be divided generally into two categories, de-

pending upon whether the boundary is treated as periodic[23,24] or

random.[25-30] The present study considers the surface to be random,

that is, the height of the surface waves at any point on the surface

is treated as a random variable.

There are two basic approaches to scattering from a randomly

rough surface. One approach introduces a scalar wave equation and

expresses the scattered field in terms of the Helmholtz integral over

elementary sources at the surface. The boundary conditions are usually

applied by assuming a pressure release surface and utilizing the
Kirchhoff approximation.[25] The other approach, developed most generally
by Middleton, treats the surface as a random distribution of point
scatterers representing inhomogeneities in an otherwise homogeneous
medium.[27-30] The interaction of the incident acoustic wave with the
point scatterers is expressed in terms of an impulse response function,
eliminating the need for solving the scalar wave equation for complex
boundary conditions. Middleton's model has been described as the most
complete theoretical model, but one which lacks experimental verifica-
tion.[31] It is the model which will be used in the present study.

I.3   The Present Study

The present study has four primary objectives. The first is
to simultaneously measure the dependence of the reverberation co-
variance on the spatial separation of the receivers in both the hori-
zontal and vertical orientations. In the process, the dependence of
the covariance on other parameters will also be measured. A thorough
analysis of the horizontal and vertical covariance will be performed.
The second objective is to develop a theoretical model of surface rever-
beration and compare it to the experimental results. The model being
used has previously been applied to the covariance of a horizontal array
with good success. Thus the present study seeks to extend the model to
the covariance of a vertical array. The third objective of this study
is to experimentally examine the first four univariate moments of the
reverberation, and apply univariate tests for normality. This will
supply some information concerning the distribution of the reverberation

process. The fourth objective involves refinement of the techniques for measurement and validation of reverberation from multiple receivers. Care must be taken in the measurement process in order to form valid sample ensembles of the reverberation. In addition, it is important to apply statistical hypothesis testing techniques to validate the sample ensembles for randomness and homogeneity before utilizing these ensembles to compute the various moments and covariance.

The present study is organized as follows. The experimental equipment and measurement techniques are described in Chapter II. The reverberation data were collected by scattering 100 μs CW pulses at a center frequency of 80 kHz from the wind-roughened surface of a fresh-water lake at a grazing angle of approximately 10.5 degrees. Approximately 1000 reverberation returns were recorded in a short period of time from nine vertical receivers and four horizontal receivers.

The theoretical model used in the present study is developed in Chapter III. A summary of Middleton's theory is given as it relates to the present study. Certain assumptions are then introduced which allow the model to be simplified to the form used by the present study. The essential assumptions are:

1. The scatterer is modeled as a perfect point reflector, i.e., scattering is omnidirectional, frequency insensitive (within the bandwidth of the signal), location insensitive, and introduces no time delay.

2. The signal is narrowband.

These and other assumptions are then applied to derive the form of the model used in the present study.

Chapter IV discusses the statistical testing of the experimental data. Assumptions inherent in the sampling process which are necessary to transform the reverberation returns into ensembles are discussed. Then various statistical tests for randomness, homogeneity, and normality are described and the results of the tests as applied to each data ensemble are given.

The experimental estimates of the covariance are given and compared to the results from the theoretical model in Chapter V. The procedure for computing the moments and covariance of the experimental data is described first. Then the moments are presented. The covariance is then analyzed as a function of time, time delay, and spatial separation for the various vertical and horizontal receivers.

Chapter VI then summarizes the study and draws some conclusions.

Chapter II is devoted to a discussion of the experimental equipment used to generate and receive the reverberation data and to a description of the recording and digitization techniques necessary for this type of study. First, a simple analysis of the sources of measurement error is performed to help establish certain requirements for the measurement system. Then the hardware configuration and measurement techniques are described which allow these measurement errors to be reduced to an acceptable level. A description of the transducers and the deployment of the experiment at the ARL:UT Lake Travis Test Station is then given. Finally, the conditions under which the data were collected are described.

II.1 Sources of Measurement Error

Several considerations are necessary in order to accurately measure reverberation coherence between spatially separated hydrophones. A reasonable reverberation to background ratio must be maintained where the background noise is due to both the ambient acoustic noise and the system electronic noise. Any feedover of the signal from one hydrophone to the other signals will also limit the accuracy of the coherence measurement. Thirdly, since the reverberation coherence is calculated experimentally from an ensemble of signals, the sample ensemble size limits the accuracy of the coherence calculations. Finally, it is necessary to maintain the phase integrity of the narrowband acoustic signals at the face of the hydrophones. Actually, it is

7

necessary only to maintain the phase difference of the acoustic signals between the hydrophone channels at the face of the hydrophones; that is, the addition of an arbitrary constant phase shift to all signals does not affect the coherence of the signals. The following discussion will analyze these various sources of inaccuracies and describe the measurement equipment and techniques used to reduce the inaccuracies to an acceptable level. Although the analysis makes use of several assumptions which, strictly speaking, may not be valid for the data used in this study, nevertheless it provides a useful insight into the relative importance of the various sources of measurement error.

To get an estimate of the effect of reverberation to noise ratio on the measurement of coherence between two hydrophones, let the two reverberation processes be represented by X_1 and X_2, which are identically distributed zero mean gaussian random processes with a variance of σ^2. Likewise, let X_{n1} and X_{n2} represent two additive white noise processes which are identically distributed zero mean gaussian random processes with a variance of σ_n^2. The reverberation plus noise processes are then $X_{1+n} = X_1 + X_{n1}$ and $X_{2+n} = X_2 + X_{n2}$. Since it is reasonable to assume that

$$E(X_1 X_{n1}) = E(X_2 X_{n2}) = 0 \qquad ,$$

then X_{1+n}, X_{2+n} are identically distributed zero mean gaussian random processes with variance of $\sigma^2 + \sigma_n^2$. Since it is also reasonable to assume that

$$E(X_2 X_{n1}) = E(X_1 X_{n2}) = E(X_{n1} X_{n2}) = 0 \qquad ,$$

then

$$\text{Cov } (X_1, X_2) = \text{Cov } (X_{1+n}, X_{2+n}).$$

The correlation coefficient between X_{1+n} and X_{2+n} is then

$$\rho_{X_{1+n}X_{2+n}} = \frac{Cov\,(X_{1+n},\,X_{2+n})}{\sigma^2 + \sigma_n^2} = \frac{Cov\,(X_1,\,X_2)}{\sigma^2 + \sigma_n^2}$$

$$= \frac{\sigma^2}{\sigma^2 + \sigma_n^2}\; \rho_{X_1 X_2} \qquad .$$

The rms reverberation to rms noise ratio is $R/N = \dfrac{\sigma}{\sigma_n}$. Thus,

$$\rho_{X_{1+n}X_{2+n}} = \frac{(\frac{R}{N})^2}{1 + (\frac{R}{N})^2}\; \rho_{X_1 X_2} \qquad .$$

This gives an expression for the measured reverberation plus noise correlation coefficient in terms of the actual reverberation-only correlation coefficient and the reverberation to noise ratio. The measured correlation coefficient is always less than or equal to the actual correlation coefficient, and the difference decreases as the correlation coefficient decreases. For example, if $R/N = 10$, the measured correlation coefficient is .99 when the actual correlation coefficient is 1.0. Thus, for a reverberation to noise ratio of 20 dB, the maximum difference in the correlation coefficients occurs for maximum correlation and reduces the measured correlation coefficient by only .01.

Now consider the effects of feedover between channels on the accuracy of the correlation coefficient. Let X_1 and X_2 be as above. Let $Y_1 = \alpha X_1$, and $Y_2 = \alpha X_2$, where α is a constant. Y_1 and Y_2 are identically distributed zero mean gaussian random processes with variance of $(\alpha\sigma)^2$. The measured reverberation signal is then the sum of the actual

reverberation signal and the feedover from the other channel, i.e.,

$$Z_1 = X_1 + Y_2$$

$$Z_2 = X_2 + Y_1$$

where Z_1 and Z_2 are the measured reverberation processes.

$$E(Z_1) = E(X_1) + E(Y_2) = 0$$

$$E(Z_1^2) = E\{(X_1 + Y_2)^2\} = E(X_1^2) + E(2X_1 Y_2) + E(Y_2^2)$$

$$= \sigma^2 + 2\alpha E(X_1 X_2) + (\alpha \sigma)^2$$

$$= (1 + 2\alpha\rho_{X_1 X_2} + \alpha^2) \sigma^2$$

Likewise, Z_2 is a zero mean gaussian random process with the same variance. The correlation coefficient between the measured reverberation processes is $\rho_{Z_1 Z_2}$:

$$\rho_{Z_1 Z_2} = \frac{E(Z_1 Z_2)}{\sigma_{Z_1} \sigma_{Z_2}} = \frac{E\{(X_1 + \alpha X_2)(X_2 + \alpha X_1)\}}{\sigma_{Z_1} \sigma_{Z_2}}$$

$$= \frac{(1 + \alpha^2) E(X_1 X_2) + 2\alpha \sigma^2}{\sigma_{Z_1} \sigma_{Z_2}}$$

$$= \frac{(1 + \alpha^2) \rho_{X_1 X_2} + 2\alpha}{1 + \alpha^2 + 2\alpha\rho_{X_1 X_2}} \quad .$$

This gives a relation between the correlation coefficient of the

measured reverberation process and the actual reverberation process as
a function of α, the feedover separation. In this case the measured
correlation coefficient is greater than or equal to the actual corre-
lation coefficient, and the difference increases as the correlation
coefficient decreases. For a feedover separation of 40 dB, i.e.,
$\alpha = .01$, the measured correlation coefficient is .02 when the actual
correlation coefficient is 0. Thus, for a channel to channel separation
of 40 dB, the maximum difference occurs when the correlation is a minimum
and increases the measured correlation coefficient by .02.

The third source of inaccuracy in measuring the reverberation
coherence is the limited size of the sample ensemble. An ensemble of
reverberation returns is collected, and from this ensemble of returns
a correlation coefficient can be calculated. The standard deviation
of the correlation coefficient as a function of the sample ensemble
size N and the correlation coefficient ρ for normally distributed
samples is:[17,32]

$$\sigma_\rho = \sqrt{\frac{1 - \rho^2}{N}} \quad .$$

The standard deviation thus increases with decreasing correlation. For
a sample ensemble size of 1000, the standard deviation is .03 for a
correlation coefficient of 0. Thus, the standard error introduced
due to the limited sample size increases with decreasing correlation
and is a maximum of .03.

If the sample ensemble size is constrained to be 1000 samples,
resulting in a maximum standard error of .03, then a crude estimate of the

minimum reverberation to background ratio and the channel to channel

separation desired to reduce measurement errors to an acceptable level

can be obtained by upper bounding the maximum difference between the

true and measured correlation coefficients by the maximum standard

error due to the limited sample ensemble size. As has been shown, a

reverberation to background ratio of 20 dB and a channel to channel

separation of 40 dB would maintain measurement errors within this

bound.

As was mentioned earlier, it is also necessary to preserve the

relative phases of the narrowband acoustic signals at the face of the

hydrophones in order to accurately determine the spatial coherence .

Phase errors will occur, however, if the measurement system introduces

different phase shifts to the different signals. These different

phase shifts may even be time-varying. There are many points at which

the measurement system can introduce different phase shifts on the

different signal channels. The hydrophone elements themselves can

have different phase responses from hydrophone to hydrophone. Since

each hydrophone has its own set of preamplifiers, amplifiers, filters,

and other associated electronics, each set of electronics can introduce

a different phase shift to that signal. When the signals are recorded

on an analog tape recorder, phase variations of the tape recorder elec-

tronics and record heads from channel to channel as well as dynamic

skew, static skew, flutter and tape stretching can all contribute to

phase errors when the signal is reproduced. Finally, during the analog-

to-digital (A/D) conversion process, phase errors will be introduced if

there are any variations in the A/D clock or A/D electronics from channel to channel. Thus, the measurement system must be carefully designed so that these phase errors can be eliminated or corrected. The techniques used to maintain the phase integrity of the acoustic signals involve a combination of electronic design, equipment calibration, special recording and digitizing techniques, and processing of the digitized signals. These techniques will be discussed in the next section.

II.2   Hardware Configuration and Measurement Techniques

The purpose of the previous section was to help clarify the reasoning that led to the choice of hardware configuration and measurement techniques used to accurately measure the reverberation coherence. This section will describe the measurement system used.

The receive system electronic equipment is divided into underwater electronics and surface electronics. The underwater electronics are located within each of the two hydrophone arrays. Each element which is used in the hydrophone arrays has associated with it a preamplifier with 70 dB of gain and a differential line driver. The surface receive electronics consist of a differential line receiver, gain and phase adjustable amplifier, bandpass filter, analog gate and summing circuit for each receive channel. The complete receive system block diagram is shown in Figure II-1.

The receive electronic equipment was designed to help minimize the electronic noise level and the feedover between chan els. Low noise preamplifiers are used which were measured to have a wideband noise
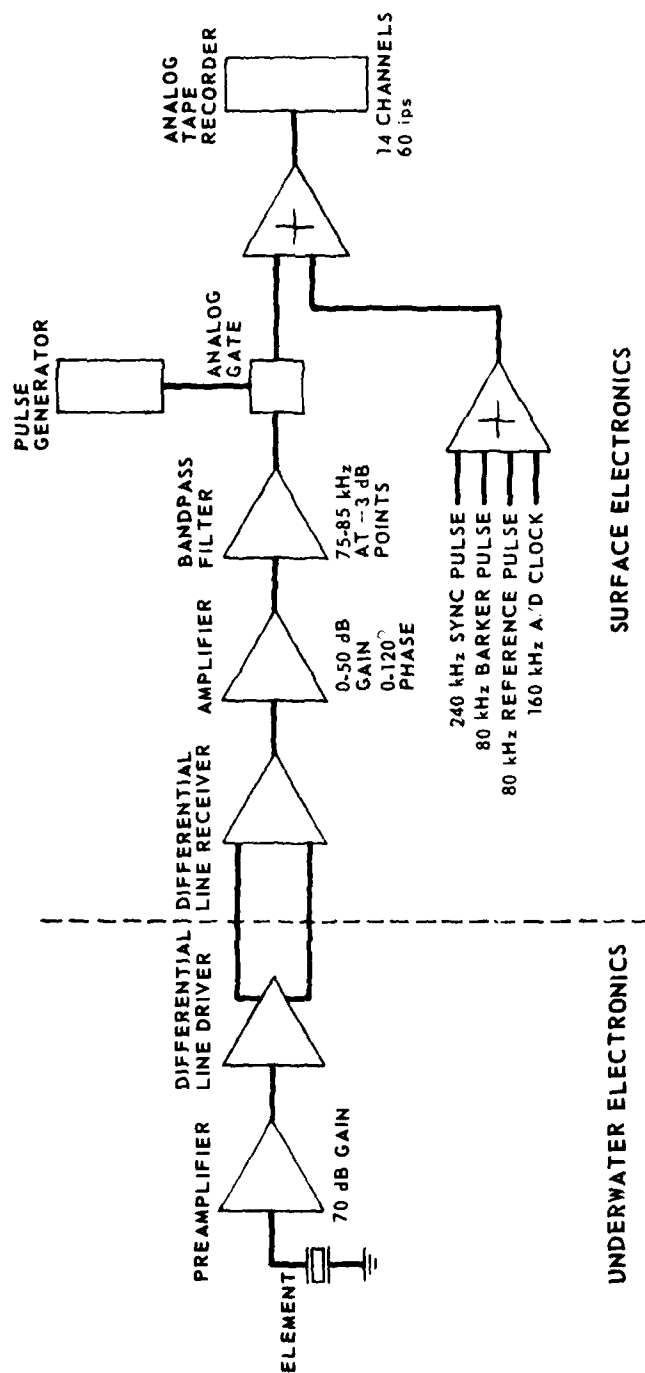
FIGURE II-1

RECEIVE ELECTRONICS BLOCK DIAGRAM
ONE CHANNEL

level related to the input with the input grounded of approximately
-110 dBV. The noise level in the 10 kHz band about 80 kHz will be
significantly less than this. A differential line driver/line receiver
combination is used with twisted pair cable to reduce the level of

feedover between channels in the cable from the arrays to the surface
electronics. Each channel also has a bandpass filter 10 kHz wide cen-
tered on 80 kHz to reduce the noise level but still provide sufficient
bandwidth for a 100 µs pulse. Figure II-2 shows a typical filter re-
sponse.

Measurements were made on this system to determine the electron-
ic noise level and the amount of feedover between channels. The elec-
tronic noise of the receive electronics at the input to the tape re-
corder with the surface amplifier set to 0 dB gain was -58 dBV ± 1 dBV.
The maximum signal level at the tape recorder input is -6 dBV, which
will give a maximum signal to electronic noise ratio of approximately
50 dB. This is well above the reverberation to electronic noise ratio
needed to ensure that the measurement error due to electronic noise is
below the measurement error due to a limited sample ensemble size.

Ambient acoustic noise was also measured immediately prior to
collecting the reverberation data. The rms reverberation to rms ambient
noise ratio was typically 30 dB or better. Thus the presence of ambient
noise did not contribute significantly to measurement error.

The feedover between channels was measured and found to be
primarily in the surface amplifier. Channels which had physically
adjacent amplifier circuits exhibited approximately -35 dB to -40 dB
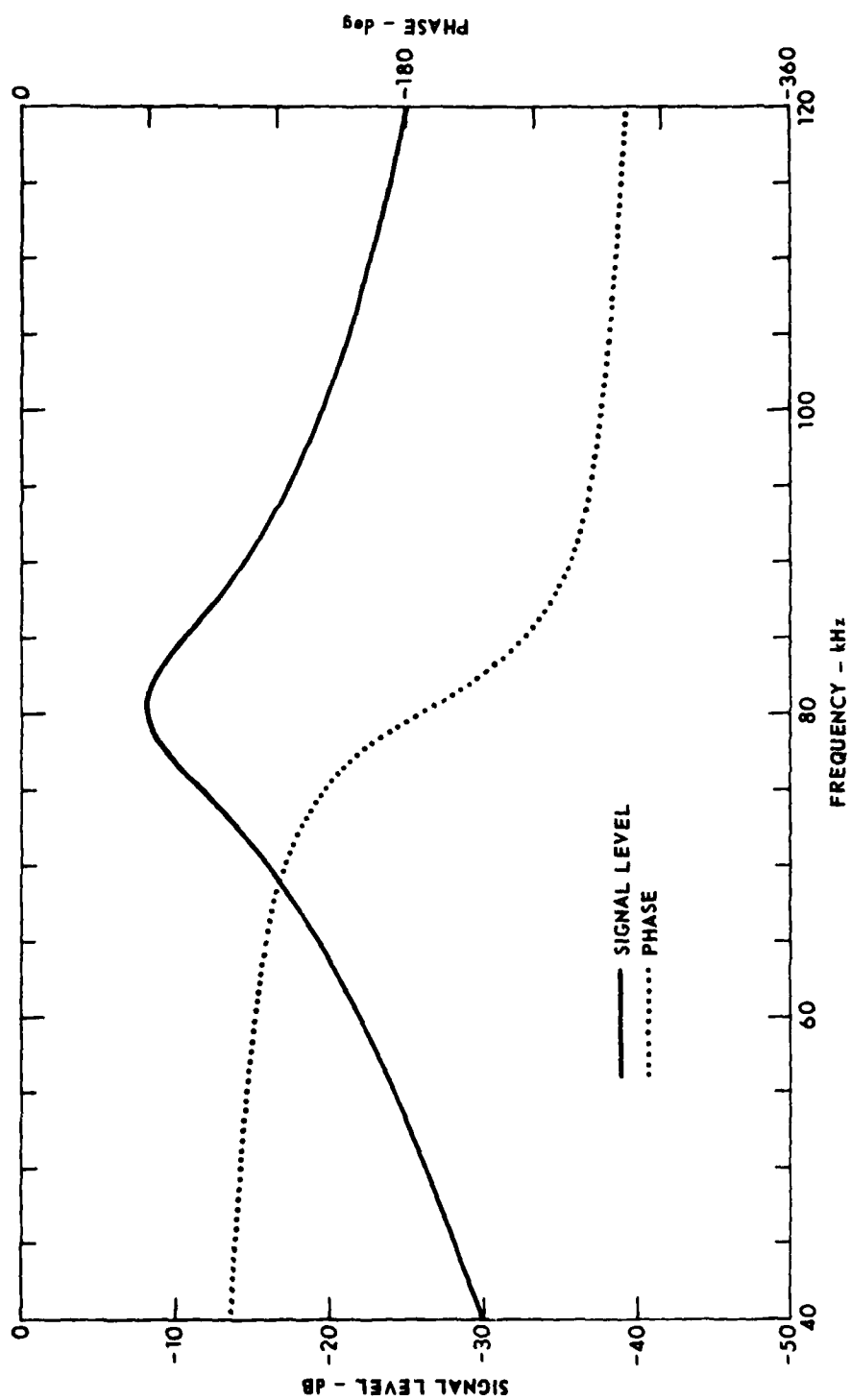
FIGURE II-2
BANDPASS FILTER RESPONSE

or feedover, while channels which were not physically adjacent had no measureable feedover.

The receive electronic equipment was also designed so that phase differences from channel to channel could be corrected during the digital processing of the data. The topside amplifier is gain and phase adjustable so that any gain and phase differences up to the inputs to the analog tape recorder can be removed. To remove these differences, an acoustic signal at 80 kHz is placed in the water in the farfield of the hydrophone arrays and is picked up by the arrays and measured at the inputs to the tape recorder. After the hydrophone arrays are oriented toward the source, the gain and phase of each channel are adjusted so that each hydrophone appears to be collinear with the other hydrophones in its array and has the same amplitude at the inputs to the analog tape recorder.

However, this calibration does not correct for phase differences due to the tape recorder electronics, reproduction process, or A/D process. To allow for this correction, several signals are summed together with each channel at the tape recorder inputs, as can be seen in Fig. II-1. A continuous sine wave at 160 kHz is provided as the A/D clock. The A/D is clocked at the zero crossings of the sine wave to provide sampling at 320 kHz. By summing the clock signal with each channel rather than recording the clock signal on only one channel or not recording a clock signal at all, any phase variations due to skew, flutter, or tape stretching can be minimized. During the reproduction and conversion process, each channel is filtered to separate the 80 kHz signal and the 160 kHz clock, and each channel is sampled with it's own clock signal.

This technique alone, though, will not correct for phase varia-
tions of the tape recorder electronics and record heads from channel to
channel, since the phase response of the tape recorder electronics and
recorder heads is not the same at 80 kHz and 160 kHz and the difference
in phase response changes from channel to channel. Thus an 80 kHz
pulsed sinusoid is summed with each channel to provide a reference
pulse for each ping. The reference pulse is digitized as a part of
the reverberation data for each channel and ping. The phase of the
reference pulse is then computed digitally and compared to the phase of
the reference pulse from an arbitrary reference channel and ping. The
digitized reverberation signal is then digitally phase shifted by an
amount which is the difference between the phase of these two reference
pulses. This is performed for every channel and ping.

However, this technique is unambiguous only when the phase
difference between two channels is less then 180°. This will not
always be the case. To compensate for large phase differences, an
80 kHz phase-encoded pulse (Barker pulse)[33] is also summed with each
channel on each ping and digitized with the reverberation data. The
Barker pulse has a particular phase-encoding that produces a very
narrow cross-correlation peak. Thus, the digitized Barker pulse is
digitally cross-correlated for each channel and ping with the Barker
pulse of the arbitrary reference channel and ping for several different
time shifts.[34] The digitized reverberation signal and reference pulse
are then shifted by the number of samples necessary to produce the
largest cross-correlation value. This is performed for every channel and
ping prior to phase shifting. Since the data are digitized at four times

the center frequency, each sample represents 90° of phase shift. Thus, the cross-correlation of the Barker pulses allows all the reverberation data and reference pulses to be aligned to within ± 90°. The reference pulses will then provide unambiguous measurements of the phase differences. It should be noted that by recording the reference and Barker pulses on every ping as well as every channel, phase variations in time are also corrected.

To minimize phase variation between channels due to the A/D equipment, the channels are digitized separately so that each channel will be processed through the same set of equipment. A 240 kHz pulsed sinusoid is summed with the reverberation signal and is filtered upon reproduction to separate the 240 kHz pulse from the reverberation signal. This pulse is used as a sync pulse to start the A/D on each ping.

The receive electronics also contains an analog gate on each channel which gates off the reverberation signal while the sync, Barker, and reference pulses occur to facilitate separating them from the reverberation signal.

II.3 Transducer Assembly

The transducers consist of one projector and two line receiving arrays. Each receiving array has 42 elements. The two receiving arrays are oriented at right angles to each other. Figure II-3 shows the relative orientation of the projector and receiving arrays, and also the spacing of the elements within the receiving arrays. Nine elements are used in the vertical array and four in the horizontal array. Each

FRONT VIEW · SIDE VIEW

CHANNEL
10.16 cm
2.54 cm
15.24 cm
15.24 cm
15.24 cm
10.16 cm
10.16 cm
10.16 cm
10.16 cm
10.16 cm
3.49 cm
17.15 cm
ARRAY CENTER
29.21 cm
44.45 cm
5.08 cm
79.69 cm
PROJECTOR
7.62 cm
3.18 cm
2.54 cm
5.08 cm
3.33 cm
4.29 cm
14 13 12 11
CHANNEL
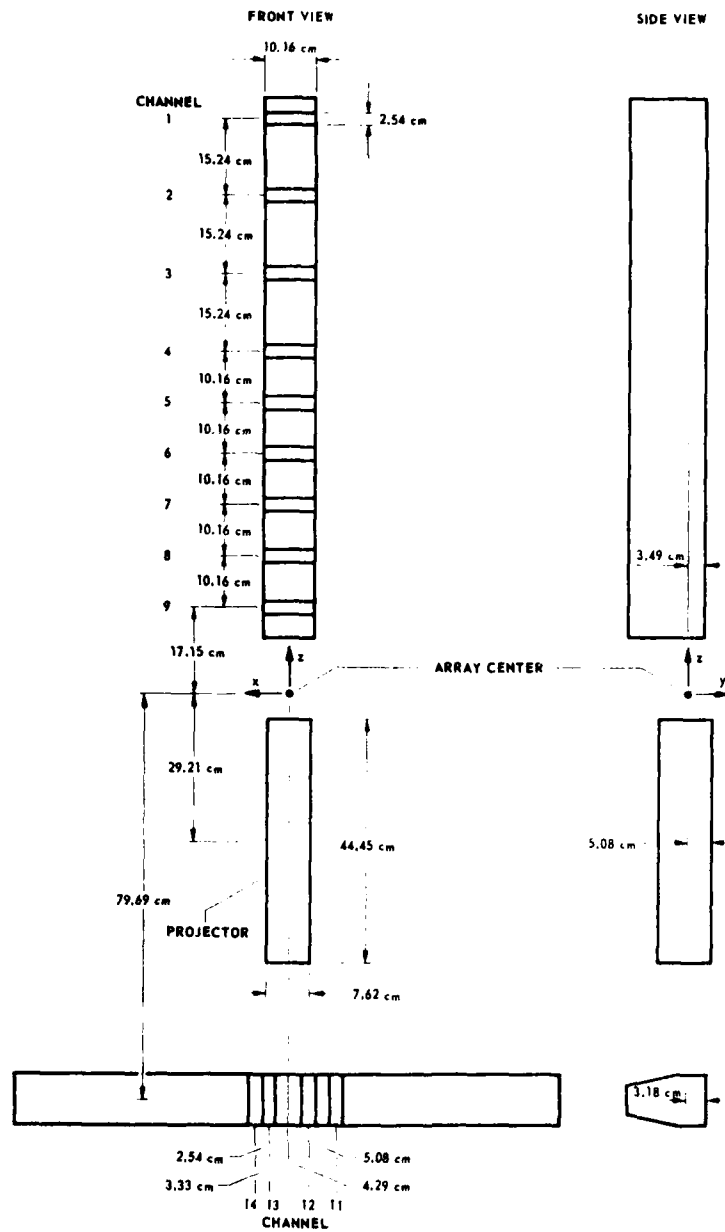
FIGURE II-3
TRANSDUCER ARRAY DIMENSIONS

element is a planar rectangular element ___ cm by ___ m. ___
ments of the vertical array have their long dimension ___ ___ ___
while the elements of the horizontal array have their long dimension
vertically. The faces of the elements in each array are ___ ___ with
the elements in that array. Directivity patterns for a single receive
element are shown in Figs. II-4 and II-5. The patterns are given for
75, 80, and 85 kHz, and are typical of the patterns for all elements.
The receive sensitivity of each receiver channel was measured at ___
and found to be approximately -107 dB re 1 V/µPa with 0 dB gain in the
topside receiver electronics.

The projector is a rectangular planar array 7.62 cm by ___ ___ m.
Its directivity patterns are shown in Figs. II-6 and II-7 at frequencies
of 75, 80, and 85 kHz. The projecting response was measured at 80 kHz
and found to be approximately 171 dB re 1 µPa/V at 1 m.

The projector and receiving arrays are mounted in a rigid framework
work and buoyed by flotation. The framework is attached to motors
which allow it to be tilted and rotated remotely. Synchro transmitters
on the tilt and rotate motors allow remote monitoring of the orientation
of the arrays. Figure II-8 is a photograph of the assembly mounted to
a tower section in air. The entire assembly was deployed on an under-
water tower in Lake Travis near the ARL:UT Lake Travis Test Station
(Fig. II-9).[37] The tower is located in approximately 40 m of water. The
center of the transducer assembly was approximately 10.? m below the
surface.
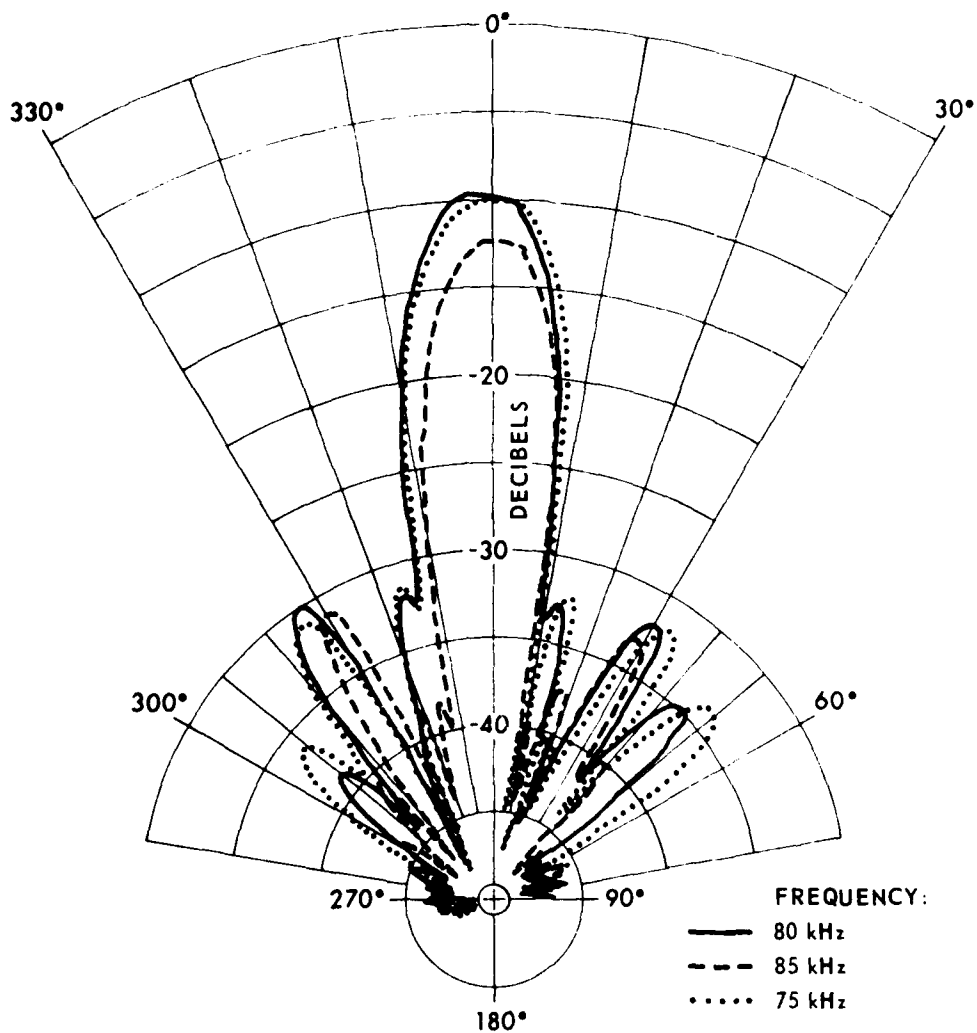
FIGURE II-4
DIRECTIVITY PATTERNS FOR A SINGLE RECEIVER ELEMENT
AT 75, 80, AND 85 kHz, MEASURED ABOUT THE LONG DIMENSION

FIGURE II-5
DIRECTIVITY PATTERNS FOR A SINGLE RECEIVER ELEMENT
AT 75, 80, AND 85 kHz, MEASURED ABOUT THE SHORT DIMENSION

ARL:UT
AS-79-2133
GRW-GA
10-24-79
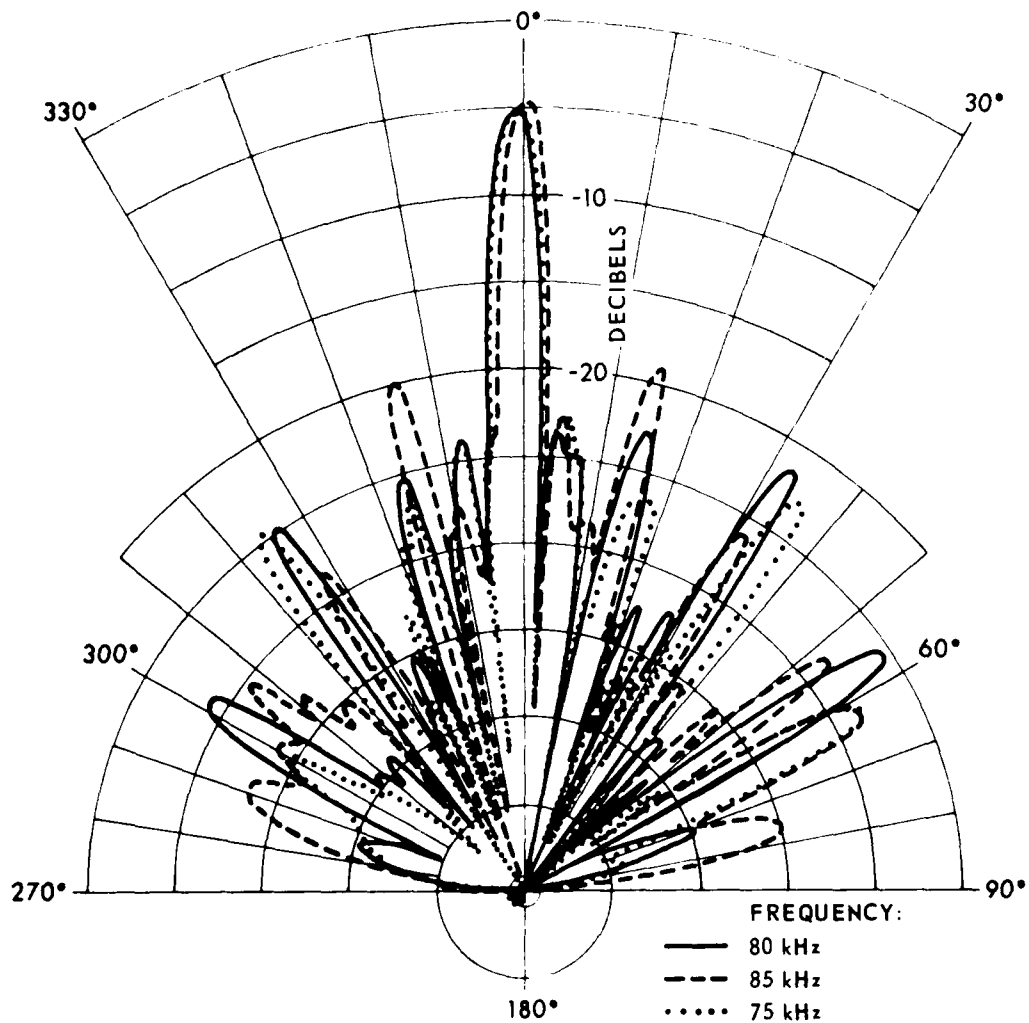
FIGURE II-6
PROJECTOR VERTICAL DIRECTIVITY PATTERNS
AT 75, 80, AND 85 kHz
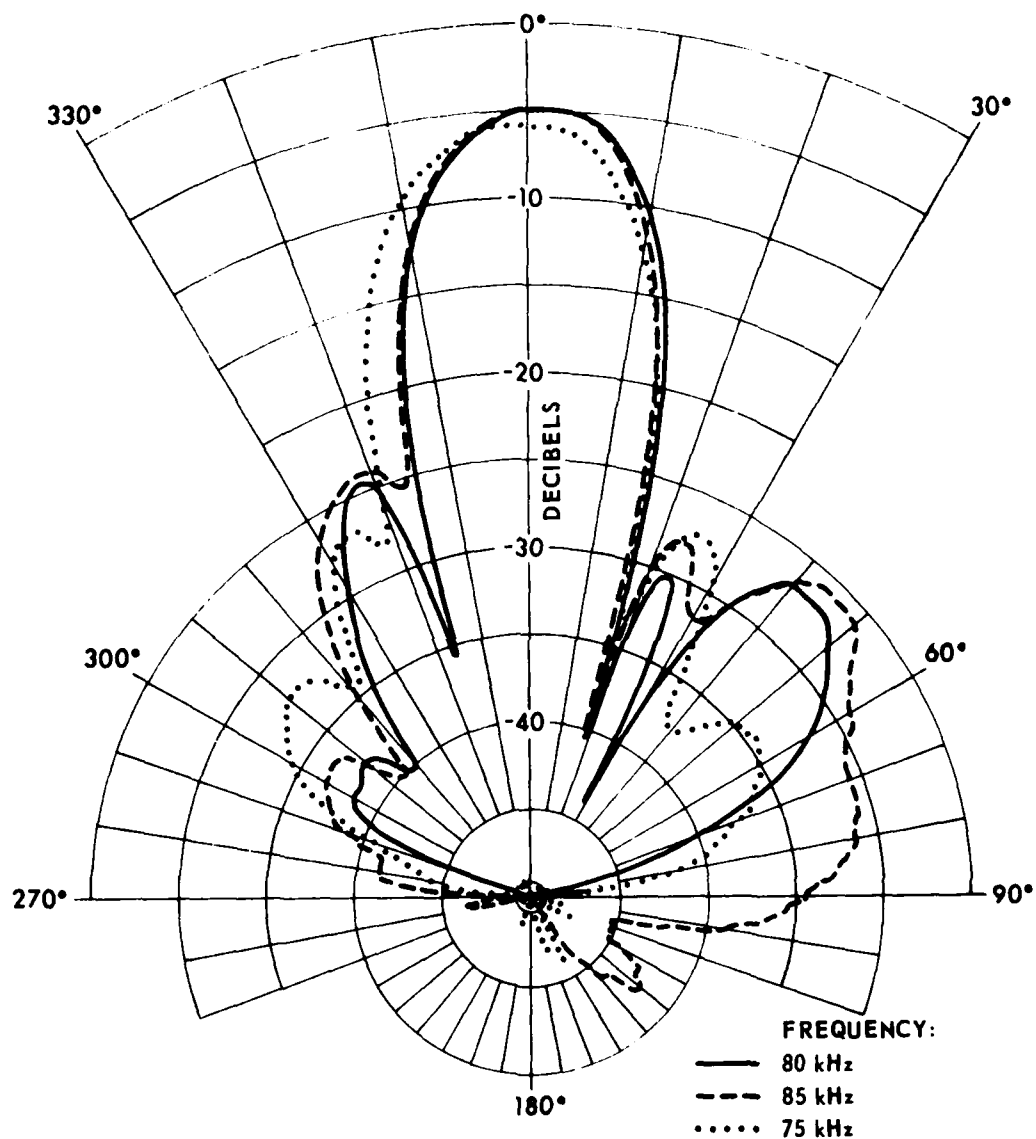
FIGURE II-7
PROJECTOR HORIZONTAL DIRECTIVITY PATTERNS
AT 75, 80, AND 85 kHz
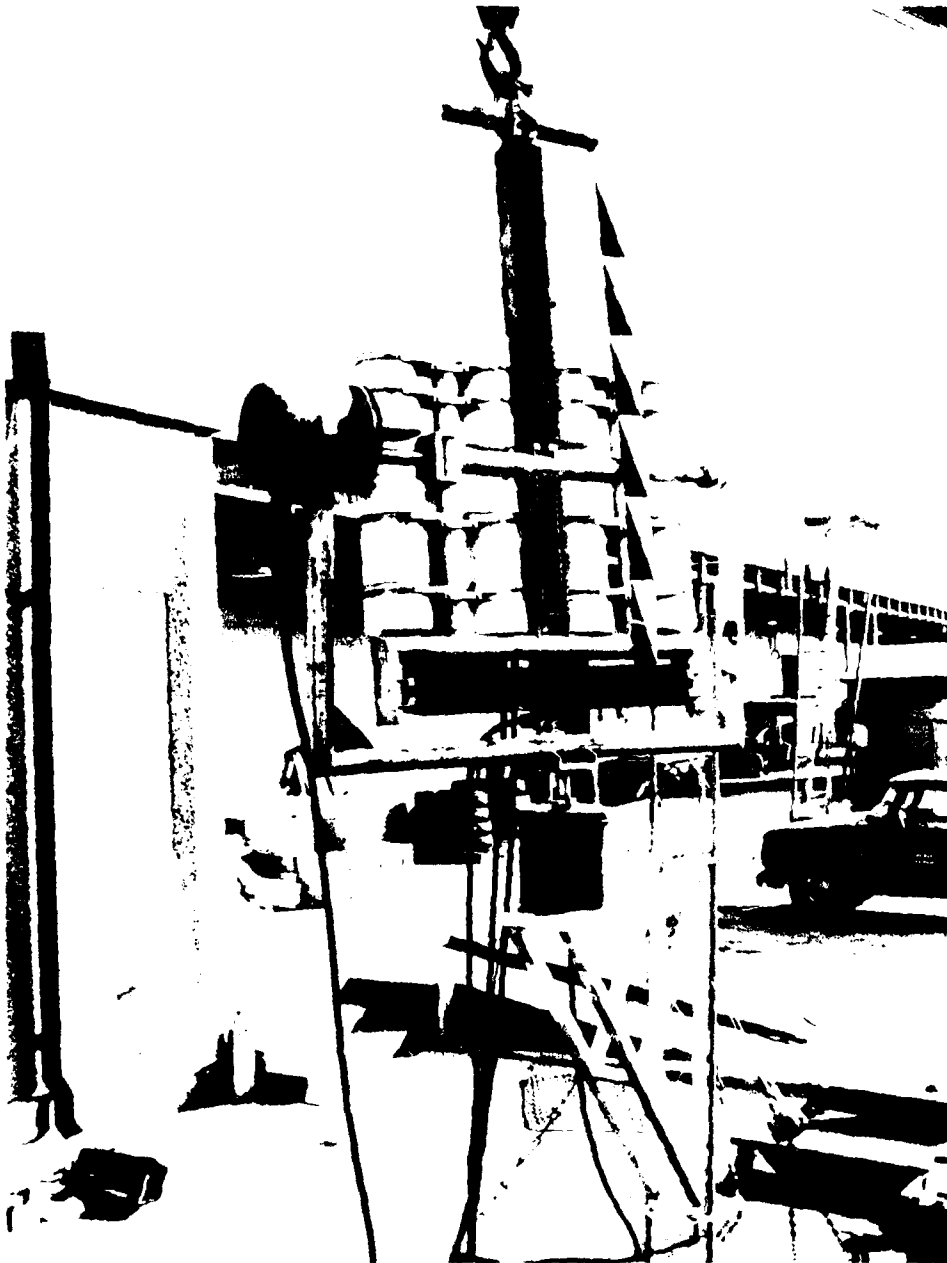
FIGURE II-8
TRANSDUCER ASSEMBLY

3673 2A
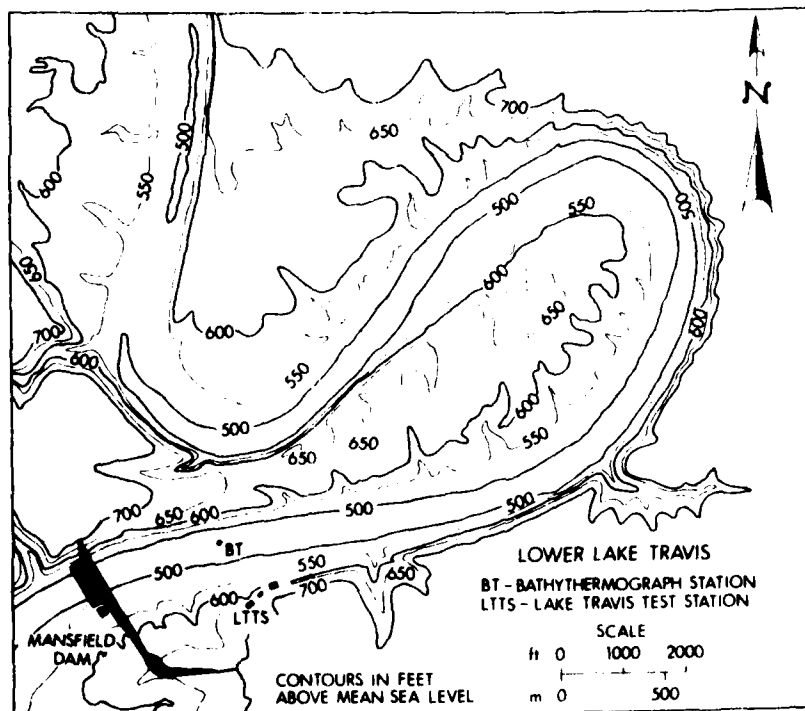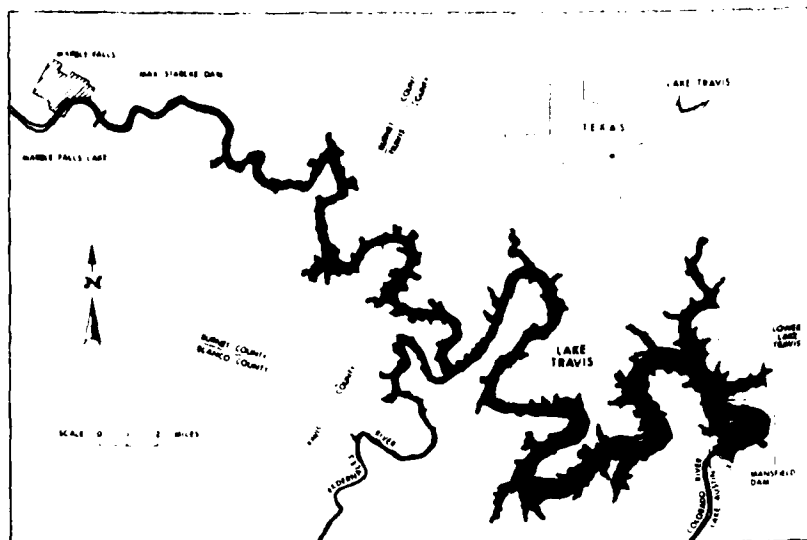
FIGURE II-9
THE LAKE TRAVIS TEST STATION

Conditions for Data Collection

A little over 1000 reverberation returns were recorded in approximately 14 minutes. A pulsed CW signal was transmitted at a center frequency of 80.0 kHz. The pulse length was 100 μs. The entire array was tilted to produce a grazing angle with the surface of approximately 10.5 degrees.

The water was isothermal to a depth of at least 20 m at a temperature of 13.8°C. The sound speed in the water was determined to be approximately 1463 m/s. The temperature of the air was 15.4°C and winds were from the north at 35-50 kph. The wave heights were estimated to be .3 to .6 m. The array was pointed approximately 47° east of north.

III. THEORETICAL MODEL

There are two fundamental approaches to the theory of
backscattering from a randomly rough surface. The "physical" model seeks
the solution of a scalar wave equation for statistically random boundary
conditions. It considers scattering from a rough surface in terms of the
statistical distribution of surface wave heights. The other approach is
the "quasiphenomenological" model, developed most generally by Middleton,
which treats reverberation as weak scattering from random point sources
representing inhomogeneities in an otherwise homogeneous medium. It
thus avoids the problem of complicated boundary conditions, but instead
requires a knowledge of the interaction of the incident sound with the
point sources in terms of an impulse response function for the point
sources. It is generally agreed that Middleton's "quasiphenomenological"
model is the most complete model of reverberation[31] but suffers from
the difficulty of having to specify a scattering function. Fortunately,
it has been shown that, at least in some cases, a very simple scattering
function works well.[17]

The remainder of this chapter is organized as follows. First
the development of Middleton's model as given in Ref. 27 is outlined.
Additional details of this development are given in Appendix A. Special
attention is given to the assumptions inherent in the model, and the
results for the covariance function are shown. Next the simplifications
which lead to the specific form of the model used in the present study
are discussed.* This includes specifying the scattering function. This

---

*This same form of the model was used by Frazer (Ref. 17).

scattering function is used in Appendix B to develop an expression for
what Middleton refers to as the elementary scattered waveform. An approxi-
mation of the covariance function which is valid for bandlimited signals
is then developed, and some additional approximations which facilitate the
numerical computation of the covariance function are discussed. Details
of the computations of the directivity patterns are given in Appendix C.

III.1   The General Model as Developed by Middleton

The following is a summary of the main features of Middleton's
model:

1. The total scattering process is a linear superposition of
    scattering from independent (in space and time) random point
    sources representing inhomogeneities in an otherwise homo-
    geneous medium. This is sufficient to specify the scatter-
    ing distribution as Poisson.

2. The interaction of sound with the scatterers is represented
    by an impulse response function.

3. General geometries and transmit and receive apertures are
    allowed.

4. General illuminating signals are allowed.

5. Reverberation from multiple receivers is considered.

6. Shadowing effects for rough surfaces are included.

7. Doppler effects due to motion of the source, receiver, and
    scatterers are included.

In Ref. 27 a characteristic function for the reverberation pro-
cess is derived based on Poisson statistics. From the characteristic
function the various moments can be determined by taking the appropriate

derivatives. An abbreviated explanation of this derivation is given

in Appendix A. The characteristic function depends upon a superposition

of elementary scattered waveforms, each representing the scattered

signal from a point source. These waveforms are determined from wave

and ray theory in a homogeneous medium and include the scattering

impulse response function. The following assumptions are made in this

development:

1. Scattering from the inhomogeneities is sufficiently weak

   that only primary scattering is considered, i.e., multiple

   scattering is ignored.

2. The probability that exactly N scattering events occur in

   a sufficiently small interval is given by the Poisson

   probability law.

3. The elementary scattered waveform for each scatterer is not

   a function of the specific scatterer; that is, the func-

   tional form of elementary scattered waveforms are identical

   for all scatterers. Also any random parameters associated

   with each scattering event have the same distribution.

   This implies that only one impulse response function is

   sufficient to describe the scattering process.

4. The scattering zone is in the farfield of the projector and

   receivers.

With these assumptions the joint (in time) characteristic func-

tion of the reverberation process is shown in Ref. 27 to be given by:

$$F_n(i\xi_1, t_1; \cdots ; i\xi_n, t_n | t^{'}, \Lambda)$$

$$= \exp\int_\Lambda \rho(\lambda;t^{'})\left\langle \exp i\{\sum_{\rho=1}^{n}\xi_\ell U(t_\ell;\lambda,\theta)\}-1\right\rangle_\theta d\lambda$$

where

$t_1,\ldots,t_n$ are the times of observation;

$t^{'}$ represents the temporal dependence of the scatter density;

Λ is the scattering region;

λ represents a point in the scattering region;

ρ is the density of scatterers at point λ and time $t^{'}$;

U is the elementary scattered waveform at time t_ℓ due to scatterers at point λ;

θ represents a set of random parameters associated with the scattering process;

and

$\langle\ \rangle_\theta$ represents the expected value with respect to the random parameters θ.

The various moments of the reverberation process are given by the appropriate derivatives of the characteristic function. For instance, if $X(t,t^{'})$ represents the reverberation process at time t due to a scatter density at time $t^{'}$, then the moments are given by the following:

$$\langle X(t,t^{'})\rangle = \int_\Lambda \rho(\lambda;t^{'})\langle U(t;\lambda,\theta)\rangle_\theta\ d\lambda$$

$$\langle X^2(t,t^{'})\rangle = \int_\Lambda \rho(\lambda;t^{'})\langle U^2(t;\lambda,\theta)\rangle_\theta d\lambda + \langle X(t,t^{'})\rangle^2$$

$$\langle X(t_1,t^{'})X(t_2,t^{'})\rangle = \int_\Lambda \rho(\lambda;t^{'})\langle U(t_1;\lambda,\theta)U(t_2;\lambda,\theta)\rangle_\theta d\lambda$$

$$+ \langle X(t_1,t^{'})\rangle \cdot \langle X(t_2,t^{'})\rangle \qquad .$$

The covariance of the process is then:

$$K_X(t_1,t_2|t') = \langle X(t_1,t')X(t_2,t')\rangle - \langle X(t_1,t')\rangle\langle X(t_2,t')\rangle$$

$$= \int_\Lambda \rho(\lambda;t')\langle U(t_1;\lambda,\theta)U(t_2;\lambda,\theta)\rangle_\theta d\lambda \qquad .$$

For spatially joint processes, for example a single projector and two receivers, the joint characteristic function of the two random processes $X^{(1)}(t_1,t')$ and $X^{(2)}(t_2,t')$ is a modification of the characteristic function given above:

$$F_{X^{(1)}X^{(2)}} = \exp\{\int_\Lambda \rho(\lambda,t')\langle\exp[i\xi_1 U_1 + i\xi_2 U_2]-1\rangle_{\theta_1,\theta_2} d\lambda\} \qquad .$$

Some of the relevant moments are given by:

$$K^{(1)}(t_1,t_2|t') = \langle X_1(t_1,t')X_1(t_2,t')\rangle$$

$$= \int_{\Lambda_1}\rho_1(\lambda,t')\langle U_1(t_1;\lambda,\theta_1)U_1(t_2;\lambda,\theta_1)\rangle_\theta d\lambda$$

$$K^{(2)}(t_1,t_2|t') = \langle X_2(t_1,t')X_2(t_2,t')\rangle$$

$$= \int_{\Lambda_2}\rho_2(\lambda,t')\langle U_2(t_1;\lambda,\theta_2)U_2(t_2;\lambda,\theta_2)\rangle_\theta d\lambda$$

$$K^{(12)}(t_1,t_2|t') = \langle X_1(t_1,t')X_2(t_2,t')\rangle - \langle X_1(t_1,t')\rangle\langle X_2(t_2,t')\rangle$$

$$= \int_{\Lambda_{12}}\rho_{12}(\lambda,t')\langle U_1(t_1;\lambda,\theta_1)U_2(t_2;\lambda,\theta_2)\rangle_\theta d\lambda \qquad .$$

III.2   The Theoretical Model as Used in the Present Study

A special case of this model is now considered. Two essential assumptions are invoked. It will be shown later that the covariance can be written as the sum of a time difference component (depending on the time difference t_2-t_1) and a time sum component (depending on the time sum t_1+t_2). It is assumed that the time sum component is negligible in comparison to the time difference component. Thus only the expression for the time difference component of the covariance is developed. This

assumption is reasonable when the transmitted signal is narrowband, i.e., the center frequency of the transmitted signal is much larger than it bandwidth. Secondly, the scatterer is modeled as a perfect point reflector, i.e., scattering is omnidirectional, frequency insensitive (within the bandwidth of the signal), location insensitive, and introduces no time delay. Since much of the scattering is from bubbles at or near the surface which have diameters much smaller than the wavelength of the transmitted sound, this assumption is a reasonable one. Other assumptions are as follows:

1. No random parameters are associated with the scattering event, i.e., there is no dependence on θ.

2. The directivity patterns of the projector and receivers are frequency insensitive within the bandwidth of the signal (narrowband signal).

3. $\rho(\lambda, t')d\lambda = \sigma_s dS$, where σ_s is the surface scatterer density and is constant, independent of position or time, and where the region of integration is over the surface of the water.

4. There is no doppler of the projector, receivers, or scatterers.

5. There are no shadowing effects.

Using these assumptions, it is shown in Appendix B that the elementary scattered waveform can be written as

$$U(t,\lambda) = \frac{\gamma \, A_R(\hat{R}_R) A_T(\hat{R}_T)}{(4\pi)^2 R_R R_T} \, V(t_r)$$

where

$$V(t_r) = \int_{-\infty}^{\infty} T_R(f) T_T(f) S_{in}(f) e^{j\omega t} \, df \quad ;$$

$$t_r = t - \frac{R_R + R_T}{c} \quad ;$$

$T_R(f)$ is the frequency response of the receiver;

$T_T(f)$ is the frequency response of the projector;

$S_{in}(f)$ is the frequency spectrum of the input electrical signal;

R_R is the distance from the receiver to the point scatterer at the coordinate λ;

R_T is the distance from the transmitter to the point scatterer at the coordinate λ;

c is the speed of sound;

$A_R(\hat{R}_R)$ is the directivity function of the receiver in the direction $\hat{R}_R$;

$A_T(\hat{R}_T)$ is the directivity function of the projector in the direction $\hat{R}_T$;

and

Y represents the response function of a scatterer which introduces no frequency shift or time delay to the scattered waveform.

Using this form of the elementary scattered waveform, the covariance of a joint process can now be written as

$$K^{(12)}(t_1, t_2 | t') = \sigma_s \int_{\Lambda_{12}} U_1(t_1, \lambda) U_2(t_2, \lambda) \, dS$$

$$= \frac{Y_1 Y_2 \sigma_s}{(4\pi)^4} \int_{\Lambda_{12}} \frac{A_{R1}(\hat{R}_{R1}) A_{R2}(\hat{R}_{R2}) A_T^2(\hat{R}_T)}{R_{R1} R_{R2} R_T^2}$$

$$\times V_1(t_{r1}) V_2(t_{r2}) \, dS$$

where

$$t_{r1} = t_1 - \frac{R_{R1}+R_T}{c}$$

$$t_{r2} = t_2 - \frac{R_{R2}+R_T}{c} \qquad .$$

This surface integral can now be evaluated numerically to compute the covariance.

This expression for the covariance can be expanded further by considering the product $V_1(t_{r1})V_2(t_{r2})$. Representing $V(t_r)$ in a quadrature formulation as

$$V(t_r) = X \cos\omega_o t_r + Y \sin\omega_o t_r$$

where ω_o is the angular center frequency of the projected signal, allows the product $V_1(t_{r1})V_2(t_{r2})$ to be written as

$$V_1(t_{r1})V_2(t_{r2}) = (X_1(t_{r1})\cos\omega_o t_{r1} +Y_1(t_{r1})\sin\omega_o t_{r1})$$

$$\times \; (X_2(t_{r2})\cos\omega_o t_{r2} +Y_2(t_{r2})\sin\omega_o t_{r2}) \qquad .$$

Multiplying these two expressions together and utilizing the trigonometric identities for the product of sine and cosine functions gives

$$V_1 V_2 = \tfrac{1}{2}[X_1 X_2+Y_1 Y_2]\cos\omega_o(\tau-\Delta R) + \tfrac{1}{2}[X_1 Y_2-Y_1 X_2]\sin\omega_o(\tau-\Delta R)$$

$$+ \tfrac{1}{2}[X_1 X_2-Y_1 Y_2]\cos\omega_o (t_{r1}+t_{r2})$$

$$+ \tfrac{1}{2}[X_1 Y_2+Y_1 X_2]\sin\omega_o (t_{r1}+t_{r2})$$

where

$$\Delta R = \frac{R_{R2}-R_{R1}}{c}$$

and the dependence of the quadrature components on t_{r1}, t_{r2} has been dropped for compactness of notation. Applying trigonometric identities

for the cosine and sine of a sum to this expression and rearranging
terms gives

$$V_1 V_2 = \tfrac{1}{2}\{[X_1 X_2 + Y_1 Y_2]\cos\omega_0 \Delta R - [X_1 Y_2 - Y_1 X_2]\sin\omega_0 \Delta R\}\cos\omega_0 t$$

$$+ \tfrac{1}{2}\{[X_1 Y_2 - Y_1 X_2]\cos\omega_0 \Delta R + [X_1 X_2 + Y_1 Y_2]\sin\omega_0 \Delta R\}\sin\omega_0 t$$

$$+ \tfrac{1}{2}[X_1 X_2 - Y_1 Y_2]\cos\omega_0(t_{r1} + t_{r2})$$

$$+ \tfrac{1}{2}[X_1 Y_2 + Y_1 X_2]\cos\omega_0(t_{r1} + t_{r2})$$

Substituting this expression for $V_1 V_2$ into the expression for the covariance
results in a time difference component (terms containing $\cos\omega_0 t$ and
$\sin\omega_0 t$) and a time sum component (terms containing $\cos\omega_0(t_{r1} + t_{r2})$ and
$\sin\omega_0(t_{r1} + t_{r2})$). For a narrowband signal the time sum terms are rapidly
varying functions over the area of integration for the covariance, since
$t_{r1} + t_{r2}$ contain the variables R_T, R_{R1}, and R_{R2}, which vary over the area
of integration. Thus the time sum component will average to approximately
zero in comparison to the time difference component of the covariance.[28]
Therefore in the expression for the covariance it is reasonable to express
the product of V_1 and V_2 as

$$V_1(t_{r1})V_2(t_{r2}) = X\cos\omega_0 t + Y\sin\omega_0 t$$

where

$$X = \tfrac{1}{2}\{[X_1(t_{r1})X_2(t_{r2}) + Y_1(t_{r1})Y_2(t_{r2})]\cos\omega_0(-\frac{R_{R2} - R_{R1}}{c})$$

$$- [X_1(t_{r1})Y_2(t_{r2}) - Y_1(t_{r1})X_2(t_{r2})]\sin\omega_0(\frac{R_{R2} - R_{R1}}{c})\}$$

$$Y = \tfrac{1}{2}\{[X_1(t_{r1})Y_2(t_{r2}) - Y_1(t_{r1})X_2(t_{r2})]\cos\omega_0(\frac{R_{R2} - R_{R1}}{c})$$

$$+ [X_1(t_{r1})X_2(t_{r2}) + Y_1(t_{r1})Y_2(t_{r2})]\sin\omega_0(\frac{R_{R2} - R_{R1}}{c})\}$$

Substituting this expression for the product of V_1 and V_2 into the equation for the covariance $K^{(12)}(t_1,t_2)$ gives the difference component

$$K_{12}(t_1,\tau) = \left\{ \frac{Y_1 Y_2 \sigma_s}{(4\pi)^4} \int_{\Lambda_{12}} \frac{A_{R1}(\hat{R}_{R1}) A_{R2}(\hat{R}_{R2}) A_T^2(\hat{R}_T)}{R_{R1} R_{R2} R_T^2} \, X dS \right\} \cos\omega_o\tau$$

$$+ \left\{ \frac{Y_1 Y_2 \sigma_s}{(4\pi)^4} \int_{\Lambda_{12}} \frac{A_{R1}(\hat{R}_{R1}) A_{R2}(\hat{R}_{R2}) A_T^2(\hat{R}_T)}{R_{R1} R_{R2} R_T^2} \, Y dS \right\} \sin\omega_o\tau \quad .$$

$$= X_{12}(t_1,\tau)\cos\omega_o\tau + Y_{12}(t_1,\tau)\sin\omega_o\tau$$

where

$$X_{12}(t_1,\tau) = \frac{Y_1 Y_2 \sigma_s}{(4\pi)^4} \int_{\Lambda_{12}} \frac{A_{R1}(\hat{R}_{R1}) A_{R2}(\hat{R}_{R2}) A_T^2(\hat{R}_T)}{R_{R1} R_{R2} R_T^2} \, X dS$$

$$Y_{12}(t_1,\tau) = \frac{Y_1 Y_2 \sigma_s}{(4\pi)^4} \int_{\Lambda_{12}} \frac{A_{R1}(\hat{R}_{R1}) A_{R2}(\hat{R}_{R2}) A_T^2(\hat{R}_T)}{R_{R1} R_{R2} R_T^2} \, Y dS \quad .$$

$X_{12}(t_1,\tau)$ and $Y_{12}(t_1,\tau)$ represent quadrature components of the difference component of the covariance. As such the difference component of the covariance can be expressed in terms of an envelope function and a phase function:

$$K_{12}(t_1,\tau) = E_{12}(t_1,\tau)\cos(\omega_o\tau + \Phi_{12}(t_1,\tau)) \quad ,$$

where

$$E_{12}(t_1,\tau) = \sqrt{X_{12}^2(t_1,\tau) + Y_{12}^2(t_1,\tau)}$$

and

$$\Phi_{12}(t_1,\tau) = \tan^{-1}\left(\frac{-Y_{12}(t_1,\tau)}{X_{12}(t_1,\tau)}\right) \quad .$$

Implementation of this model on a computer is facilitated by several additional approximations:

1. The function $V(t_r)$ is approximated from experimental measurements.

2. The surface integral is evaluated numerically, using the Simpson's integration technique.

3. The directivity functions of the projector and receivers are computed from the theoretical response for planar arrays.

The function $V(t_r)$ represents the input electrical signal after it has been filtered by the projector and receiver. It can be measured experimentally for the particular projector, receiver, and signal used by projecting at an omnidirectional, frequency insensitive (within the narrowband assumption) target and recording the received echo. This echo is used to represent $V(t_r)$, within an amplitude scale factor. The onset of the echo, which would represent the time $t_r=0$, cannot be precisely defined, since the exact distance between the projector and target is generally difficult to determine to the required degree of accuracy. Thus a reasonable point on the received echo is picked and defined as the point $t_r=0$. Quadrature samples of the received echo are obtained by directly sampling $V(t_r)$,[35] and the quadrature components of $V(t_r)$ are computed for any required time t_r by linear interpolation on the quadrature samples of the received echo. For t_r less than zero or greater than the extent of the echo, $V(t_r)$ is defined as zero.

The waveform $V(t_r)$ was measured experimentally by transmitting a 100 μs CW pulse centered at 80 kHz at a fluid-filled spherical lens[36] with a diameter of 15.2 cm and recording the echo received by the arrays from the sphere. The sphere was at the same depth as the arrays and at a range of approximately 100 m. The envelope and phase of the received echo on each receiving hydrophone is given in Figs. III-1 and III-2.

The surface integrals are evaluated numerically using the Simpson's integration technique. This integration technique evaluates an integral by summing over fixed step sizes. The integral of a function $f(x)$ with respect to the variable x between the limits a and b is approximated by

$$\int_a^b f(x)dx = \frac{\Delta x}{3} \sum_{n=1}^{N+1} mf(a+(n-1)\Delta x)$$

where

Δx is the chosen step size;

N is the integer closest to $\frac{b-a}{\Delta x}$;

and

$$m = \begin{cases} 1, & \text{if } n = 1 \text{ or } N + 1 \\ 2, & \text{if } n \text{ is even} \\ 4, & \text{if } n \text{ is odd.} \end{cases}$$

The step size Δx is chosen to provide the desired accuracy for the integration.

To evaluate the surface integral required for the covariance computation, the integration is performed over the variables t' and ϕ,
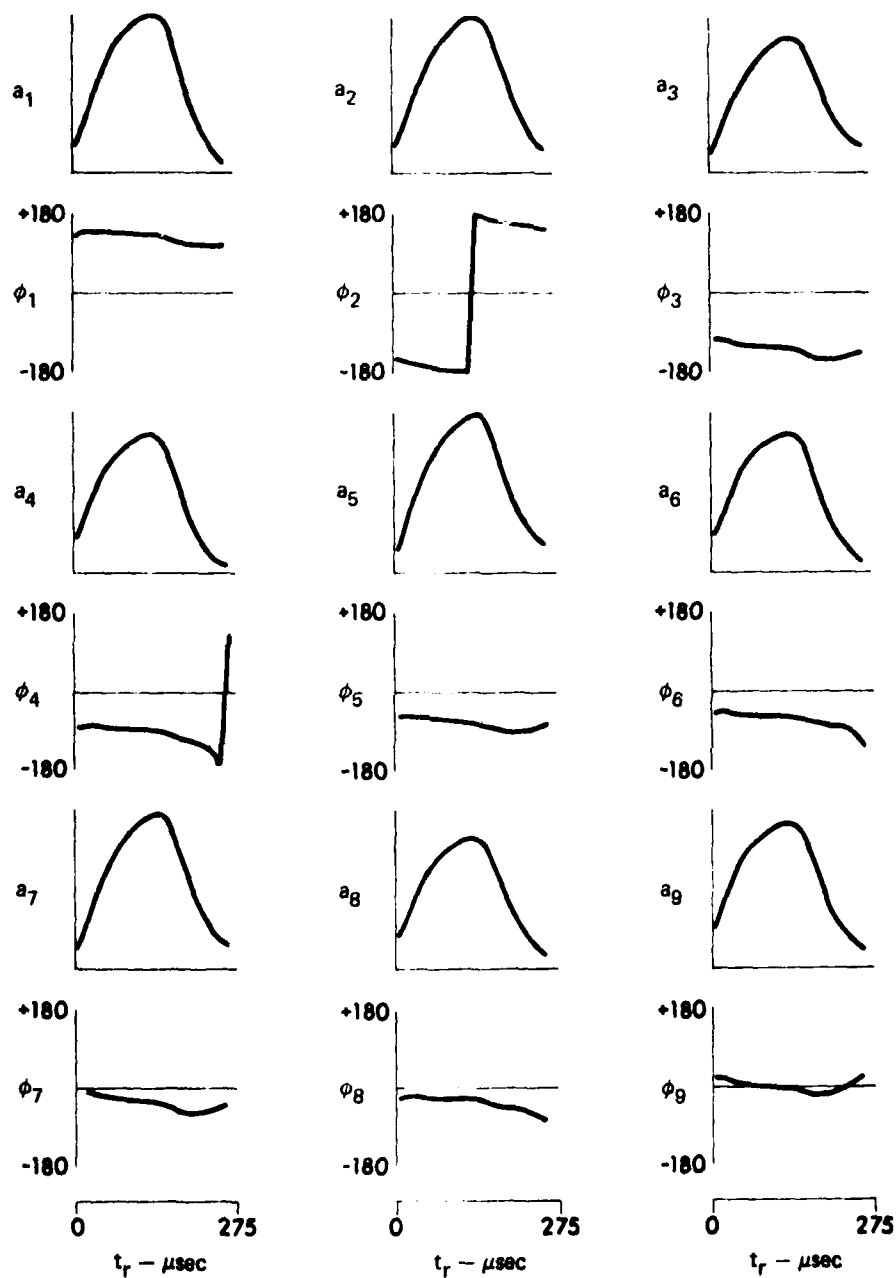
FIGURE III-1
THE AMPLITUDES a_i AND PHASES ϕ_i OF THE WAVEFORMS $V_i(t_r)$
FOR THE VERTICAL ARRAY
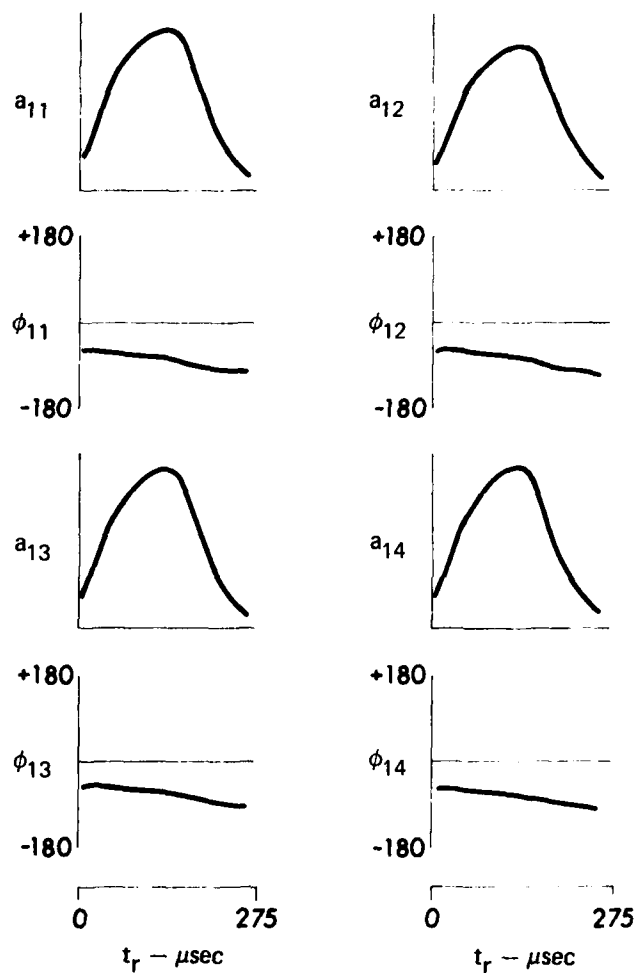
FIGURE III-2
THE AMPLITUDES a_i AND PHASES ϕ_i OF THE WAVEFORMS $V_i(t_r)$
FOR THE HORIZONTAL ARRAY

with the transformation

$$dS \rightarrow wc^2 t_T dt_T d\phi$$

where ϕ is the azimuthal angle to a point scatterer, and t_T is the time

of the scattering event relative to the beginning of the transmission.

The transformation factor w is a function of both ϕ and t_T, and is

given in explicit form in Appendix C. For the parameters of this

study, w was very close to 1. Since $R_T = ct_T$, then

$$\frac{1}{R_T^2} dS = \frac{w}{t_T} dt_T d\phi \qquad .$$

The Simpson's integration technique is used to evaluate both integrals,

with the t_T integration performed first since the limits of the t_T

integration turn out to be ϕ dependent.

The quadrature components of the covariance are then

$$X_{12}(t_1,\tau) = \frac{Y_1 Y_2 \sigma_s}{(4\pi)^4} \int_{\phi_L}^{\phi_U} \int_{t_L}^{t_U} \frac{A_{R1}(\hat{R}_{R1}) A_{R2}(\hat{R}_{R2}) A_T^2(\hat{R}_T)}{R_{R1} R_{R2} t_T} Xw dt_T d\phi$$

$$Y_{12}(t_1,\tau) = \frac{Y_1 Y_2 \sigma_s}{(4\pi)^4} \int_{\phi_L}^{\phi_U} \int_{t_L}^{t_U} \frac{A_{R1}(\hat{R}_{R1}) A_{R2}(\hat{R}_{R2}) A_T^2(\hat{R}_T)}{R_{R1} R_{R2} t_T} Yw dt_T d\phi$$

where the area of common scatterers A_{12} determines the limits on the ϕ

and t_T integrations. Figure III-3 shows the common scattering region

for two horizontal receivers and a projector. Only scatterers which were

illuminated between the times t_{1L} and t_{1U} contribute to the waveform

of receiver 1 at time t_1, where t_{1L} and t_{1U} are given by

44

COMMON SCATTERING REGION

ϕ_U

ϕ_L

t_{2U}

t_{1U}

t_{1L}

t_{2L}

RECEIVER 2

PROJECTOR

RECEIVER 1

$t_{2U} = t_1 + \tau - \dfrac{R_{R2}}{c}$

$t_{2L} = t_1 + \tau - \dfrac{R_{R2}}{c} - T$

$t_{1U} = t_1 - \dfrac{R_{R1}}{c}$
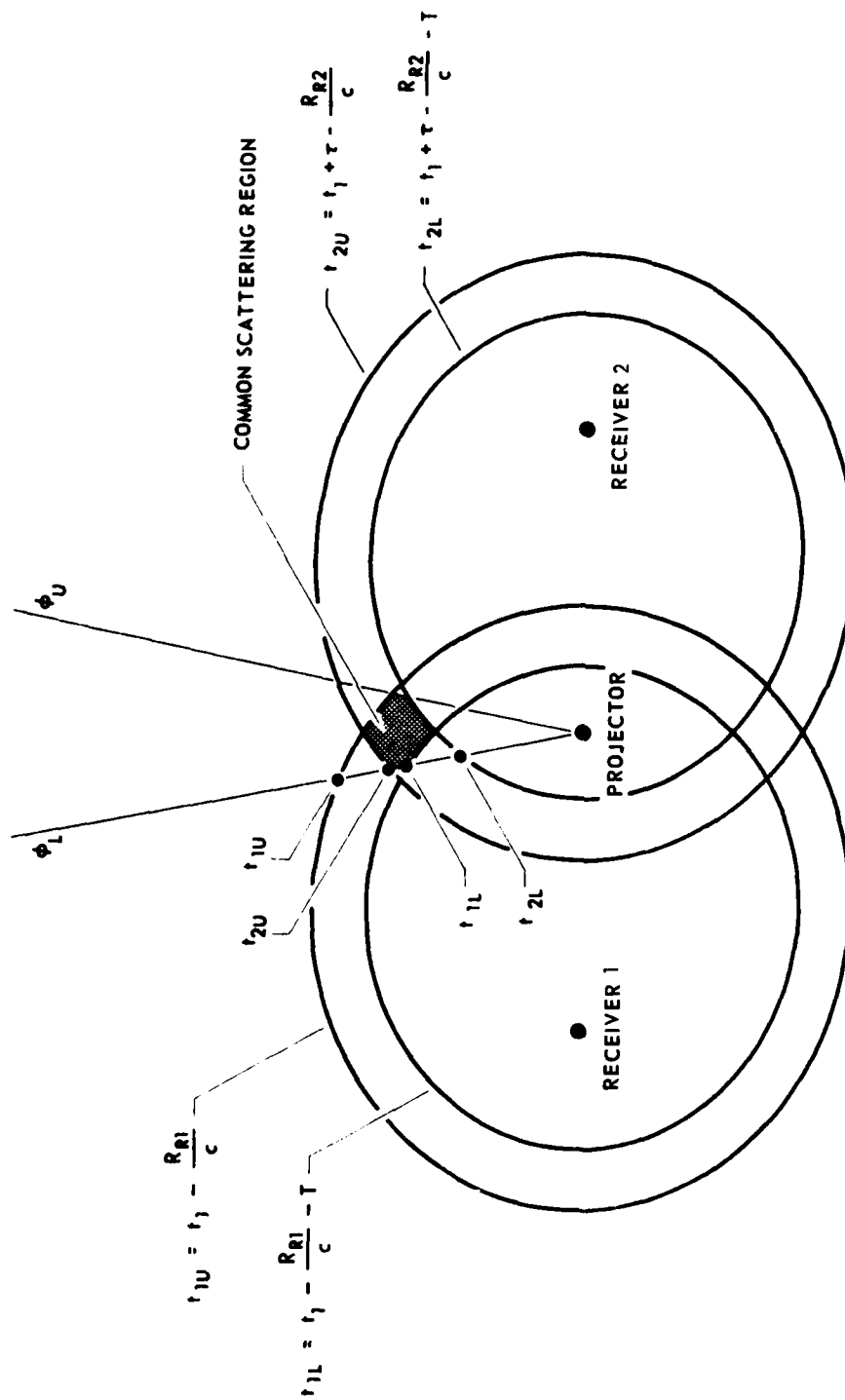
$t_{1L} = t_1 - \dfrac{R_{R1}}{c} - T$

FIGURE III-3

SURFACE VIEW OF COMMON SCATTERING REGION (From Ref. 17)

$$t_{1L} = t_1 - \frac{R_{R1}(t_{1L})}{c} - T$$

$$t_{1U} = t_1 - \frac{R_{R1}(t_{1U})}{c}$$

where T is the transmitted pulse length. Likewise, only the scatterers which were illuminated between the times t_{2L} and t_{2U} contribute to the waveform of receiver 2 at time $t_2 = t_1 + \tau$, where t_{2L} and t_{2U} are given by

$$t_{2L} = t_1 + \tau - \frac{R_{R2}(t_{2L})}{c} - T$$

$$t_{2U} = t_1 + \tau - \frac{R_{R2}(t_{2U})}{c}$$.

Thus the scatterers which contribute to both receivers at both times t_1 and t_2 are those which were illuminated between the times t_L and t_U, where t_L and t_U are given by

$$t_L = \max[t_{1L}, t_{2L}]$$

$$t_U = \min[t_{1U}, t_{2U}]$$.

The above equations for t_{1L}, t_{1U}, t_{2L}, and t_{2U} are solved iteratively in order to determine the limits for the t_T integration.

The limits on the ϕ integration are much easier to determine, and in fact depend only on the horizontal directivity pattern of the projector. The limits are chosen so that most of the projected sound is within the chosen limits. If the sidelobes of the projector are sufficiently low, it can be assumed that to a good approximation the scatterers are illuminated only by the main lobe of the projector. The limits are then typically chosen to include only the main lobe.

The directivity functions used in the covariance calculation are computed from the theoretical response for planar, shaded elements. The projector is bizonally shaded in both dimensions, while the receiving elements are bizonally shaded in the long dimension and unshaded in the short dimension. The projector's directivity function is given by

$$A(\hat{R}_T) = \frac{\sin X + \frac{1}{2}\sin(\frac{X}{2})}{\frac{5X}{4}} \cdot \frac{\sin Y + \frac{1}{2}\sin(\frac{Y}{2})}{\frac{5Y}{4}}$$

where

$$X = \frac{\omega_o}{2c} \ell_{TV}\sin\alpha_T\cos\beta_T \quad ;$$

$$Y = \frac{\omega_o}{2c} \ell_{TH}\sin\alpha_T\sin\beta_T \quad ;$$

$\hat{R}_T$ is a unit vector from the projector to the point scatterer with respect to a coordinate system centered on the projector, as illustrated in Fig. III-4;

ℓ_{TV} is the vertical length of the projector;

ℓ_{TH} is the horizontal length of the projector; and

α_T and β_T are spherical angular coordinates, represented by the angles α and β in Fig. III-4.

Likewise, the directivity function for the horizontal receivers is given by

$$A(\hat{R}_{Ri}) = \frac{\sin X + \frac{1}{2}\sin(\frac{X}{2})}{\frac{5X}{4}} \cdot \frac{\sin Y}{Y}$$

and for the vertical receivers is given by

$$A(\hat{R}_{Ri}) = \frac{\sin X}{X} \cdot \frac{\sin Y + \frac{1}{2}\sin(\frac{Y}{2})}{\frac{5Y}{4}}$$
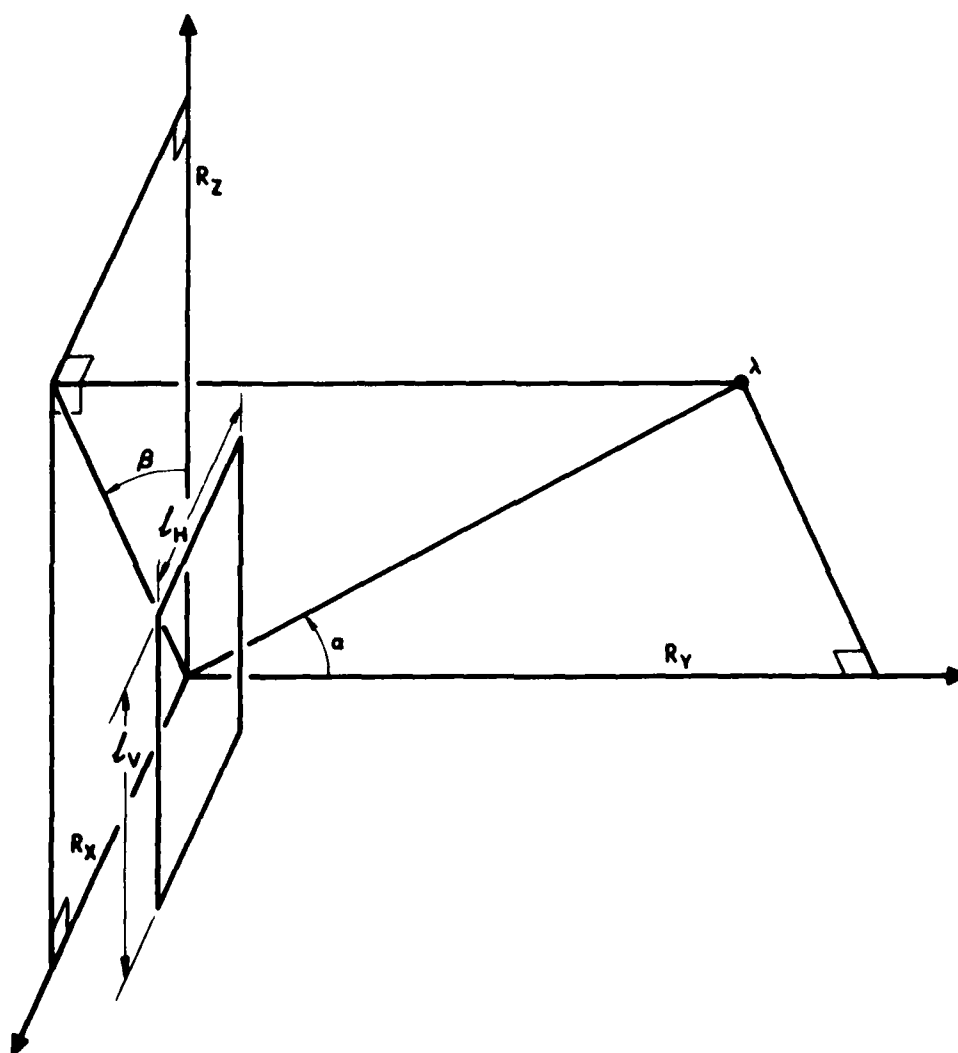
FIGURE III-4
COORDINATE SYSTEM CENTERED AT AN ELEMENT OF THE ARRAY

where

$$X = \frac{\omega_o}{2c} \ell_{RiV} \sin\alpha_{Ri} \cos\beta_{Ri} \quad ;$$

$$Y = \frac{\omega_o}{2c} \ell_{RiH} \sin\alpha_{Ri} \sin\beta_{Ri} \quad ;$$

$\hat{R}_{Ri}$ is a unit vector from the ith receiver to the point scatterer

with respect to a coordinate system centered on the receiver;

ℓ_{RiV} is the vertical length of the ith receiver;

ℓ_{RiH} is the horizontal length of the ith receiver; and

α_{Ri} and β_{Ri} are spherical angular coordinates represented by the

angles α and β in Fig. III-4.

Details of the computation of the directivity functions in terms of the

variables of integration t_T and ϕ are given in Appendix C.

A comparison of the computed and measured directivity patterns

for the projector is given in Figs. III-5 and III-6 for a frequency

of 80 kHz. The corresponding directivity patterns for a typical re-

ceiver element are given in Figs. III-7 and III-8.

The steps sizes for the t_T and ϕ integrations were chosen to

achieve an accuracy of at least one percent. A step size of 2.5×10^{-6} s

was found to be adequate for the t_T integration. The required step

size for the ϕ integration was found to depend upon whether the elements

were separated vertically or horizontally. The integrand of the ϕ inte-

gration for vertically separated elements changed only slowly over the

range of ϕ. Thus a step size of 2 degrees was sufficient. However,

for horizontal separations the integrand changed more rapidly. For

separations out to 5 cm, a step size of 1 degree was sufficient, but

for a separation of 7.5 cm, a 0.5 degree step size was necessary.
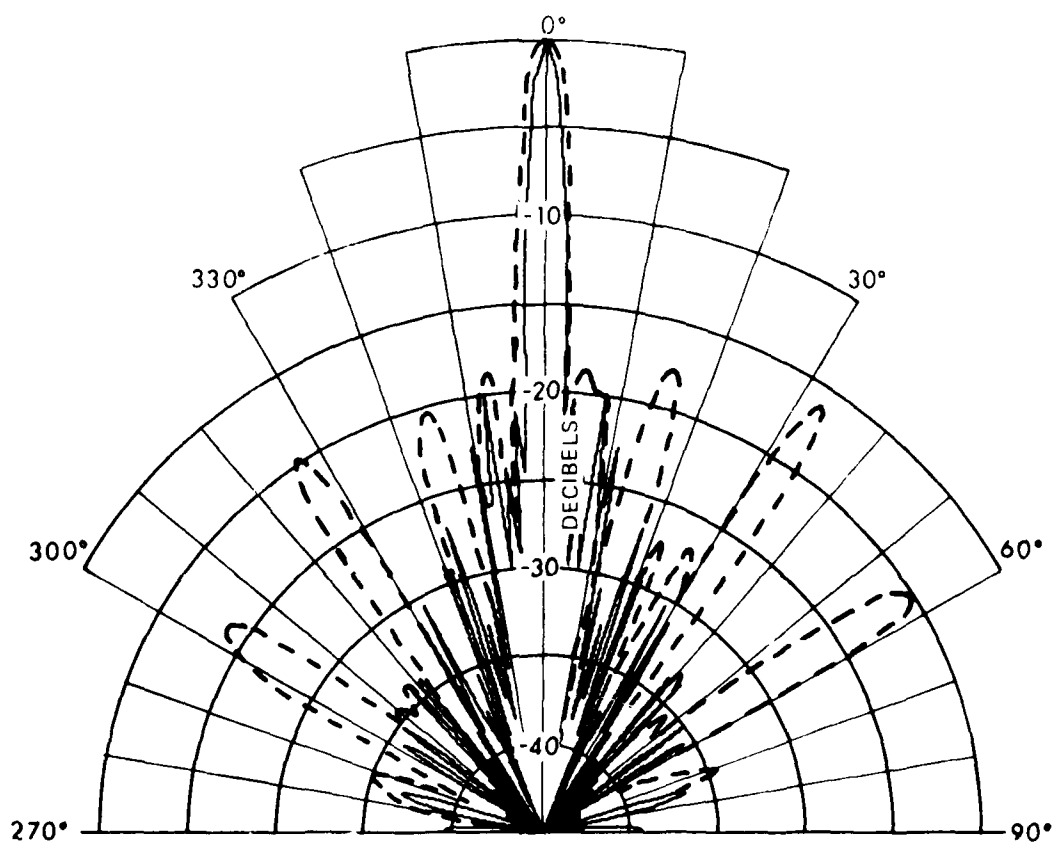
FIGURE III-5
COMPARISON OF COMPUTED AND MEASURED
PROJECTOR VERTICAL BEAM PATTERN

---- MEASURED PATTERN
———— COMPUTED PATTERN
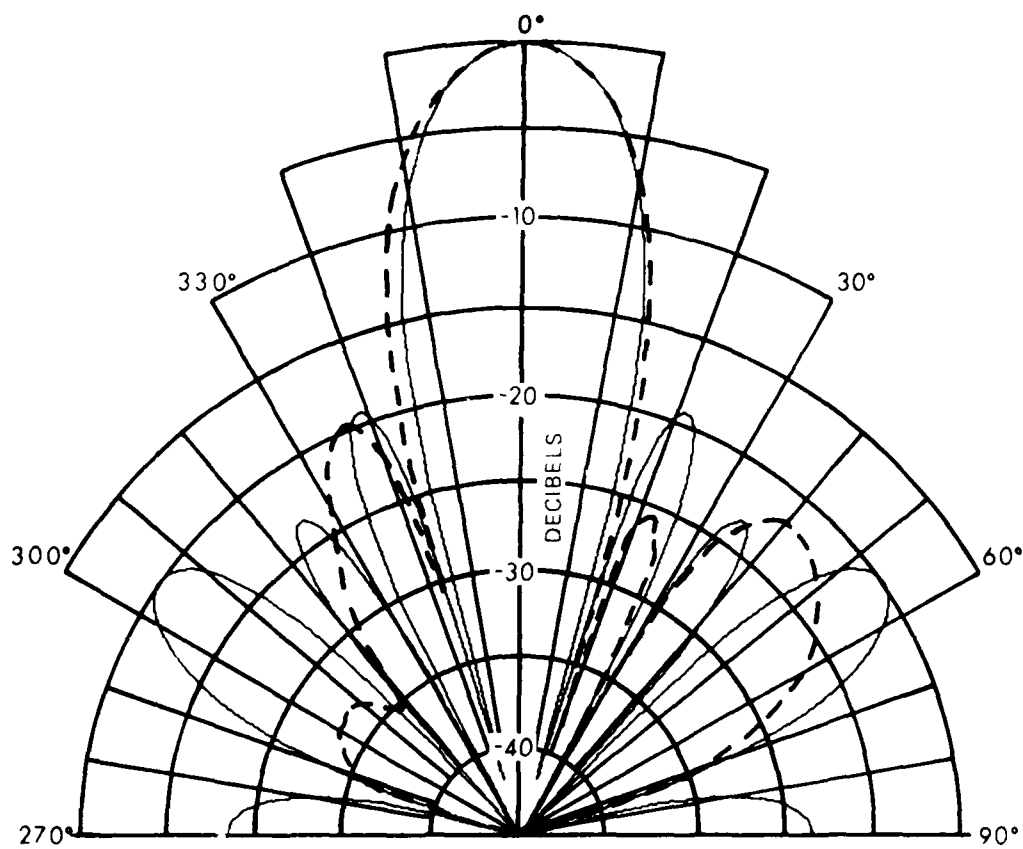
FIGURE III-6
COMPARISON OF COMPUTED AND MEASURED
PROJECTOR HORIZONTAL BEAM PATTERN

— — — — —   MEASURED PATTERN
————————   COMPUTED PATTERN
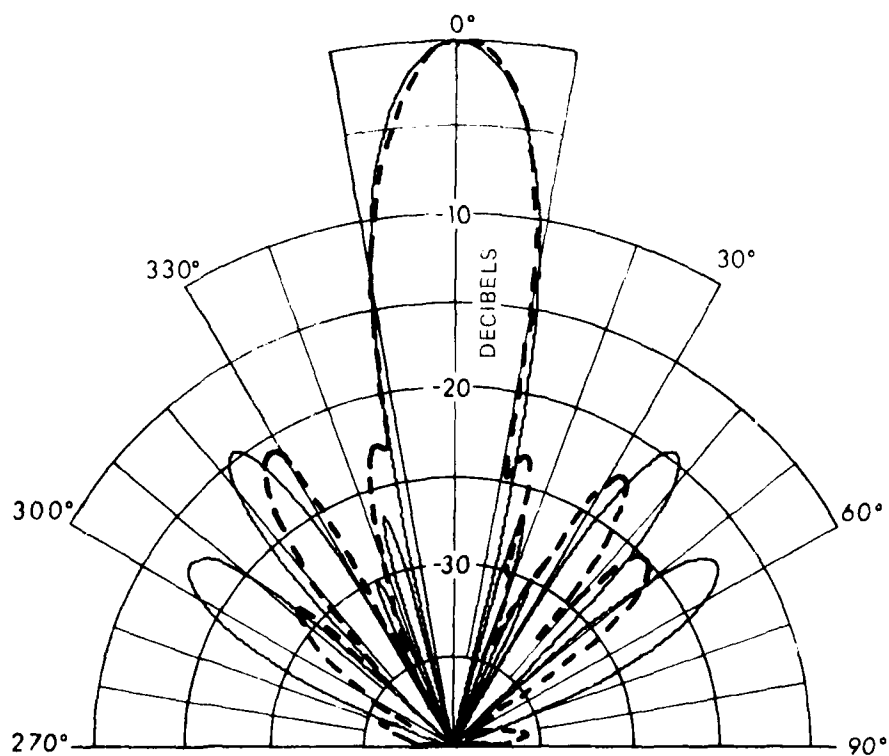
FIGURE III-7
COMPARISON OF COMPUTED AND MEASURED RECEIVER
BEAM PATTERN IN THE LONG DIMENSION AT 80 kHz

— — — — — MEASURED PATTERN
———————— COMPUTED PATTERN
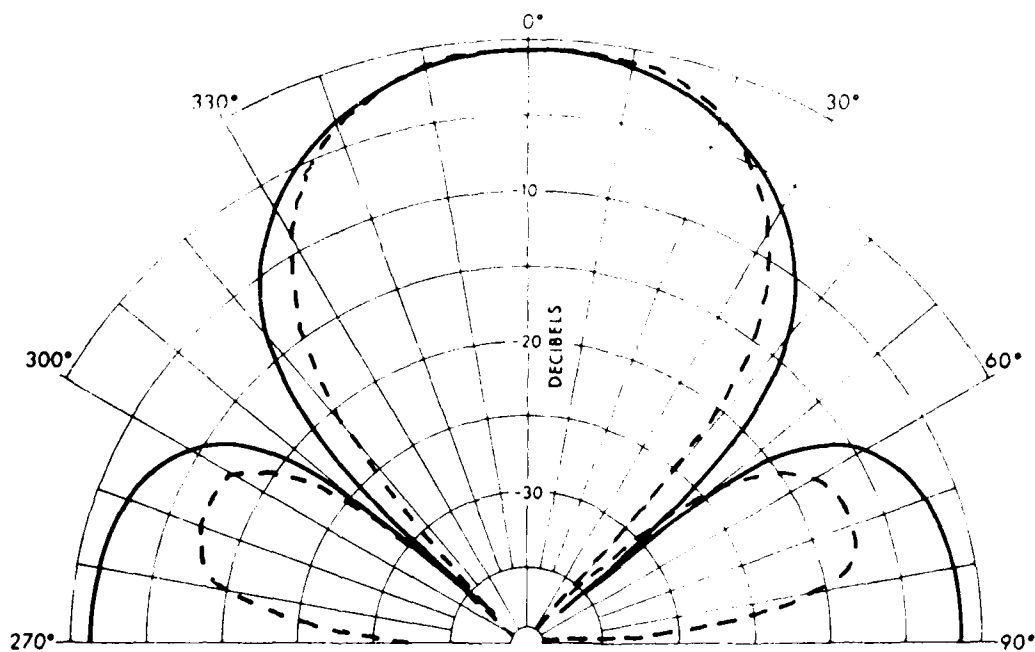
FIGURE III-8
COMPARISON OF COMPUTED AND MEASURED RECEIVER
BEAM PATTERN IN THE SHORT DIMENSION AT 80 kHz

―――――― COMPUTED PATTERN
― ― ― ― MEASURED PATTERN

Further spacings required such small step sizes that in view of the negligible levels of coherence between these spacings, the theoretical computations were not performed. The ϕ integration was performed over the limits from -15 to 15 degrees.

IV. STATISTICAL TESTING OF SAMPLE DATA

The reverberation field is sampled to form experimental ensembles, and various statistical tests are performed on the ensembles to validate the sample data. This chapter discusses the sampling procedure, including the assumptions inherent in the sampling process. The statistical tests are also discussed, and the results from applying these tests to the sample data are presented.

IV.1   Formation of Sample Ensembles

The electrical signals produced at the output of each receiving element by the acoustic reverberation are treated in this study as continuous time random processes, denoted by $v_i(t,\omega)$, where i indexes the particular random process ($1 \leq i \leq 13$), t represents the observation time relative to the beginning of the pulsed transmission, and ω indexes the particular realization of the random process which was generated from the parent population Ω of all possible realizations of the random process. For this study, $1 < \omega < 1084$. For a fixed ω, $v_i(t,\omega)$ is a particular realization, or sample function, of the ith random process.

The continuous time random process $v_i(t,\omega)$ is sampled in time during the analog-to-digital (A/D) processing for each realization. The sampled function is denoted by $v_i(t_n,\omega)$, where t_n denotes one of the discrete times at which the sampling occurred. For this study, $1 \leq n \leq 3200$, where the sampling occurred at four times the center frequency of the transmission, or 320 kHz. Thus the reverberation process was sampled for a total time of 10 ms.

For a fixed t_n and receiver element i, the collection of all $v_i(t_n,\omega)$, $1<\omega<1084$ represents a finite sample set of a random variable, and is referred to as a sample ensemble. To be a valid sample ensemble, the sampling assumptions must be met: each sample of the ensemble must be independent and identically distributed, i.e., the samples are a random collection of realizations of the random variable $v_i(t_n,\omega)$ for a fixed t_n and i. The results of testing the ensembles for randomness are presented in a later part of this chapter.

The A/D conversion not only reduces the continuous time process to a discrete time process, but it also quantizes the value of the signal at each time into one of a finite number of discrete values. A 12-bit A/D converter was used for the digitization. The instantaneous value of the electrical signal was thus converted to an integer in the range of -2048 to $+2047$, giving a dynamic range of approximately 66 dB. Thus the samples of the random process are no longer continuously valued, but instead take on discrete values. This aspect of the sampling has a significant effect upon the statistical testing of the ensembles. Most of the statistical tests assume that sampling is from a continuous distribution and thus no two or more samples will have precisely the same value. This assumption cannot always be met when the samples are quantized into a finite number of values. Thus the statistical tests must be adjusted to account for ties in the sample data.

The previous discussion has served to point out the assumptions inherent in the technique used by this study to form sample ensembles. The data upon which the computations in this study are made are limited ensembles of quantized, finite range, discrete time, random processes.

It is assumed that these data adequately represent continuously valued, continuous time random processes. Generally, the statistical tests account for the fact that the data is a limited ensemble of samples from a continuous distribution and also generally account for quantization effects which lead to ties in the data. Thus finite ensemble size and quantization are not significant limitations. The limited dynamic range of the sampled data must be considered during data collection and digitization to ensure that virtually the entire distribution of values of the reverberation process falls within the available dynamic range of the data collection and digitization system. It must be assumed that the extreme tails of the distribution of the random process which were not included in the sampled data due to limited dynamic range contribute negligibly to the results of this study. Observation of the sampled data indicated that only occasionally was the value of the reverberation process outside the dynamic range of the A/D converter, so that it is felt that the dynamic range is also not a significant limitation.

IV.2   Statistical Testing of Ensembles

Since the reverberation is treated as a random process and the reverberation ensemble as a random sampling of the parent population of the random process, then it is assumed that the ensembles consist of random variables which are independent and identically distributed. In an attempt to verify that the collection of reverberation events forms a valid ensemble, each ensemble was tested for randomness or independence. Since the elements of a valid ensemble must be not only independent but also identically distributed, further tests for homogeneity were also

applied to each ensemble.[38,59] An ensemble was accepted as a valid sample ensemble if the hypotheses of randomness and homogeneity could not be rejected by these tests at a reasonable level of significance.

After the sample ensembles were verified, they were then tested for normality. That is, each ensemble was tested to determine if it represented a sampling from a normal parent population.

IV.2.1 General Remarks on Hypothesis Testing

One of the requirements of hypothesis testing is to establish a criterion for accepting or rejecting an hypothesis for an ensemble or group of ensembles. Before engaging in a discussion of the details of statistical hypothesis testing, a few qualitative remarks may help to clarify the criterion chosen in this study. The basic "output" of an hypothesis test upon which this criterion is usually based is the probability of making a mistake by rejecting the test hypothesis. That is, an hypothesis test is performed on an ensemble and the basic result of the test is this probability. Typically if this probability is small, that is, the probability of erring by rejecting the hypothesis is small, then the hypothesis can be rejected for the ensemble with some degree of confidence, while keeping in mind that there is some small probability of being wrong.

In the present study many ensembles are obtained, one at each sample time for each channel. Instead of accepting or rejecting individual ensembles, as is typically done, it is desirable to either accept or reject the entire set of ensembles for each channel. That is, it is desirable to either accept or reject the hypothesis being tested for each channel over the entire 10 ms of the recorded reverberation returns.

Of course, this acceptance technique assumes that the property of the

data which is being tested, such as normality or homogeneity, does not

change during the 10 ms reverberation return. This may not always be the

case,[15,41] and thus it may be necessary to accept one segment of the data

while rejecting another segment.

In any case it is necessary to establish a procedure which

will allow the acceptance or rejection of the entire set, or some segment of

the entire set, of ensembles for each channel. One such procedure is to

examine the percentage of ensembles which have a small probability of

erring. If a disproportionately large percentage of the ensembles have

small probabilities of erring by rejecting the hypothesis, then it is

reasonable to reject the hypothesis for the entire set of ensembles. On

the other hand, if the percentage of ensembles with small probabilities

is commensurate with the level of probabilities, then the hypothesis is

accepted for the entire set of ensembles. For example, if approximately

10 percent of the ensembles have a probability of making a mistake less

than or equal to 0.1, then the hypothesis can be accepted. If, however,

the percentage of ensembles is significantly different from 10 percent,

then the hypothesis is rejected at this level of 0.1. The probability

of making a mistake by rejecting the hypothesis is referred to as the

probability of making a Type I error, and is denoted by α. The level

at which an hypothesis is tested is referred to as the level of signif-

icance. In this study, the level of significance was chosen to be 0.1

for all the hypothesis tests.

Having qualitatively discussed the results of an hypo-

thesis test and established a criterion for accepting or rejecting an

hypothesis, a more detailed discussion of the general procedures for applying these tests is appropriate. Each of the statistical tests applied in this study tests a single null hypothesis H_0 against a single alternative hypothesis H_1. No testing is performed against multiple hypotheses. For example, the test for randomness tests the null hypothesis

$$H_0: \quad \text{the sample ensemble is random,}$$

against the alternative hypothesis

$$H_1: \quad \text{the sample ensemble is not random.}$$

To accept the alternative hypothesis H_1 is to reject the null hypothesis H_0. No attempt is made to discriminate between various types of non-randomness in the test itself. However, the particular test chosen may be more sensitive to one class of nonrandomness than another. Thus the test should be chosen which is most sensitive to the type of nonrandomness expected in the data in order to produce results which can be confidently relied upon.[39]

Hypothesis testing is performed by first computing a test statistic which is a function of the sample ensemble being tested. For example, denoting the random variables of the sample ensemble by $v_i(t_n,\omega)$ and the test statistic by $T_i(t_n)$, then

$$T_i(t_n) = F(v_i(t_n,\omega))$$

where F is some function which defines the particular test being used. The test statistic is itself therefore a random variable which has (perhaps unknown) probability distributions under H_0 and H_1. That is, if the sample ensemble meets the criteria of the null hypothesis, then the test statistic will have a particular probability distribution. If

the sample ensemble meets the criteria of the alternative hypothesis, then the test statistic will have a (hopefully) different probability distribution.

The probability distribution of the test statistic under the null hypothesis is generally known or can be approximated. From this distribution, the probability of obtaining or exceeding the value of the statistic which was calculated from the sample ensemble, assuming the sample ensemble met the criteria of the null hypothesis, can be calculated. If this probability is small, then the assumption of the null hypothesis is rejected and the alternative hypothesis is accepted. This probability was referred to previously as the probability of making a Type I error, and is designated α. Thus α is the probability of announcing H_1 when H_0 is true, written as

$$\alpha = P(H_1 | H_0) \qquad .$$

The probability α provides a measure of the confidence with which the alternative hypothesis can be accepted. If α is very small, then there is little chance of making an error in announcing H_1, and thus one can be confident about announcing H_1. However, if α is not small, then H_1 cannot be reliably accepted and instead H_0 is accepted. Unfortunately, the value of α provides no indication of the confidence with which H_0 can be accepted. In order to confidently accept H_0, the probability of announcing H_0 when H_1 is true, written as $P(H_0 | H_1)$, must be known to be small. This probability is known as the probability of making a Type II error and is designated by β, i.e.,

$$\beta = P(H_0 | H_1) \qquad .$$

$1-\beta$ is sometimes referred to as the power of a test. To calculate this probability, the distribution of the test statistic under the alternative hypothesis must be known. This distribution is generally not known for the types of tests used in this study. Thus, the best that can be said is that if H_1 cannot be accepted, then H_0 cannot be reliably rejected.

In an attempt to minimize this deficiency, several criteria are applied to hypothesis tests in an effort to define a test which will most likely be the most powerful test to use. One of the most common criteria is asymptotic relative efficiency (ARE). It is a comparison of the efficiency of one test to another test, and is defined as follows. Let N_A be the number of samples that test A requires to achieve a power $1-\beta$ at a given significance level α, and let N_B be the number of samples that test B requires to achieve the same power at the same significance level. Tests A and B test the same null hypothesis H_0 against the same alternative hypothesis H_1 and each has test statistics which are asymptotically normally distributed. The ARE is the ratio of N_A to N_B (N_A/N_B) in the limit as N_A and N_B go infinity and as H_1 goes to H_0.

The ARE is useful primarily as a comparison of several different tests to the same reference test. While the magnitude of the ARE has only a limited meaningfulness, a comparison of the ARE of several comparable tests is generally a good indication of the ranking of the power of the tests.[40] Thus the test with the largest ARE is usually the most powerful test. If the tests are nonparametric, i.e., no assumption is made as to the form of the probability distribution

of the sample ensemble (except possibly for continuity or some other
rather general assumptions), then usually a most powerful parametric test
is used as the reference test from which the ARE of the nonparametric
tests are determined. In this study, the tests for randomness, indepen-
dence, homogeneity, and one test for normality are all nonparametric tests.

Alternatively, an empirical method is often used with
parametric tests to estimate the efficiency of various tests when the
distribution of the test statistic under the alternative hypothesis is
unknown. The sample ensemble is assumed to have a certain distribution
under the alternative hypothesis, and from this distribution the distri-
bution of the test statistic under the alternative hypothesis is empiri-
cally calculated for various sample sizes. It is then possible to compute
the power of the test from this empirical distribution. This procedure
is usually repeated for a number of different sample ensemble distribu-
tions. In this way the power of several tests can be compared for a
number of different distributions to determine the test which generally
has the largest power over the widest class of distributions. Alterna-
tively, if the sample data is known a priori to come from one of a
restricted class of distributions, then a test can be chosen which has
the largest power over this restricted class of distributions. In this
study, three of the tests for normality are parametric tests.

The tests used in this study were generally selected to
provide the most power for the type of data being tested and the likely
alternatives. The runs up and down test was used as a test for random-
ness, while the Kolmogorov-Smirnov two-sample test and the Wilcoxon rank-

sum test were used for testing homogeneity. The four tests for normality were Pearson's test of skewness, Pearson's test of kurtosis, D'Agostino's test, and the Kolmogorov-Smirnov one-sample test. The (two-tailed) level of significance was chosen to be 0.1 for all tests.

The tests were performed on each of the 3200 ensembles from each of the 13 channels. For each test, the probability of a Type I error was computed and compared to the level of significance. The percentage of the 3200 ensembles from each channel that failed a particular test, i.e., that had a probability of a Type I error below the level of significance, was also computed. In order to determine if the hypothesis being tested should be accepted for all 3200 ensembles, the results of a particular test were treated as outcomes from independent, repeated Bernoulli trials.[15] That is, in this scheme two outcomes from a test are possible: the probability of a Type I error α is greater than or equal to the significance level, or it is less than the significance level. The probability that α is less than the significance level under the null hypothesis is just the value of the significance level. That is, for a significance level of 0.1 there is a probability of 0.1 that α will be less than 0.1 if the null hypothesis is true. If this probability is denoted by p, then for all the tests considered in this study,

$$p = \text{Prob}[\alpha < 0.1] = 0.1 \quad .$$

According to the binomial law, the probability that, out of n independent outcomes each with a probability p of having a value of α less than the significance level, k or more of the outcomes will actually have values of α less than the significance level is given by

$$B(k;n,p) = \sum_{i=k}^{n} \binom{n}{i} p^{i}(1-p)^{n-i}$$

This binomial distribution has a mean of np and a standard deviation of $[np(1-p)]^{1/2}$. For a particular test the number k of outcomes which had values of $\alpha < 0.1$ were determined and the resulting binomial probability was computed for each channel. If this probability was small, less than 0.05, indicating that too many outcomes were below the significance level, or if it was large, greater than .95, indicating too few outcomes, then the null hypothesis was rejected in favor of the alternative hypothesis for that channel. If the probability was greater than 0.05, then the null hypothesis could not be confidently rejected.

This technique assumes that the outcomes are independent. It will be shown in the next chapter that the reverberation used for this study has a correlation time of approximately 250 µs. Thus tests performed on ensembles representing sample times which are less than 250 µs apart may not have independent outcomes, although it is difficult to determine the precise relationship between the correlation of the reverberation process and the dependence of the outcomes of a test. The approach taken in this study to attempt to extract independent test outcomes was to select the outcome of the test from every 80th ensemble, corresponding to a time separation of 250 µs, from the set of 3200 ensembles from each channel. These 40 values of α were then examined to determine the number k of values less than 0.1, and this number was used to compute the binomial probability.[15] Thus n=40 in the computations of the binomial probability.

IV.3.3   Testing for Randomness

Tests for randomness test the null hypothesis:

H_0: all n! possible permutations of the n members of
        the sample ensemble were equally likely to have
        been the permutation which actually occurred,

against the alternative hypothesis:

H_1: certain permutations are more likely to occur than
        others.

For all permutations to be equally likely, the occurrence of the samples
must be independent, that is, the occurrence of any one sample has no
effect on the occurrence of any other sample. Thus a test for random-
ness is also a test for independence. The runs up and down test was
used in the present study as a test for randomness.

IV.3.3.1 The runs up and down test

A run is the unbroken sequence of
similar events.[49] The total number of runs in an ensemble can be used
as a test of the randomness of the ensemble. If the ensemble can be
naturally separated into two distinct classes, then these two classes
could be chosen as the set of similar events. For instance, if it were
desired to determine if the toss of a coin were "fair," then the coin
could be tossed a number of times and the result of the toss recorded.
The total number of unbroken sequences of heads and tails could be
determined. Either too many or too few runs would indicate that the
coin toss was not random. In this case the observations consist of
only two different classes, "heads" and "tails," and these two classes
form a natural set of similar events.

1.0

1.1

1.25   1.4   1.6

2 5

2 2

2 0

1.8
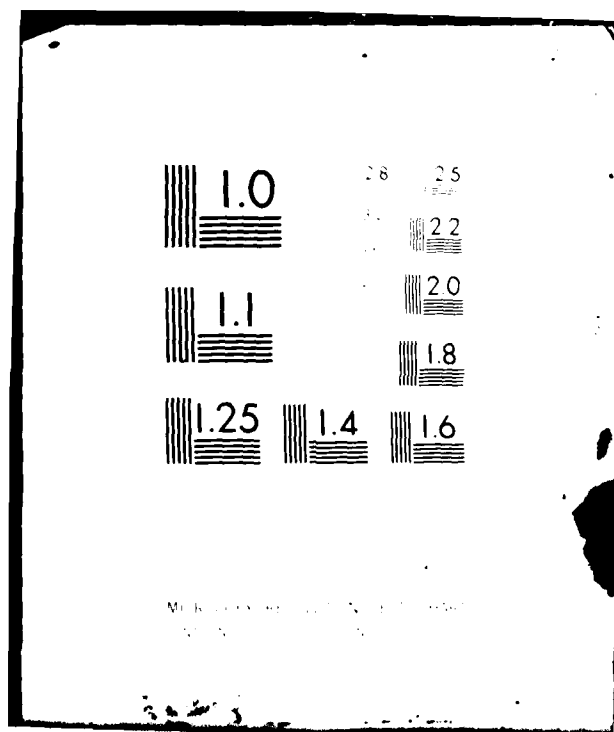
In the present study, the reverberation samples cannot be so easily divided into two distinct classes since the samples are continuously valued and thus take on a range of values. One possibility is to test the sign of the difference between the samples and the sample mean.[41] However, if the distribution of the samples is symmetric about the mean, which is very likely the case for reverberation, then this test will be insensitive to any changes in the variance of the distribution which might have occurred during the collection of the sample ensemble.[39] That is, the sample ensemble may not be random due to a lack of homogeneity, but the test will fail to detect it. A test of this sort is a test only of the randomness of the signs and not a test of the randomness of the samples.

An alternative pair of events which is more suitable for an ensemble of continuously valued samples is an unbroken sequence of increasing or decreasing observations. Although the probability distribution associated with the total number of runs of this type is different from the probability distribution associated with the previously described runs, it can still be calculated. The total number of runs r in a sample ensemble of size n is asymptotically normally distributed with mean and variance given by:[40]

$$\mu = \frac{2n-1}{3}$$

$$\sigma^2 = \frac{16n-29}{90} \quad .$$

Thus the statistic r is transformed to a normal deviate

$$\frac{r-\mu}{\sigma}$$

and is referenced to the normal distribution function. Since the exact distribution of r is discrete and the normal approximation is continuous, a continuity correction is applied by reducing the absolute value of $r-\mu$ by $\frac{1}{2}$. The test statistic is then:

$$Z = \frac{sgn(r-\mu) \cdot [\,|r-\mu|-.5\,]}{\sigma}$$

where $sgn(\cdot)$ is the sign function.

To guard against nonrandomness due to either too few runs (Z significantly less than zero) or too many runs (Z significantly greater than zero), the absolute value of Z is used as the test statistic. The test is then referred to as a two-tailed test. The distribution of $|Z|$ under the null hypothesis can be easily determined from the distribution of Z, and the significance level of $|Z|$ can be calculated from the significance level of Z.[42] Denoting the distribution function of Z by $F_Z(z)$ and the distribution function of $|Z|$ by $F_{|Z|}(z)$, then since Z has a symmetric density function about zero,

$$F_{|Z|}(z) = 2F_Z(z) - 1 \quad , \quad z \geq 0 \quad .$$

Since

$$\alpha = P(H_1|H_0) = P(|Z|>z) = 1 - F_{|Z|}(z) \quad ,$$

then

$$\alpha = 2(1-F_Z(z)) = 2P(Z>z) \quad , z \geq 0 \quad .$$

Thus the calculated value z of the test statistic $|Z|$ can be related to the normal distribution function and the resulting probability of exceeding that value can be multiplied by 2 to determine the significance level for $|Z|$.

The runs up and down test assumes that there are no tied observations. If ties do occur, only adjacent tied values could possibly affect the number of runs. In order to account for ties, the ties are handled so as to produce the minimum possible number of runs and then the maximum possible number of runs. The probabilities associated with the minimum and maximum number of runs are computed to provide upper and lower bounds on the level of significance.

The ARE of this test was found to be zero with respect to several distribution-free and parametric tests.[40] However, even though its efficiency is low, the power will be large due to the large number of samples employed in this study. The test was chosen for use because of its simplicity and economy as compared to a more efficient test such as the Kendall rank correlation test for randomness.

The results from the runs up and down test are displayed graphically in Figs. IV-1 through IV-4. The plots show the probability of a Type I error for each of the 3200 ensembles of each channel. The percentage of probabilities below the value of 0.1 are computed for each channel and indicated on the plots. The percentages are based on all 3200 samples and not on an independent sampling of the ensembles. The two values represent probabilities associated with the minimum and maximum number of runs and can be considered as bounds on the true percentage. It can be seen from these plots that there was not significantly more than 10% of these probabilities below 0.1. It will be shown later that probabilities based on independent Bernoulli trials were not small enough to reject the random hypothesis. Thus the entire set of
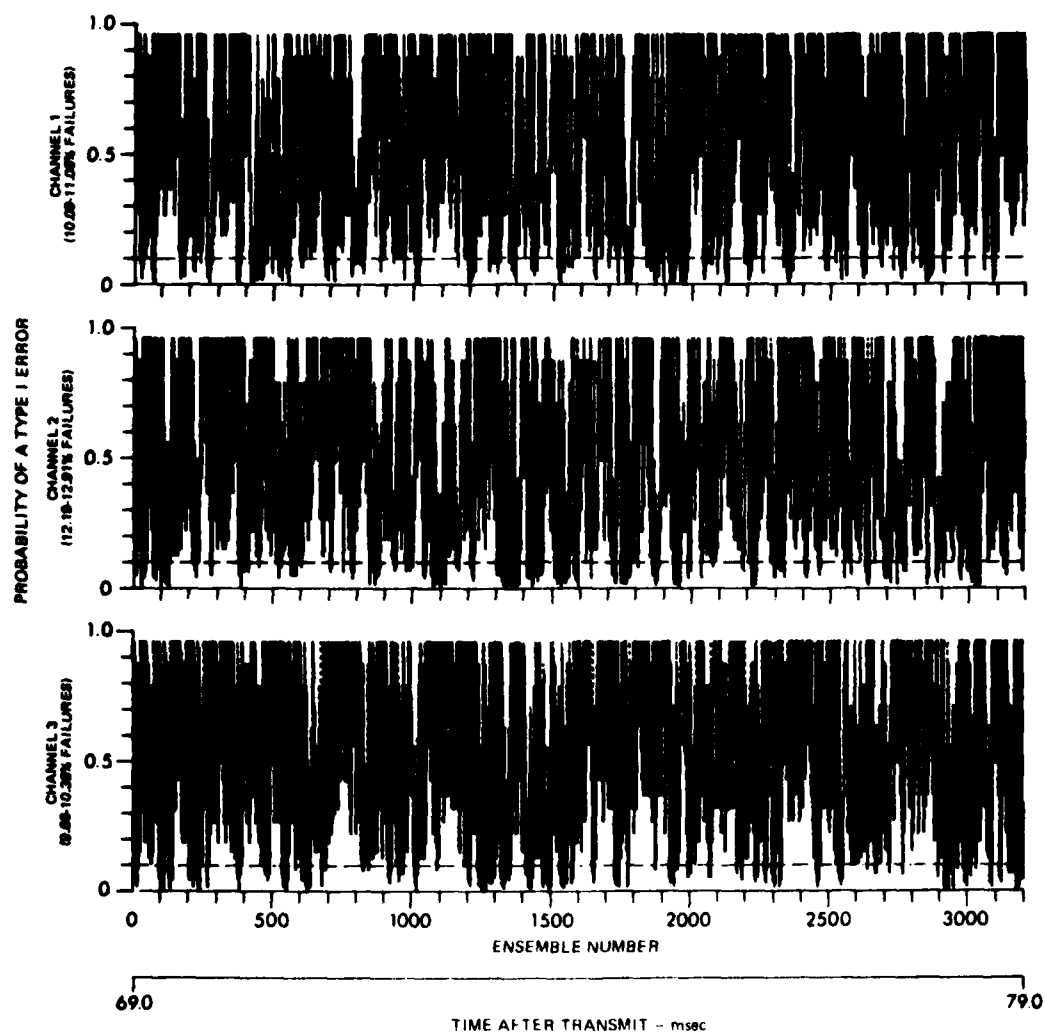
FIGURE IV-1
THE RUNS UP AND DOWN TEST FOR RANDOMNESS, CHANNELS 1-3
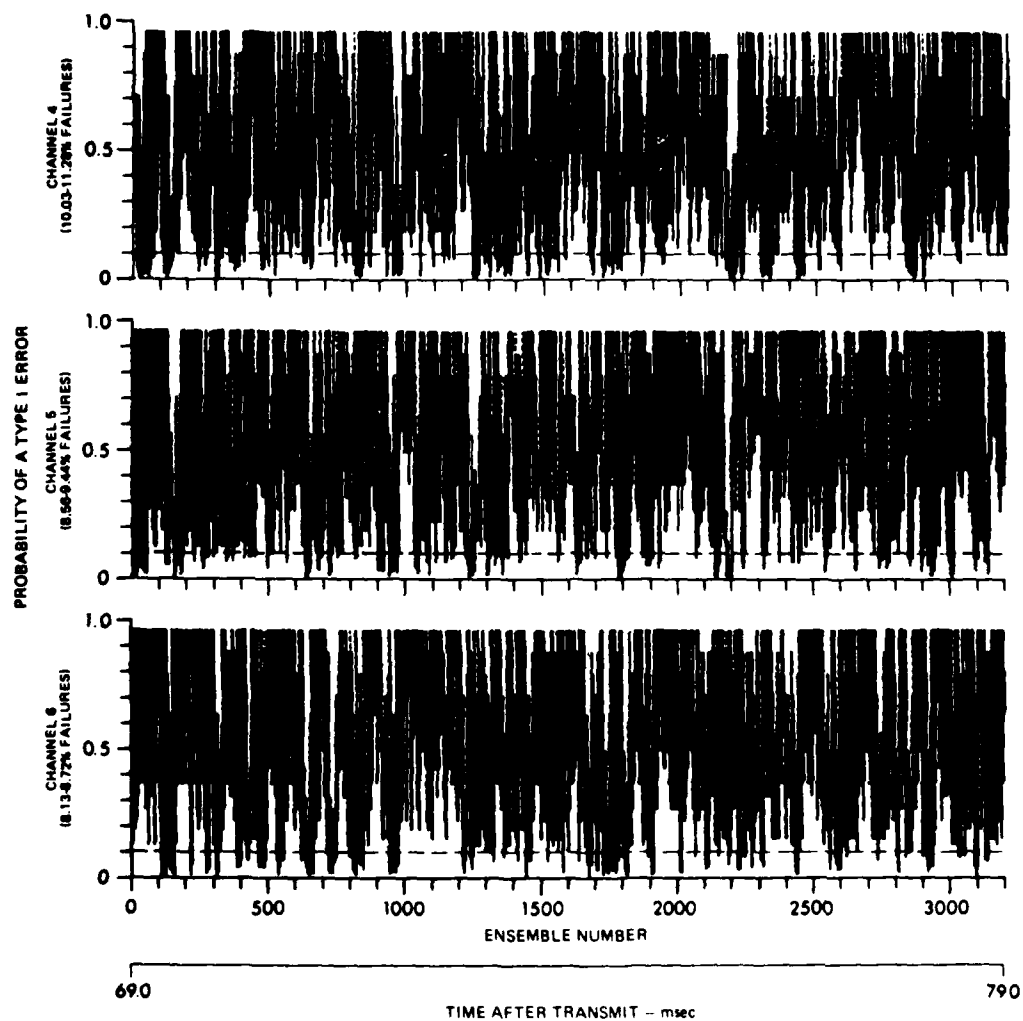
FIGURE IV-2
THE RUNS UP AND DOWN TEST FOR RANDOMNESS, CHANNELS 4-6
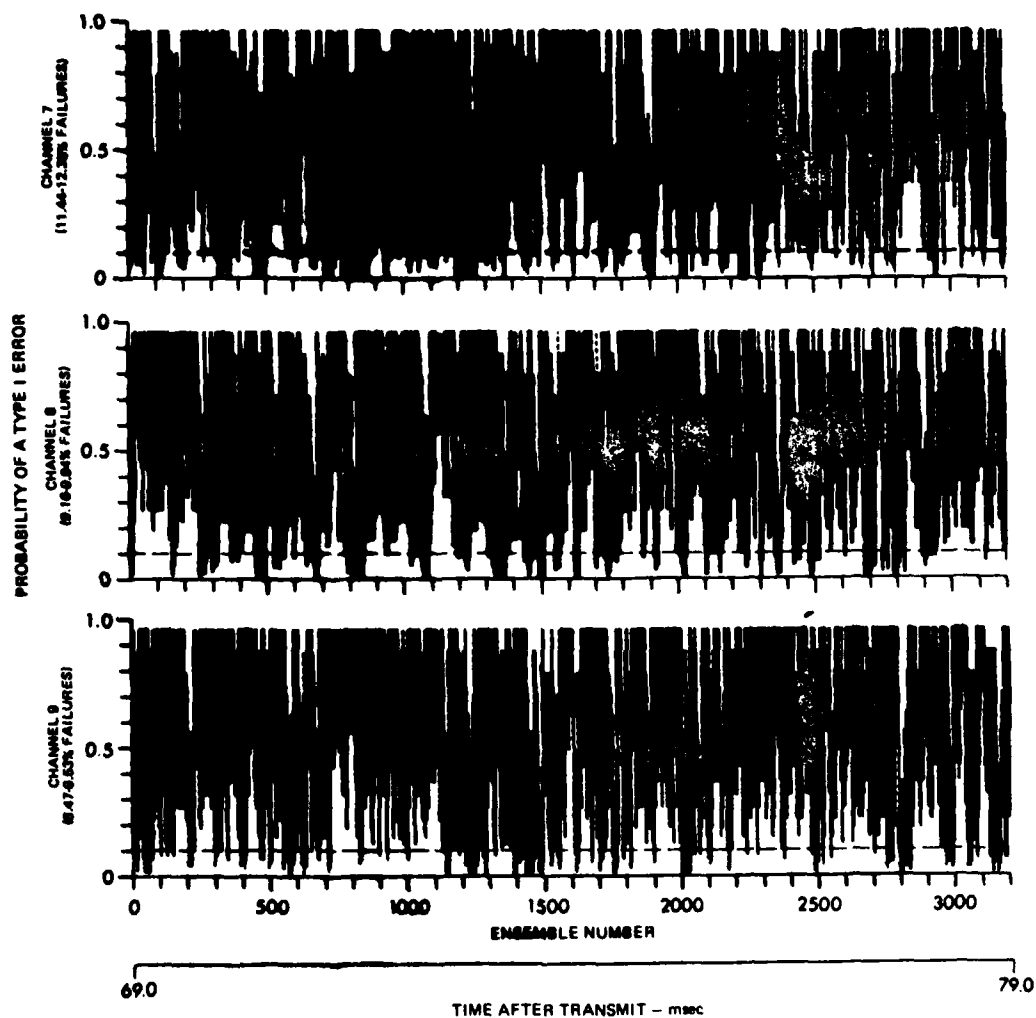
FIGURE IV-3
THE RUNS UP AND DOWN TEST FOR RANDOMNESS, CHANNELS 7-9
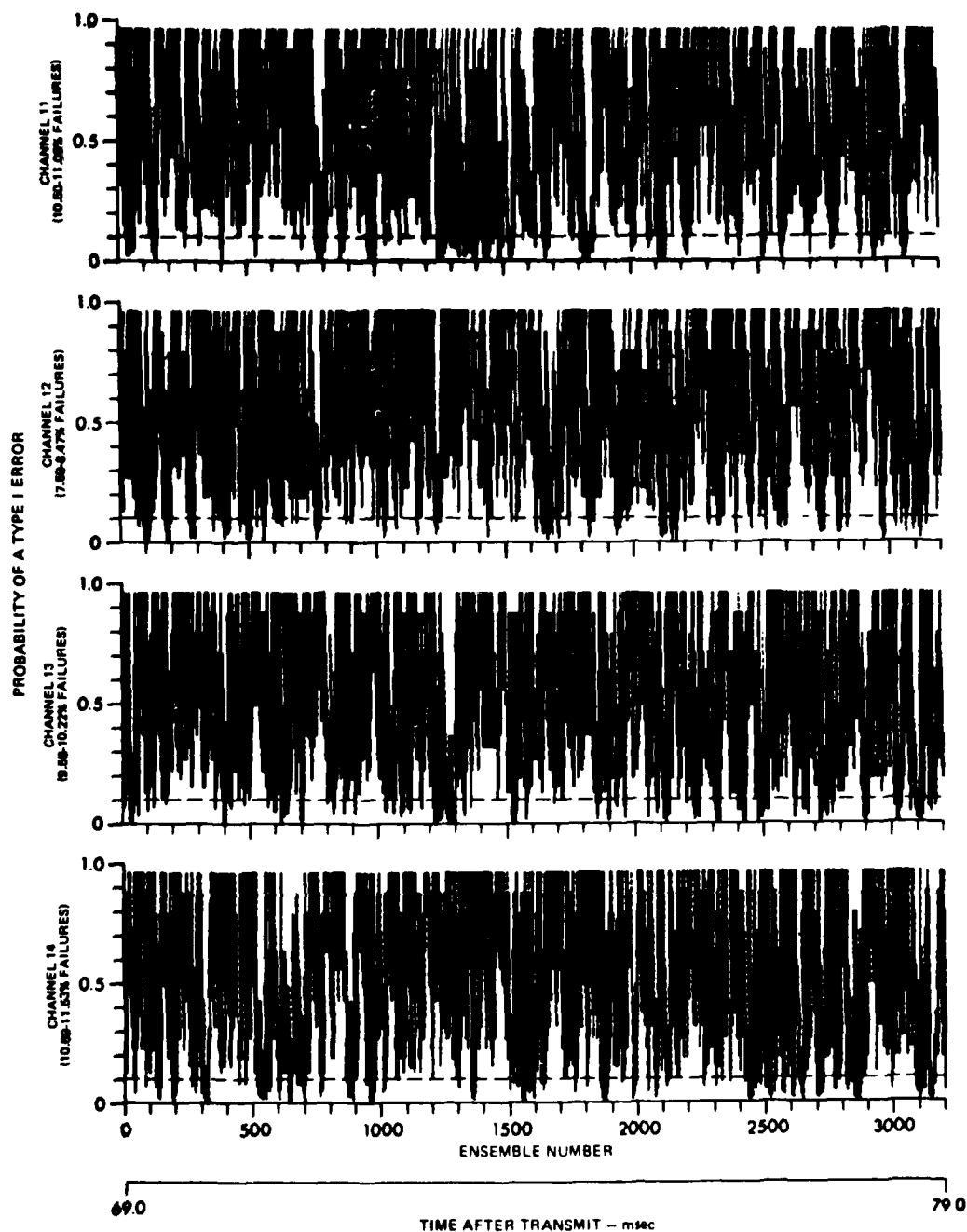
FIGURE IV-4
THE RUNS UP AND DOWN TEST FOR RANDOMNESS, CHANNELS 11-14

ensembles for all channels was accepted as random, that is, randomness

could not be reliably rejected.

The tests for randomness were performed only

on the last 500 samples from each ensemble, instead of the entire 1084

samples. The results of the next section will show that the entire

1084 samples were not homogeneous, but that the last 500 samples of

each ensemble were more nearly homogeneous. Thus all of the statistical

analysis was performed only on the last 500 samples of each ensemble.

IV.2.3 Testing for Homogeneity

The non-parametric tests for homogeneity employed in

this study divide the sample ensemble into two sub-ensembles of length

n and m and test that the two sub-ensembles are identically distributed.

Specifically, they test the null hypothesis:

H_0: each of the possible combinations of sub-ensembles, one

of length n and the other of length m, obtainable from the

total ensemble of length n + m was equally likely to have

become the one which was actually obtained;

against the alternative hypothesis:

H_1: certain combinations of sub-ensembles are more likely than

others.

For the null hypothesis to be true, the two sub-ensembles must be

identically distributed. Since the most likely source of inhomogeneity

in the reverberation data is a change in reverberation intensity

between the beginning and the end of the recording of the data (approx-

imately a 14 minute period of time) the two sub-ensembles initially

consisted of the first 500 samples and the second 500 samples of the

ensemble. Two tests for homogeneity were employed. The first one to be described is the Kolmogorov-Smirnov two-sample test. The second is the Wilcoxon rank-sum test.

IV.2.3.1 The Kolmogorov-Smirnov Two-Sample Test

The test statistic for the Kolmogorov-Smirnov two-sample (KS-2) test is the maximum absolute difference between the empirical cumulative distribution functions of the two sub-ensembles, denoted D_{mn}. Although the exact distribution of D_{mn} can be calculated,[43] for large sample sizes the Smirnov approximation is more useful.[44] If D_{mn} is transformed to the statistic Z, where

$$Z = D_{mn} \sqrt{\frac{m \cdot n}{m+n}}$$

then Z has as its limiting distribution the Smirnov distribution. With a correction for continuity, Z becomes[44]

$$Z = D_{mn} \sqrt{\frac{m \cdot n}{m+n}} + C$$

where

$$C = \frac{2}{3\sqrt{n}} \quad \text{for } n = km, \ k = 1,2,3.....$$
$$= \frac{2}{5\sqrt{n}} \quad \text{for } n \neq km \quad .$$

The Smirnov distribution $F(z)$ was approximated as

$$
F(z) = \begin{cases}
0 & , \quad -\infty < z < .22 \\
\frac{\sqrt{2\pi}}{z} \exp\left(\frac{-\pi^2}{8z^2}\right) & , \quad .22 \leq z \leq .80 \\
1 - 2[\exp(-2z^2) - \exp(-8z^2) + \exp(-18z^2)] & , \quad .80 < z \leq 3.15 \\
1 & , \quad z > 3.15 \quad .
\end{cases}
$$

The probability of a Type I error is

$$\alpha = 1 - F(z) \quad .$$

The probability of a Type I error is plotted in Figure IV-5 for all 3200 ensembles of channel 11 using the first 1000 samples of each ensemble. Slightly over 30% of the ensembles had a probability of Type I error under 0.1, indicating a lack of homogeneity between the first 500 and second 500 samples of these ensembles. Figure IV-6 gives a strong indication of the source of the inhomogeneity. 100-sample estimates of the variance were computed throughout each ensemble of 1084 samples and are plotted for every 32nd ensemble of the entire set of 3200 ensembles from channel 11. Since the variance is proportional to the intensity of the reverberation, this plot is indicative of the change in reverberation intensity during the approximately 14 minutes necessary to record the 1084 reverberation returns and the 10 ms during which the returns were digitized. It is obvious that the reverberation intensity was significantly lower during the first part of the data recording period, after which it increased to a maximum, then decreased somewhat and was relatively stable during the last part of the 14 minute recording period. The change of the reverberation intensity for a single ensemble is shown in Fig. IV-7 and further demonstrates the change in reverberation intensity which is characteristic of all the ensembles. Thus it was felt that this change in intensity was the cause of the lack of homogeneity in the data set. Since the intensity over the last 500 samples of each ensemble appears to be more stable, the last 500 samples should be more nearly homogeneous. For this reason it was decided to restrict all further analysis of the reverberation returns to the last 500 samples of each ensemble.
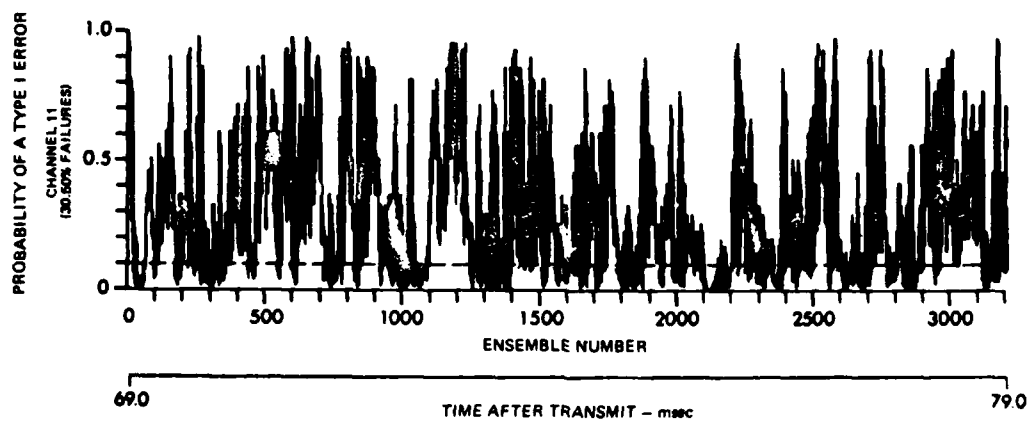
FIGURE IV-5
THE KOLMOGOROV-SMIRNOV TWO-SAMPLE TEST FOR HOMOGENEITY, CHANNEL 11
1000 SAMPLES PER ENSEMBLE
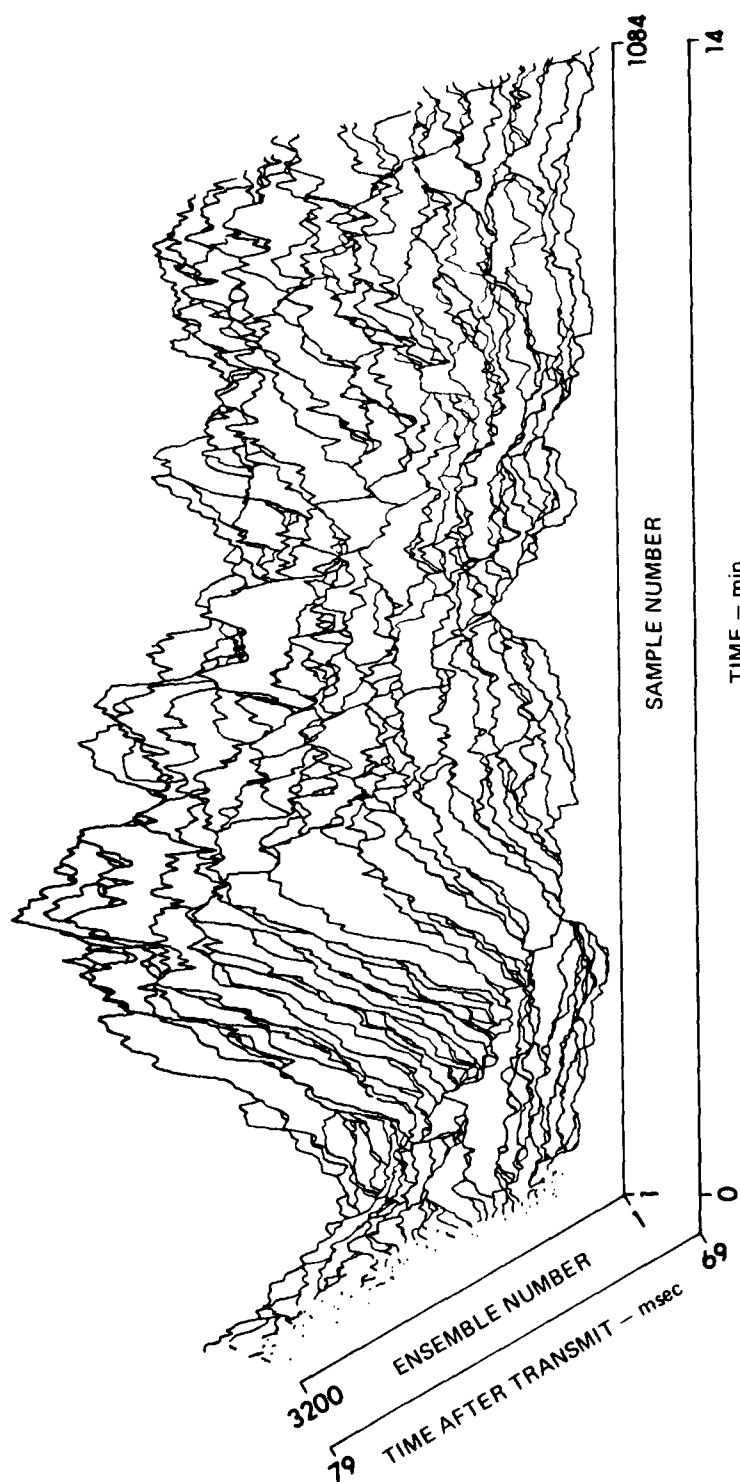
FIGURE IV-6
REVERBERATION INTENSITY, CHANNEL 11
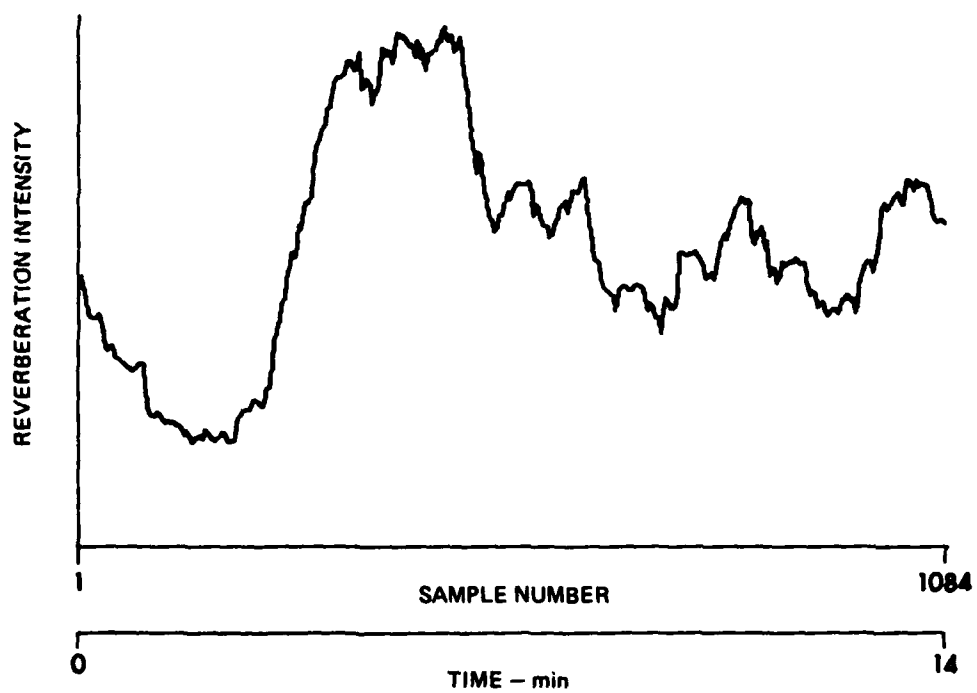
FIGURE IV-7
REVERBERATION INTENSITY, CHANNEL 11
ENSEMBLE NUMBER 601

Figures IV-8 through IV-11 display the results of the KS-2 test for all 13 channels, utilizing only the last 500 samples of each ensemble. The percentage of samples below the threshold of 0.1 varies generally between 10 and 20 percent. These percentages indicate that there is still some inhomogeneity even in the last 500 samples, but it is not as severe as in the first 1000 samples. Even though this inhomogeneity is present, it was felt that it would not be a severe limitation to the rest of the analysis.

It can be observed that physically adjacent channels in the vertical array fail the KS-2 test in approximately the same regions. For example, channels 1-3 (Fig. IV-8) all fail significantly in the region between ensembles 2200-2300. However, there are some exceptions also, like the region around ensemble 2000, where channel 3 fails but channels 1 and 2 do not. In general, this similarity in the failure regions indicates a high degree of correlation between these channels. Examination of the four horizontal channels (Fig. IV-11) shows little similarity between adjacent channels, which would indicate a lower level of correlation.

IV.2.3.2 The Wilcoxon Rank-Sum Test

The rank of a sample within an ensemble represents its relative size within the ensemble. The smallest sample has a rank of 1, the next smallest a rank of 2, and so forth. If the ensemble is divided into two sub-ensembles of length n and m ($n \leq m$), then the Wilcoxon rank-sum statistic W is the sum of the ranks of the samples from the sub-ensemble of length n among the entire n+m samples.
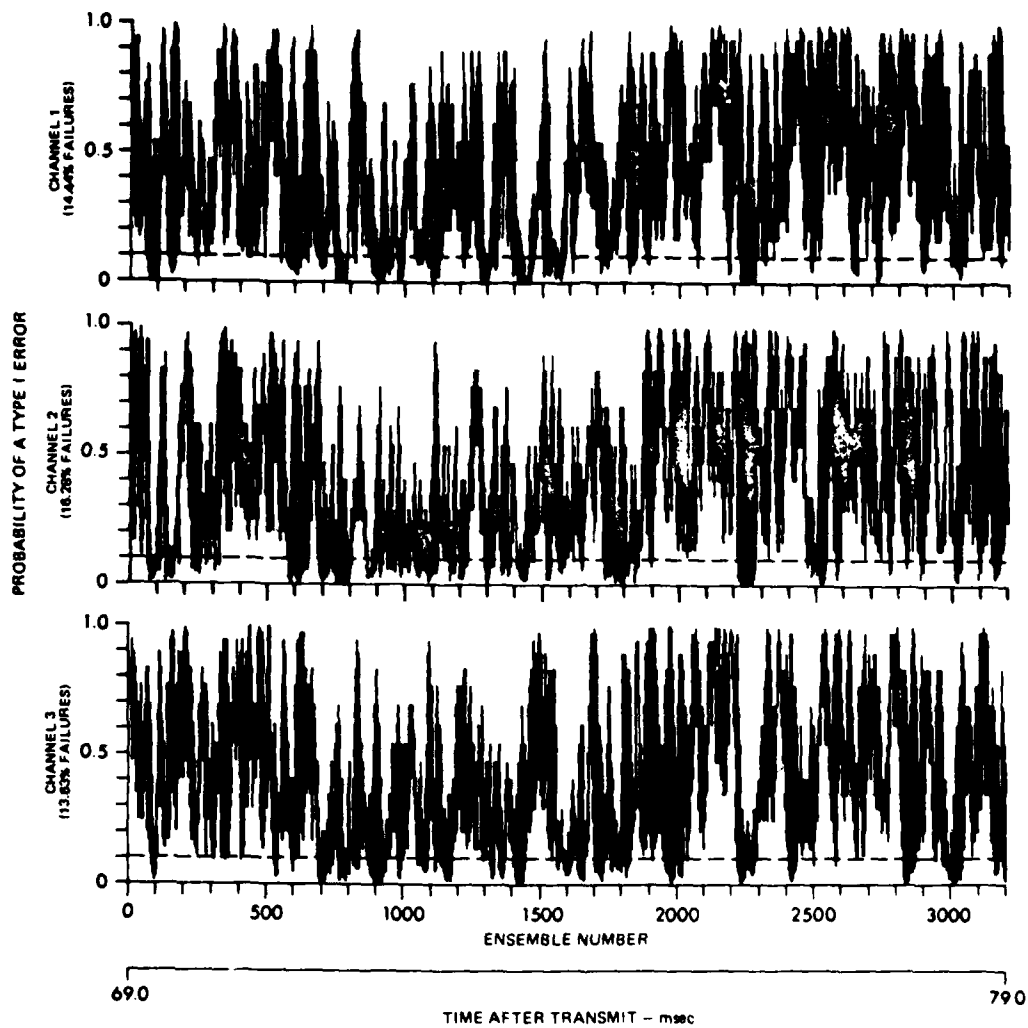
FIGURE IV-8
THE KOLMOGOROV-SMIRNOV TWO-SAMPLE TEST FOR HOMOGENEITY, CHANNELS 1-3
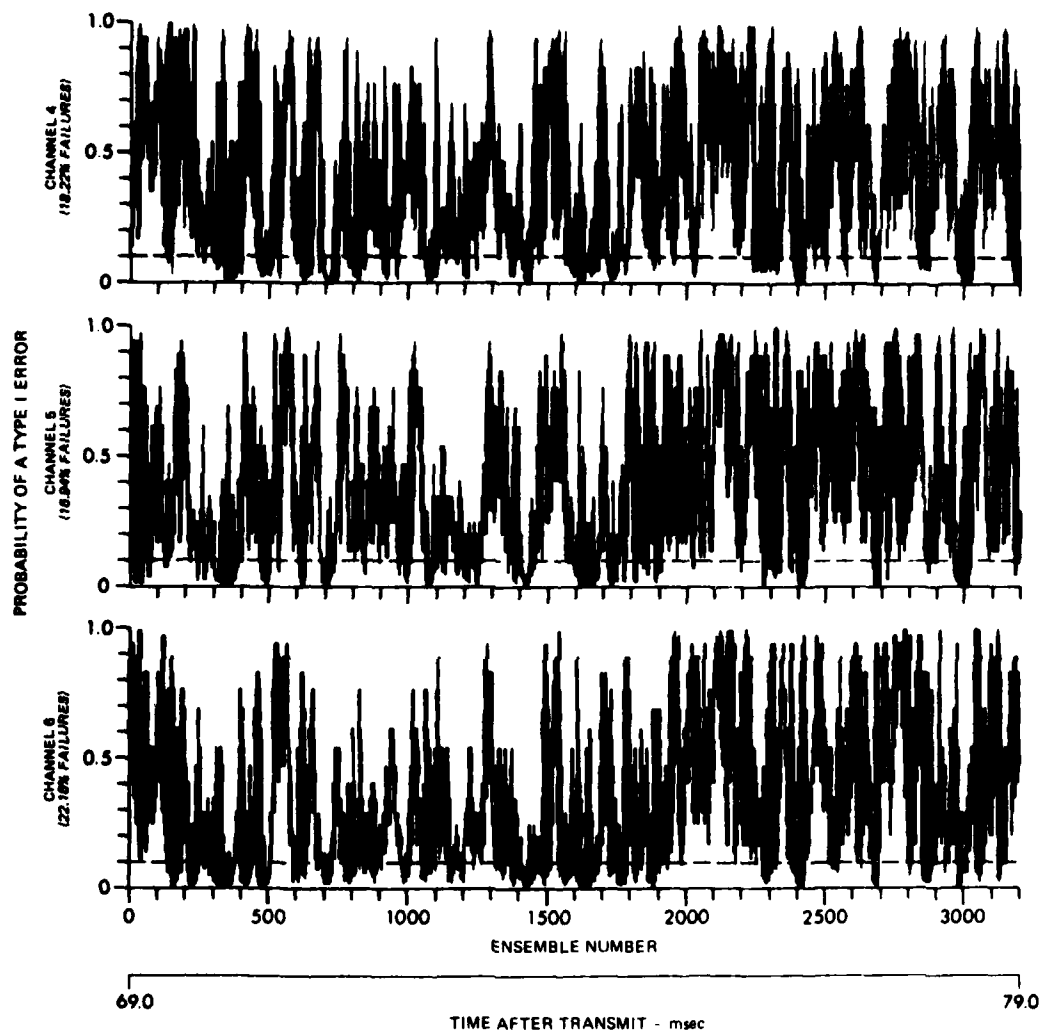
FIGURE IV-9
THE KOLMOGOROV-SMIRNOV TWO-SAMPLE TEST FOR HOMOGENEITY, CHANNELS 4-6
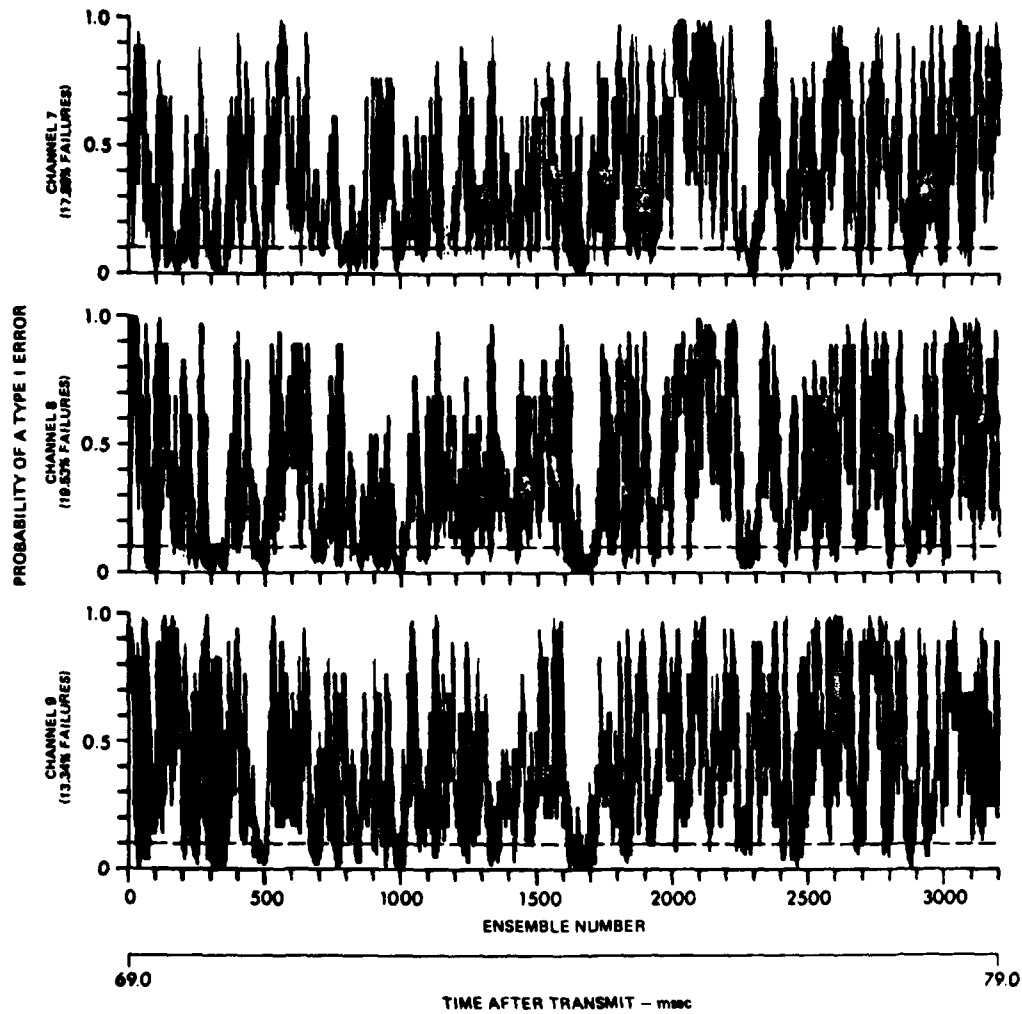
FIGURE IV-10
THE KOLMOGOROV-SMIRNOV TWO-SAMPLE TEST FOR HOMOGENEITY, CHANNELS 7-9
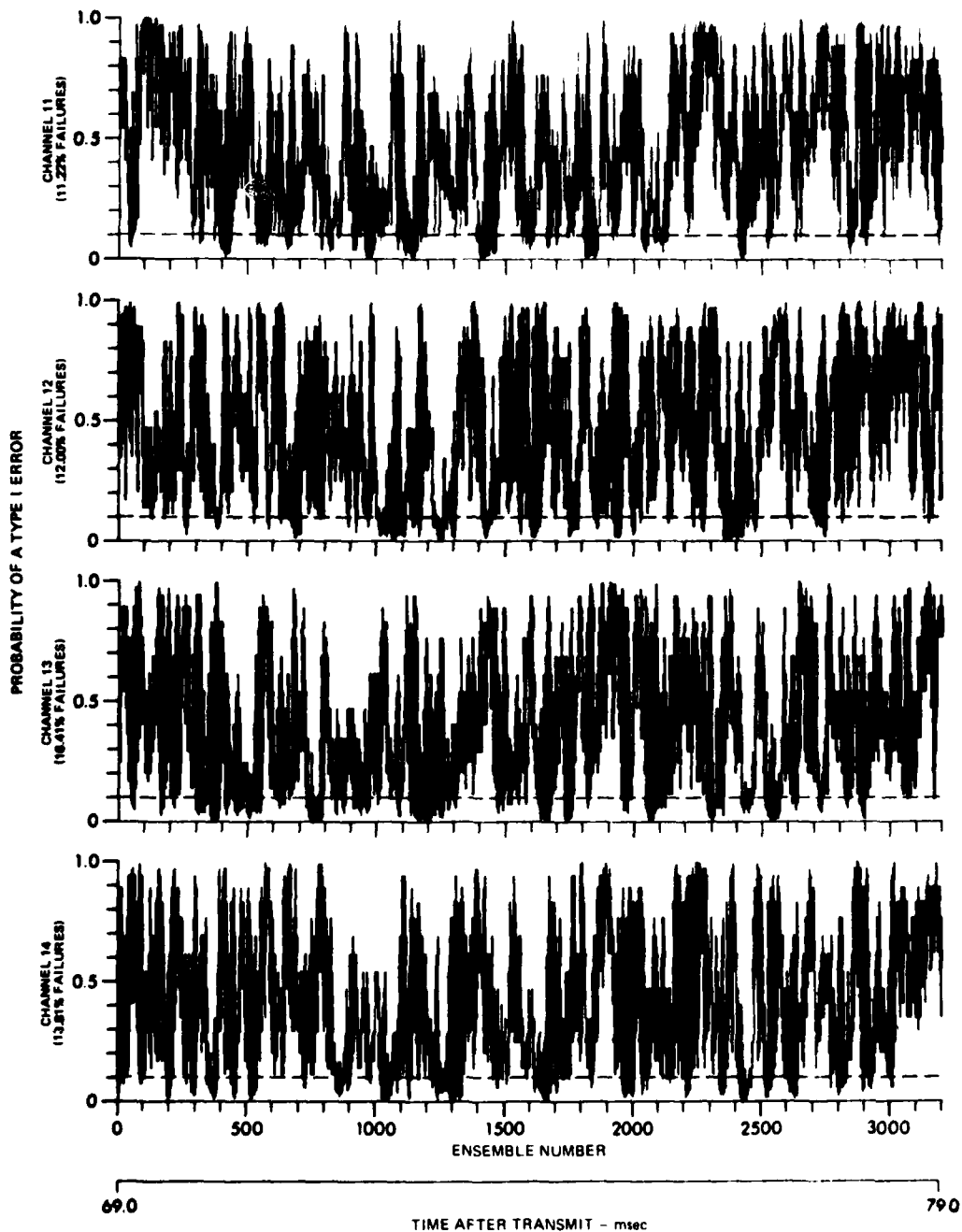
FIGURE IV·11
KOLMOGOROV-SMIRNOV TWO-SAMPLE TEST FOR HOMOGENEITY, CHANNELS 11·14

The exact null distribution of W is known and has a mean $\overline{W}$:

$$\overline{W} = \tfrac{1}{2}n(n+m+1)$$

and a variance S_w^2:

$$S_w^2 = \frac{nm(n+m+1)}{12}$$

and is symmetric about the mean.[40] The distribution is asymptotically normal so that for large sample sizes the normal approximation with continuity correction can be used, where the $N(0,1)$ deviate is

$$Z = \frac{sgn(W-\overline{W}) \cdot [|W-\overline{W}|-.5]}{S_w}$$

The two-tailed version of the test was used, so $|Z|$ was referred to the normal probability distribution. A correction for the normal approximation was also applied.[45] The calculated value z of the test statistic $|Z|$ was referenced to the normal probability distribution to determine the probability P_1 of exceeding that value. P_1 was then reduced by the factor

$$\frac{n^2+m^2+nm+n+m}{20nm(n+m+1)} \cdot g(z)$$

where $g(z) = 2\pi^{-\frac{1}{2}}(z^3-3z)\exp(-z^2/2)$.

This reduced probability was multiplied by 2 for the two-tailed level of significance.

The Wilcoxon rank-sum test assumes that there are no tied observations. To account for ties, the test statistic W is computed by handling ties so that W is as small as possible, and then as large as possible. The associated probabilities are assumed to provide a bound on the true probability.

The test is particularly sensitive to inhomogeneities due to unequal locations, but will also detect other differences. For testing for unequal locations between populations which have identical shapes and variances, the Wilcoxon test has an ARE which is no lower than .864 relative to the two-sample t test.[40] It is more powerful than the KS-2 test for detecting changes in location of normal populations. In general, the Wilcoxon test is more powerful or almost as powerful as other non-parametric tests for detecting changes in location.

The upper and lower limits of the two-tailed probability of a Type I error are plotted in Figs. IV-12 through IV-15. Although a few channels have significantly more than 10% failures (as much as about 15%), most channels have less than 10% failures. This indicates that there is not a significant inhomogeneity due to a change in location. It also indicates that the Wilcoxon test is not as sensitive as the KS-2 test to the type of inhomogeneities which are present. A comparison of the results from the Wilcoxon and KS-2 tests shows that in virtually every instance in which the Wilcoxon test failed, the KS-2 test also failed. However, the opposite was not true. Thus the Wilcoxon test did not detect inhomogeneities which were not already detected by the KS-2 test.

IV.2.4 Summary of Results of Tests for Randomness and Homogeneity

The purpose of the tests for randomness and homogeneity was to determine if the collection of ensembles for each channel could be considered to contain independent, identically distributed random variables.
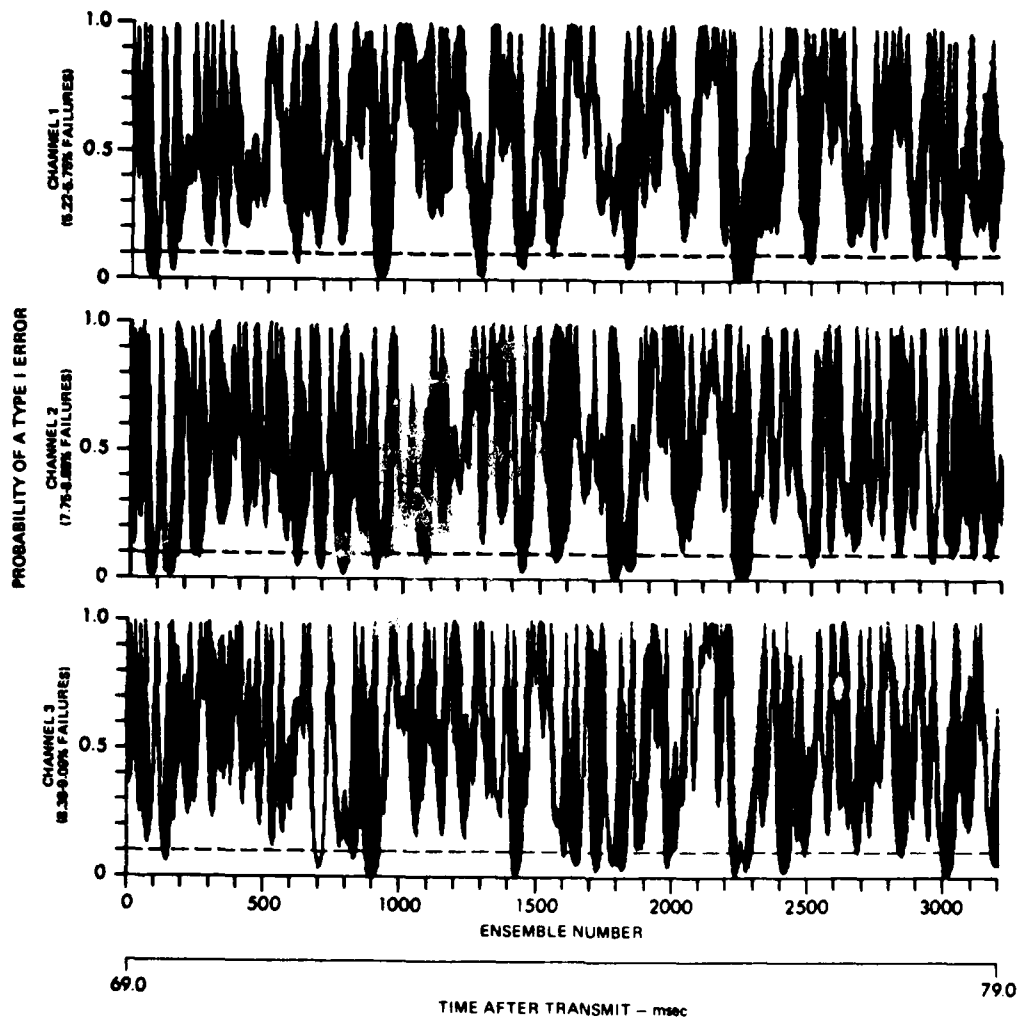
FIGURE IV-12
THE WILCOXON RANK-SUM TEST FOR HOMOGENEITY, CHANNELS 1-3
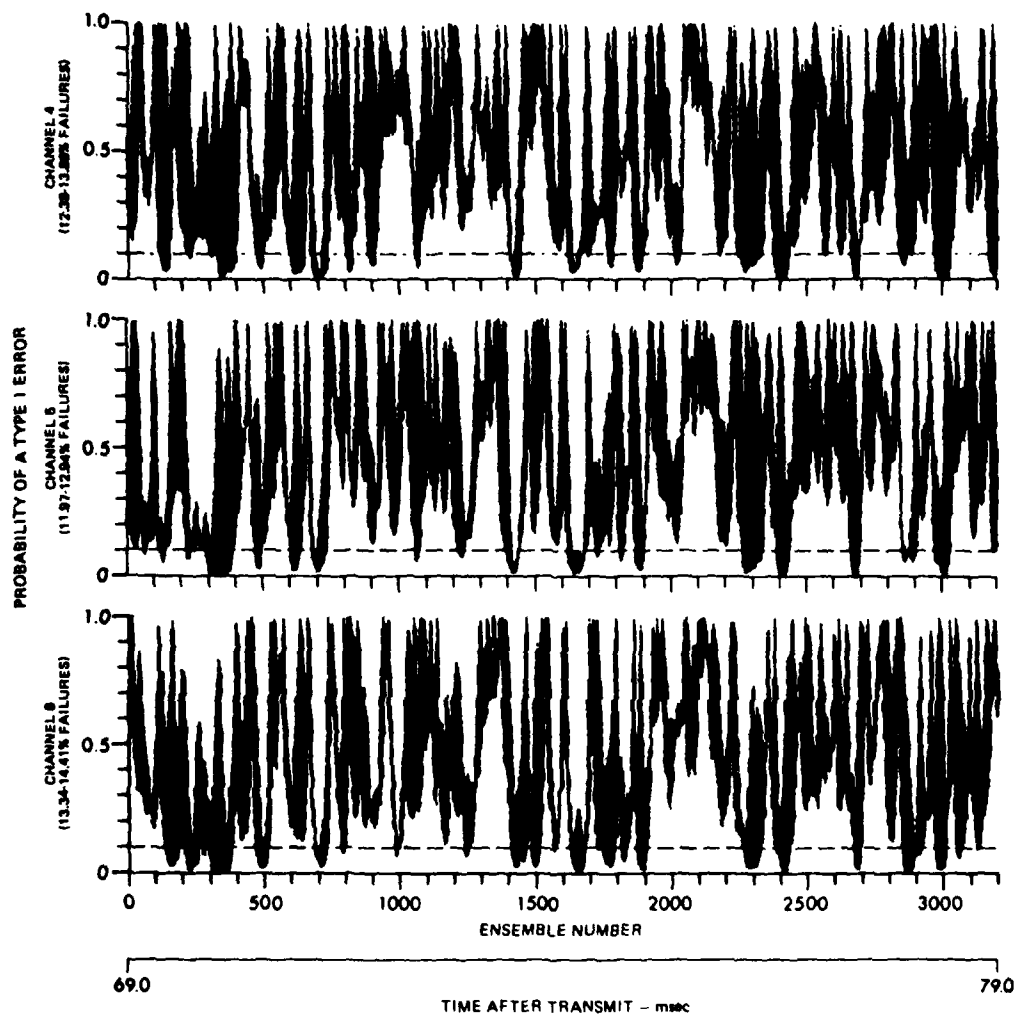
FIGURE IV-13
THE WILCOXON RANK-SUM TEST FOR HOMOGENEITY, CHANNELS 4-6

88
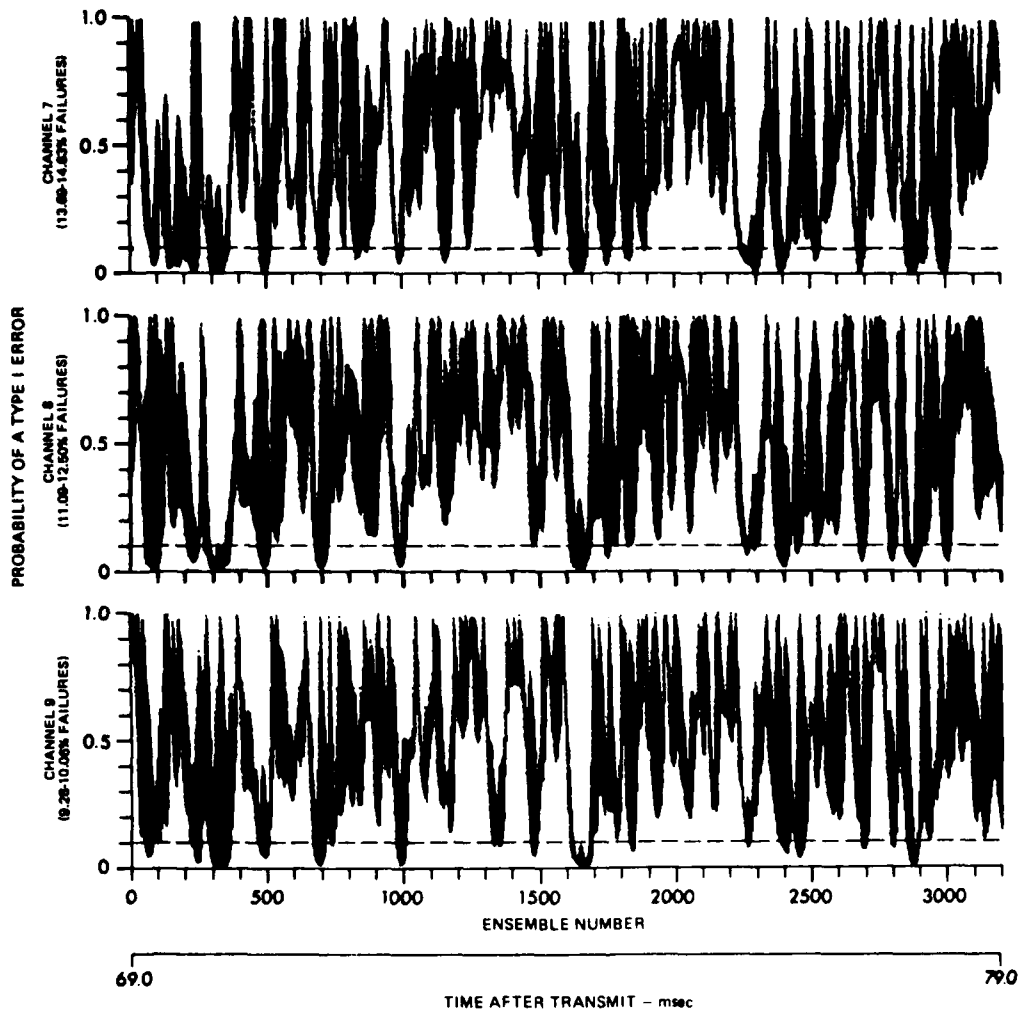
FIGURE IV-14
THE WILCOXON RANK-SUM TEST FOR HOMOGENEITY, CHANNELS 7-9
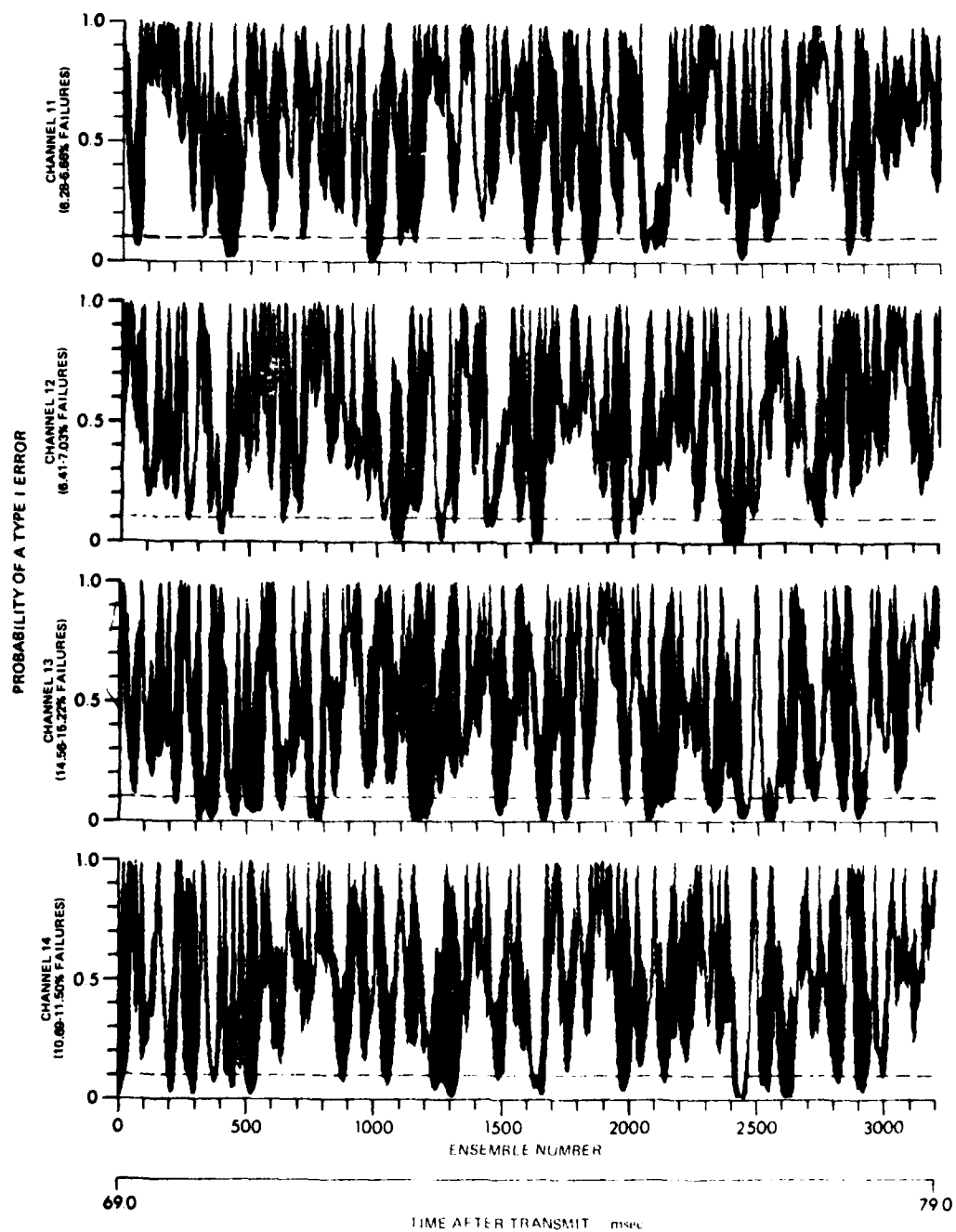
FIGURE IV-15
WILCOXON RANK-SUM TEST FOR HOMOGENEITY, CHANNELS 11-14

Three statistical tests were applied, one test for randomness and two tests for homogeneity. As was described earlier, the probability of a Type I error for every 80th ensemble was compared to the level of significance of 0.1 and the total number of probabilities below this level were tabulated for each channel. The probability that this number or more would be below the level of significance was computed for each channel and each of the three tests. The results are reproduced in Table IV.1. Although there are some probabilities below .05 or greater than .95 for one test of a particular channel, this condition did not occur for the other tests for that channel. For example, the binomial probability resulting from the runs test for channel 5 has a value of .99, but the KS-2 test and Wilcoxon tests do not exhibit such extreme probabilities. Thus considering the three tests together, the assumption of a statistically valid ensemble, i.e., consisting of i.i.d. random variables, cannot be confidently rejected for this channel or any of the channels. Therefore the collection of reverberation ensembles was accepted as valid ensembles for all channels.

IV.2.5 Testing for Normality

Each ensemble of each channel was further tested for univariate normality using four different tests: Pearson's test of skewness, Pearson's test of kurtosis, D'Agostino's test, and the Kolmogorov-Smirnov one-sample test. Each one tests the null hypothesis:

H_0: the samples of the ensemble consist of random variables

drawn from a normal parent population;

TABLE IV.1

BINOMIAL PROBABILITY OF k OR MORE OUTCOMES BELOW
THE LEVEL OF SIGNIFICANCE FOR THE STATISTICAL
TESTS FOR RANDOMNESS AND HOMOGENEITY

Channel Number

Statistical Test

	Runs	KS-2	Wilcoxon
1	.58-.58	.10	.10-.10
2	.78-.78	.04	.10-.10
3	.78-.78	.21	.58-.78
4	.21-.21	.04	.78-.78
5	.99-.99	.10	.58-.78
6	.78-.92	.37	.21-.37
7	.04-.10	.10	.04-.04
8	.58-.58	.02	.04-.10
9	.21-.37	.10	.21-.21
11	.10-.10	.92	.99-.99
12	.37-.37	.78	.78-.92
13	.37-.37	.04	.21-.21
14	.10-.10	.21	.58-.58

against the alternative hypothesis:

H_1: the samples are not normal.

No a priori values were assigned to the mean and variance of the ensembles; that is, the tests for normality were not testing to determine if the ensembles were normally distributed with a particular mean and variance. Rather, the mean and variance were assumed to be the sample mean and variance computed from each ensemble. Designating the ith sample from an ensemble of size N by X_i, then the sample mean m and the sample variance s^2 are given by

$$m = \frac{1}{N} \sum_{i=1}^{N} X_i$$

$$s^2 = \frac{1}{N-1} \sum_{i=1}^{N} (X_i - m)^2 \quad .$$

IV.2.5.1 Pearson's Test of Skewness

The test statistic for Pearson's test of skewness is just the sample skew $\sqrt{b_1}$, given by

$$\sqrt{b_1} = \frac{m_3}{m_2^{3/2}}$$

where $\quad m_3 = \frac{1}{N} \sum_{i=1}^{N} (X_i - m)^3$

$$m_2 = \frac{N-1}{N} s^2 \quad .$$

The skew is asymptotically normally distributed[46] with a mean of zero and a variance of[47]

$$\frac{6(N-2)}{(N+1)(N+3)} \quad .$$

Thus for large sample sizes, the sample skew can be transformed to .e

N(0,1) deviate

$$Z = \frac{\sqrt{b_1}}{\sqrt{\frac{6(N-2)}{(N+1)(N+3)}}}$$

and Z can be referenced to the normal distribution function to determine the probability of a Type I error. For a two-tailed test, the test statistic is $|Z|$ and the resulting probability is multipled by 2, as usual. An empirical study of this and other tests for normality over a wide class of alternative distributions has shown that it is one of the more powerful tests for normality when used in conjunction with Pearson's test of kurtosis, described in the next section.[48]

Results from this test are displayed in Figs. IV-16 through IV-19. The percentage of failures for each channel ranged from approximately 17% to 29%, indi iting some departure from normality. There does not appear to be any correlation between the failure regions of the skewness test and the failure regions of the KS-2 test, which is some small indication that the level of inhomogeneity present in the data was not sufficient to upset the skewness test.

IV.2.5.2 Pearson's Test of Kurtosis

The test statistic for this test is just the sample kurtosis b_2, given by

$$b_2 = \frac{m_4}{m_2^2}$$

where $\quad m_4 = \frac{1}{N} \sum_{i=1}^{N} (X_i - m)^4$.

The distribution of the kurtosis only very slowly approaches the normal
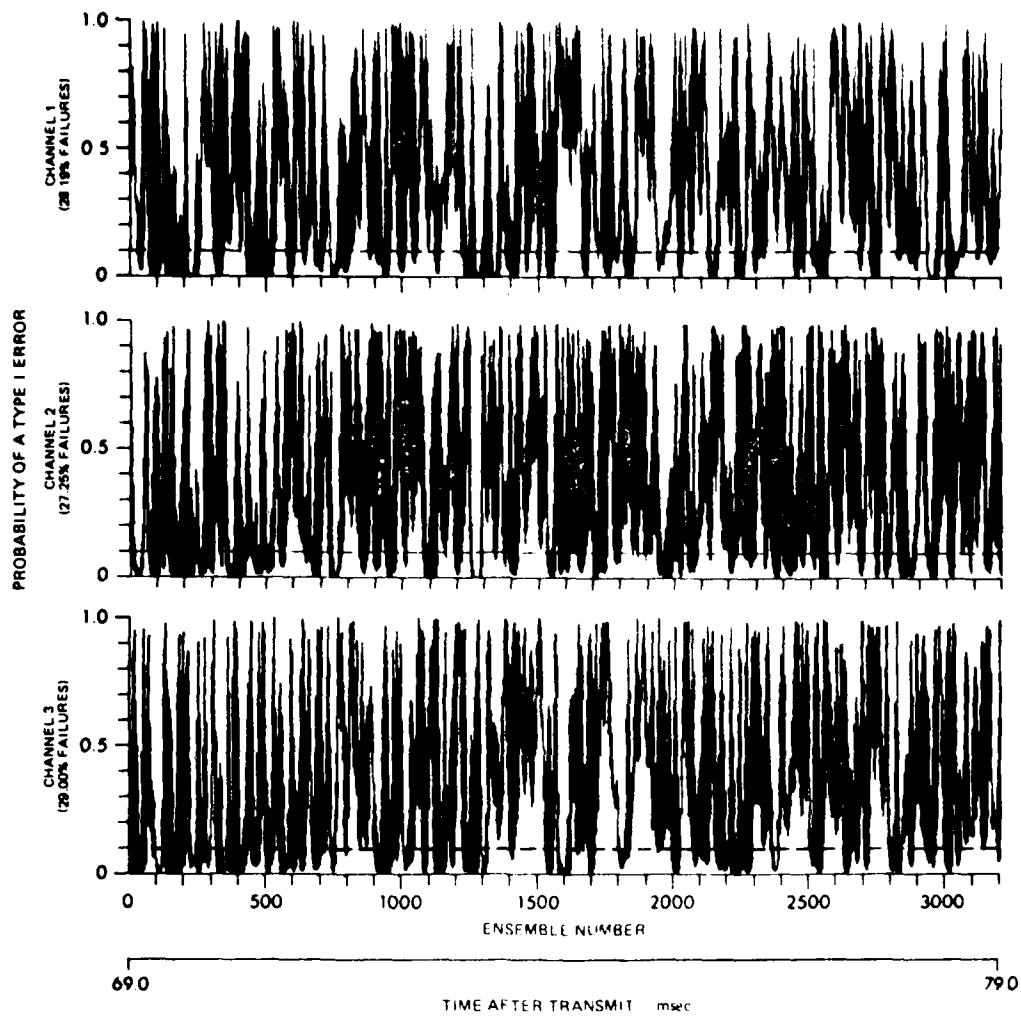
FIGURE IV-16
PEARSON'S TEST OF SKEWNESS FOR NORMALITY, CHANNELS 1-3
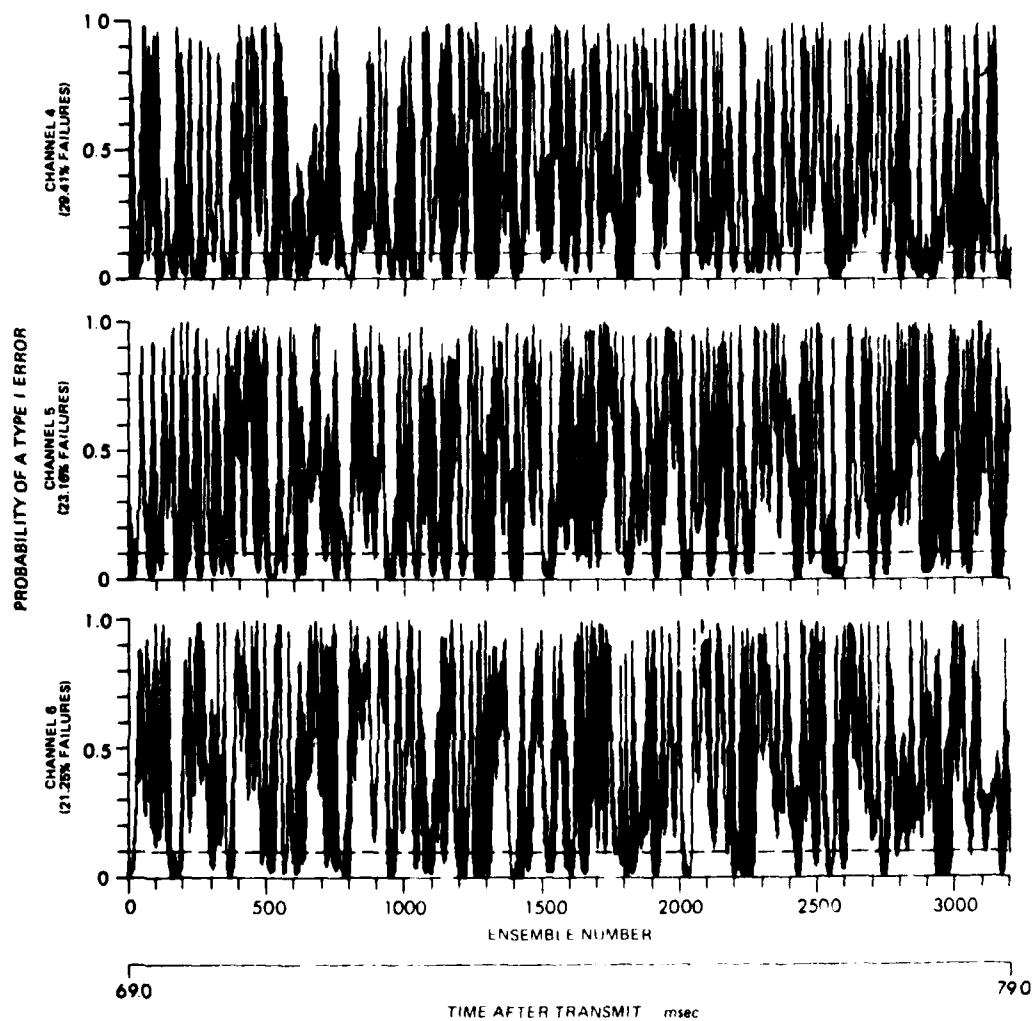
FIGURE IV-17
PEARSON'S TEST OF SKEWNESS FOR NORMALITY, CHANNELS 4 6
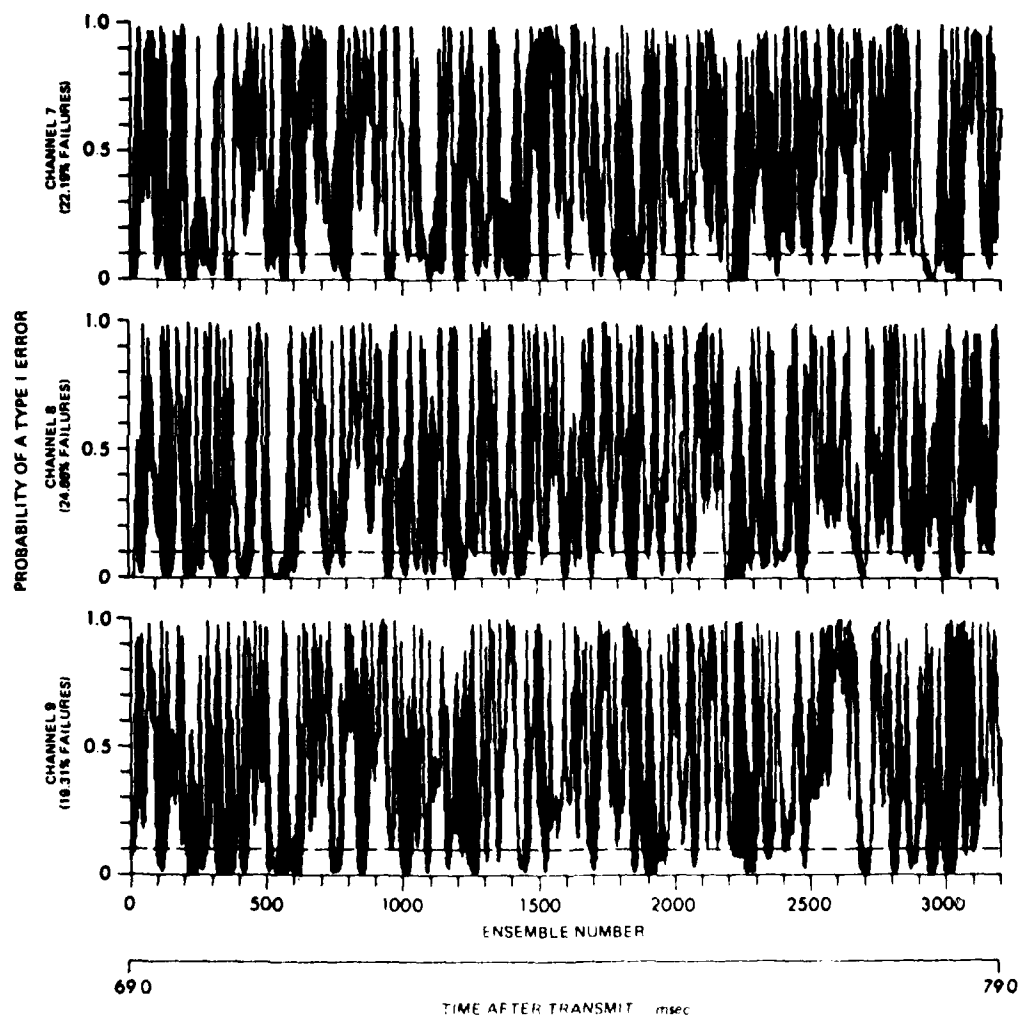
FIGURE IV-18
PEARSON'S TEST OF SKEWNESS FOR NORMALITY, CHANNELS 7-9
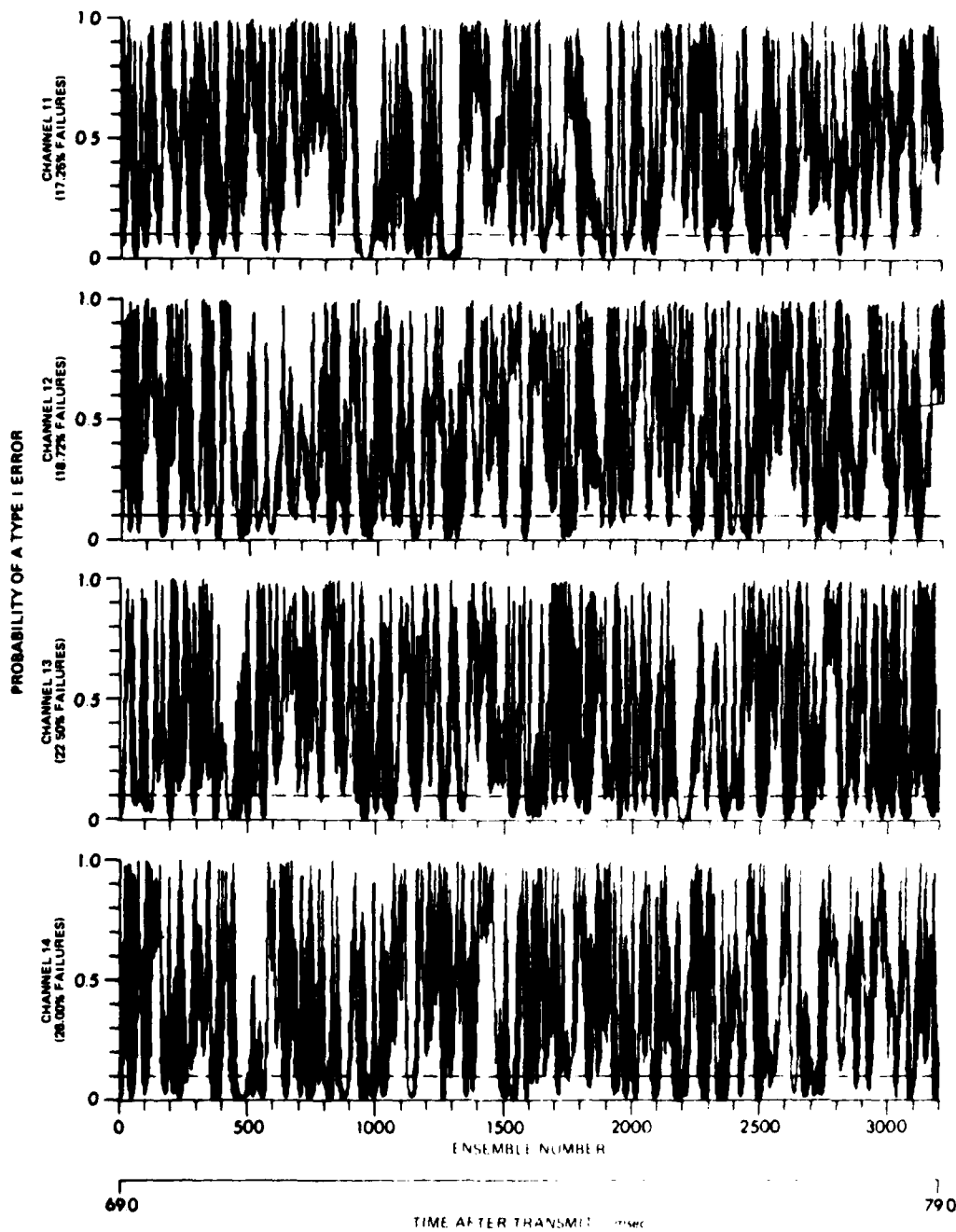
FIGURE IV-19

PEARSON'S TEST OF SKEWNESS FOR NORMALITY, CHANNELS 11-14

distribution, which makes the normal distribution unsuitable as an approximate distribution. Rather, the distribution is usually approximated by the Pearson Type IV curve,[46] although other approximations have been used.[49] Because of the difficulty of calculating these distributions, the probability of a Type I error was not calculated for this statistic. Instead, Figs. IV-20 through IV-23 are plots of the statistic b_2 itself with an indication of the upper and lower bounds of b_2. Values of b_2 outside these bounds result in a two-tailed probability less than 0.1. These upper and lower bounds were derived by Pearson using the Type IV curve.[46] The percentage of points outside these bounds is indicated on each plot.

The percentage of failures varied from approximately 24% to almost 60%, indicating a significant deviation of the kurtosis from its value under the normal distribution. The kurtosis is generally larger than expected, which implies that the tails of the sample distribution are larger than the normal tails. These larger tails would be expected if there were a greater number of large amplitude returns. Taken together, the tests of skewness and kurtosis indicate that the reverberation returns were significantly non-normal, with most of the difference due to a larger kurtosis.

IV.2.5.3 D'Agostino's Test for Normality

The test statistic D for this test is

$$D = \frac{T}{N^2 \sqrt{m_2}}$$

where $\displaystyle T = \sum_{i=1}^{N} \left(i - \frac{N+1}{2}\right) \cdot X_i$.
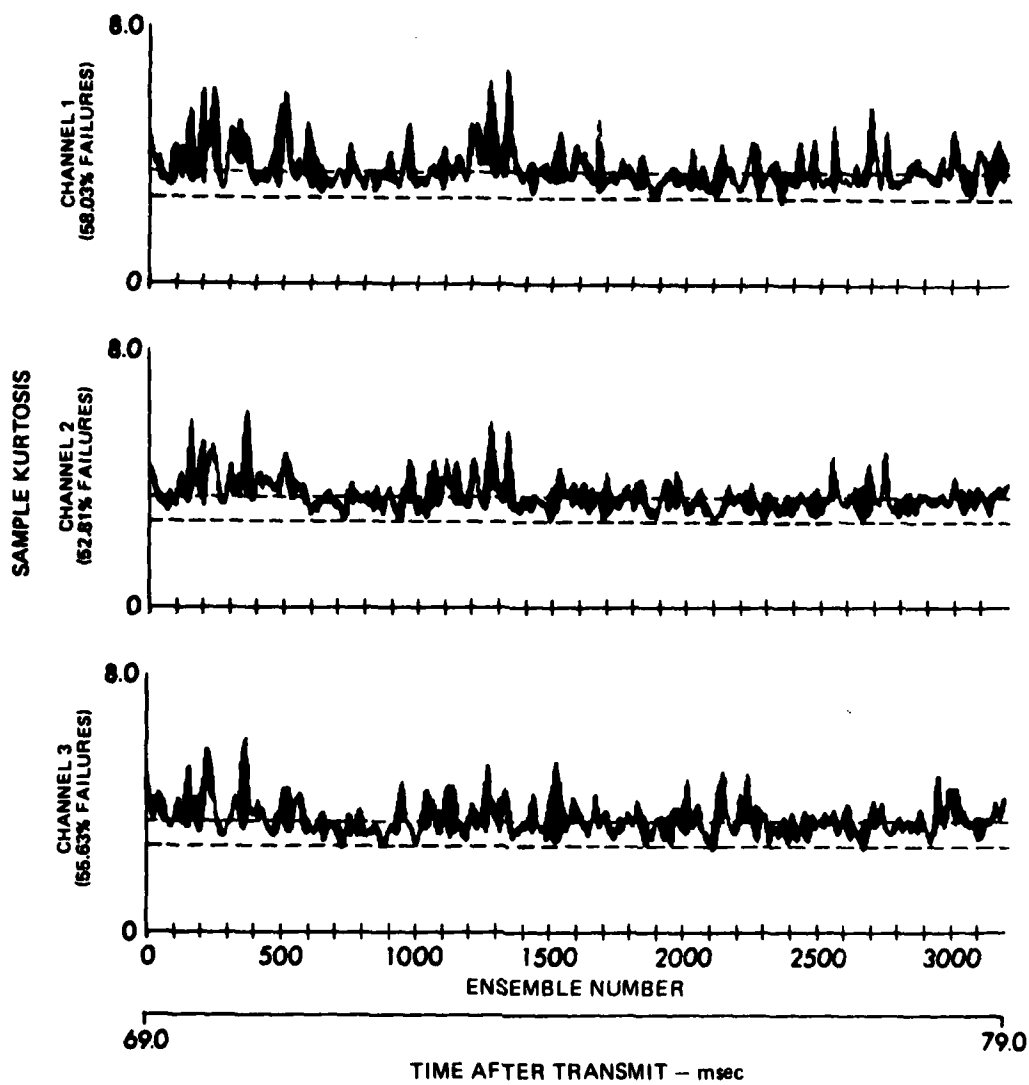
FIGURE IV-20
PEARSON'S TEST OF KURTOSIS FOR NORMALITY, CHANNELS 1-3
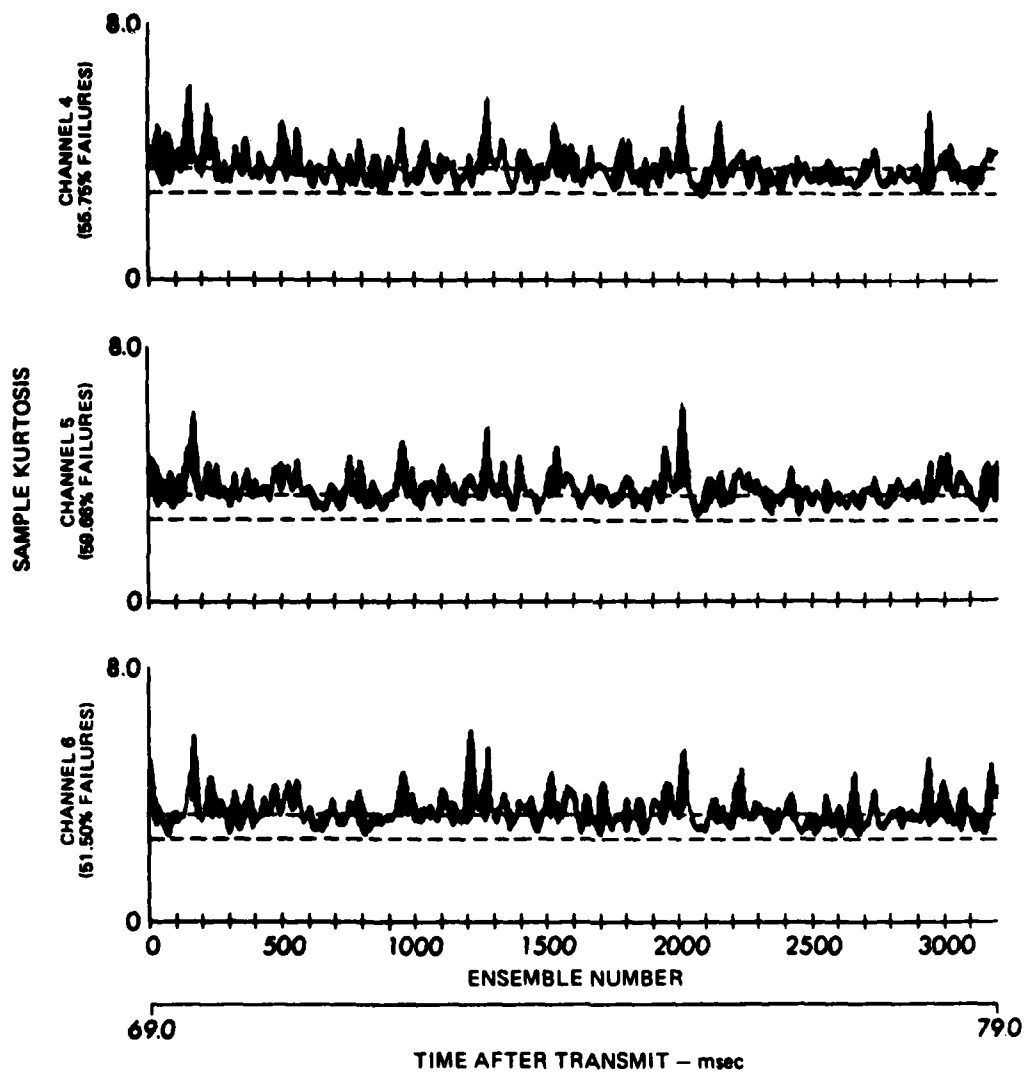
FIGURE IV-21
PEARSON'S TEST OF KURTOSIS FOR NORMALITY, CHANNELS 4-6
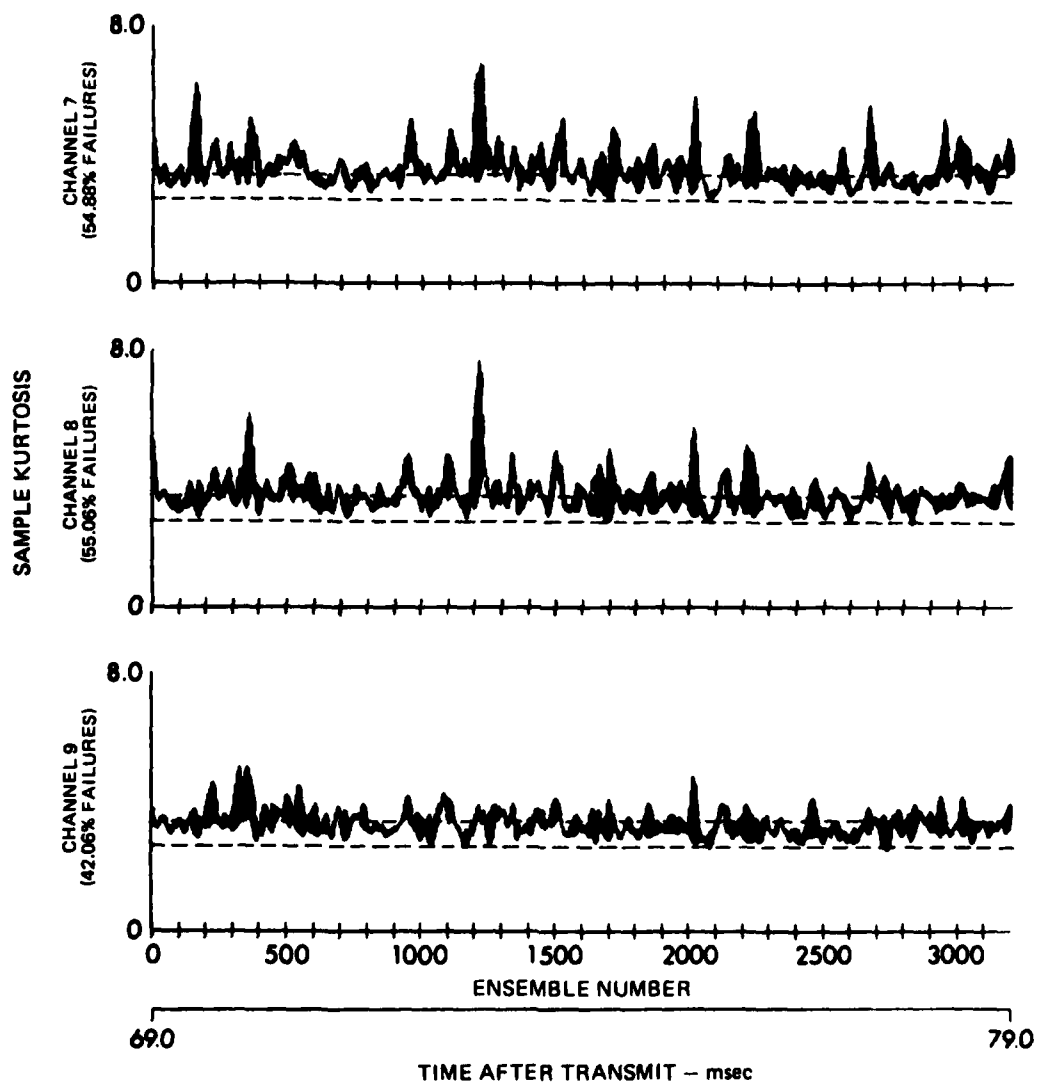
FIGURE IV-22
PEARSON'S TEST OF KURTOSIS FOR NORMALITY, CHANNELS 7-9
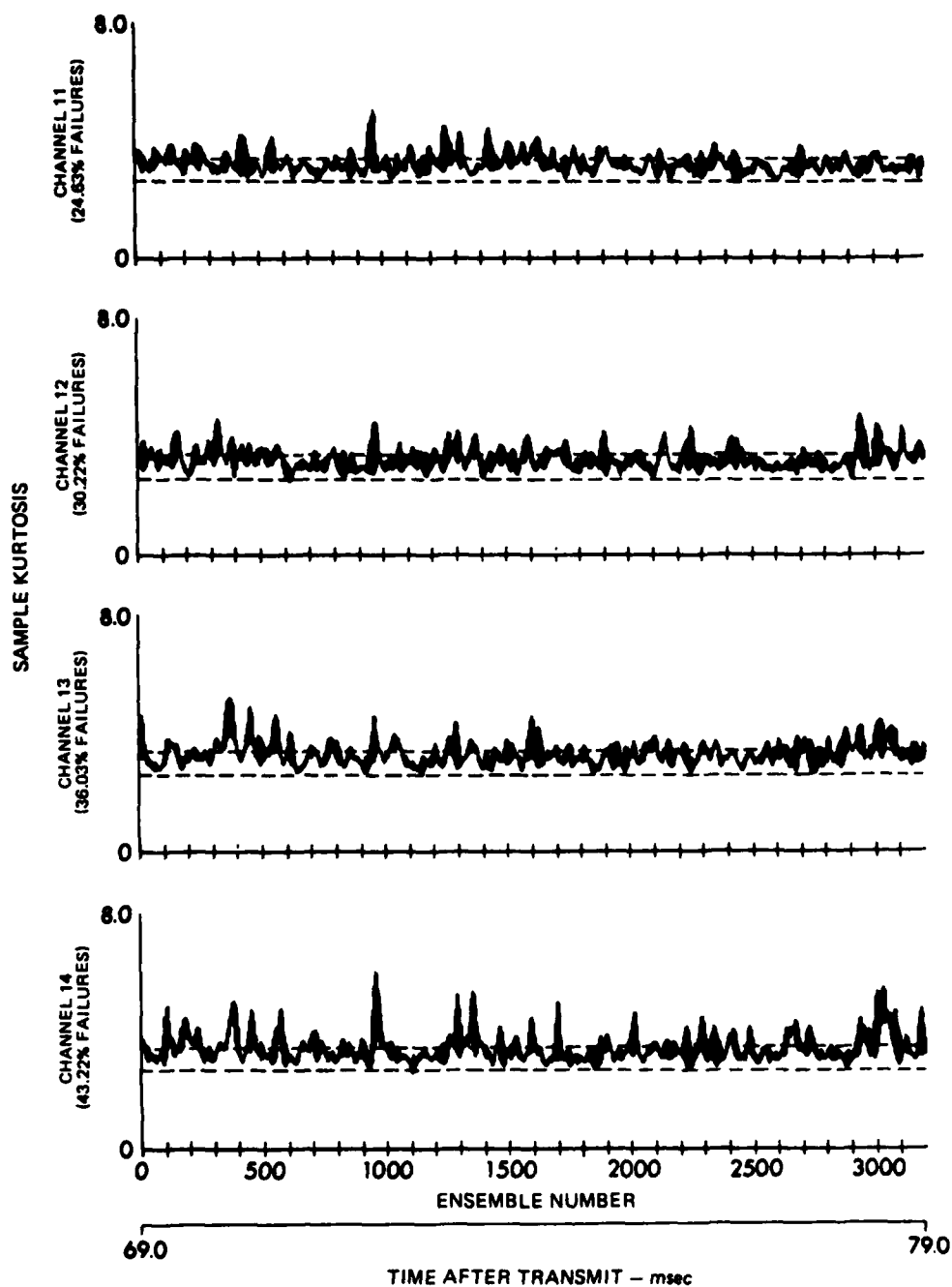
FIGURE IV-23
PEARSON'S TEST OF KURTOSIS FOR NORMALITY, CHANNELS 11-14

ARL:UT
AS-80-1708
GRW - GA
11 - 7 - 80

The expected value of D and its asymptotic standard deviation are approximately given by

$$E(D) \simeq \frac{1}{2\sqrt{\pi}} \left[\frac{N-1}{N} \left(1 + \frac{1}{4(N-1)} + \frac{1}{32(N-1)^2} - \frac{5}{128(N-1)^3} \right) \right]^{\frac{1}{2}}$$

and

$$\text{asd}(D) \simeq \frac{0.029986}{\sqrt{N}} .$$

Although the distribution of D is asymptotically normal, it is more accurate to transform D to a normal deviate using Cronish-Fisher expansions. The statistic is first standardized by the transformation

$$Y = \frac{D-E(D)}{\text{asd}(D)} .$$

Then a Cornish-Fisher expansion using the first four moments of D is used to transform to the N(0,1) deviate Z[51]:

$$Z = Y - [\tfrac{1}{6}\gamma_1 (Y^2-1) + \tfrac{1}{24}\gamma_2 (Y^3-3Y) - \tfrac{1}{36}\gamma_1^2 (4Y^3-7Y)]$$

where

$$\gamma_1 \simeq \frac{-8.463}{\sqrt{N}}$$

$$\gamma_2 \simeq \frac{107.9}{N} .$$

A two-tailed test is performed, so $|Z|$ is referenced to the normal distribution and the resulting probability is multiplied by 2 to determine the probability of a Type I error. An empirical power study has been performed over a wide class of alternative distributions and indicates that this test has good power over most of the distributions.[50]

The probability of a Type I error is plotted in Figs. IV-24 through IV-27 for each of the channels. A high degree of correlation can be observed between these results and the results from the kurtosis test. Both tests have approximately the same
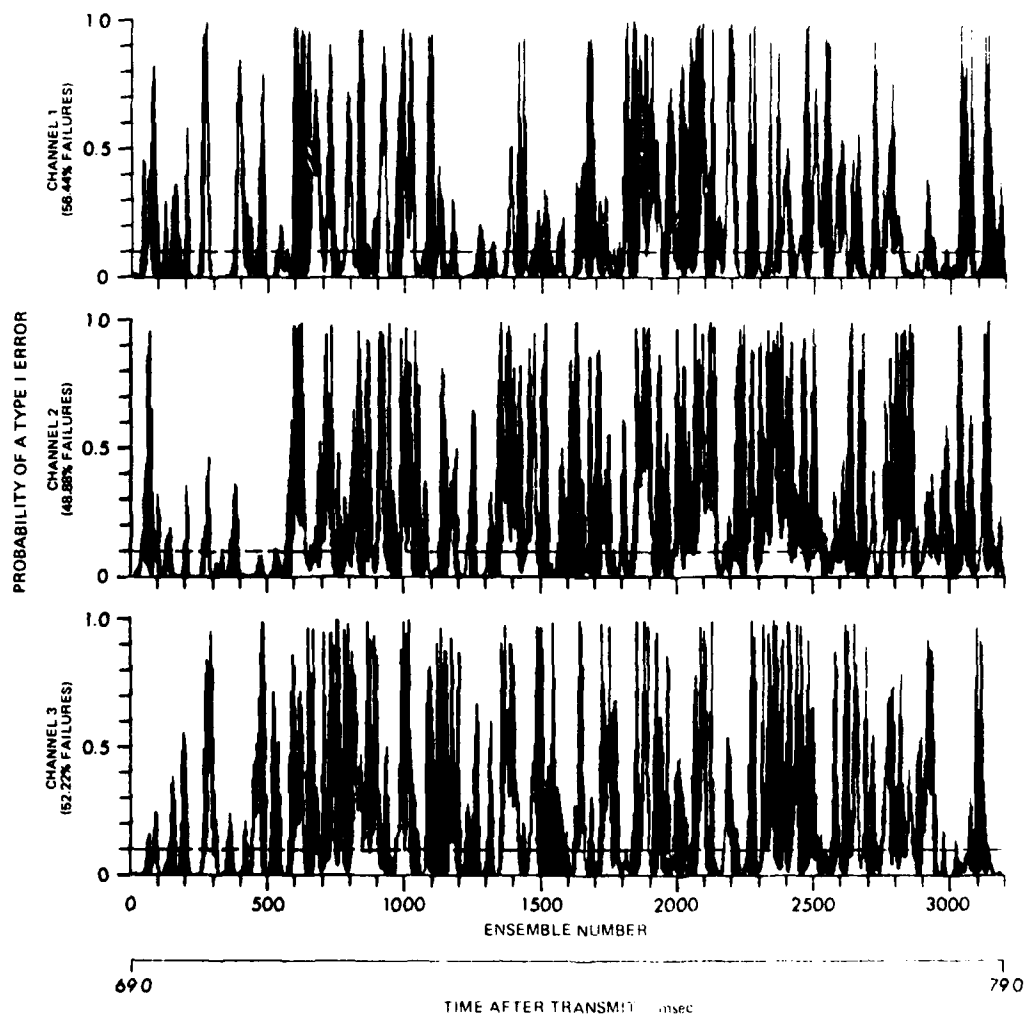
FIGURE IV-24
D'AGOSTINO'S TEST FOR NORMALITY, CHANNELS 1-3
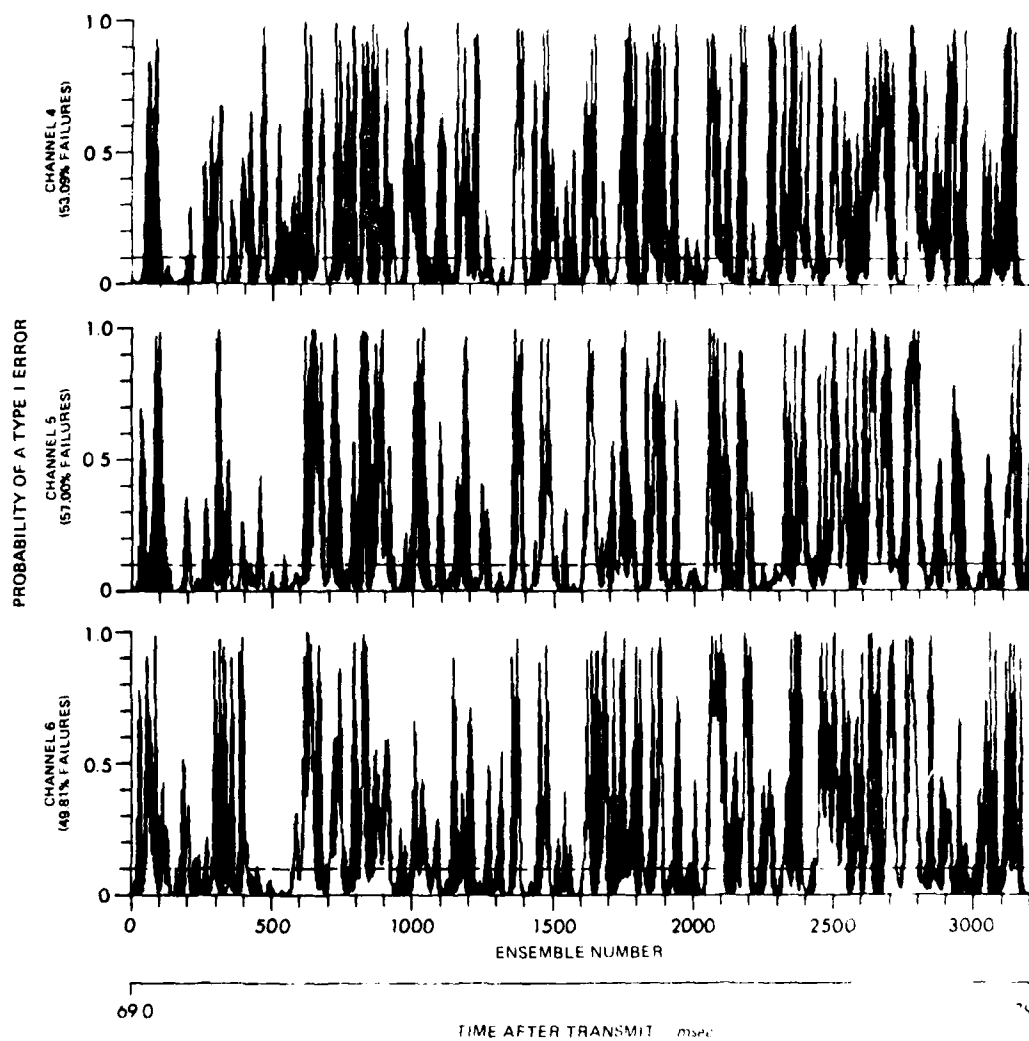
FIGURE IV-25
D'AGOSTINO'S TEST FOR NORMALITY, CHANNELS 4-6
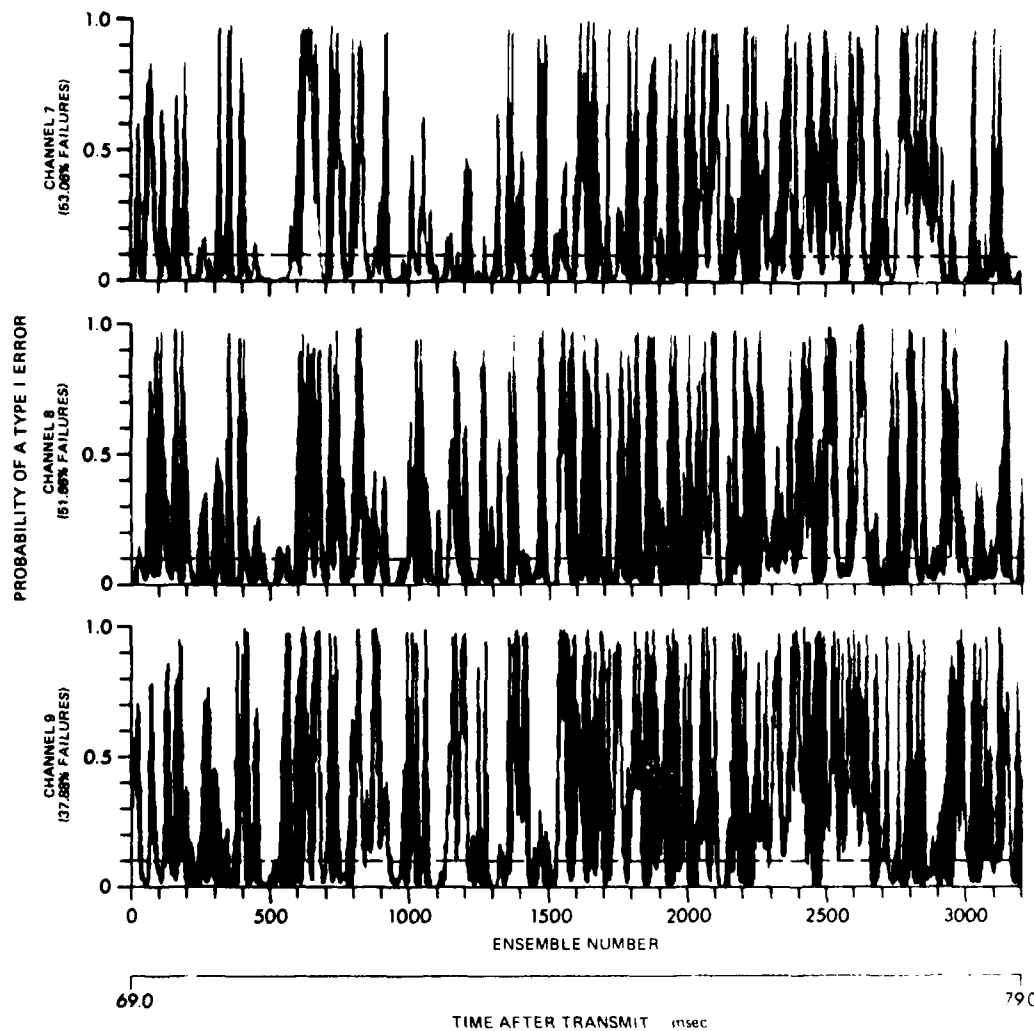
FIGURE IV-26
D'AGOSTINO'S TEST FOR NORMALITY, CHANNELS 7-9
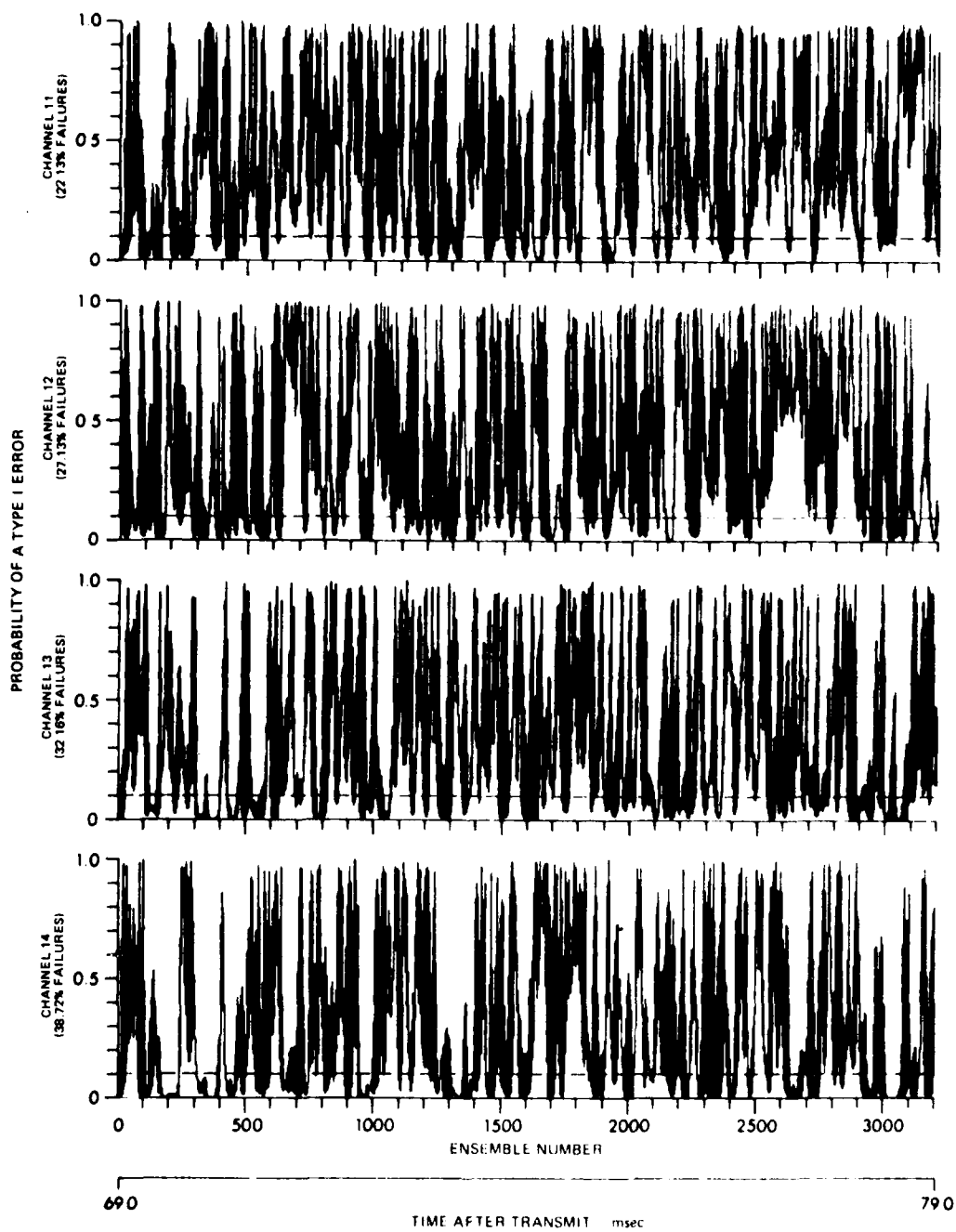
FIGURE IV-27
D'AGOSTINO'S TEST FOR NORMALITY, CHANNELS 11-14

percentage of failures for each channel, and the failures occur in the

same regions. Thus it appears that D'Agostino's test and the kurtosis

test have approximately the same power for the type of distributions

encountered in these reverberation data, and both indicate a signifi-

cant departure of the data from normality.

IV.2.5.4 The Kolmogorov-Smirnov One-Sample Test

The test statistic D_N for the Kolmogorov-

Smirnov one-sample (KS-1) test is the maximum absolute difference

between the empirical cumulative distribution function of the data

and the theoretical distribution function. The distribution of D_N

depends on N, the number of samples, but is independent of the theoreti-

cal distribution function.[52] As a test for normality, the theoretical

distribution is the normal distribution with a mean and variance given

by the sample mean and sample variance of the ensemble being tested.

The exact distribution of D_N can be calculated,[52,53] but for large

sample sizes the Smirnov approximation can be used. If D_N is transformed

to the statistic Z, where

$$Z = \sqrt{N} \ D_N \quad ,$$

then Z has as its limiting distribution the Smirnov distribution. The

approximation to the Smirnov distribution has been discussed in an

earlier section of this chapter.

As a goodness-of-fit test, the KS-1 test is

generally superior to the Chi-square test.[40] However, as a test for

normality, it generally has less power than the skewness and kurtosis tests

or D'Agostino's test.[48] The results from the KS-1 test, presented in

Figs. IV-28 through IV-31, tend to confirm its poor performance as a test for normality against the type of distributions encountered in these data.

Much of the poor performance of the KS-1 test can be attributed to the use of the sample mean and variance instead of the true (but unknown) mean and variance. The distribution of the test statistic for the KS-1 test is derived on the assumption that all parameters of the theoretical distribution function are known. When parameters are unknown and must be estimated from the data, the distribution of the test statistic is generally different, and in fact depends on the theoretical distribution function. Thus the probability of a Type I error computed from the test statistic distribution derived under the condition that parameters are known will generally be different from the true probability of a Type I error when parameters are estimated. Usually the test will be more conservative;[57] that is, the probability of a Type I error computed in this way will be larger than its true value, resulting in fewer rejections of the null hypothesis at a given significance level than if the probability of a Type I error had been computed from the true distribution function. The conservative nature of the test when parameters are estimated is demonstrated in these results. As can be seen, every channel had less than 1% failures, compared to typically 50% failures from the kurtosis test of D'Agostino's test. At a level of significance of 0.1, approximately 10% failures would be expected even if the data were normal. Although efforts have been made to compute the distribution function of the KS-1 test when parameters are estimated,[57-63] the results are extremely difficult to apply and were not attempted in this study.
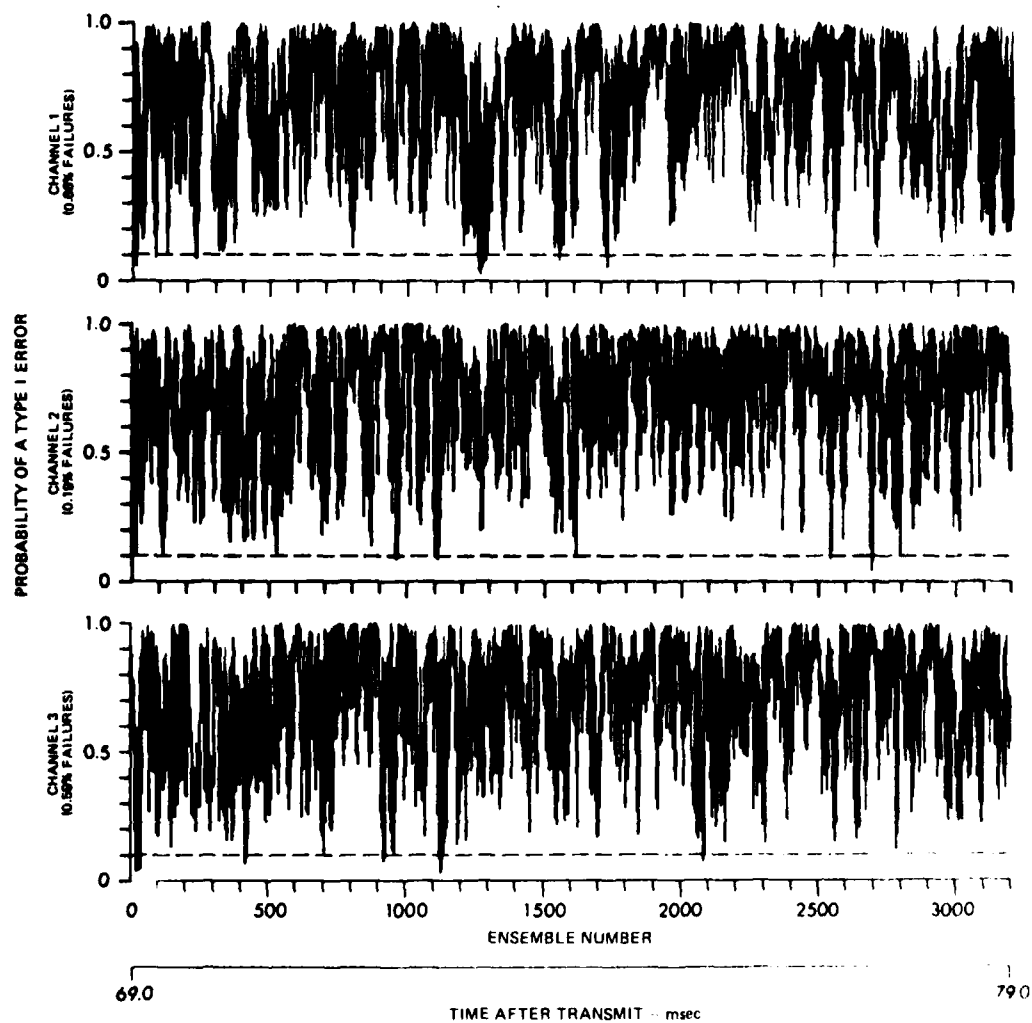
FIGURE IV - 28
THE KOLMOGOROV-SMIRNOV ONE-SAMPLE TEST FOR NORMALITY, CHANNELS 1 3
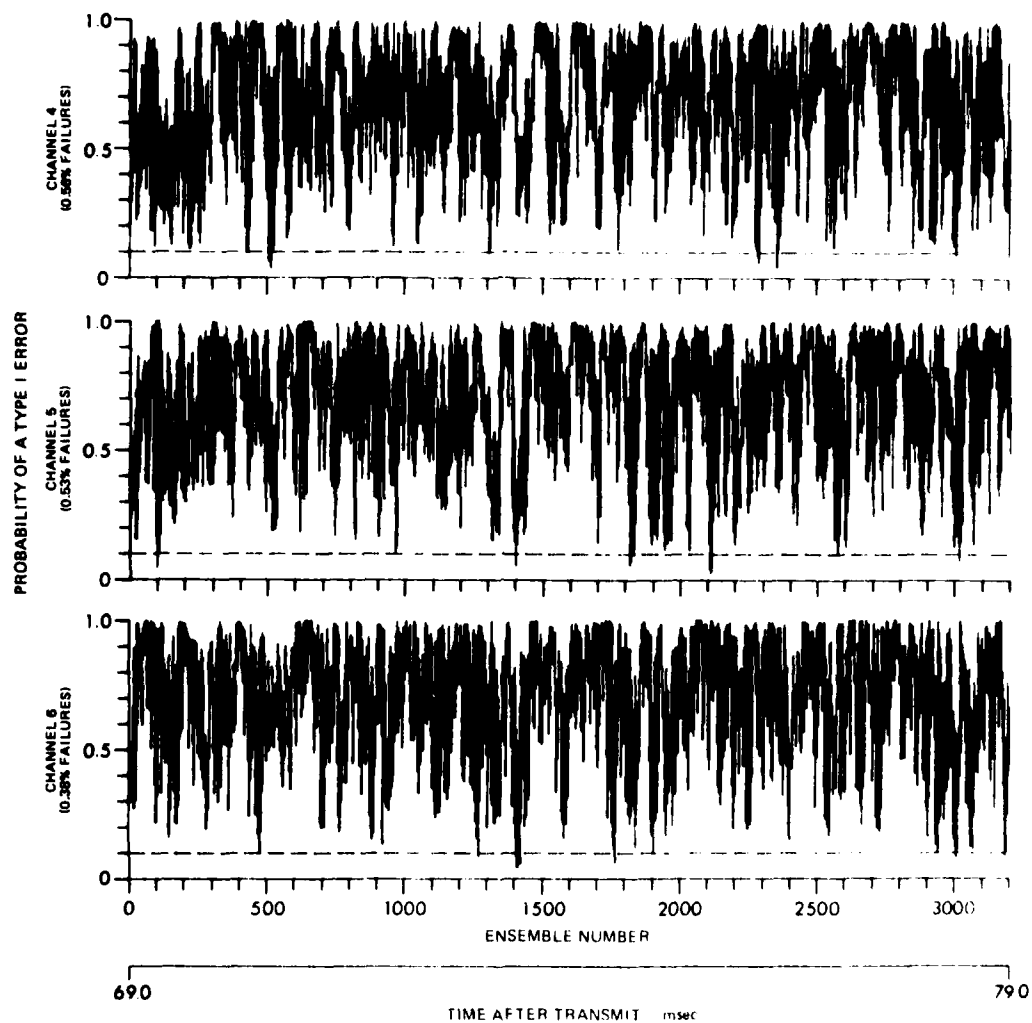
FIGURE IV-29
THE KOLMOGOROV-SMIRNOV ONE SAMPLE TEST FOR NORMALITY, CHANNELS 4-6
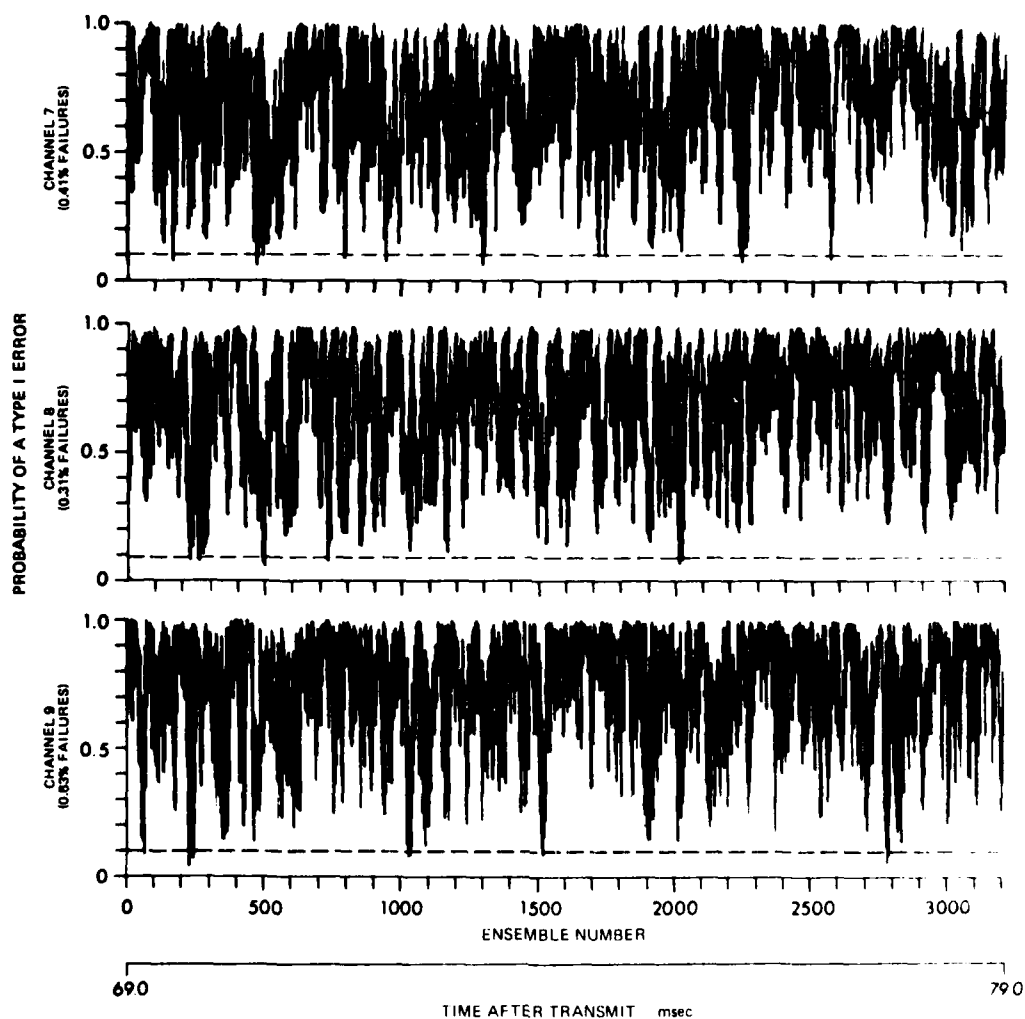
FIGURE IV-30
THE KOLMOGOROV-SMIRNOV ONE-SAMPLE TEST FOR NORMALITY, CHANNELS 7-9
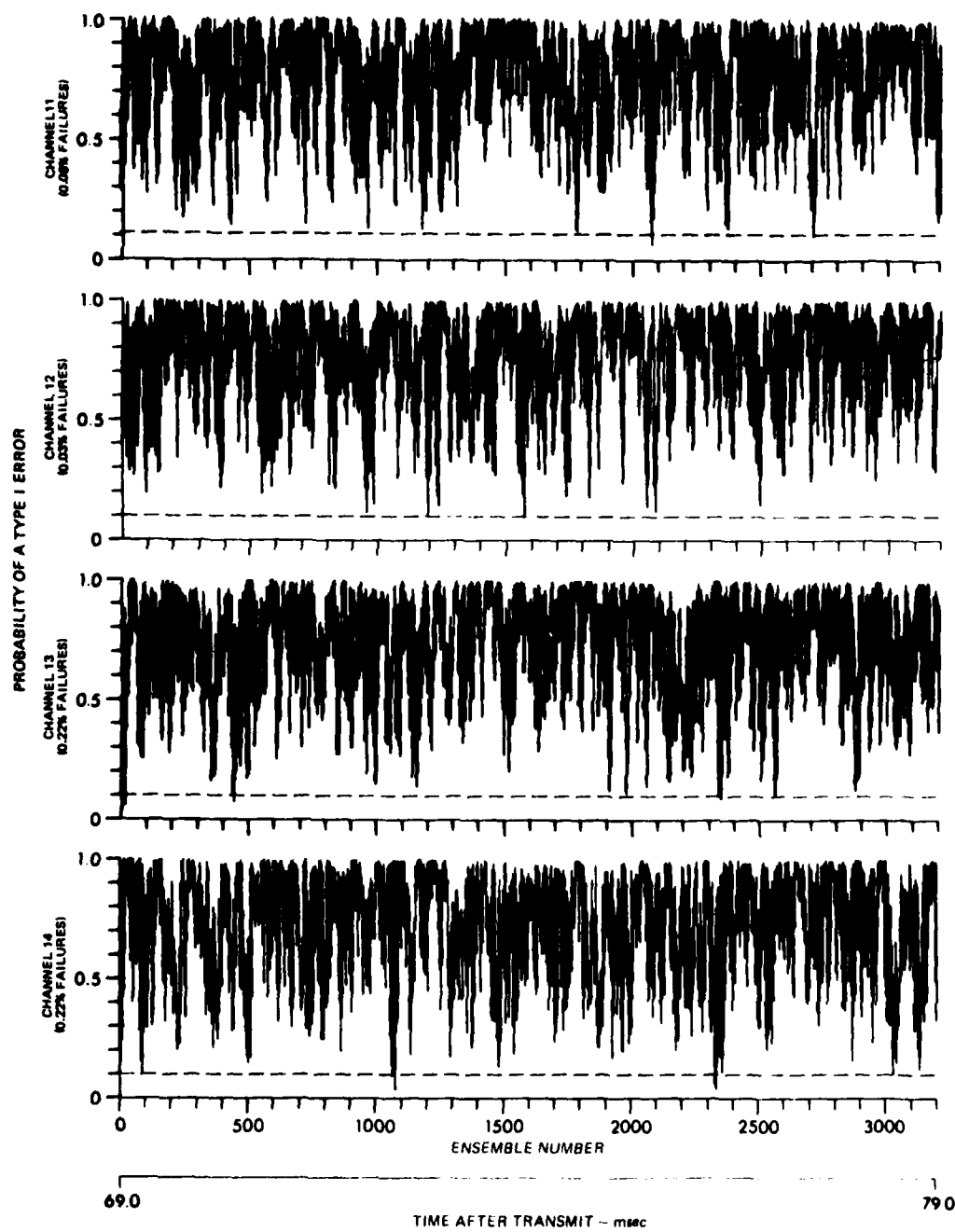
FIGURE IV-31
KOLMOGOROV-SMIRNOV ONE-SAMPLE TEST FOR NORMALITY, CHANNELS 11 14

IV.2.6 Summary of Results of Tests for Normality

Four different tests for normality were applied to all 13 channels of data. The probability of a Type I error from every 80th ensemble was compared to the level of significance of 0.1 and the resulting binomial probability was computed. On all channels, the results from the D-test and the kurtosis test indicated a near-zero probability that the collection of ensembles from each channel was normally distributed. The skew test resulted in binomial probabilities less than .05 for all channels except 6, 9, 11, 12, and 13. For these channels the probabilities were .1, .1, .21, .37, and .58, respectively. Since the D-test and the kurtosis test rejected these channels, it was felt that the hypothesis of normality could be confidently rejected for all 13 channels. The KS-1 test was not applied to the determination of normality due to the extremely conservative nature of the test as it was implemented with the sample mean and variance.

IV.3 Summary of the Statistical Testing

All thirteen channels of the reverberation data have been tested for randomness, homogeneity, and normality for all 3200 ensembles formed during the 10 ms reverberation return. Only the last 500 samples of each ensemble were used, since the reverberation intensity was more uniform during this last half of the observation period. The runs up and down test indicated that all the data were random at a two-tailed level of significance of 0.1. The KS-2 test for homogeneity indicated that there was some lack of homogeneity in the data (10 to 20 percent of the ensembles of each channel failed at a 10 percent significance level) although the inhomogeneity was judged not to be too

severe. Some sequences of ensembles were more nearly homogeneous than

others. For example, ensembles 1801-2200, which will be examined in

some detail in the next chapter, had less than 10 percent failures

for all channels except 11, 13, and 14. For these channels the failure

rate was 19.25, 10.5, and 12.0 percent, respectively.

The data were also tested for normality. The tests indicated

some skewness and a significant amount of kurtosis. Pearson's test

of kurtosis and D'Agostino's test typically indicated a 50 percent

failure rate. The tests for normality were apparently not adversely

affected by the overall lack of homogeneity. There appeared to be no

correlation between ensembles which failed the homogeneity tests and

those which failed the tests for normality. Ensembles 1801-2200, which

were generally homogeneous, failed the tests for normality at approxi-

mately the same rate as the rest of the ensembles. Although previous

tests of surface reverberation for normality have indicated no signifi-

cant departures from normality,[41] it has not yet been determined under

what conditions a departure from normality is to be expected. That is,

it is not known what acoustic, geometric, or environmental conditions

most affect the statistical distribution of surface reverberation. In

particular, it is possible that the large surface wave heights encounter-

ed in the present study tended to result in backscattered sound with

larger amplitudes and thus distributions of this backscattering with

larger than normal tails, which would account for the large kurtosis

observed. Thus it is felt that the lack of normality in no way conflicts

with previous results.

V. MOMENTS AND COVARIANCE

The previous chapter presented the results of various tests to determine the validity of the sample data, that is, to determine if valid sample ensembles could be constructed. In addition, these ensembles were tested to determine if their underlying distribution was gaussian. Since the ensembles were shown to be non-gaussian, a closer examination of the sample moments provides insights into the type of underlying distribution from which the data were sampled. Examples of techniques whereby the sample moments are used to approximate a distribution are Pearson curves, Gram-Charlier series, and Cornish-Fisher expansions.[51] Although the present study will not attempt to estimate the distribution of the data, the mean, variance, skew, and kurtosis will be examined in this chapter in some detail.

After an examination of the moments, the spatial and temporal covariance of the reverberation will be extensively analyzed. Many statistical techniques for the detection of signals in the presence of reverberation depend upon a knowledge of the covariance of the reverberation. For this reason the covariance is an important statistical parameter to study. Of course, most of these techniques assume that the reverberation is zero-mean gaussian, so that the covariance of the reverberation is the only statistical parameter necessary to completely specify the distribution function of the reverberation. For non-gaussian distributions, the covariance may not be the only parameter necessary to specify the distribution, and the detection techniques

116

based on non-gaussian reverberation may require more than just a knowledge of the covariance. Nevertheless, the covariance of the reverberation remains an important parameter in the statistical description of the process.

This chapter is organized as follows. The equations for the numerical calculation of the mean, variance, skew, kurtosis, and co-variance are given. The sum and difference components of the sample co-variance are discussed, along with the technique for normalizing the covariance. The mean, variance, skew, and kurtosis are then presented and analyzed as a function of time for all 13 channels. The rest of the chapter is then an analysis of the covariance as a function of time, time-difference, and spatial separation. The experimental results are compared to the theoretical model. It is found that while the theoretical predictions of the covariance between the horizontal elements agree quite well with the experimental results, the predictions of the vertical covariance differ quite significantly from the experimental results. An explanation of this difference is put forth, and changes to the model which would possibly bring the vertical predictions into agreement with the experimental results are proposed.

V.1 Numerical Computation of the Moments and Covariance

The rth population moment about the mean of $v_i(t)$, the random process from the ith channel at time t, is given by

$$\mu_r(t,i) = \left\langle (v_i(t) - \mu_1'(t,i))^r \right\rangle$$

where

$$\mu_1'(t,i) = \left\langle v_i(t) \right\rangle \quad .$$

The sample ensemble estimate of $\mu_r(t,i)$ at the time t_n is

$$m_r(t_n,i) = \frac{1}{N} \sum_{\omega=1}^{N} \left(v_i(t_n,\omega) - m_1^{\cdot}(t_n,i)\right)^r$$

where

$$m_1^{\cdot}(t_n,i) = \frac{1}{N} \sum_{\omega=1}^{N} v_i(t_n,\omega)$$

and is the sample estimate of the mean,

N = number of samples in the ensemble, and

$v_i(t_n,\omega)$ = the sample of the reverberation return from the ith

channel at time t_n from ping ω.

The sample estimate of the skew is

$$\sqrt{b_1(t_n,i)} = \frac{m_3(t_n,i)}{m_2^{3/2}(t_n,i)}$$

and the kurtosis is

$$b_2(t_n,i) = \frac{m_4(t_n,i)}{m_2^{2}(t_n,i)} \qquad .$$

The numerical computation of the covariance is more involved.
The covariance is shown to consist of sum and difference components.
Only the difference component is considered in this study. The
covariance is

$$\kappa_{ij}(t,t+\tau) = \left\langle \left(v_i(t)-\mu_1^{\cdot}(t,i)\right)\left(v_j(t+\tau)-\mu_1^{\cdot}(t+\tau,i)\right)\right\rangle \qquad .$$

Writing the reverberation signals in their quadrature representative
gives

$$\kappa_{ij}(t,t+\tau) = \left\langle (X_i(t)\cos\omega_o t + Y_i(t)\sin\omega_o t - \left\langle X_i(t)\cos\omega_o t + Y_i(t)\sin\omega_o t \right\rangle) \right.$$

$$\cdot (X_j(t+\tau)\cos\omega_o(t+\tau) + Y_j(t+\tau)\sin\omega_o(t+\tau)$$

$$\left. - \left\langle X_j(t+\tau)\cos\omega_o(t+\tau) + Y_j(t+\tau)\sin\omega_o(t+\tau) \right\rangle) \right\rangle \quad .$$

Carrying out the multiplication, utilizing identities for the product of cosine and sine functions, and rearranging terms results in

$$\kappa_{ij}(t,t+\tau) = X_d \cos\omega_o\tau + Y_d \sin\omega_o\tau$$

$$+ X_s \cos2\omega_o(t+\tau/2) + Y_s \sin2\omega_o(t+\tau/2)$$

where

$$X_d = \tfrac{1}{2}\left\langle \overline{X}_i(t)\overline{X}_j(t+\tau) + \overline{Y}_i(t)\overline{Y}_j(t+\tau) \right\rangle$$

$$X_s = \tfrac{1}{2}\left\langle \overline{X}_i(t)\overline{X}_j(t+\tau) - \overline{Y}_i(t)\overline{Y}_j(t+\tau) \right\rangle$$

$$Y_d = \tfrac{1}{2}\left\langle \overline{X}_i(t)\overline{Y}_j(t+\tau) - \overline{Y}_i(t)\overline{X}_j(t+\tau) \right\rangle$$

$$Y_s = \tfrac{1}{2}\left\langle \overline{X}_i(t)\overline{Y}_j(t+\tau) + \overline{Y}_i(t)\overline{X}_j(t+\tau) \right\rangle$$

and

$$\overline{X}_i = X_i - \left\langle X_i \right\rangle , \text{ etc.}$$

It is assumed that the variables t and τ have no random components. Thus the covariance can be written as the sum of a difference component and a sum component:

$$\kappa_{ij}(t,t+\tau) = \kappa_d + \kappa_s$$

where

$$\kappa_d = X_d \cos\omega_o\tau + Y_d \sin\omega_o\tau$$

$$= E_d \cos(\omega_o\tau + \phi_d)$$

and

$$\kappa_s = X_s \cos2\omega_o(t+\tau/2) + Y_s \sin2\omega_o(t+\tau/2)$$

$$= E_s \cos2\omega_o(t+\tau/2+\phi_s) \quad .$$

The difference component is so called because of its dependence upon the difference in observation times, while the sum component depends upon their sum. The envelope and phase of the sum and difference components can be written in terms of their quadrature components in the usual way.

The present study is concerned only with the difference component of the covariance. It can be shown that, in the case of the variance, the envelope of the sum component is always less than or equal to the envelope of the difference component. Since

$$E_d^2 = X_d^2 + Y_d^2$$

and

$$E_s^2 = X_s^2 + Y_s^2$$

then

$$E_d^2 - E_s^2 = \left\langle \overline{X}_i^2(t) \right\rangle \left\langle \overline{Y}_i^2(t) \right\rangle - \left\langle \overline{X}_i(t)\overline{Y}_i(t) \right\rangle^2$$

where for the variance, $i = j$ and $\tau = 0$. From Schwarz's inequality,

$$\left\langle \overline{X}_i(t)\overline{Y}_i(t) \right\rangle^2 \leq \left\langle \overline{X}_i^2(t) \right\rangle \left\langle \overline{Y}_i^2(t) \right\rangle \qquad .$$

Thus

$$E_d^2 - E_s^2 \geq 0$$

and

$$E_d \geq E_s \qquad .$$

Therefore the difference component envelope is always greater than or equal to the sum component envelope. It will be shown later that the sum component of the variance was actually much smaller than the difference component for the segment of the data which was analyzed.

It can also be argued that when estimates of the covariance are computed from sample ensembles, the time variable t will have a random

component ϵ due to time sampling errors during the A/D conversion or motion of the receivers.[17,28] If this ϵ is such that $\omega_o \epsilon$ is uniformly distributed from $-\pi$ to π, then taking the expected value over the cosine and sine functions will cause the sum component of the sample covariance to be zero. Even if ϵ is not so distributed, any random error in t at all will decrease the contribution of the sum component to the sample covariance. Since it appears that the difference component of the covariance is the dominant component, the present study is limited to an examination of only the difference component. Further references to the covariance are intended to include only the difference component unless otherwise stated.

The sample estimates of the quadrature components of the difference component of the covariance are given by

$$x_{ij}(t,\tau) = \frac{1}{2}\frac{1}{N}\sum_{\omega=1}^{N}(\overline{X}_i(t,\omega)\overline{X}_j(t+\tau,\omega) + \overline{Y}_i(t,\omega)\overline{Y}_j(t+\tau,\omega))$$

$$= \frac{1}{2N}\sum_{\omega=1}^{N}(X_i(t,\omega)X_j(t+\tau,\omega) + Y_i(t,\omega)Y_j(t+\tau,\omega))$$

$$- \frac{1}{2}\left[\frac{1}{N}\sum_{\omega=1}^{N}X_i(t,\omega)\frac{1}{N}\sum_{\omega=1}^{N}X_j(t+\tau,\omega) + \frac{1}{N}\sum_{\omega=1}^{N}Y_i(t,\omega)\right.$$

$$\left.\cdot \frac{1}{N}\sum_{\omega=1}^{N}X_j(t+\tau,\omega)\right]$$

$$y_{ij}(t,\tau) = \tfrac{1}{2}\frac{1}{N}\sum_{\omega=1}^{N}\left(\overline{X}_i(t,\omega)Y_j(t+\tau,\omega) - Y_j(t,\omega)\overline{X}_j(t+\tau,\omega)\right)$$

$$= \frac{1}{2N}\sum_{\omega=1}^{N}\left(X_i(t,\omega)Y_j(t+\tau,\omega) - Y_i(t,\omega)X_j(t+\tau,\omega)\right)$$

$$- \tfrac{1}{2}\left[\frac{1}{N}\sum_{\omega=1}^{N}X_i(t,\omega)\frac{1}{N}\sum_{\omega=1}^{N}Y_j(t+\tau,\omega) - \frac{1}{N}\sum_{\omega=1}^{N}Y_i(t,\omega)\right.$$

$$\left.\cdot \frac{1}{N}\sum_{\omega=1}^{N}X_j(t+\tau,\omega)\right]$$

The sample estimates of the envelope and phase are then

$$e_{ij}(t,\tau) = \sqrt{x_{ij}^2(t,\tau) + y_{ij}^2(t,\tau)}$$

$$\phi_{ij}(t,\tau) = \tan^{-1}\left(\frac{-y_{ij}(t,\tau)}{x_{ij}(t,\tau)}\right) \qquad ,$$

and the sample estimate of the difference component of the covariance is

$$k_{ij}(t,\tau) = e_{ij}(t,\tau)(\cos \phi + \phi_{ij}(t,\tau)) \qquad .$$

The covariance can be normalized so that its value is in the range of -1 to +1. The normalized covariance is

$$\widetilde{k}_{ij}(t,\tau) = \frac{k_{ij}(t,\tau)}{\sqrt{k_{ii}(t,0)k_{jj}(t+\tau,0)}}$$

The normalized envelope is given by

$$\widetilde{e}_{ij}(t,\tau) = \frac{e_{ij}(t,\tau)}{\sqrt{e_{ii}(t,0)e_{jj}(t+\tau,0)}}$$

and the phase is unaffected by normalization.

The covariance is referred to as a cross-covariance for $i \neq j$. If $i = j$, then the covariance is an auto-covariance. An auto-covariance

at $\tau = 0$ is just the variance. The normalized covariance is sometimes referred to as the correlation coefficient.

The quadrature components of the reverberation returns were obtained by sampling the received waveforms directly,[35] i.e.,

$$X_i(t,\omega) = v_i(t,\omega)$$

and

$$Y_i(t,\omega) = v_i(t + \frac{1}{4f_o}, \omega) \quad ,$$

where f_o is the center frequency of the transmitted signal. The method of obtaining $Y_i(t,\omega)$ directly from the received waveform is an approximation consistent with the narrowband assumption.[35]

V.2 Moments of the Reverberation Processes

The sample mean, variance, skew, and kurtosis are plotted for 200 ensembles, representing a time duration of 0.622 ms, centered about a time after transmit of 75.25 ms. Much of the analysis of the covariance is also centered about this time. The short time duration of the plots allows the oscillatory nature of these moments to be observed.

V.2.1 Sample Mean

The sample means for all 13 channels are shown in Figs. V-1 through V-4. Since an absolute calibration of the receivers was not maintained throughout the recording and digitization process, the magnitudes of the means have little significance. That is, gain differences which occurred between channels during recording or digitization will be reflected in the computed means. Thus these plots represent the sample mean only to within an undetermined scale factor which is different for each channel. The same is true of the sample variance
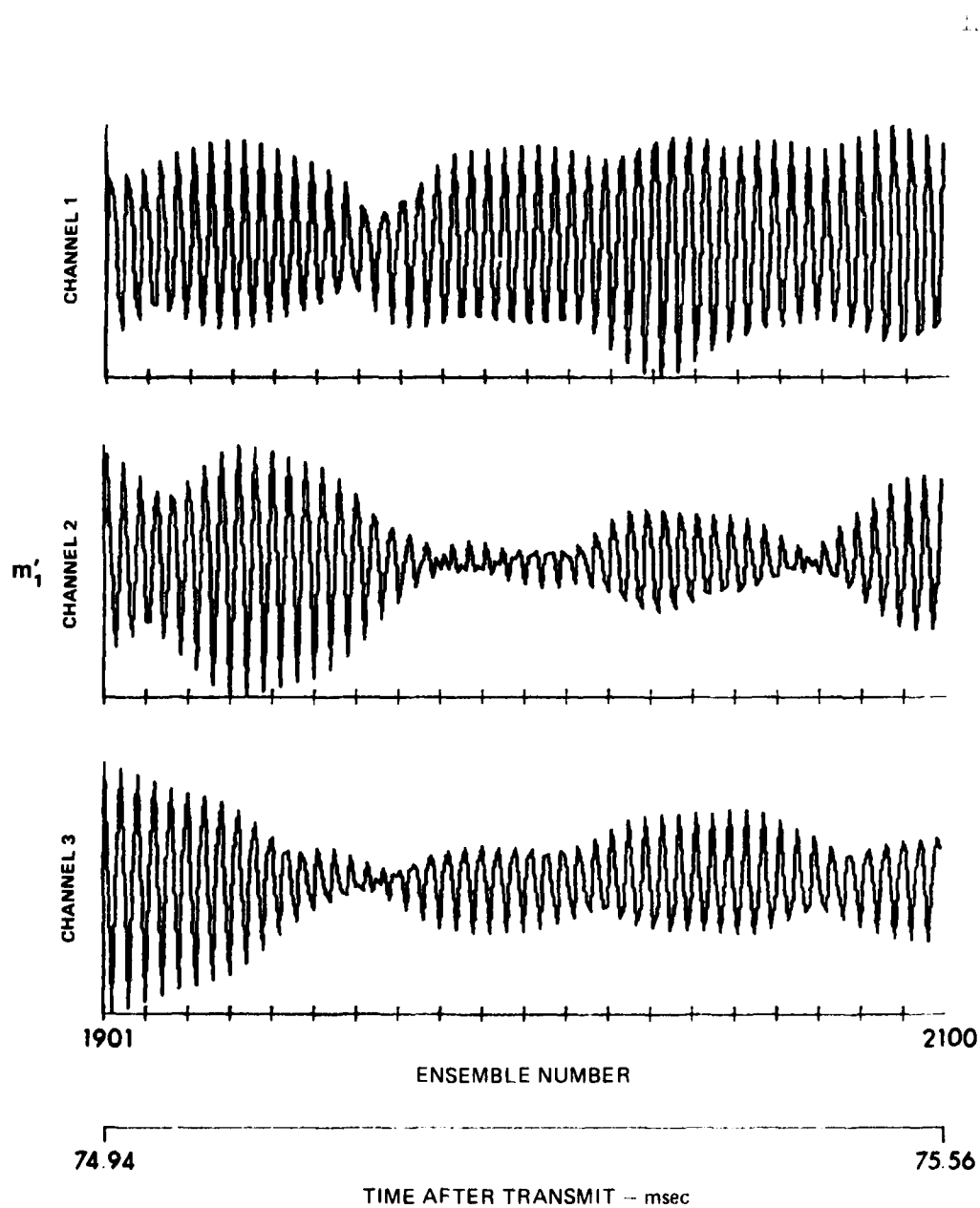
FIGURE V-1
SAMPLE MEAN, CHANNELS 1-3
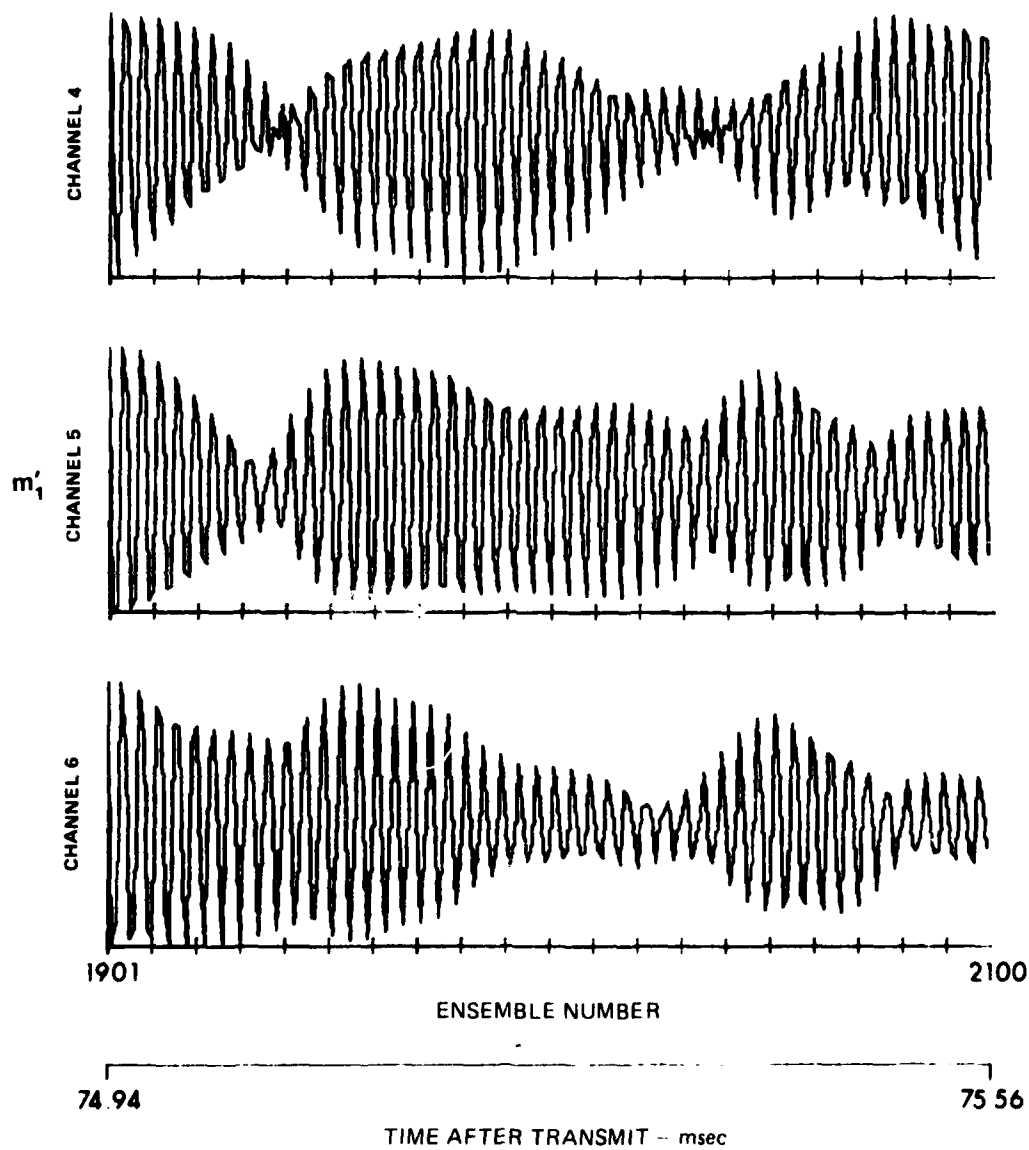
FIGURE V-2
SAMPLE MEAN, CHANNELS 4-6

CHANNEL 7

CHANNEL 8

m_1'

CHANNEL 9

1901

ENSEMBLE NUMBER

2100

74.94

75.56

TIME AFTER TRANSMIT – msec
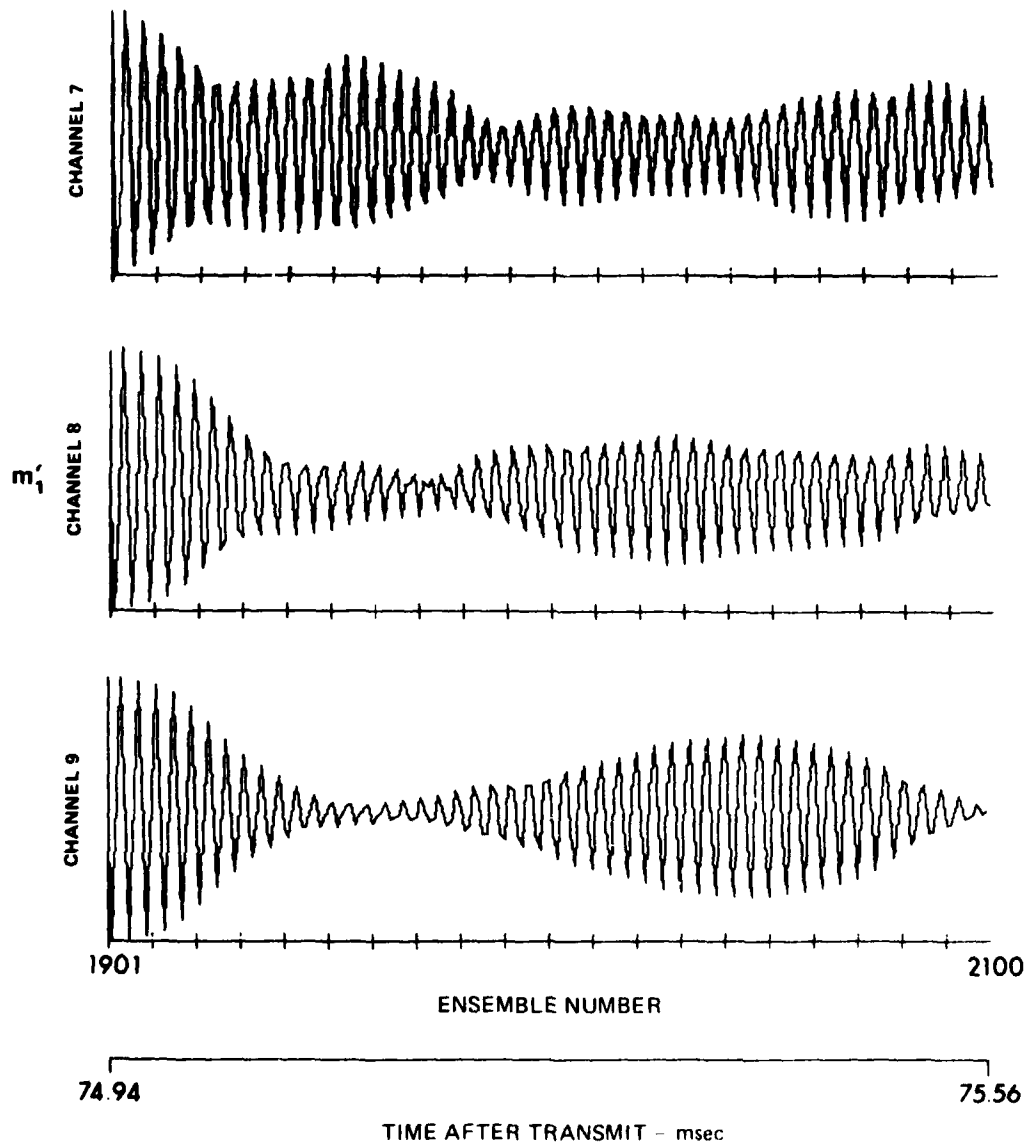
FIGURE V-3
SAMPLE MEAN, CHANNELS 7-9

m'_1

CHANNEL 11

CHANNEL 12

CHANNEL 13

CHANNEL 14

1901   2100

ENSEMBLE NUMBER

74.94   75.56

TIME AFTER TRANSMIT — msec
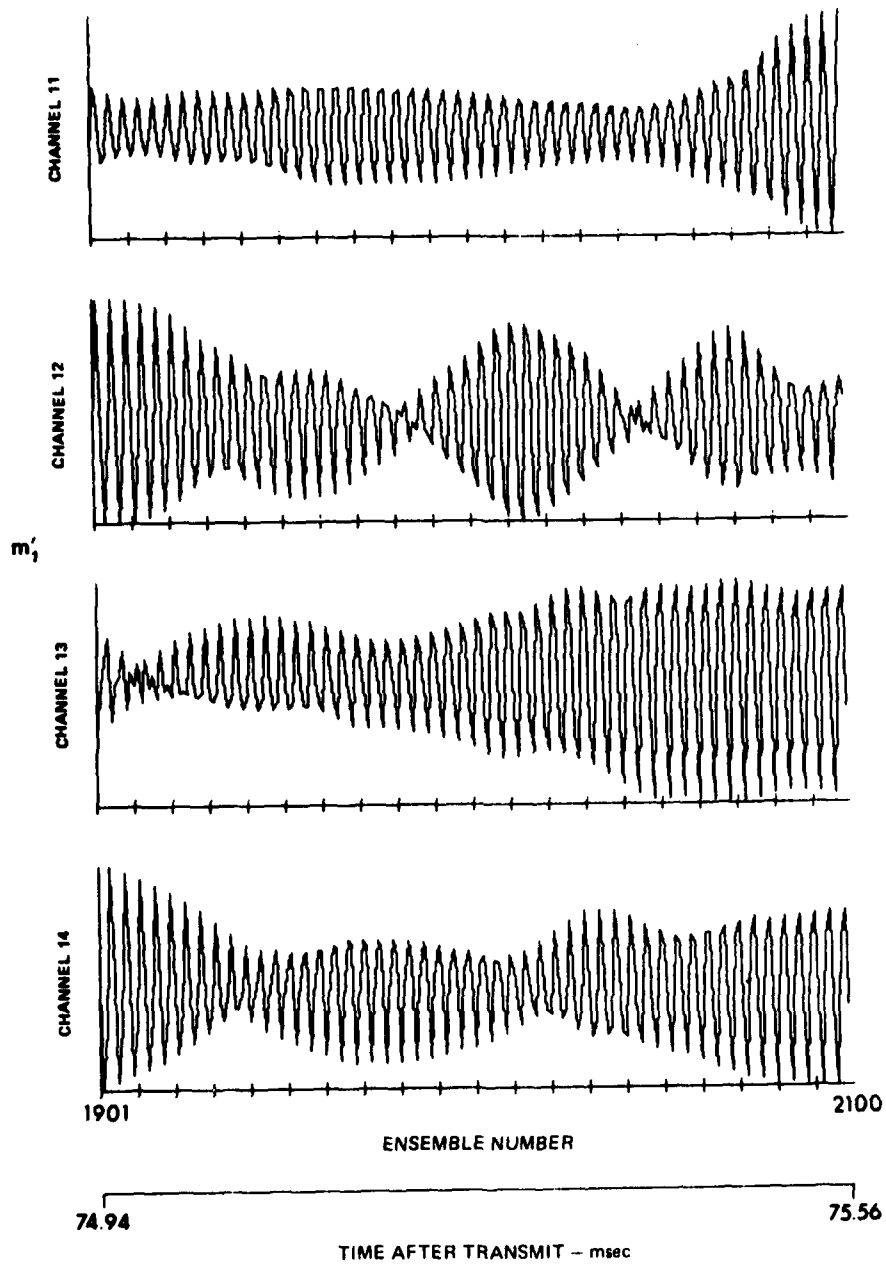
FIGURE V-4
SAMPLE MEAN, CHANNELS 11-14

which is shown later. However, the ratio of the mean to the square

root of the variance is independent of any scale factors. In spite of

this limitation, it is still possible to estimate the statistical

significance of the amplitude of the mean. The ratio of the mean to

the square root of the variance provides one measure of the significance

of the mean. For the data shown here, a typical value for this ratio

is .07. The Student's t-test for zero-mean of normal samples indicates

that for this ratio the mean can be accepted as zero at a 12% signifi-

cance level. Although the data are not normal, nevertheless this is

some indication that the mean is not statistically large.

Another measure of the statistical significance of the

sample mean is its sampling variance, given by[51]

$$\text{var}(m_1') = \frac{1}{N}\mu_2 \quad .$$

The sampling variance is a measure of the spread of the sample estimate

of a statistical parameter (in this case the sample mean) about its

true value. Using the sample estimate m_2 in place of the population

moment μ_2, it was found that most of the values of the mean fell within

plus or minus one standard deviation of zero. Essentially all of the

values were within two standard deviations of zero. This also indicates

that the sample mean is not statistically large.

Even though the sample mean is not statistically differ-

ent from zero, observation of Figs. V-1 through V-4 shows that the means

are not completely random about zero but rather oscillate at the trans-

mitted frequency ω_o. This is to be expected from a bandlimited signal

if the random component of t is small since

$$\left\langle v_i(t) \right\rangle = \left\langle X_i(t)\cos\omega_0 t + Y_i(t)\sin\omega_0 t \right\rangle$$

$$= \left\langle X_i(t) \right\rangle \cos\omega_0 t + \left\langle Y_i(t) \right\rangle \sin\omega_0 t$$

$$= \overline{E}_i(t)\, \cos(\omega_0 t + \overline{\phi}_i(t))$$

where $\qquad \overline{E}_i(t) = \sqrt{\left\langle X_i(t) \right\rangle^2 + \left\langle Y_i(t) \right\rangle^2}$

and $\qquad \overline{\phi}_i(t) = \tan^{-1}\left(\dfrac{-\left\langle Y_i(t) \right\rangle}{\left\langle X_i(t) \right\rangle} \right)$.

Thus the mean of a bandlimited signal is also bandlimited and centered
at the frequency ω_0. Any random component of t will have the effect of
reducing the amplitude of the mean. However, it is apparent in the pres-
ent data that this random component is sufficiently small that the
oscillatory factor is preserved. Therefore, it can be concluded that,
although from a statistical point of view the mean is small, nevertheless
it contains a periodic component at the center frequency ω_c.

V.2.2 Sample Variance

The sample variance for all 15 channels is shown in
Figs. V-5 through V-8. The actual sample variance is plotted along
with the difference component of the sample variance. It can be seen
that the variance does contain a component at a frequency of $2\omega_c$, but
that it is small compared to the difference component. The sampling
variance of the variance is given by[51]

$$\mathrm{var}(m_2) = \frac{1}{N}\left(\mu_4 - \mu_2^2 \right) \qquad .$$

Approximating μ_4 and μ_2 by m_4 and m_2, and recalling that $b_2 = \dfrac{m_4}{m_2^2}$,

the sampling variance can be estimated as
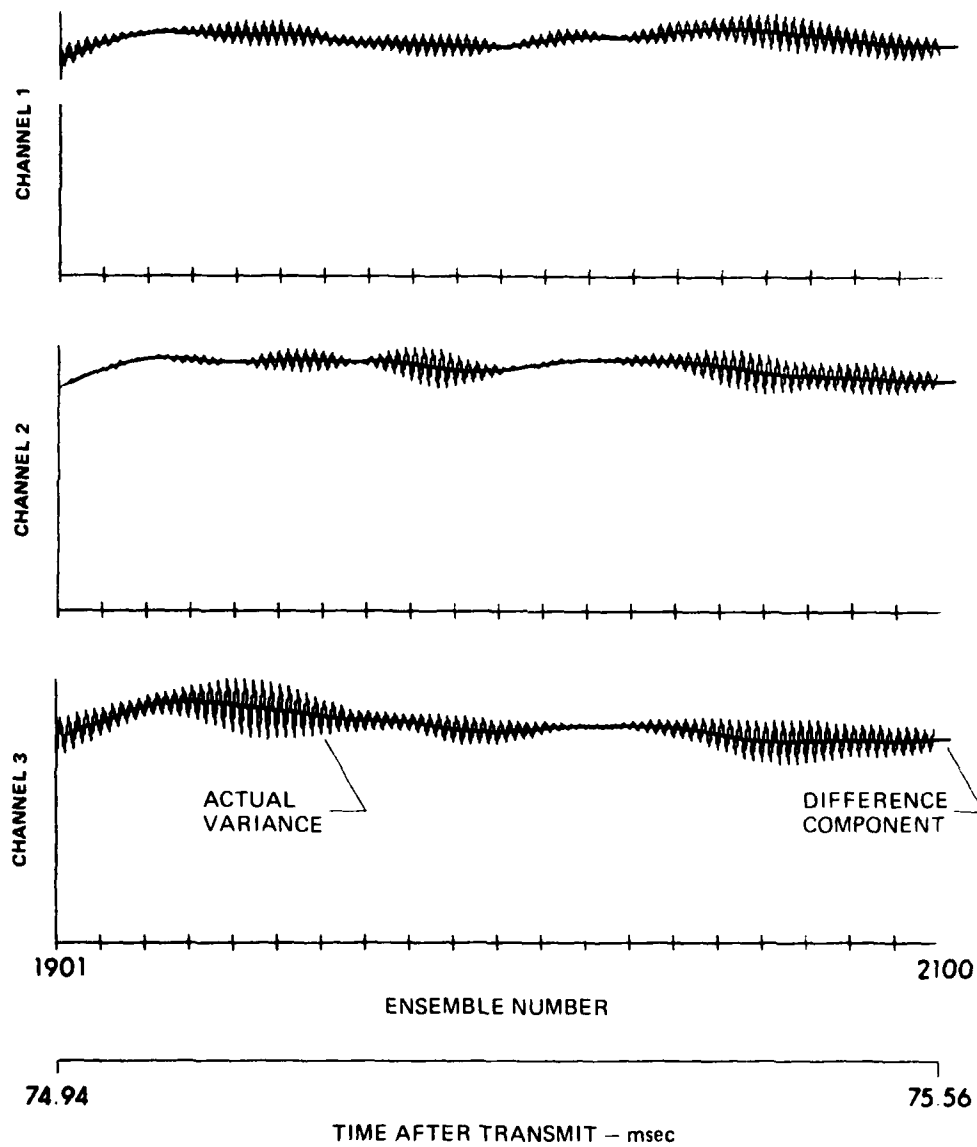
FIGURE V-5
COMPARISON OF ACTUAL VARIANCE AND
DIFFERENCE COMPONENT, CHANNELS 1-3
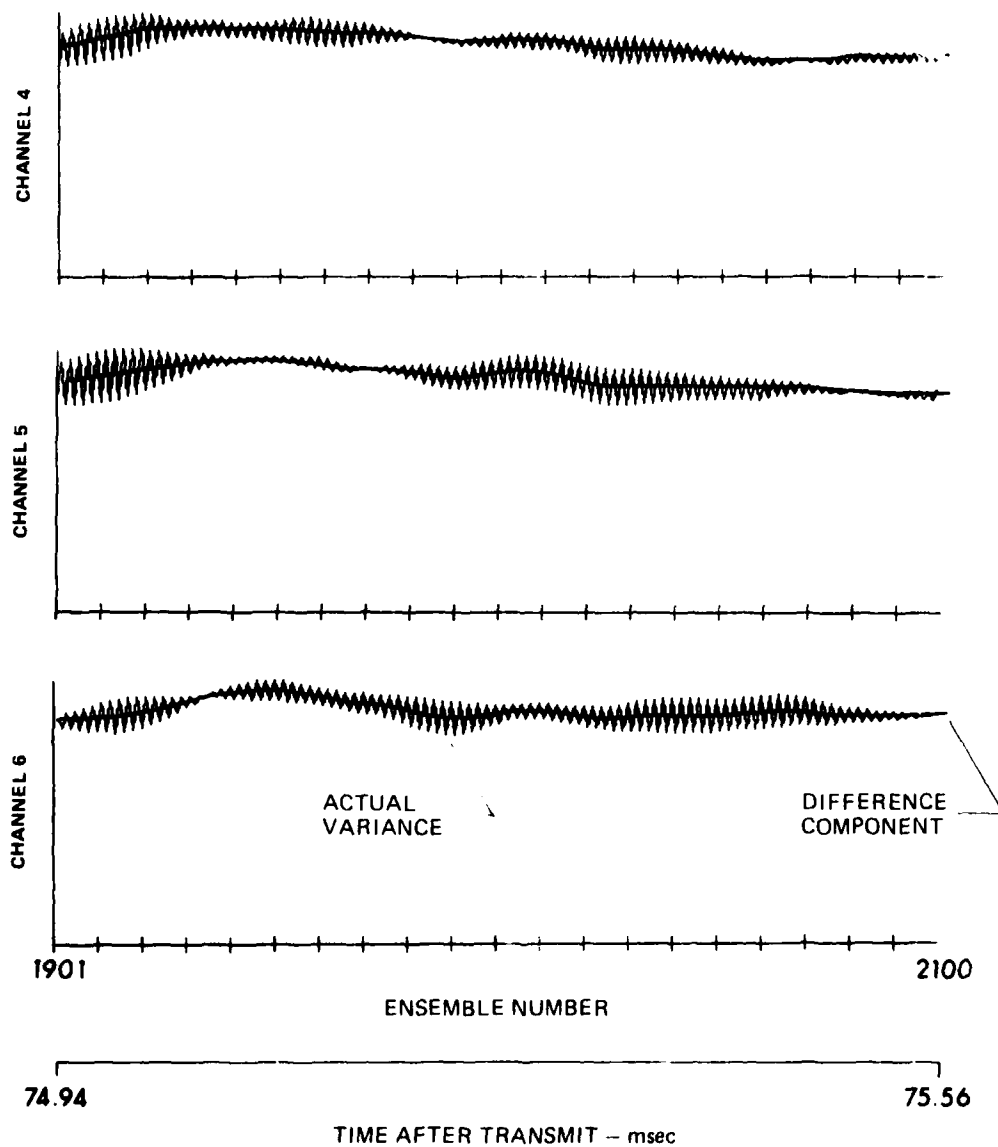
FIGURE V-6
COMPARISON OF ACTUAL VARIANCE AND
DIFFERENCE COMPONENT, CHANNELS 4-6
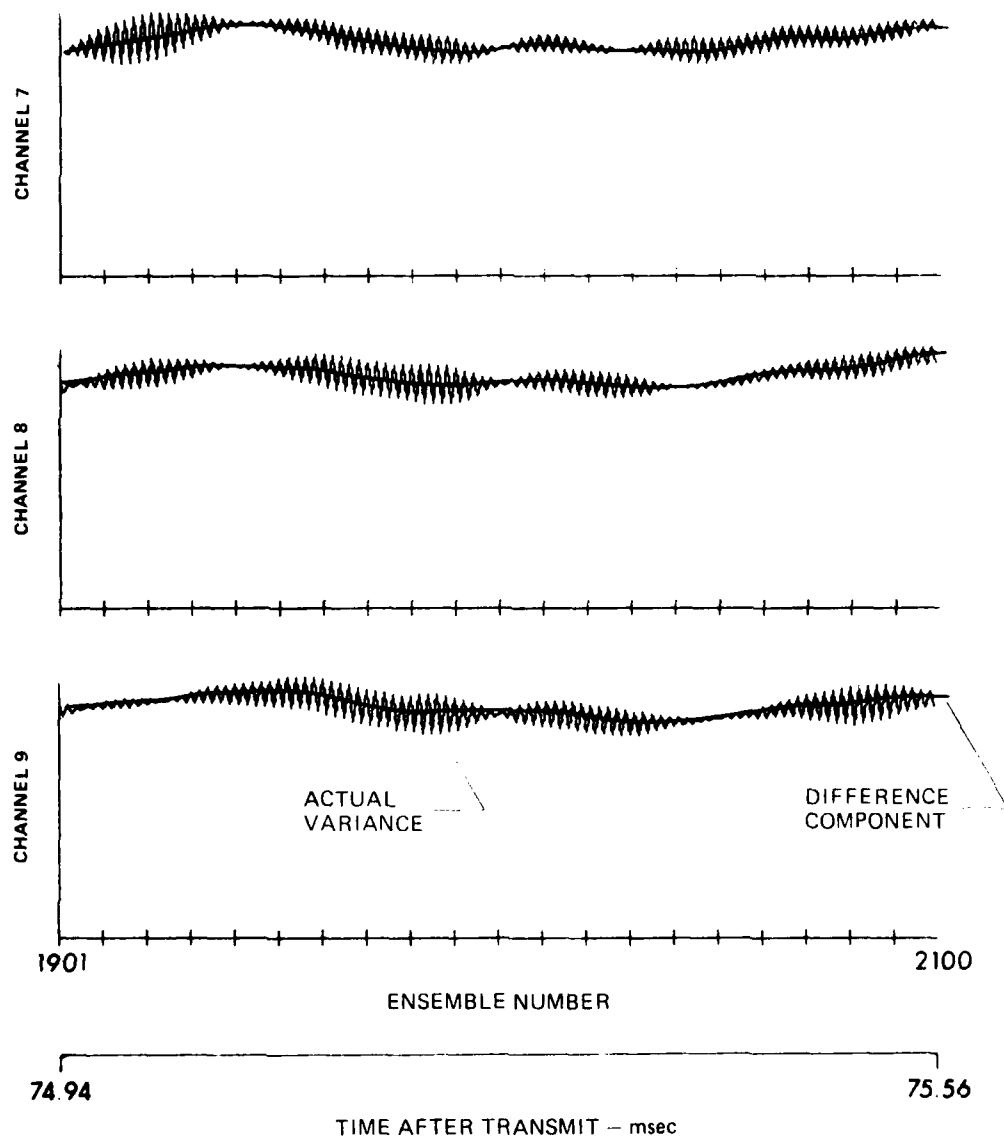
FIGURE V-7
COMPARISON OF ACTUAL VARIANCE AND
DIFFERENCE COMPONENT, CHANNELS 7-9
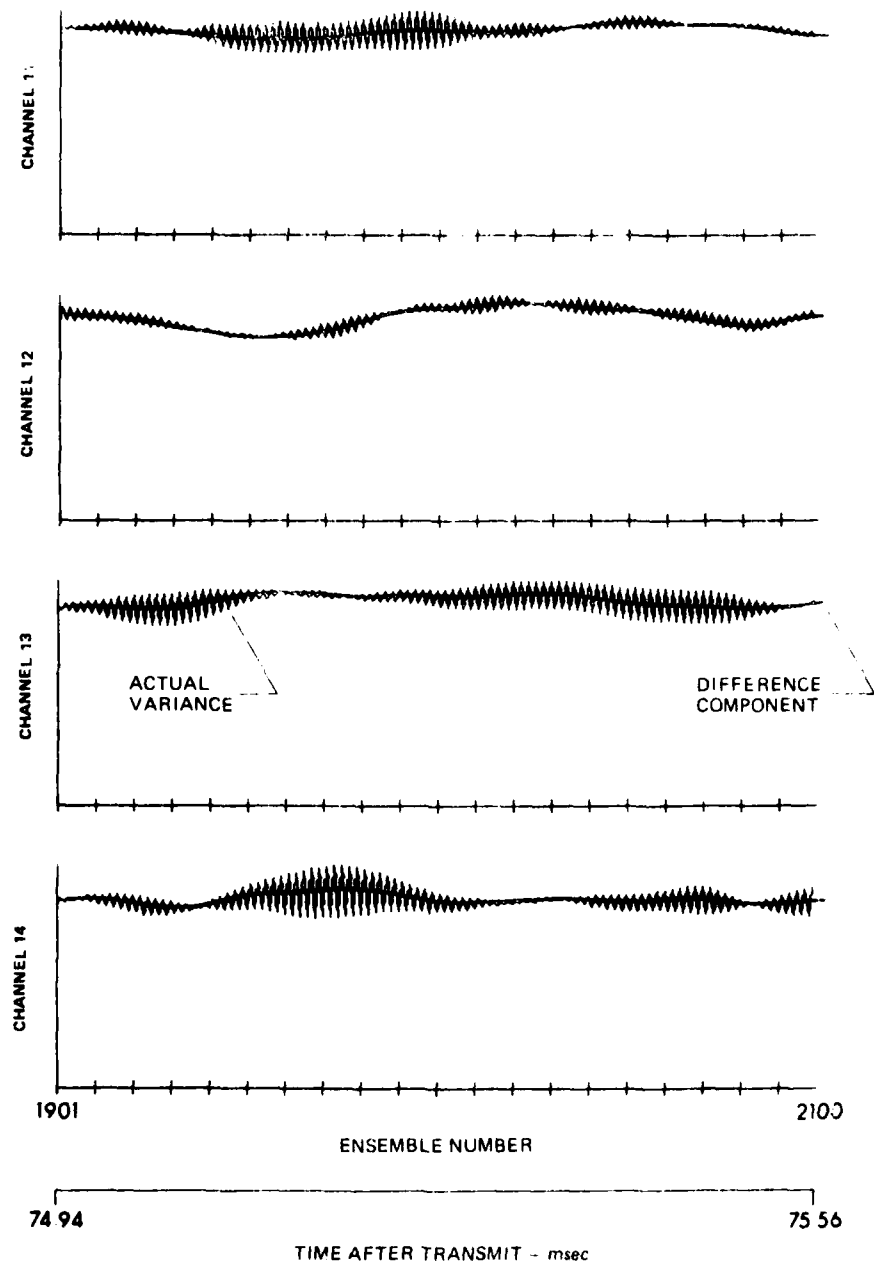
FIGURE V-8
COMPARISON OF ACTUAL VARIANCE AND
DIFFERENCE COMPONENT, CHANNELS 11-14

$$\text{variance}^1 = \frac{1}{n} \left(h_j - 1 \right) m_j \qquad .$$

For the data shown here, the variance is nearly within . . . . . . one standard deviation of the difference component of the variance, where the standard deviation of m_j is just the square root of . . . . . The variance was rarely more than two standard deviations of the difference component. Thus the sum component is not . . . . even though, as in the case of the mean, the sum component is not random but rather contains a periodic factor. This oscillation of the mean and variance has been predicted.[16]

V.2.3 Sample Skew

The estimates of the sample skew are plotted in figures V-9 through V-12. The sample skew is symmetric about zero and appears to oscillate at ω_o. However, since samples of the skew are taken only at time intervals of $\frac{2\pi}{\omega}$, an oscillation at ω will . . . . . . an oscillation at ω_o. Since the skew component . . . . It is more reasonable to assume the oscillation is at ω_o. . . . . . test of skewness indicates that the present ensemble can be accepted as normal at a 10% level of significance if the skew is within . . . . of zero. It can be observed that many values of the skew fall . . . . . of these bounds due to the periodic component of the skew. . . . . . mality is rejected, not because the skew was on the average significantly different from zero, but because a number of the individual values of the skew were outside the confidence limits due to the periodic component of the skew.
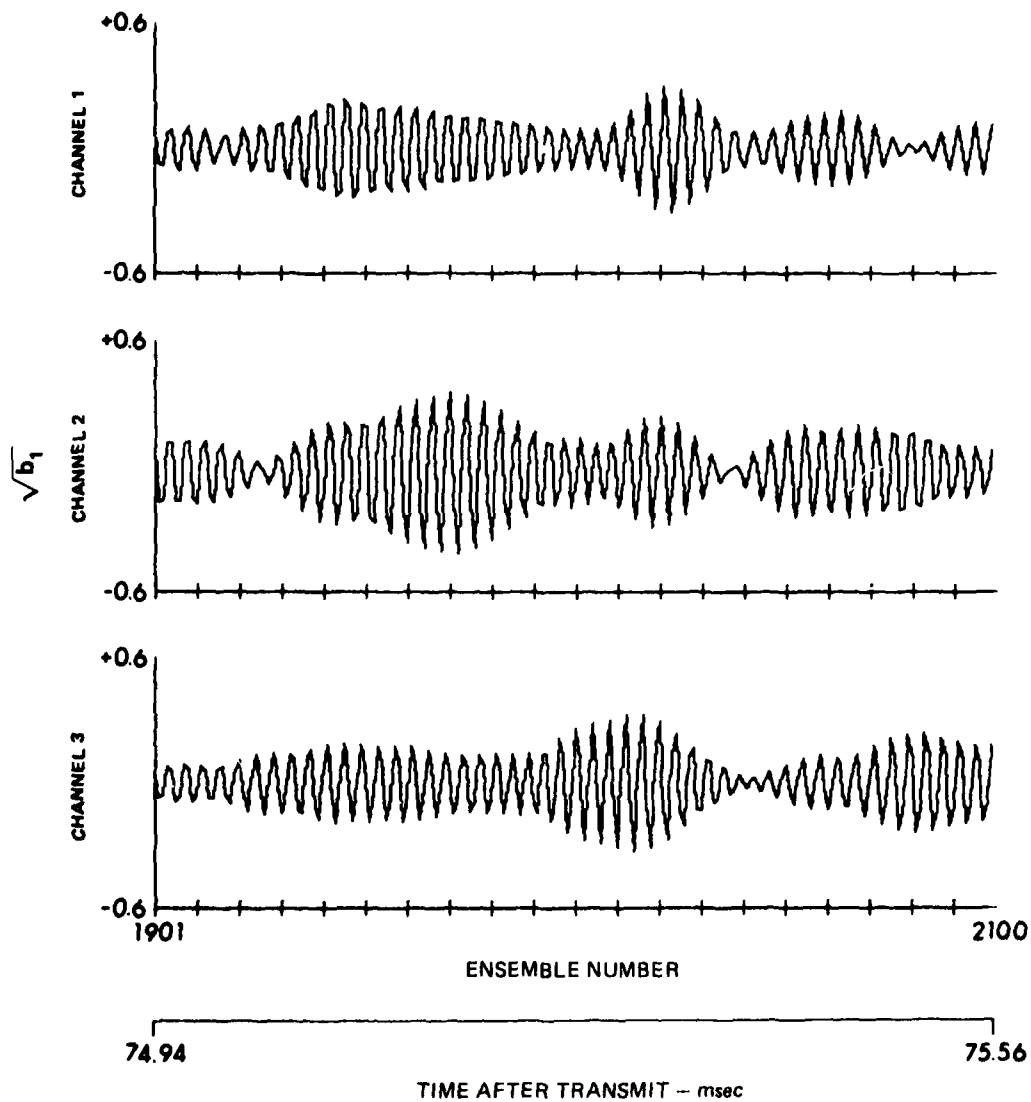
FIGURE V-9
SAMPLE SKEW, CHANNELS 1-3
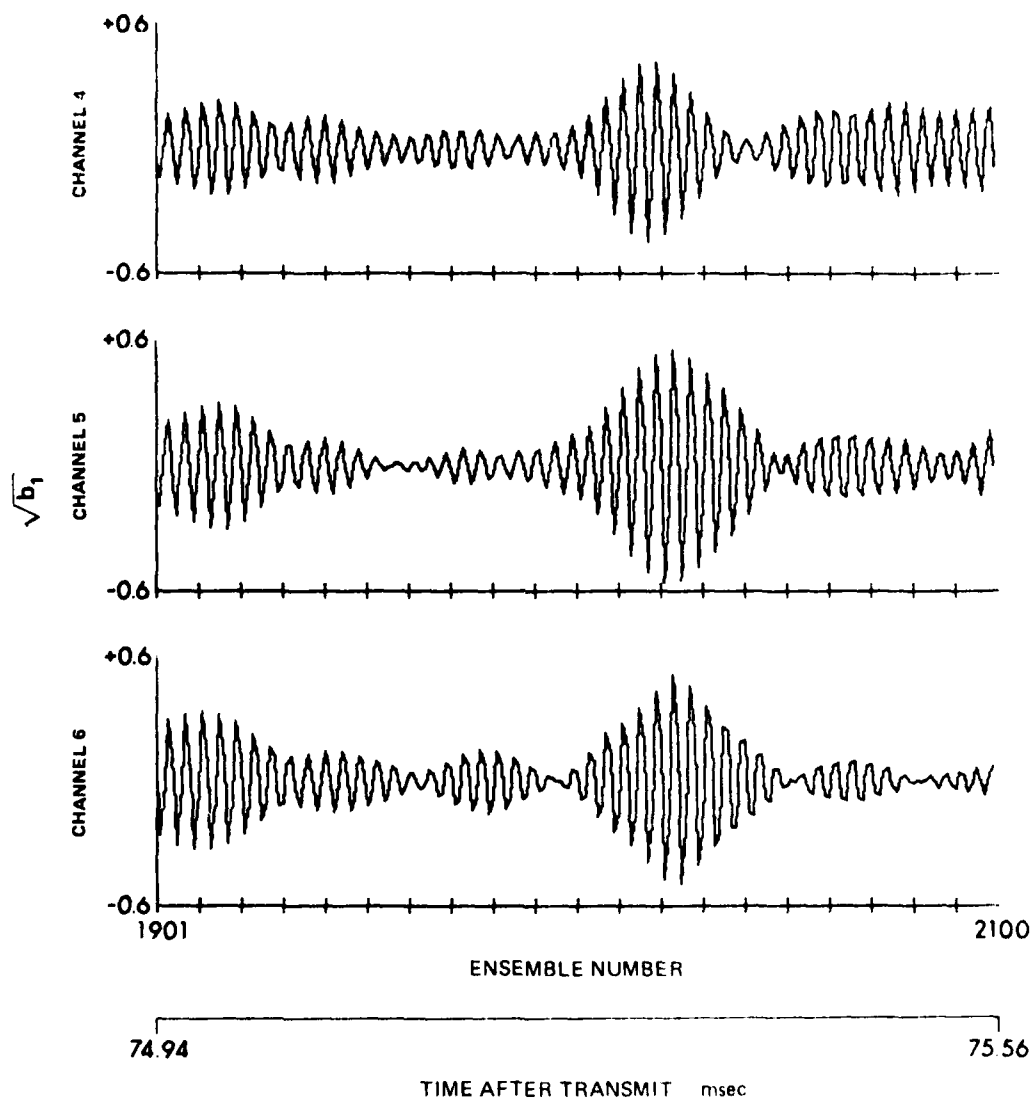
FIGURE V-10
SAMPLE SKEW, CHANNELS 4-6
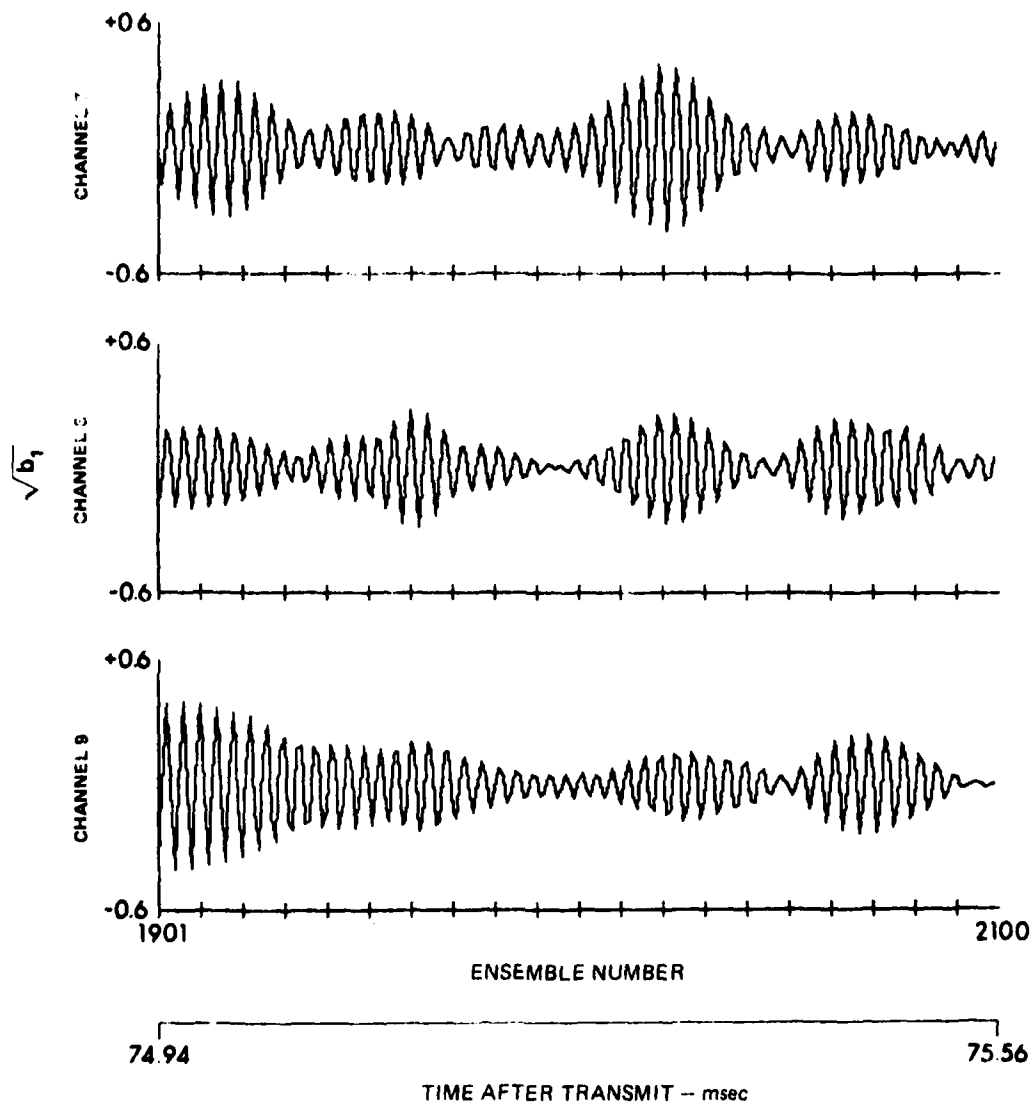
FIGURE V-11
SAMPLE SKEW, CHANNELS 7-9
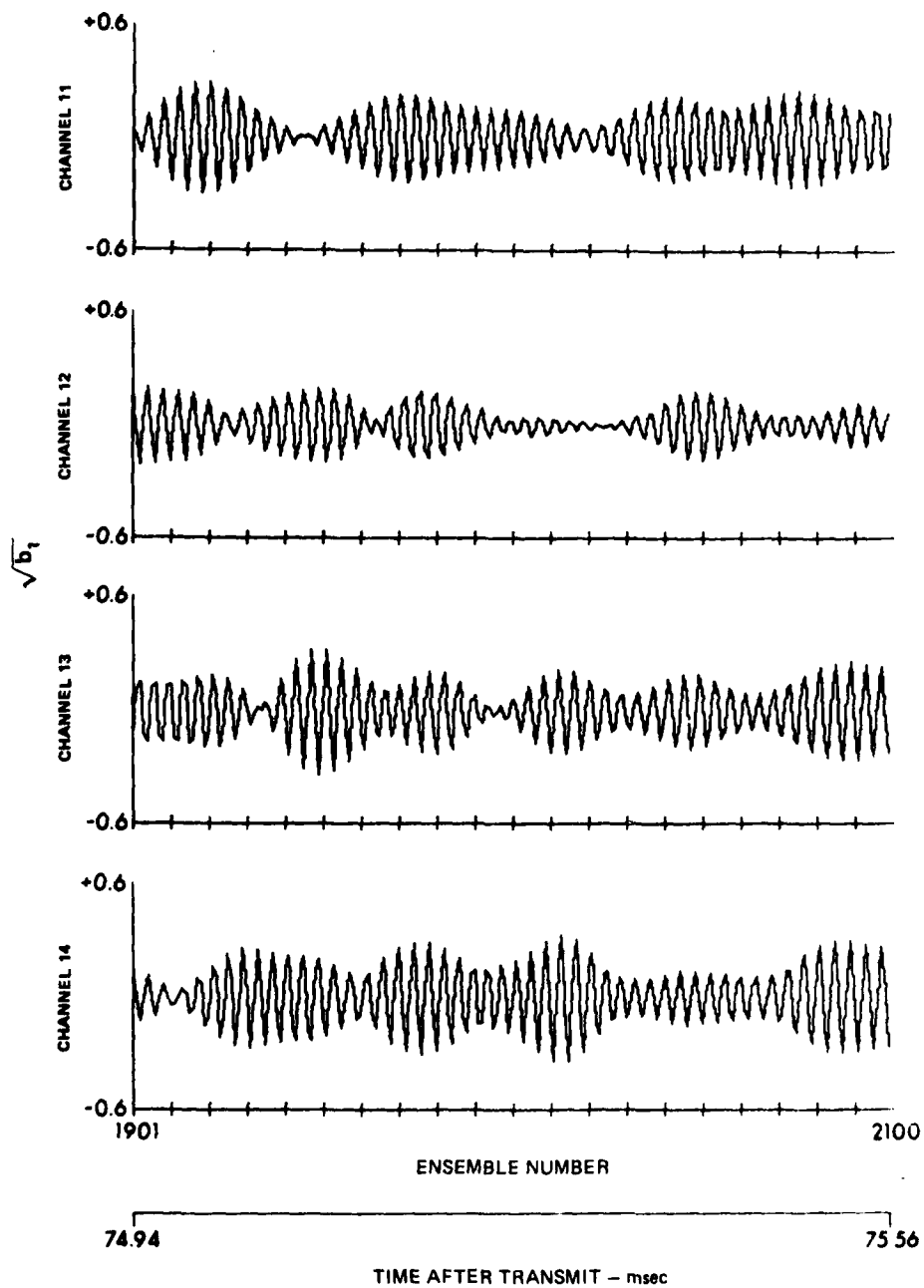
FIGURE V-12
SAMPLE SKEW, CHANNELS 11-14

V.2.4   Sample Kurtosis

Plots of the sample kurtosis are shown in Figs. V-13 through V-16. Oscillations are evident and appear to be at a frequency of $2\omega_o$, although they are probably at $4\omega_o$. A normal distribution has a kurtosis of 3. These samples are generally significantly larger than 3. The 10% confidence limits for Pearson's test of kurtosis are 2.67 - 3.37.[46] Most of the values of the kurtosis are above the upper limit. The values of the kurtosis are not distributed symmetrically about the normal value of 3. Rather, the kurtosis is on the average larger than 3. Thus the periodic component of the kurtosis is not the dominant factor in causing a rejection of normality, as was the case for the skew.

V.3   The Covariance

This section examines only the difference component of the covariance. Both the sample estimates from the experimental data and the theoretical results from the point-scatter model are presented. This section is developed as follows. The difference component of the variance over the entire 10 ms digitization interval is discussed first. Then the auto-covariance as a function of τ is presented and analyzed. The cross-covariance as a function of spatial separation for $\tau=0$ is then compared for the horizontal and vertical arrays. The covariance for $\tau \neq 0$ is presented and the section concludes with a discussion of the failure of the theoretical model to adequately predict the spatial dependence of the covariance for the vertical array.

V.3.1   The Difference Component of the Variance

Figures V-17 through V-20 are plots of the sample difference component of the variance over the entire 10 ms of the
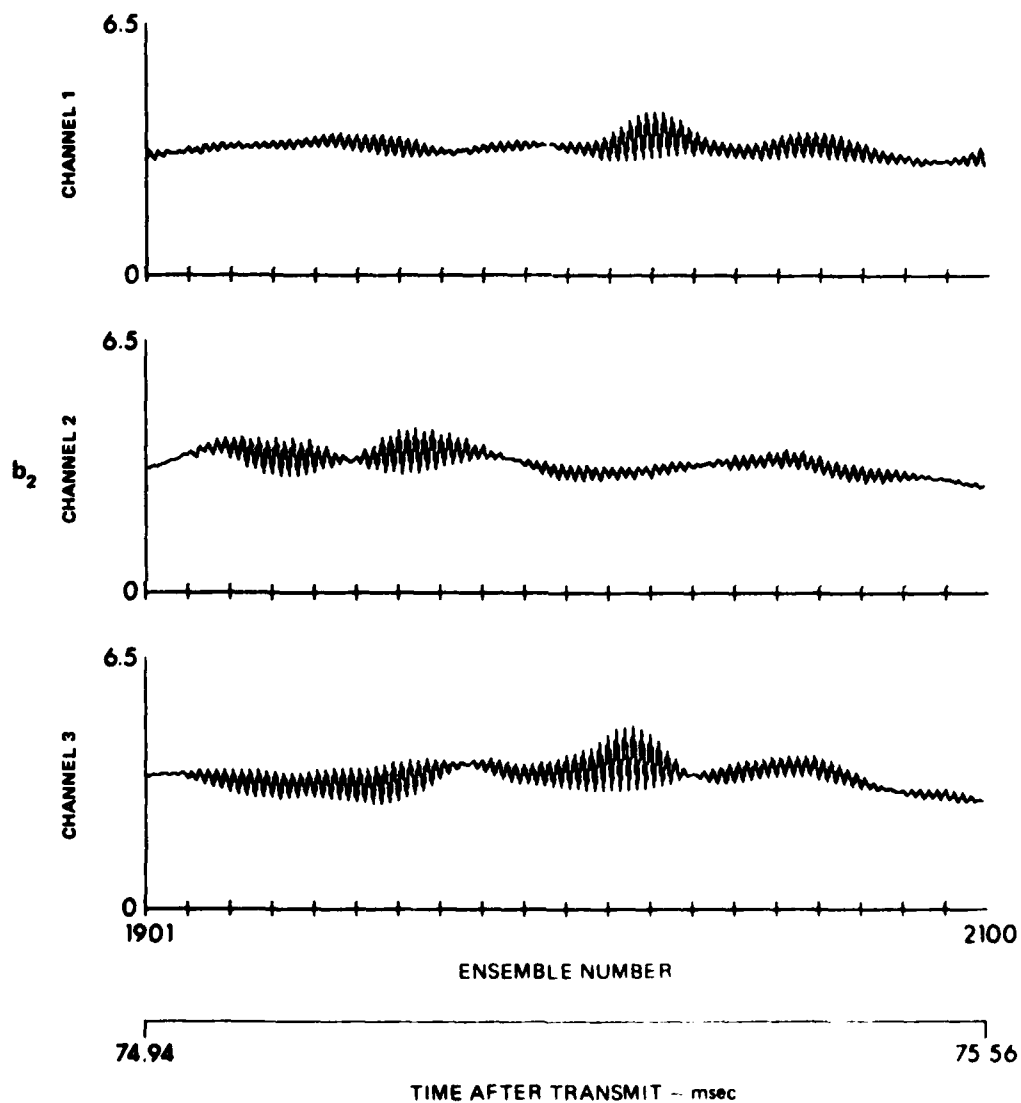
FIGURE V-13
SAMPLE KURTOSIS, CHANNELS 1-3
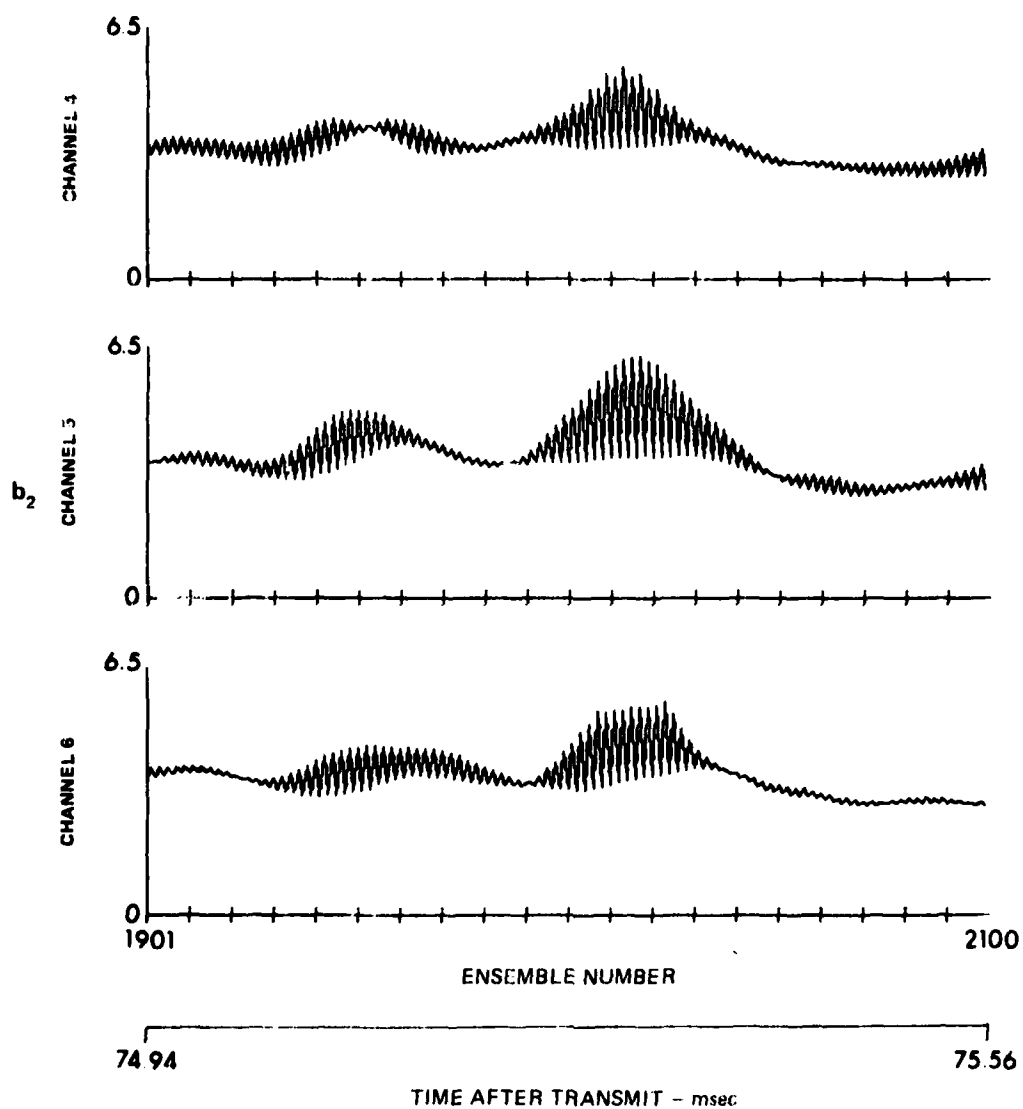
FIGURE V-14
SAMPLE KURTOSIS, CHANNELS 4-6
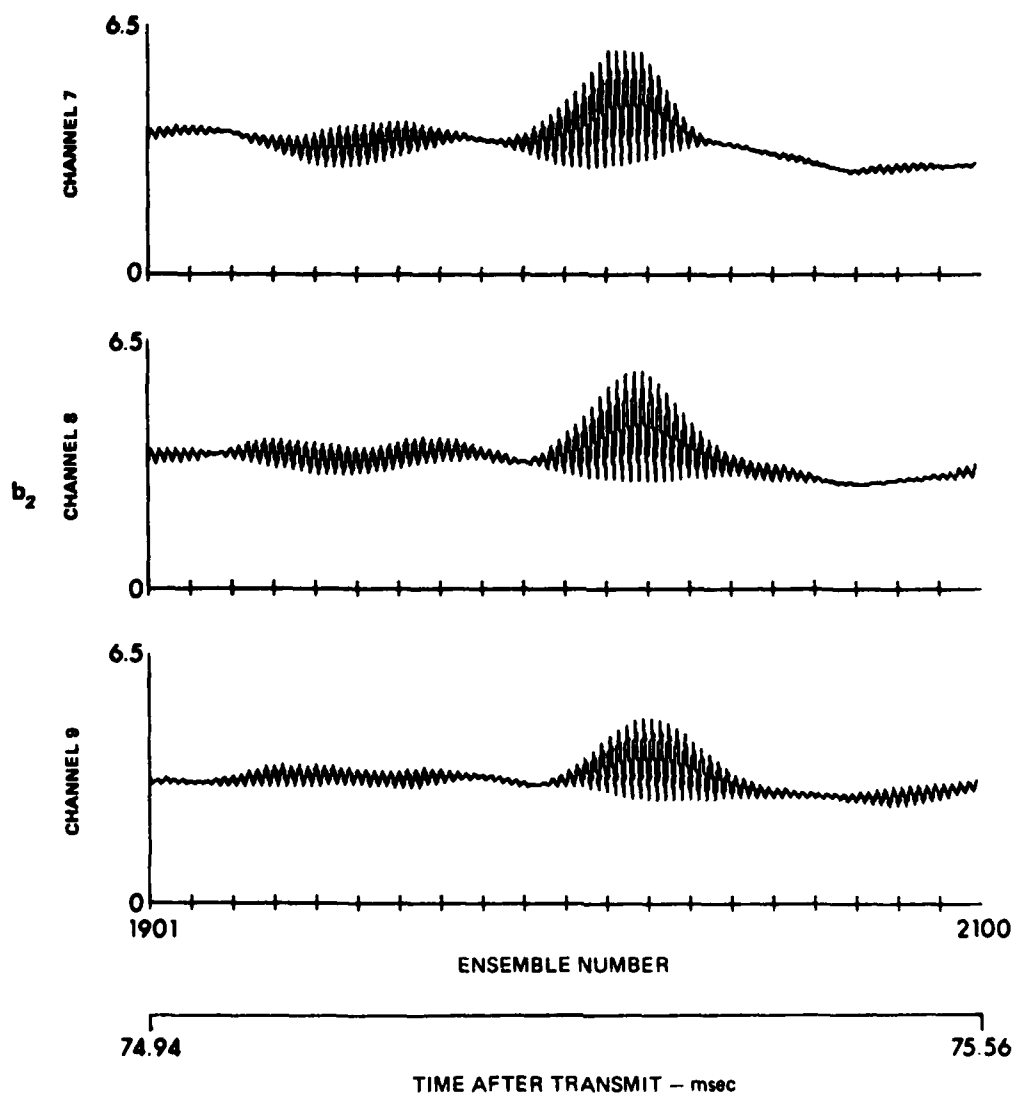
FIGURE V-15
SAMPLE KURTOSIS, CHANNELS 7-9
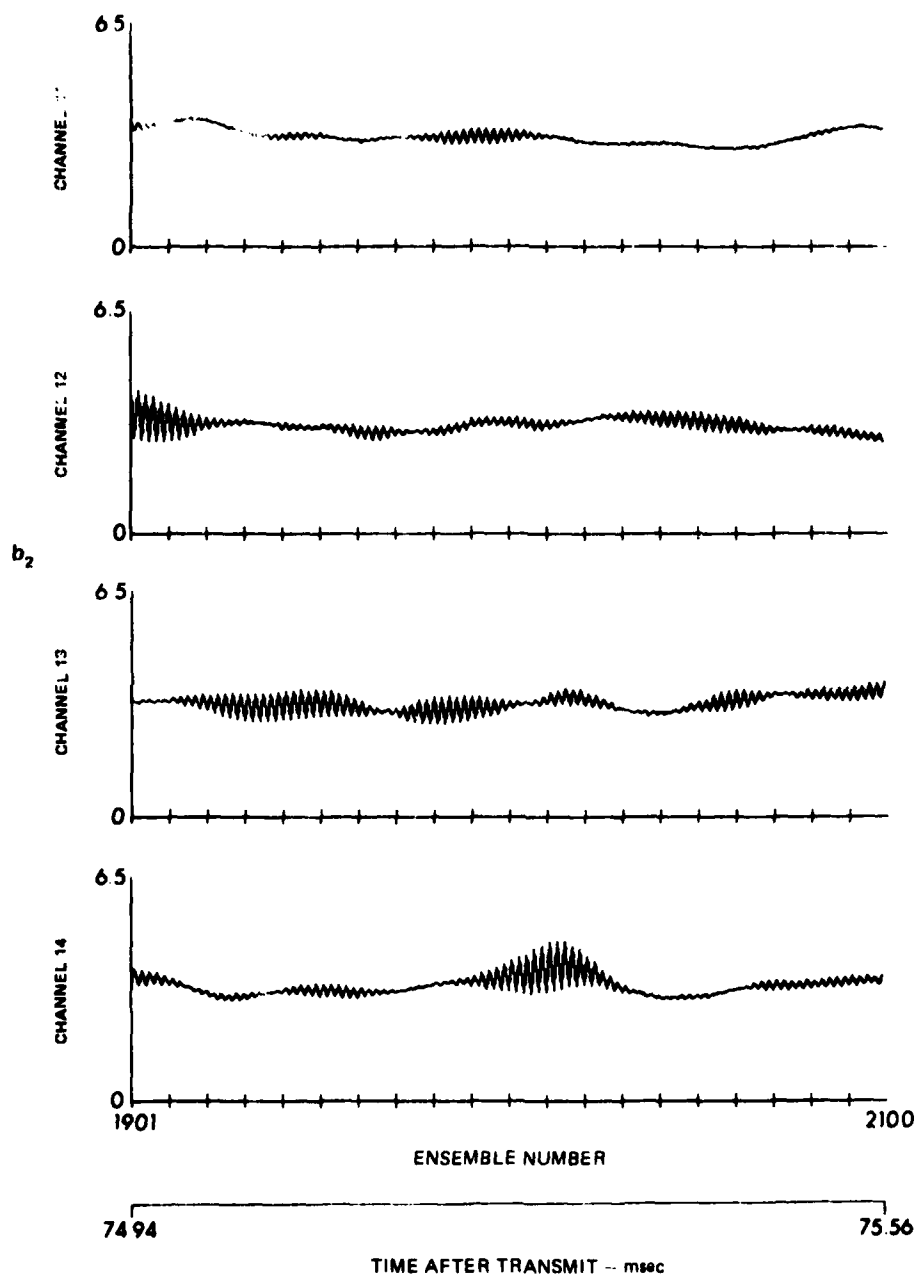
FIGURE V-16
SAMPLE KURTOSIS, CHANNELS 11-14

ARL·UT
AS·81·17
GRW·GA
1 9·81
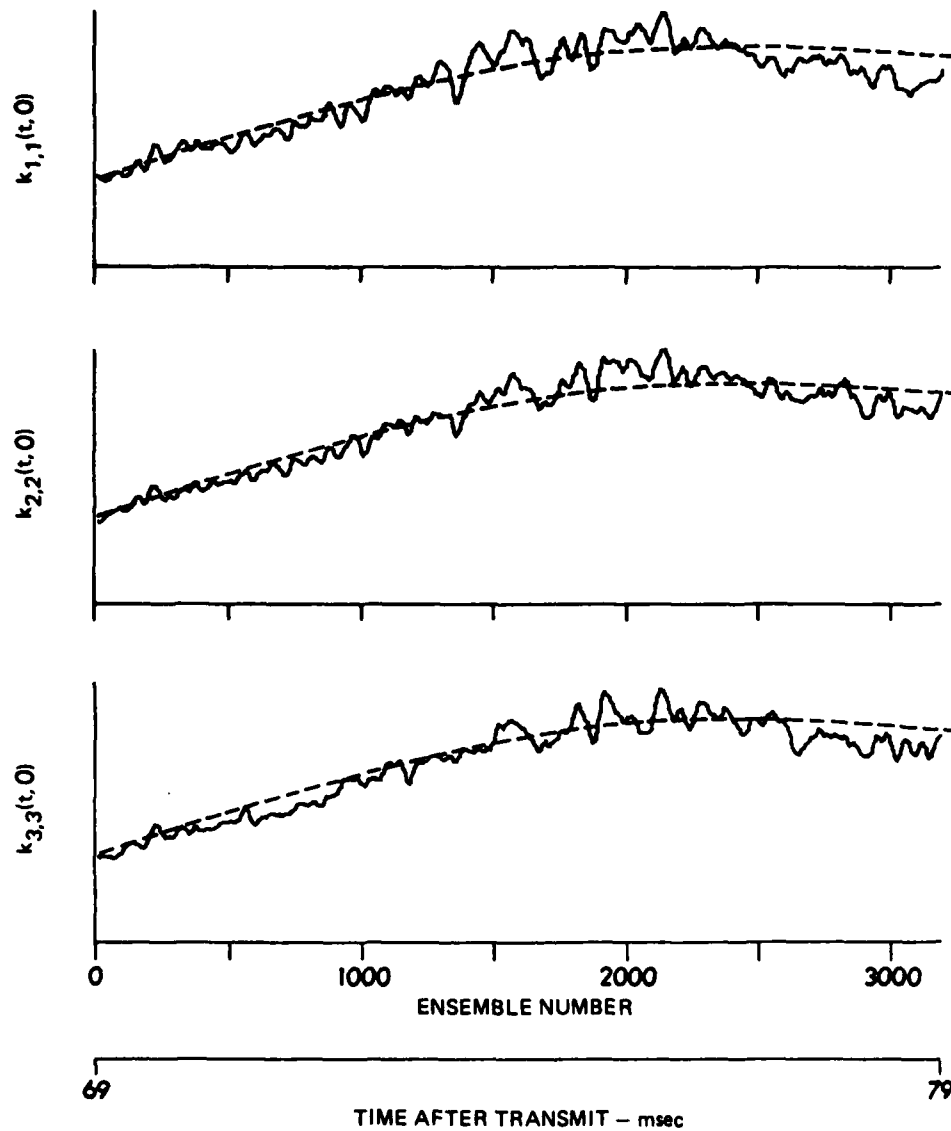
FIGURE V-17
COMPARISONS OF EXPERIMENTAL AND THEORETICAL VARIANCES
CHANNELS 1-3

——————— EXPERIMENTAL
– – – – – – THEORETICAL
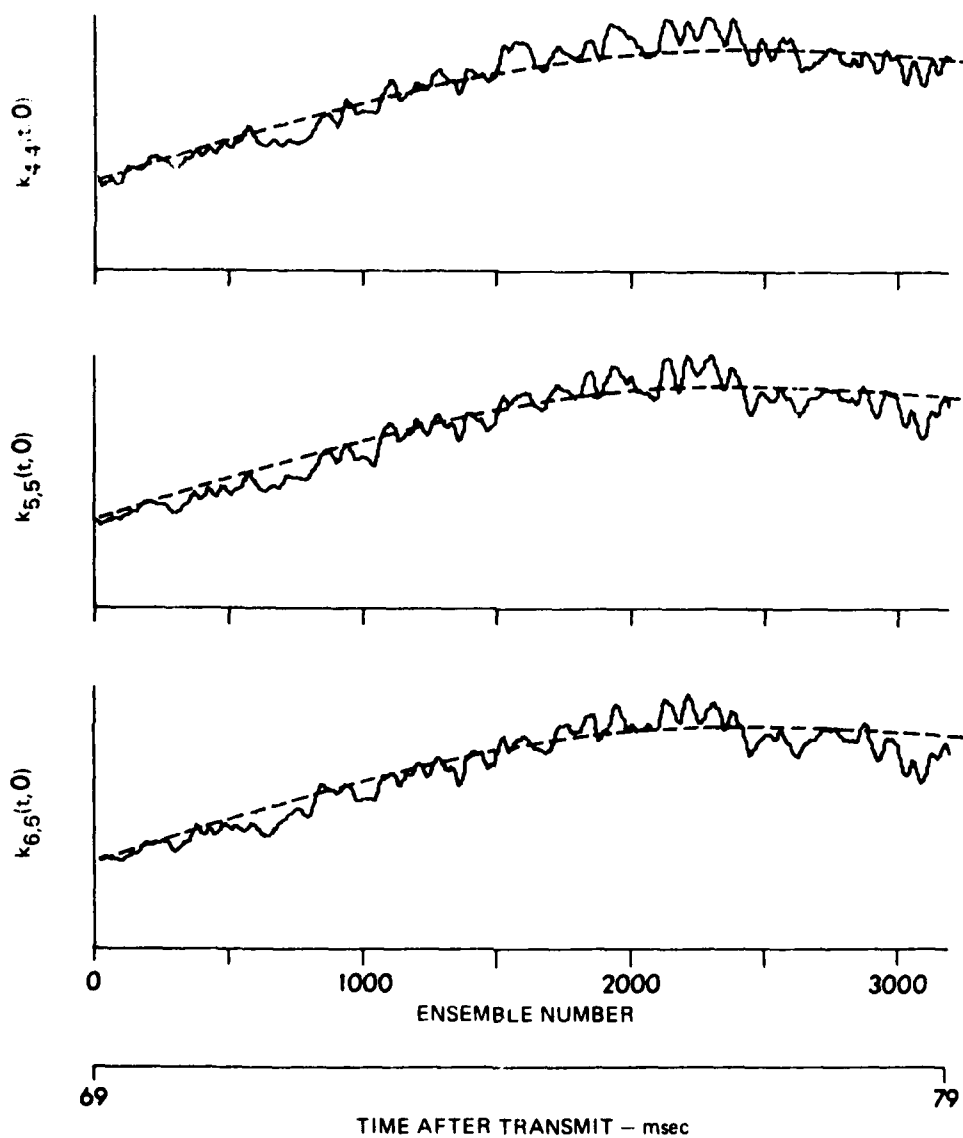
FIGURE V-18
COMPARISONS OF EXPERIMENTAL AND THEORETICAL VARIANCES
CHANNELS 4-6

——————— EXPERIMENTAL
— — — — — THEORETICAL
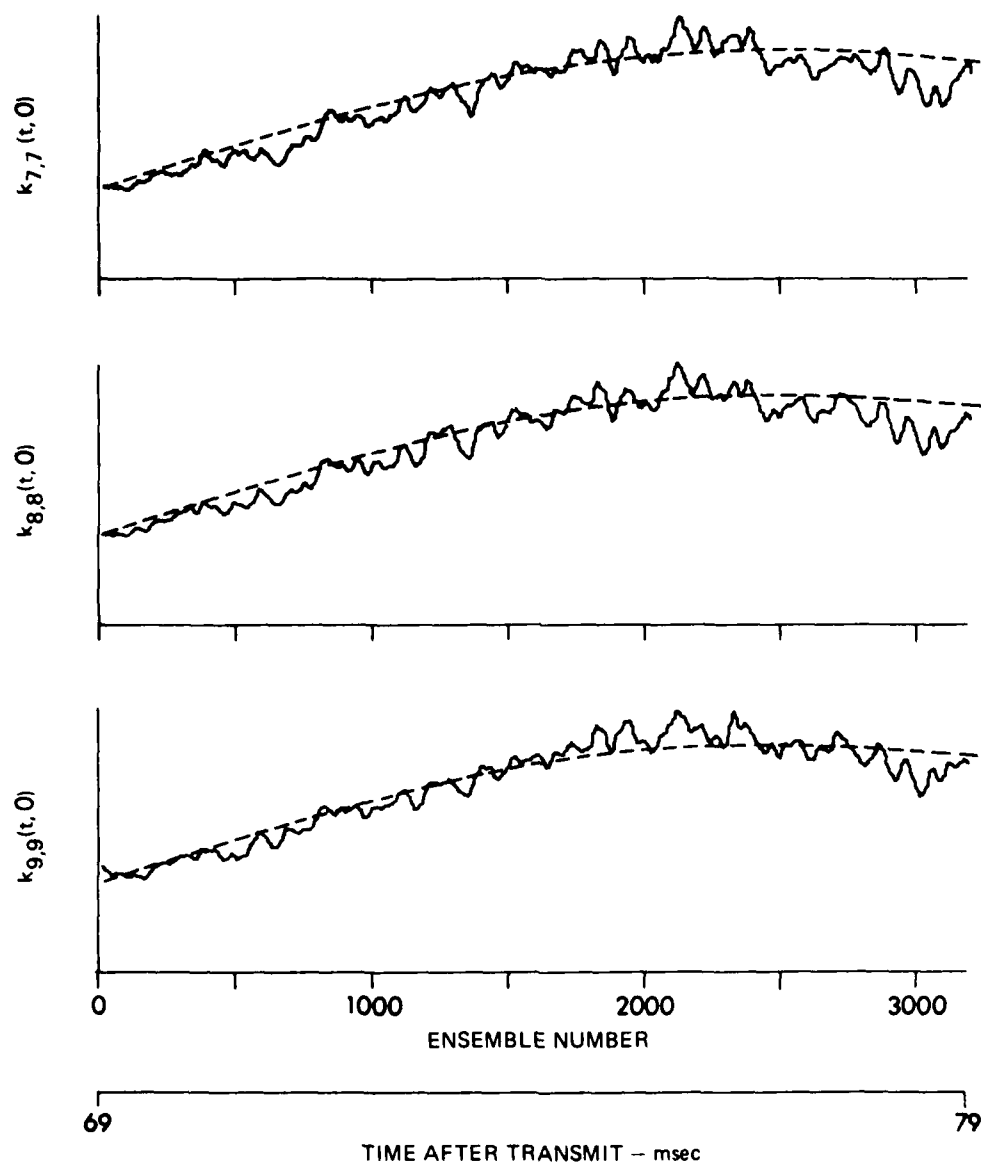
FIGURE V-19
COMPARISONS OF EXPERIMENTAL AND THEORETICAL VARIANCES
CHANNELS 7-9

———— EXPERIMENTAL
— — — — THEORETICAL
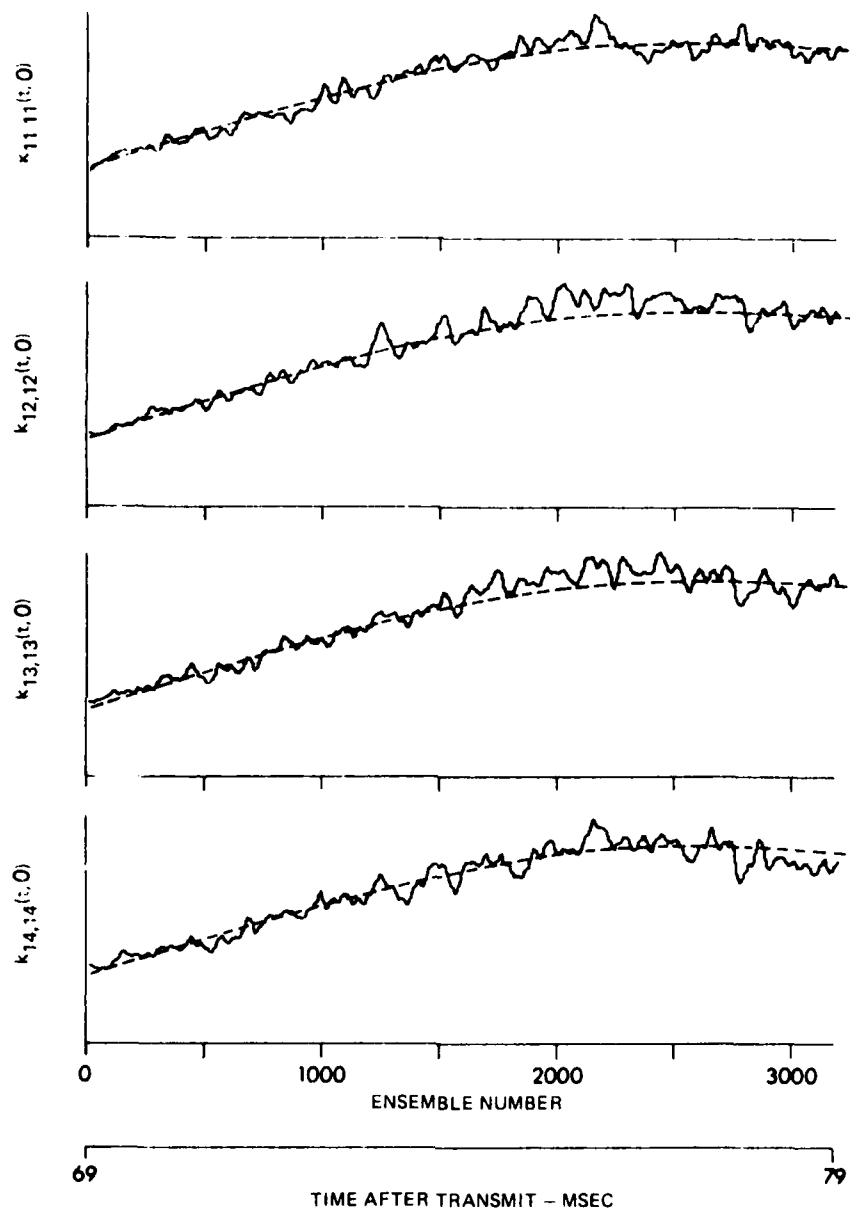
FIGURE V-20
COMPARISONS OF EXPERIMENTAL AND THEORETICAL VARIANCES
CHANNELS 11-14

——————— EXPERIMENTAL
— — — — — — THEORETICAL

digitized reverberation returns for all 13 channels. Also plotted is the theoretical difference component of the variance. Good agreement is attained between the sample and theoretical estimates. The fluctuations of the sample variance can be attributed to sampling errors due to the finite ensemble size.

Since the variance represents the intensity of the reverberation, most of the following analysis of the covariance was performed at a time when the variance was the largest in order to maximize the reverberation-to-ambient noise ratio. As can be seen from the plots, the reverberation intensity increases to a maximum during this 10 ms and then begins to decrease slightly by the end of the 10 ms data segment. This change in the intensity is due primarily to the vertical directivity of the projector. The time chosen for most of the covariance analysis was 75.25 ms after transmit, which is approximately the maximum of the reverberation intensity on each channel.

V.3.2 Auto-covariance

The sample estimates of the normalized envelopes $\tilde{e}_{ii}(t,\tau)$ and phases $\phi_{ii}(t,\tau)$ of the auto-covariances for the horizontal and vertical arrays are shown in Figs. V-21 and V-22. Observation of the auto-covariance permits examination of the dependence of the covariance on τ independently of its dependence upon spatial separation. The normalized auto-covariance envelope has, by definition, a maximum of 1 at $\tau=0$. Also an examination of the equations for the phase of the difference component shows that the phase must be zero at $\tau=0$.

It can be observed that the auto-covariance decreases to approximately zero for $\tau = \pm 250$ μs. It is usually stated that the
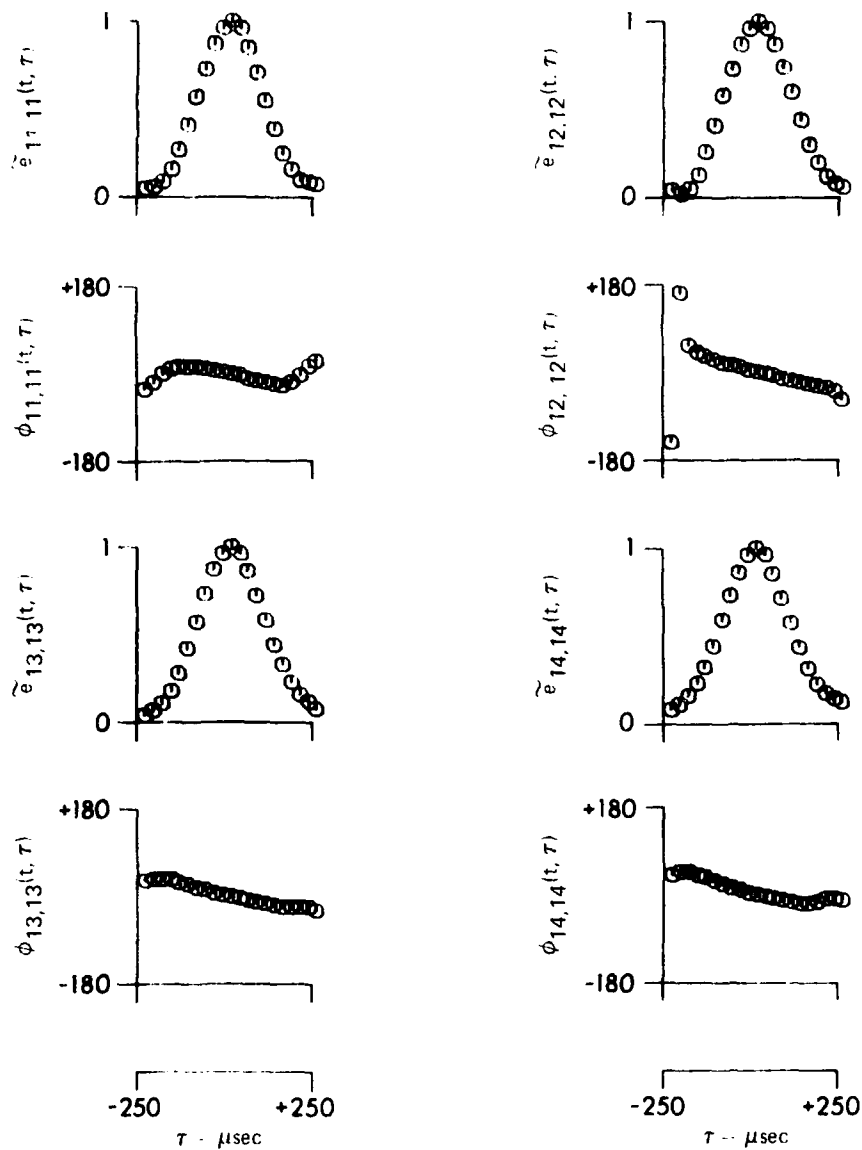
FIGURE V-21
NORMALIZED ENVELOPES AND PHASES OF SAMPLE ESTIMATES
OF THE AUTOCOVARIANCE OF THE HORIZONTAL RECEIVERS
AS A FUNCTION OF τ FOR t = 75.25 msec
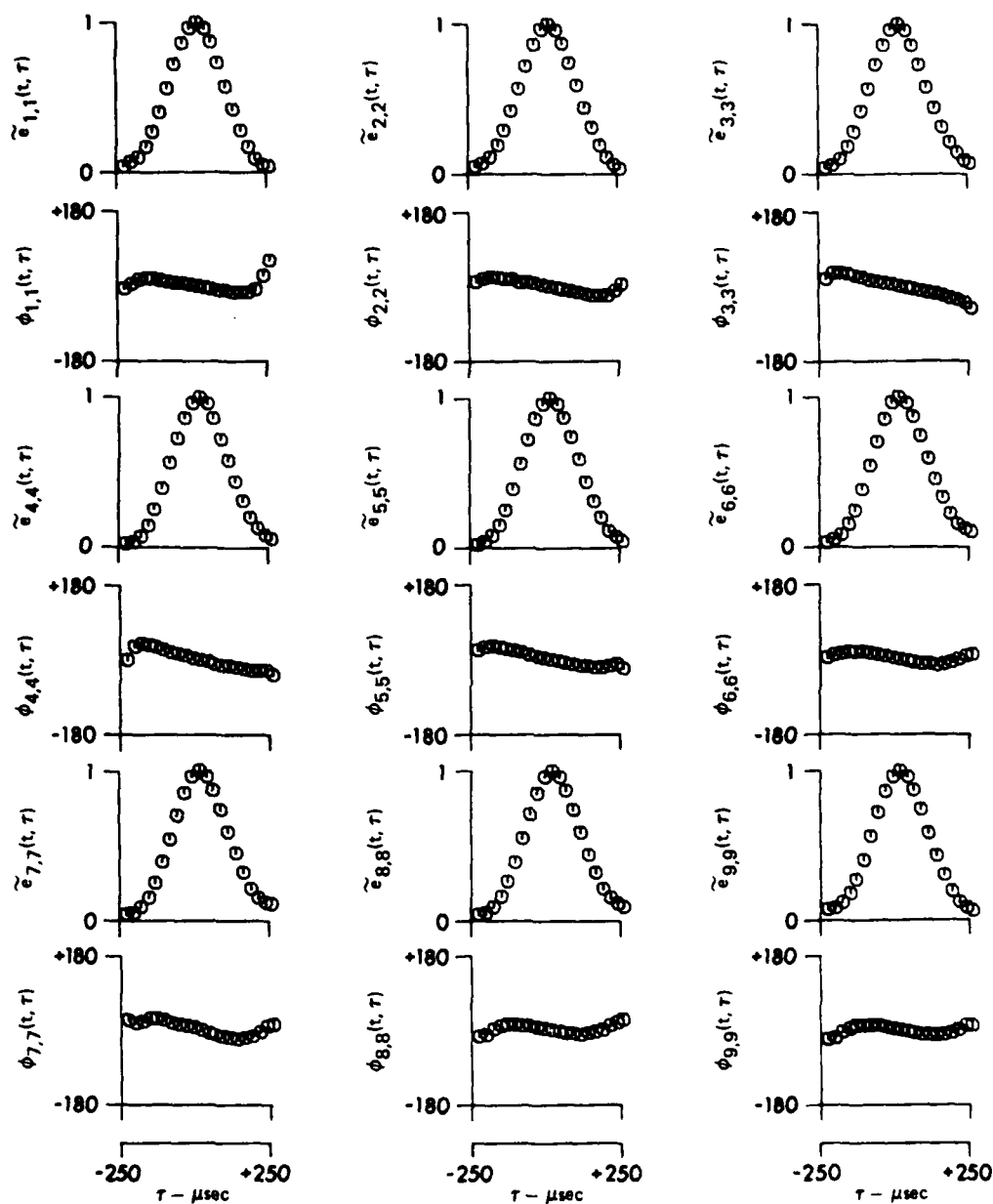
FIGURE V-22
NORMALIZED ENVELOPES AND PHASES OF SAMPLE ESTIMATES
OF THE AUTOCOVARIANCE OF THE VERTICAL RECEIVERS
AS A FUNCTION OF τ FOR t = 75.25 msec

covariance decreases to zero in a time interval equal to one pulse length. However, the covariance envelope has a value of about 0.5 at the time interval of 100 μs, the pulse length used in this study. This apparent discrepancy can be resolved by pointing out that the usual statement is valid only for extremely narrowband signals, i.e., long pulse lengths. For wider bandwidths, the frequency responses of the projector and receiver filter the transmitted signal more severely and result in an increase in the duration of the covariance beyond the time interval of one pulse length. The transmitted pulse, after being filtered by the projector and receivers, is represented by the waveforms $V_i(t_r)$ and is shown in Figs. III-1 and III-2 for all thirteen receivers. It can be seen that the envelope of the transmitted pulse has a duration of approximately 275 μs after being filtered. Thus it appears that the covariance decreases to zero in a time interval approximately equal to the length of the transmitted pulse after it has been filtered by the projector and receivers.

This effect has been observed by others.[16,17] Figure V-23 shows representative envelopes of the auto-covariance and the filtered transmitted signal for one receiver from Frazer[17] and from the present study. In both cases the pulse length was 100 μs; however, after being filtered, the durations of the transmitted pulses were different. The time interval of the auto-covariances are also different and in both cases correspond approximately to the length of the filtered transmitted pulses. This agreement tends to confirm the conclusion that the time interval of the covariance is related to the filtered transmitted pulse length. It also points out that a valid theory of the covariance of surface reverberation needs to take into account the
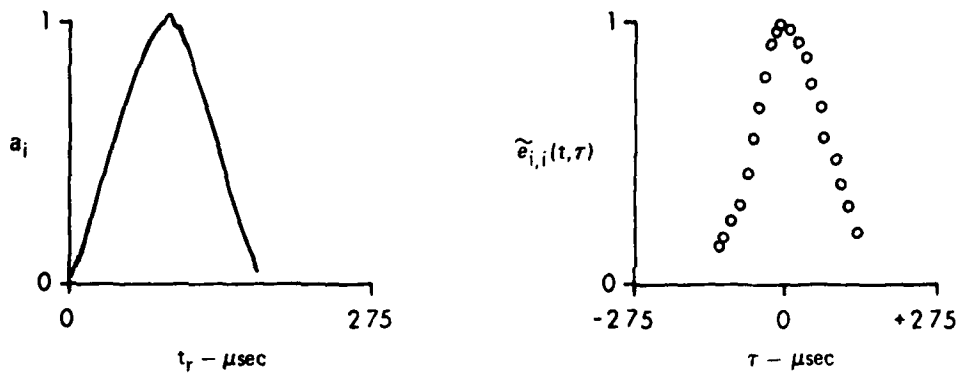
(a) $V_i(t_r)$ AND AN AUTOCOVARIANCE ENVELOPE FROM FRAZER
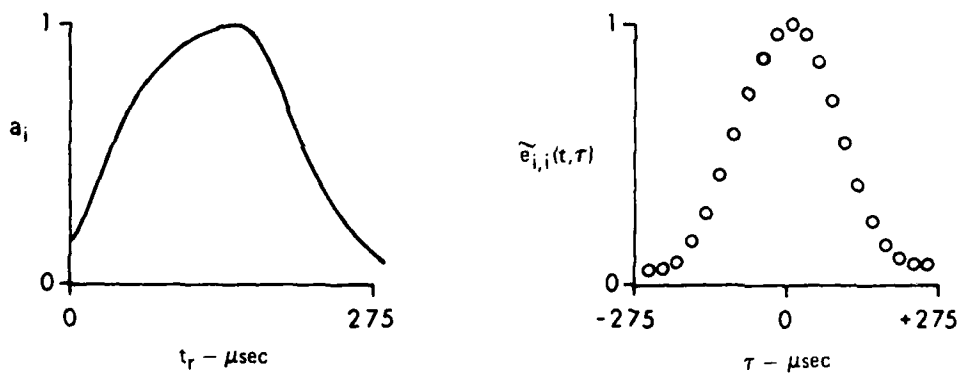
(b) $V_i(t_r)$ AND AN AUTOCOVARIANCE ENVELOPE FROM THE PRESENT STUDY

FIGURE V-23
A COMPARISON OF A REPRESENTATIVE WAVEFORM $V_i(t_r)$
AND A REPRESENTATIVE ENVELOPE $\widetilde{e}_{i,i}(t, \tau)$ OF THE
AUTOCOVARIANCE FROM FRAZER AND PRESENT STUDY

bandwidth and pulse length of the transmitted signal and the frequency responses of the projector and receivers.

The symmetry of the auto-covariance envelopes and phases in Figs. V-21 and V-22 is also of note. The envelopes have approximately even symmetry about $\tau=0$ while the phases exhibit an odd symmetry. These conditions are sufficient to specify the reverberation as being locally stationary, at least at this observation time t. A random process is locally stationary at the time t if the auto-covariance is an even function of τ, i.e.,

$$k_{ii}(t,\tau) = k_{ii}(t,-\tau)\qquad.$$

The local stationarity of reverberation from short pulsed CW transmissions has also been previously demonstrated.[16]

Figures V-24 and V-25 are similar to Figs. V-21 and V-22 but in addition include the theoretical estimates of the envelopes and phases of the auto-covariances. As can be seen, excellent agreement between the theoretical and experimental estimates is obtained for both the envelopes and the phases. This is true of both the horizontal and vertical arrays. In particular, the time extent of the auto-covariance predicted by the model is in good agreement with the experimental results. Thus it appears that at least in this case the model is correctly taking into account the bandwidth, pulse length, and frequency responses of the projector and receivers. Similar excellent agreement has been obtained previously for a horizontal array using the same model.[17] This confirmation provides increased confidence in the model for the cases examined.

There appears to be some similarity between the phases of the auto-covariance and the phases of the waveforms $V_i(t_r)$ in Figs. III-1
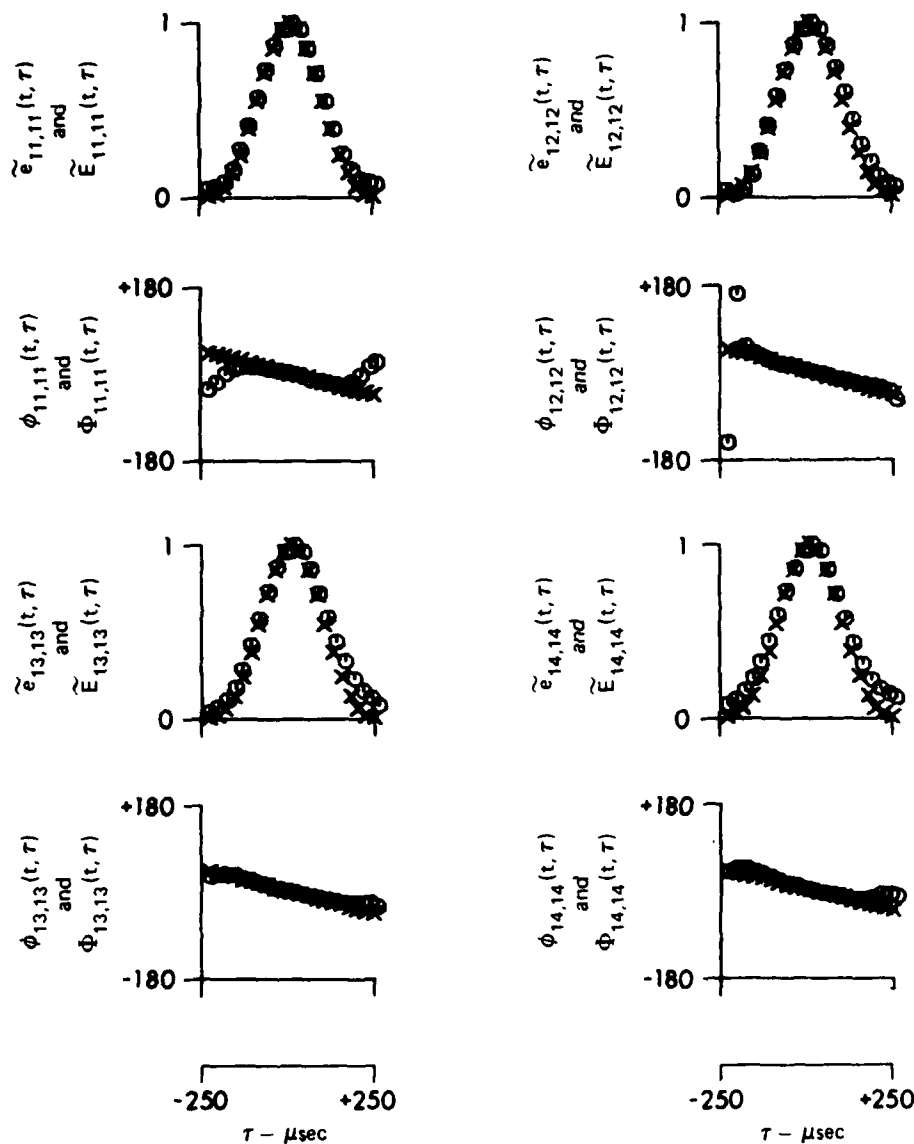
FIGURE V-24

COMPARISONS OF NORMALIZED ENVELOPES AND PHASES OF SAMPLE
ESTIMATES AND THEORETICAL ESTIMATES OF THE AUTOCOVARIANCE
OF THE HORIZONTAL RECEIVERS AS A FUNCTION OF τ FOR t = 75.25 msec

O – SAMPLE ESTIMATE
X – THEORETICAL ESTIMATE

FIGURE V-25
COMPARISONS OF NORMALIZED ENVELOPES AND PHASES OF
SAMPLE ESTIMATES AND THEORETICAL ESTIMATES OF THE
AUTOCOVARIANCE OF THE VERTICAL RECEIVERS
AS A FUNCTION OF τ FOR t = 75.25 msec

O – SAMPLE ESTIMATE
X – THEORETICAL ESTIMATE

ARL:UT
AS-81-142
GRW - GA
2 - 24 - 81

and III-2. The similarity is more apparent for the theoretical

estimates and to a lesser extent for the experimental estimates. The

actual magnitudes of the phases of $V_i(t_r)$ are not reflected in the phases

of the auto-covariances, but rather the change in phase during the

extent of $V_i(t_r)$. The shift of the phases of $V_i(t_r)$ for the different

receivers of the vertical array represents the slight path length

differences from the sphere to the vertical receivers; the horizontal

receivers exhibit no such shifts since their closer spacing resulted

in insignificant path length differences when pointed directly at the

sphere. This shift in the phases for the vertical array is not observable

in the phases of the auto-covariances of the vertical array. However,

the changes in phase during the extent of the waveforms $V_i(t_r)$ can be

correlated with similar changes in phase during the extent of the auto-

covariances of the same channels. Considering the dependence of the

theoretical model upon the waveforms $V_i(t_r)$, the similarity of the

phases of $V_i(t_r)$ and the phases of the theoretical estimate of the

auto-covariances is not too surprising. Some of the experimental esti-

mates of the phase appear to also have shapes similar to their corre-

sponding phases for $V_i(t_r)$, but some do not. Although Frazer has reported

a noticeable similarity between the experimental phases of the auto-

covariance and the phases of $V_i(t_r)$,[17] the present data do not con-

clusively show this similarity.

To this point, the auto-covariances have been examined

as a function of τ only at one time t. Figure V-26 shows the auto-

covariance for channel 1 as a function of both t and τ over the entire

10 ms of digitized reverberation. Both the unnormalized envelope

$e_{1,1}(t,\tau)$ and the normalized envelope $\tilde{e}_{1,1}(t,\tau)$ are shown, along with
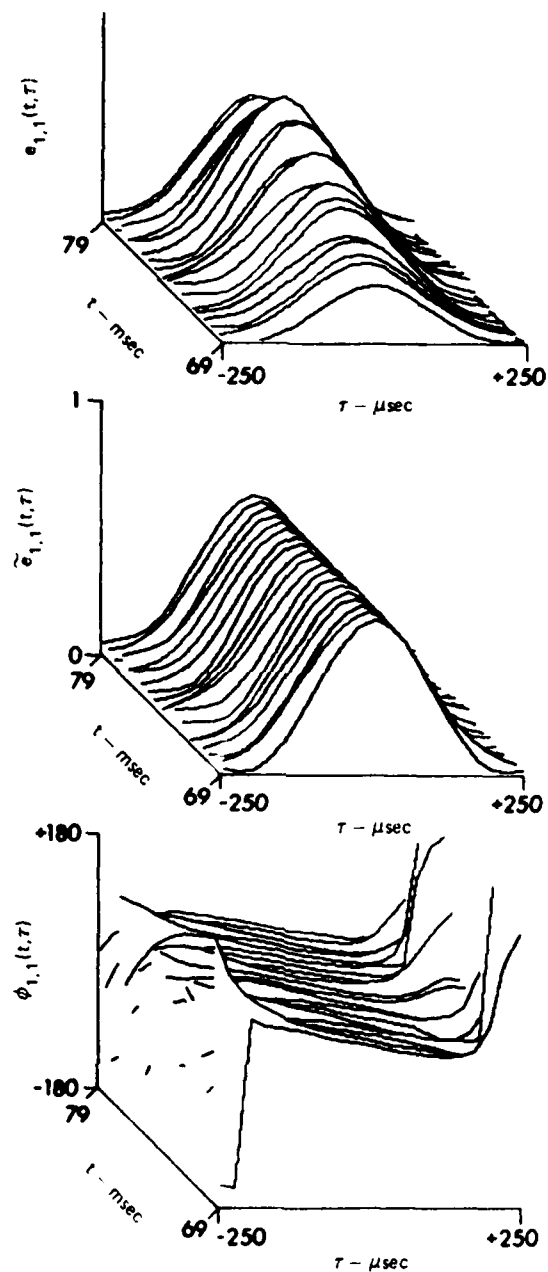
FIGURE V-26
UNNORMALIZED AND NORMALIZED ENVELOPES AND PHASES
OF SAMPLE ESTIMATES OF THE AUTOCOVARIANCE OF
CHANNEL 1 AS A FUNCTION OF t AND τ

the phase $\phi_{1,1}(t,\tau)$. The unnormalized envelope demonstrates the change

in reverberation intensity during the 10 ms interval. The maximum of

the unnormalized covariance increases with time for most of the interval

before it begins to decrease again toward the end. This change has been

observed in the variance shown previously. The change is due to the

vertical directivity of the projector. That is, the reverberation

returns from the earlier times are caused by scattering from the surface

which is illuminated from an off-axis angle of the projector's vertical

directionality response. Thus the reverberation intensity is less. As

time increases, the surface which is illuminated by the on-axis, or

maximum, vertical response of the projector begins to contribute to the

reverberation return, resulting in an increase in reverberation intensity.

The grazing angle between the projector and surface at the earliest time

of 69 ms is 11.2 degrees, decreasing to 9.8 degrees at 79 ms. The change

in angle is 1.4 degrees, which is less than the vertical beamwidth of

the projector. Thus the entire digitized reverberation return was

caused by scattering only from the main lobe of the projector. It

should be noted that spreading losses and the vertical directionality

of the receiver will also affect the change in reverberation intensity

with time. However, these effects were insignificant for the period

of time which is observed here.

　　　　This change in the covariance with time points out one

form of non-stationarity which reverberation characteristically has.

A random process is said to be wide-sense stationary in an interval if

its auto-covariance is a function only of τ within an interval of time,

i.e.,

$$k_{ii}(t,\tau) = k_{ii}(\tau) \quad , \quad t_1 \leq t \leq t_2 \quad .$$

It is obvious from Fig. V-26 that the unnormalized auto-covariance
changes with time; thus it is not wide-sense stationary. However, the
unnormalized auto-covariance does appear to represent a locally
stationary process at each time due to the symmetry of its envelope and
phase about τ at each time. Even though the unnormalized covariance
is not wide-sense stationary, it does exhibit one property of a wide-sense
stationary process: the covariance has its maximum at $\tau=0$ for each
time t. On the other hand, the normalized auto-covariance does appear
to represent a wide-sense stationary process over the interval
69 ms $\leq$ t $\leq$ 79 ms since the normalized envelope and phase change little
in this interval. If the unnormalized auto-covariance $k_{ii}(t,\tau)$ repre-
sents a random process $X_i(t)$, then the normalized auto-covariance
represents a normalized random process $\widetilde{X}_i(t)$, where

$$\widetilde{X}_i(t) = \frac{X_i(t)}{\sqrt{k_{ii}(t,0)}} \quad .$$

Thus this technique for normalizing the random process $X_i(t)$ has, in
this instance, removed much of its non-stationarity. This need not
be the case in general though. In particular, Fig. V-26 displays only
the difference component of the covariance. The actual covariance may
be non-stationary, even when normalized, due to contributions from
the sum term.[56]

V.3.3   The Covariance for $\tau=0$

The previous sections have analyzed the temporal depen-
dence of the variance and auto-covariance. The spatial dependence of

the covariance is addressed in this section, and the joint spatial-
temporal covariance is discussed in the following section. The spatial
covariance for the horizontal array is presented first, followed by the
vertical spatial covariance.

The envelope of the normalized covariance between the
horizontal elements at $\tau=0$ as a function of spatial separation of the
elements is shown in Fig. V-27. The envelope of the covariance
decreases rather significantly within a spatial separation of just a
few wavelengths. In fact, the envelope has decreased to a value of 0.1
in just over four wavelengths.

It is of interest to quantify the error associated with
the sample estimate of the covariance due to the finite sample size.
The sampling variance of the normalized covariance is given by[51]

$$\text{var}(\tilde{k}_{i,j}) = \frac{\kappa_{i,j}^2}{N} \left\{ \frac{\mu_{22}}{\mu_{11}^2} + \frac{1}{4} \left(\frac{\mu_{40}}{\mu_{20}^2} + \frac{\mu_{04}}{\mu_{02}^2} + \frac{2\mu_{22}}{\mu_{20}\mu_{02}} \right) \right.$$

$$\left. - \left(\frac{\mu_{31}}{\mu_{11}\mu_{20}} + \frac{\mu_{13}}{\mu_{11}\mu_{02}} \right) \right\}$$

where
$$\mu_{rs} = \left\langle (v_i - \mu_1'(i))^r (v_j - \mu_1'(j))^s \right\rangle$$

and
$$\kappa_{i,j} = \frac{\mu_{11}}{\sqrt{\mu_{20}\mu_{02}}} \quad .$$

The time dependence has been suppressed for compactness of notation. If
either r or s is zero, then the bivariate population moment μ_{rs}
reduces to its corresponding univariate moment. The usual procedure

FIGURE V-27
COMPARISON OF THE THEORETICAL AND EXPERIMENTAL DEPENDENCE
OF THE ENVELOPE OF THE NORMALIZED COVARIANCE ON SPATIAL
SEPARATION FOR THE HORIZONTAL ARRAY

$\tau = 0$

$t = 75.25$ msec

1.0

1.1

1.25 1.4 1.6

2.8 2.5

2.2

2.0

1.8
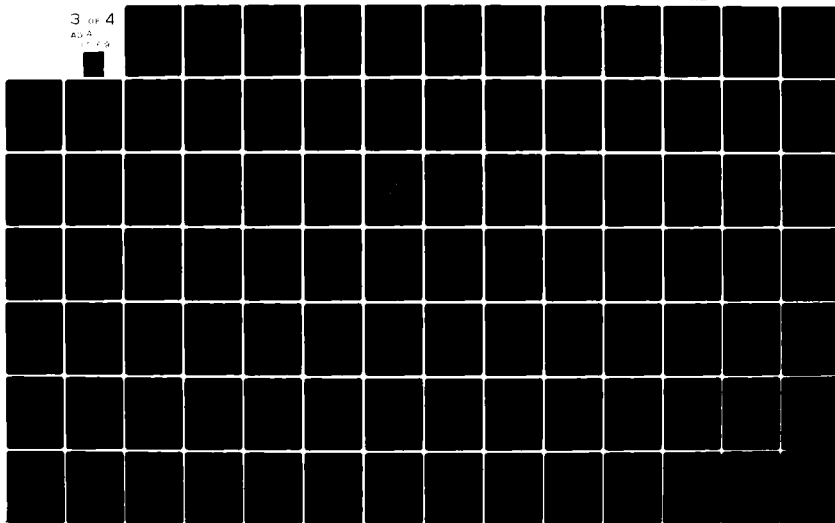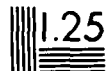
when the population moments are unknown is to replace the population

moments with their sample estimates m_{rs} in order to evaluate the sample

variance. In the present study, the sample moments m_{22}, m_{31}, and m_{13}

have not been calculated. However if the joint random processes are

jointly normal, then

$$var(\widetilde{k}_{i,j}) = \frac{1}{N} (1-\kappa^2_{i,j})^2 \quad ,$$

which can be approximated as

$$var(\widetilde{k}_{i,j}) = \frac{1}{N} (1-\widetilde{k}^2_{i,j})^2 \quad .$$

The standard deviation of the sample estimate of the normalized co-

variance is just the square root of the sampling variance. Even though

the present data are not normal, this normal approximation was used

to quantify the sampling errors.

The error bars in Fig. V-27 represent one standard de-

viation of the sample estimate above and below the measured envelope of

the covariance. Since the envelopes of the covariance from the four

largest separations are all within one standard deviation of the value

of 0.1, no statistical significance can be placed upon the changes in

the envelope at these separations. However, it is significant to note

that the envelope remains at 0.1 instead of going to zero at these

separations.

Theoretical estimates of the envelope of the covariance

were made at the first three separations and are also shown in Fig. V-27.

It can be seen that good agreement is obtained at these separations

between the experimental and theoretical estimates. Theoretical esti-

mates were not made at the larger separations due to the significant increase in computer cost required to make the numerical integrations converge at these separations.

Similar agreement between the theoretical and experimental estimates of the horizontal covariance has been obtained by Frazer using the same theoretical model.[17] However, Frazer obtained larger values of covariance than were obtained in the present study. The theoretical and experimental results from Frazer and the present study are compared in Fig. V-28. At a separation of 0.05 m, for example, Frazer obtained a covariance envelope of 0.6 while 0.3 was obtained in the present study. It is significant to note that the theoretical model correctly predicted the envelope of the covariance in both cases, even though the values were significantly different. This is an indication that the model is correctly taking into account the experimental differences which caused these significantly different results. It is felt that the wider horizontal transmit beamwidth used in the present study was the primary factor which resulted in the smaller values of covariance. The present study employed a horizontal transmit beamwidth of 15 degrees, compared to 10 degrees used in Frazer's experiment. The wider beamwidth insonifies more "off-axis" scatterers on the surface, which tends to decrease the covariance between horizontal receivers. Thus these results from the present study tend to confirm the results obtained by Frazer.

Figure V-27 showed the covariance as a function of spatial separation at only one time t. It is also of interest to know

FIGURE V-28
COMPARISON OF THE THEORETICAL AND EXPERIMENTAL DEPENDENCE OF THE
ENVELOPES OF THE NORMALIZED COVARIANCE ON SPATIAL SEPARATION
FOR THE HORIZONTAL ARRAYS OF WILSON AND FRAZER
$\tau = 0$

if there is any significant change in the spatial covariance over the

10 ms observation interval. Figure V-29 shows the envelopes of the

normalized covariance at $\tau=0$ as a function of time for the six separa-

tions of the horizontal array. It can be observed that the envelope

of the covariance does not change significantly over the 10 ms interval

for each separation. The random fluctuations which are present are

all less than two standard deviations of the mean value of the envelope

over the interval; thus any apparent changes can be attributed to

sampling errors due to the finite sample size of the ensembles. Since

the envelopes do not change significantly with time, the spatial depen-

dence demonstrated in Fig. V-27 for one time will be approximately

the same for all other times in the 10 ms interval.

The actual covariance is determined not only by the

envelope but also by the phase. Figure V-30 contains plots of the phase

of the covariance at $\tau=0$ as a function of time for each of the six

separations of the horizontal array. The most obvious feature to note

is that the separations which have significantly non-zero values for

the envelopes also have phases which are constant with time, whereas

the separations with small envelope values appear to have phases which

change approximately linearly with time. Specifically, $\phi_{13,14}(t,0)$ and

$\phi_{11,12}(t,0)$, representing separations of 2.5 and 5.0 cm respectively,

are reasonably constant with time, while the other phases change sig-

nificantly. It can also be observed that the four phases which change

are all very similar, i.e., they all begin at approximately 180 degrees

and decrease linearly at about the same rate.
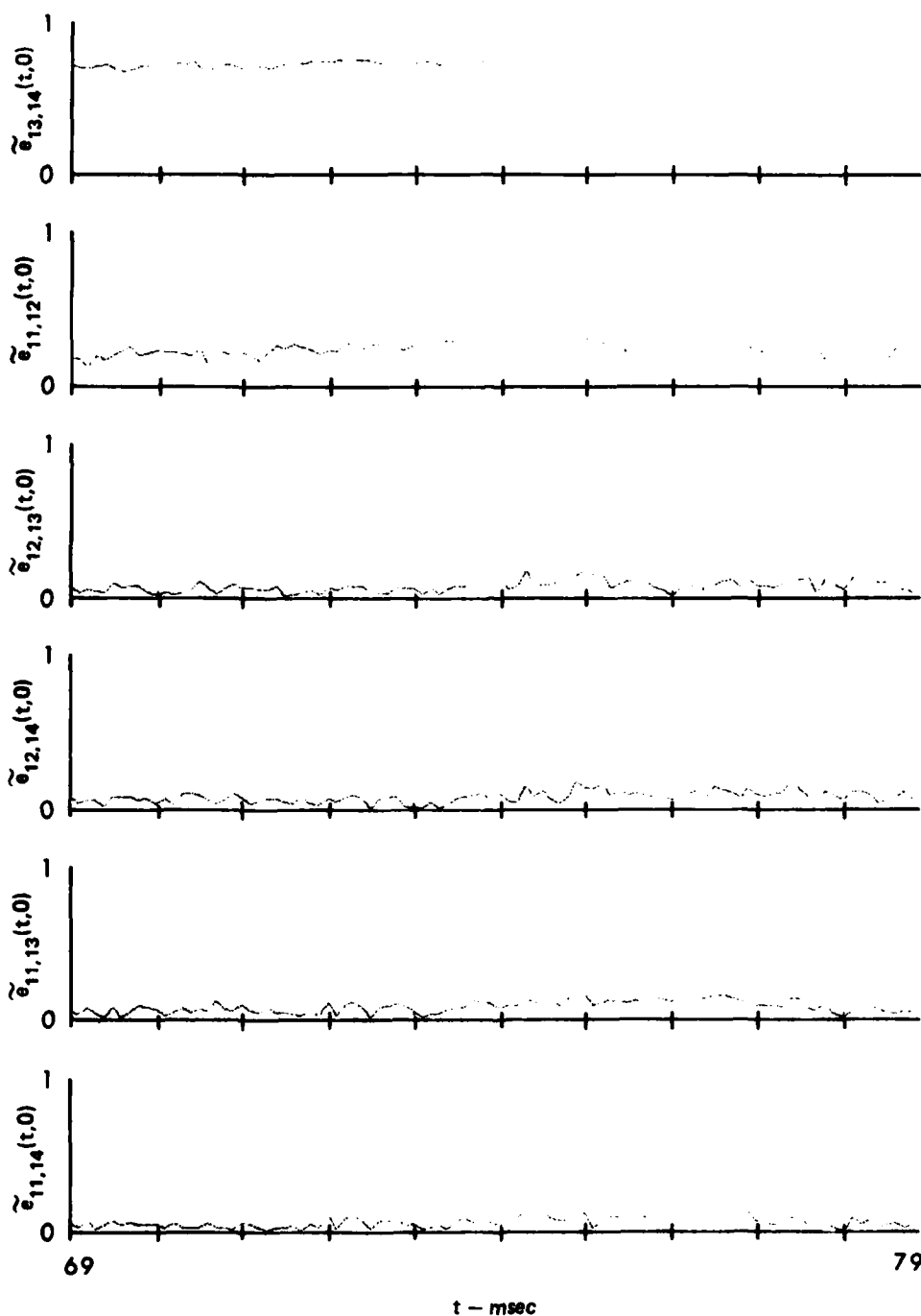
FIGURE V-29
THE DEPENDENCE OF THE EXPERIMENTAL ENVELOPES
OF THE NORMALIZED COVARIANCE ON TIME AT $\tau = 0$
FOR THE HORIZONTAL ARRAY
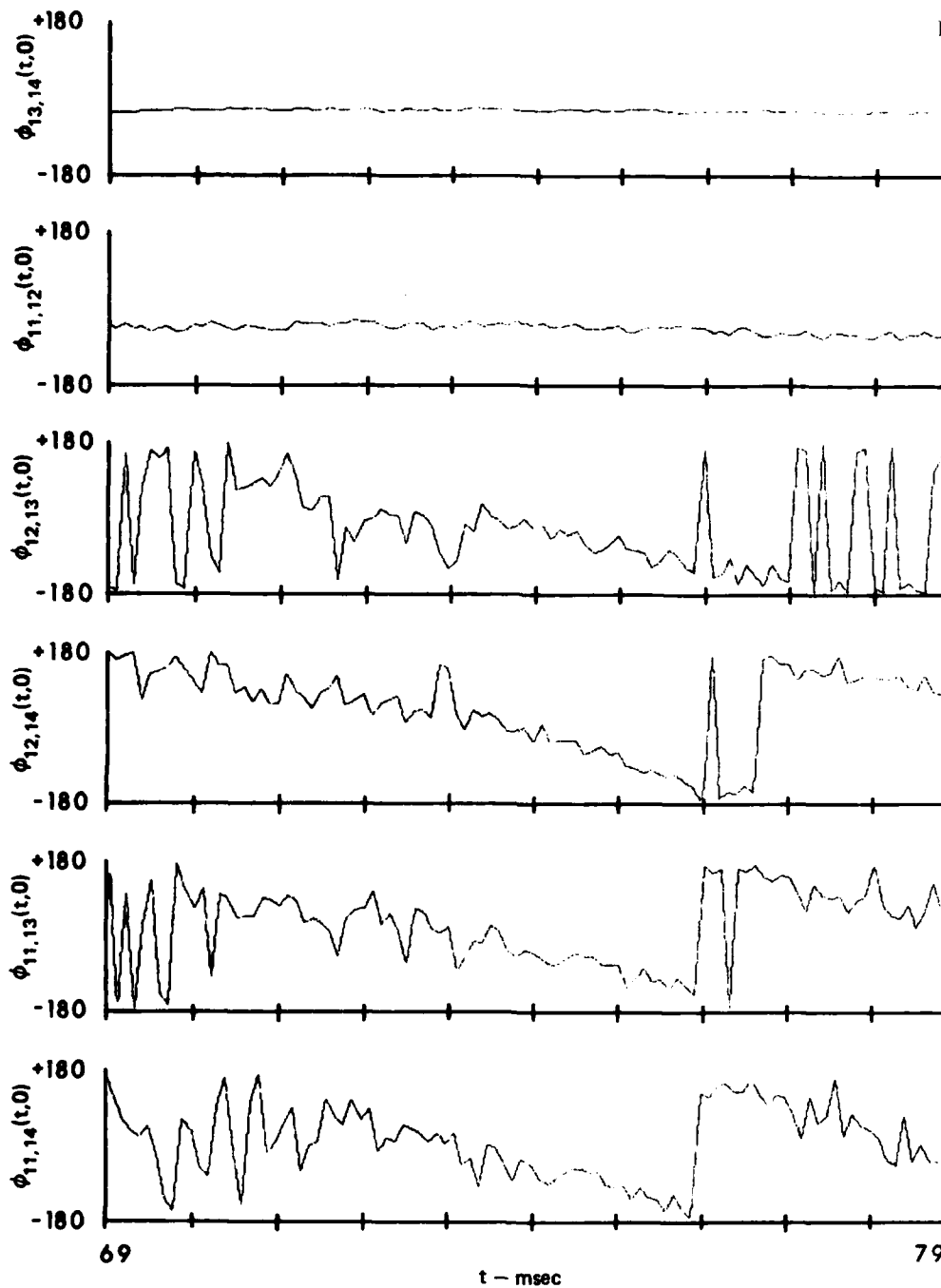
FIGURE V-30
THE DEPENDENCE OF THE EXPERIMENTAL PHASES OF
THE NORMALIZED COVARIANCE ON TIME AT $\tau = 0$
FOR THE HORIZONTAL ARRAY

A non-zero phase implies that the effective scattering
center is off-axis azimuthally, indicating a non-uniform surface scatter
density in the azimuthal angle. A change in the phase of the horizontal
covariance with time is indicative of a change in the bearing angle
to the effective scattering center with range; thus the scatter density
changes with range as well. However, it is curious that this change in
phase with range is only noticeable at the larger separations, which
have smaller values of covariance. One possible explanation is that
some sort of secondary scattering is occurring which is causing the
effects described here, but is observable only when the covariance from
the primary scattering is negligible. However, at this point no
mechanism for secondary scattering which would account for these effects
is known. It should be noted that this change in phase with time was
also observed by Frazer.[17] Also of note is the fact that while
$\phi_{13,14}(t,0)$ and $\phi_{11,12}(t,0)$ are constant with time, they are also
non-zero, indicating a non-uniform surface scatter density. Thus
for the significant levels of covariance, the actual covariance is
somewhat less than the envelope of the covariance and does not change
significantly with time over the observed interval.

Theoretical estimates of the envelope and phase of the
normalized covariance as a function of time for $\tau=0$ have also been made
at three horizontal separations, and are compared with the experimental
results in Figs. V-31 and V-32. The theoretical envelope values are
almost constant throughout the 10 ms interval. The envelopes $\widetilde{E}_{11,12}(t,0)$
and $\widetilde{E}_{13,14}(t,0)$ are consistently slightly larger than the experimental
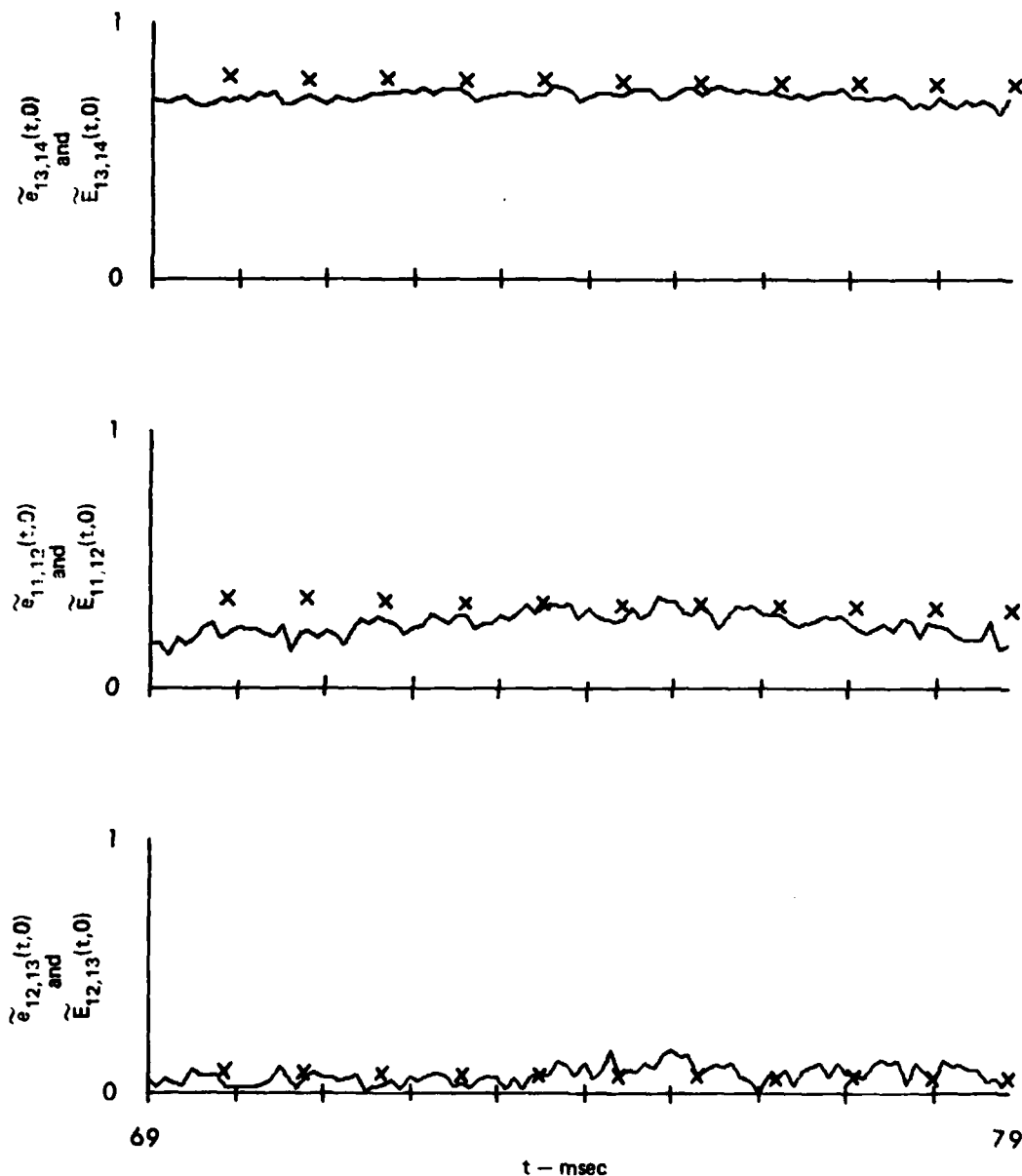
FIGURE V-31
COMPARISON OF THE THEORETICAL AND EXPERIMENTAL
DEPENDENCE OF THE ENVELOPES OF THE NORMALIZED
COVARIANCE ON TIME AT $\tau = 0$ FOR
THE HORIZONTAL ARRAY

—— EXPERIMENTAL
✕ THEORETICAL
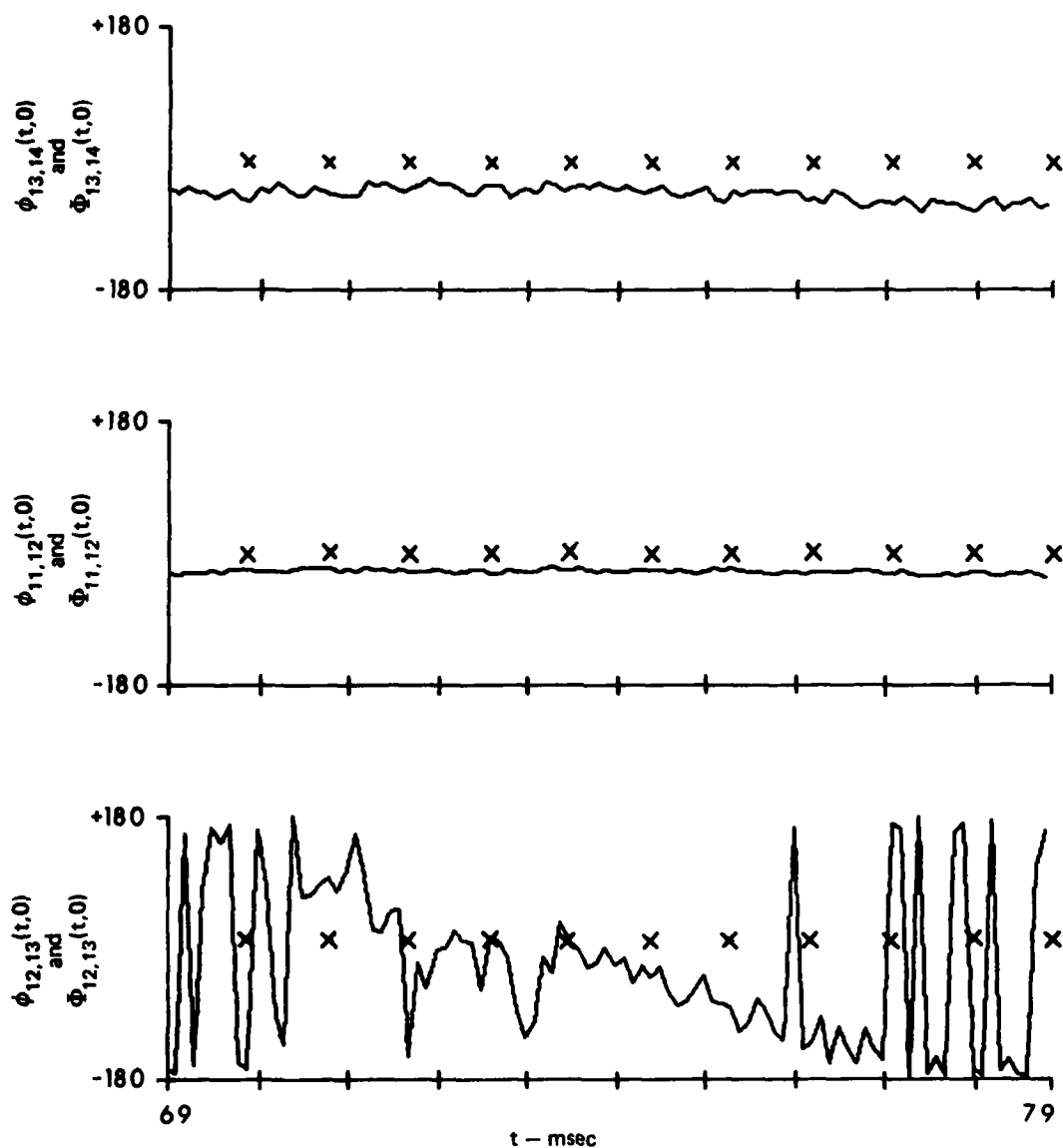
FIGURE V-32
COMPARISON OF THE THEORETICAL AND EXPERIMENTAL
DEPENDENCE OF THE PHASES OF THE NORMALIZED
COVARIANCE ON TIME AT $\tau = 0$ FOR
THE HORIZONTAL ARRAY

—— EXPERIMENTAL
✕ THEORETICAL

values, but the agreement is still good. $\tilde{E}_{12,13}(t,0)$ agrees very well with the experimental results.

The theoretical phases are also constant over the 10 ms interval. In fact, the phases are all very close to zero for the three separations. This is to be expected since the model assumes a uniform scatter density at the surface. As has already been stated, the phases $\phi_{11,12}(t,0)$ and $\phi_{13,14}(t,0)$ are also constant with time but different from zero. Thus the covariance predicted by the model will be greater than the experimental covariance, even though the theoretical and experimental envelopes agreed well, because the magnitudes of the experimental phases were greater than the theoretical phases. It should also be noted that the mechanism causing $\phi_{12,13}(t,0)$ to change with time is completely unaccounted for in the model.

The previous discussion has examined only the horizontal spatial dependence of the covariance. In a similar manner, the spatial dependence of the covariance for the vertical array will now be presented. Figure V-33 displays the envelope of the normalized covariance at $\tau=0$ as a function of spatial separation for the vertical array. Unlike the horizontal array, some pairs of elements have identical spacings. Thus more than one value of the envelope of the covariance occurs at some separations. It is of interest to determine if the covariance at a specified separation is dependent upon the position of the elements on the vertical array. As an indication of this dependence, error bars representing one standard deviation of the sample covariance above and below the mean envelope value at each separation are provided
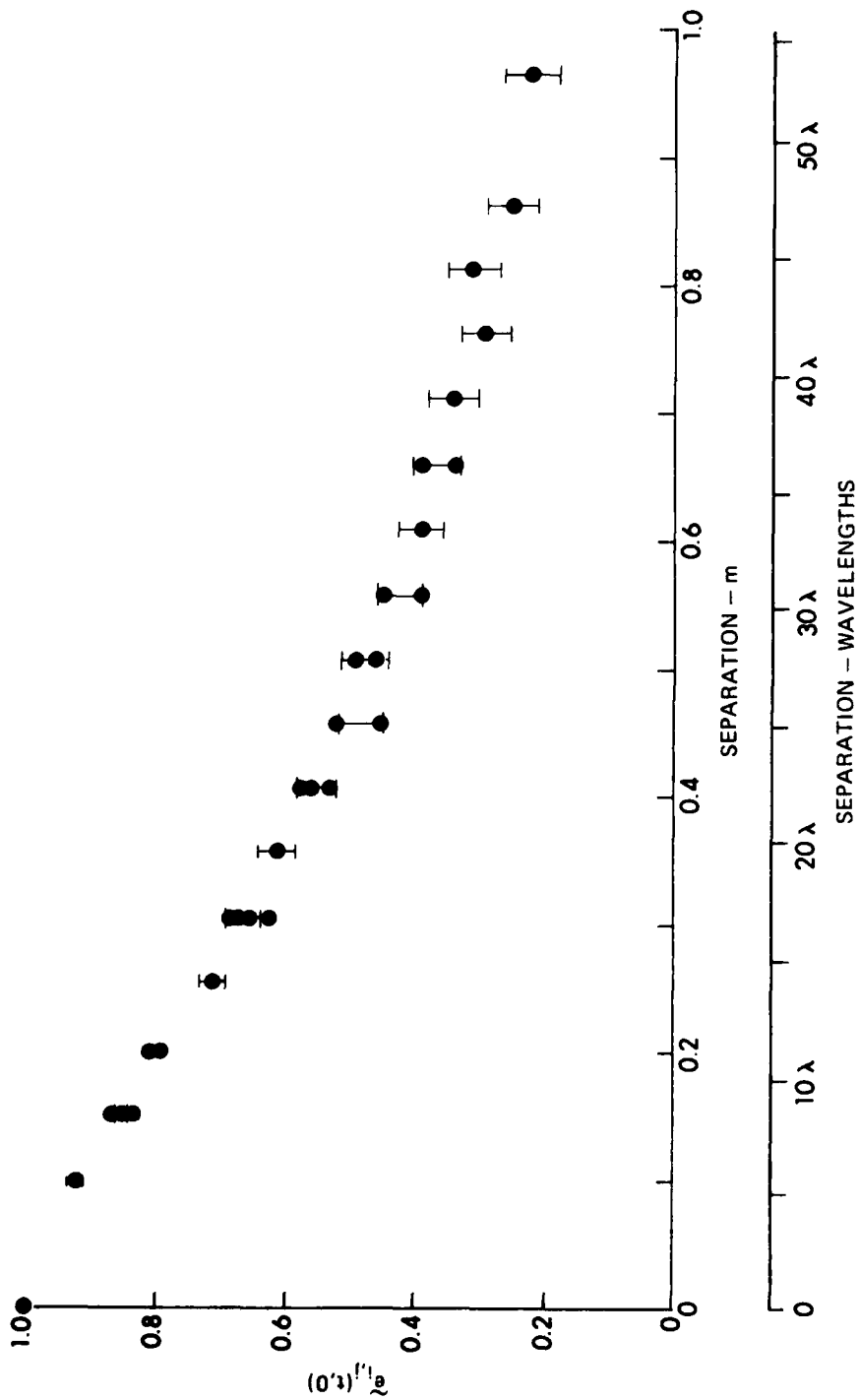
FIGURE V-33

THE DEPENDENCE OF THE EXPERIMENTAL ENVELOPE OF THE NORMALIZED
COVARIANCE ON SPATIAL SEPARATION FOR THE VERTICAL ARRAY

$\tau = 0$

$t = 75.25$ msec

on the plot in Fig. V-33. Most values of the envelope are within one

standard deviation of the mean value at each separation. They are all

certainly within two standard deviations. Any differences between the

various values of the envelopes at each separation are not statistically

significant and can be attributed to sampling errors due to a finite

ensemble size. Thus the envelope of the covariance is not affected

by the position of the pair of elements on this vertical array.

The covariance, though, is determined not only by its

envelope, but also by its phase. If the phase of the covariance

changes with respect to the position on the array, then the covariance

will also. Figure V-34 shows the covariance as a function of separation

on the vertical array. It can be seen that the covariances in general

differ significantly from their envelope values, indicating a non-zero

phase. Also, there is a greater range of values of the covariance at

separations which occur at more than one location on the array. Thus

the covariance does change with position on the array. Furthermore,

this change can be attributed to the change of the phase of the co-

variance with position. The phase will be examined in more detail later.

However, the most striking observation about the vertical

covariance is that it maintains a significant level at much larger

separations than the horizontal covariance. Figure V-35 compares the

vertical and horizontal envelopes of the covariance. The values shown

for the vertical array represent the mean value of the envelope at

each separation. The envelope of the vertical covariance decreases

monotonically with increasing separation, but even the covariance at a
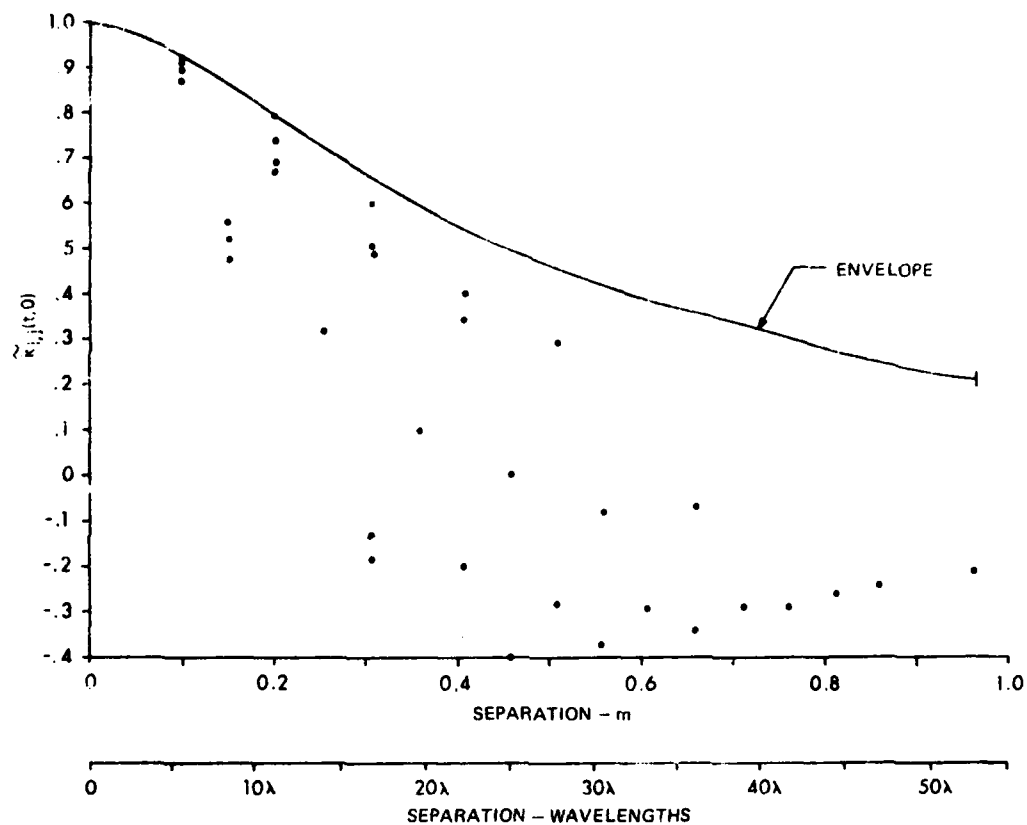
FIGURE V-34
THE DEPENDENCE OF THE EXPERIMENTAL ESTIMATE OF THE NORMALIZED
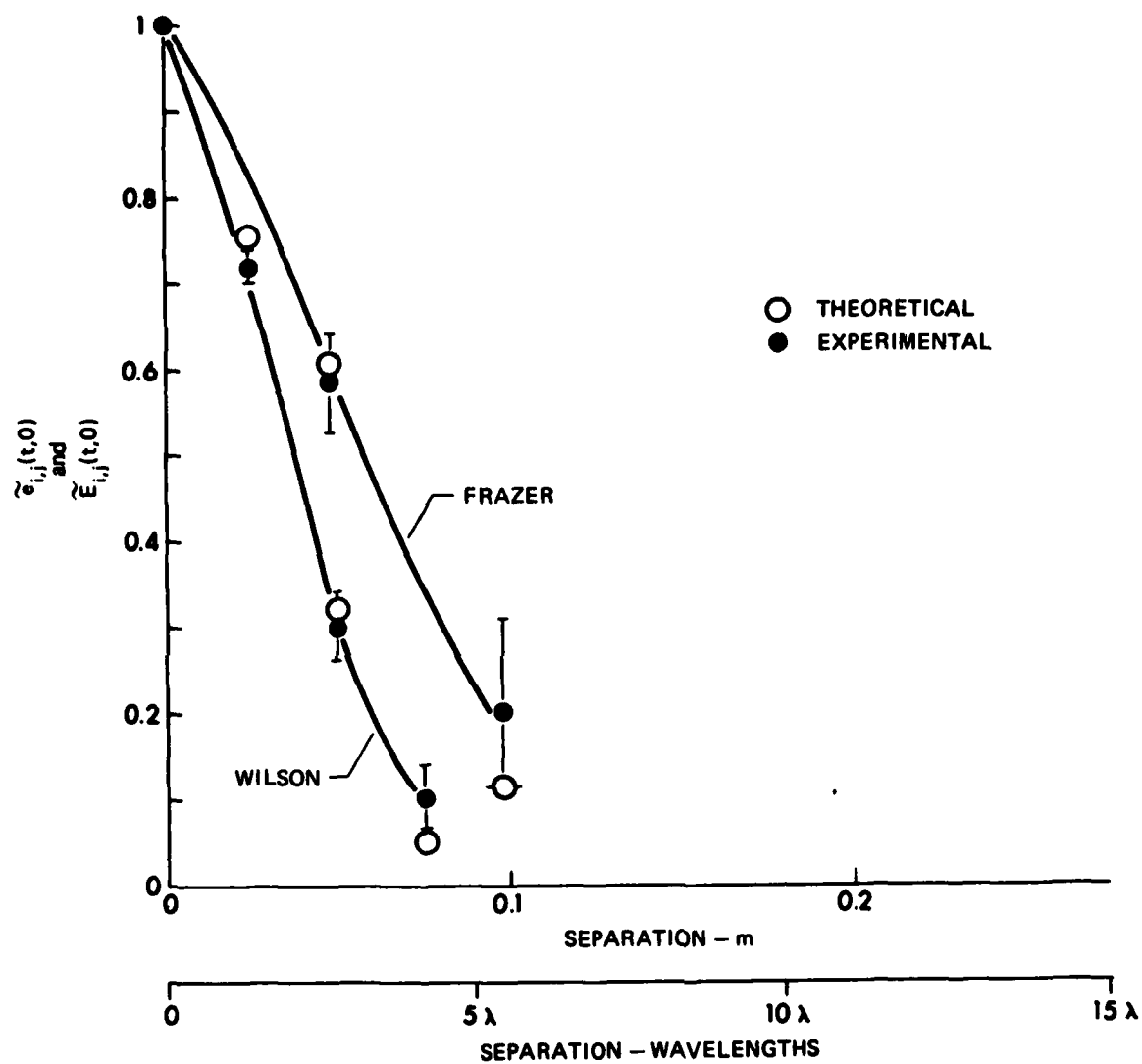**COVARIANCE ON SPATIAL SEPARATION FOR THE VERTICAL ARRAY**
$\tau = 0$ $t = 75.25$ msec
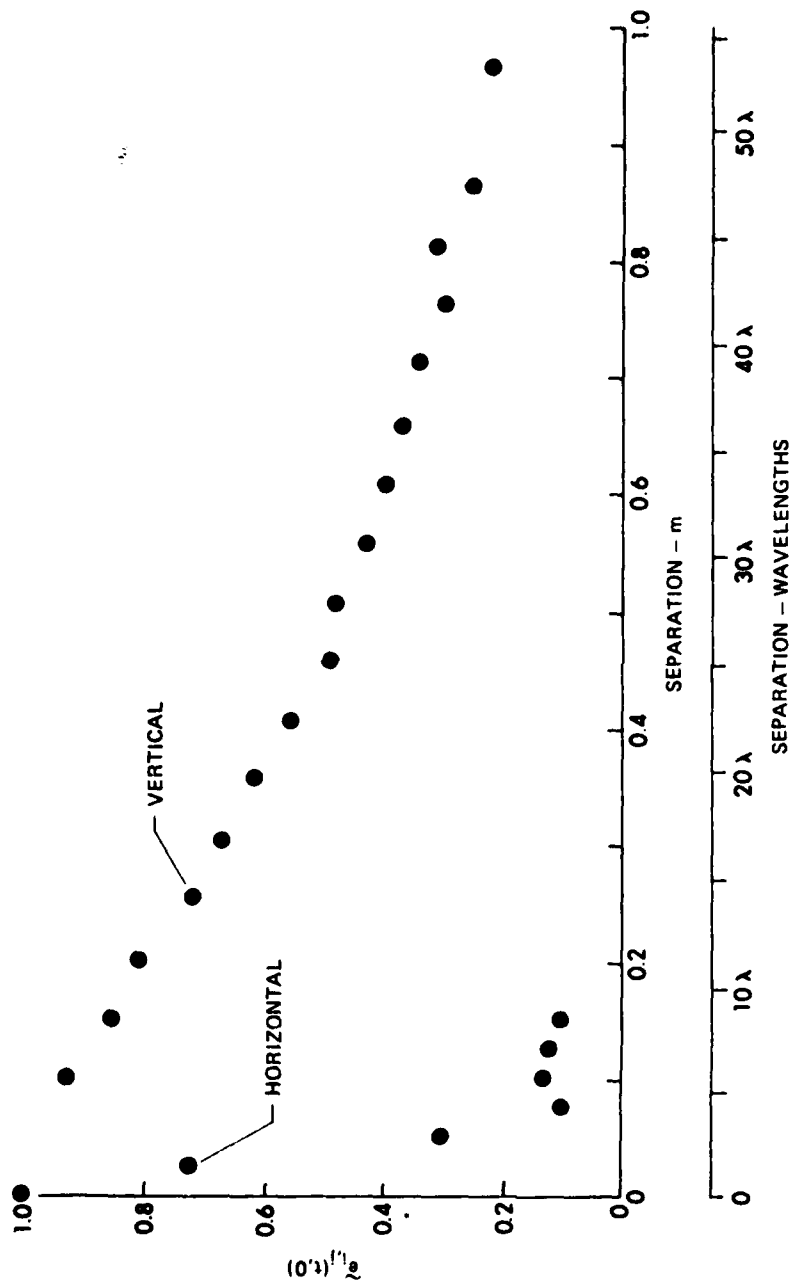
FIGURE V-35

COMPARISON OF THE VERTICAL AND HORIZONTAL DEPENDENCE OF THE
ENVELOPES OF THE NORMALIZED COVARIANCE ON SPATIAL SEPARATION

$\tau = 0$

$t = 75.25$ msec

separation of greater than 50 wavelengths has an envelope value greater than 0.2. By comparison, the envelope of the horizontal covariance has decreased to the same value in approximately 3 wavelengths. As another example, the envelope of the vertical covariance has a value of 0.5 at approximately 25 wavelengths, whereas the envelope of the horizontal covariance has this value at approximately 2 wavelengths.

The vertical covariance was also computed from the theoretical model. Figure V-36 compares the envelopes of the experimental and theoretical estimates of the normalized covariance at $\tau=0$. As can be seen the theoretical predictions are not at all in agreement with the experimental estimates. The model did predict a covariance which was larger for the vertical array than the horizontal array, but the covariance it predicted for the vertical array was much larger than what was actually obtained experimentally. Considering how well the model predicted the dependence of the horizontal covariance on separation, and the dependence of both the vertical and horizontal auto-covariance on time and time difference (t and τ), its failure for the vertical covariance was quite unexpected. However, a close examination of the simplifying assumptions which were introduced into the model revealed the probable reasons for the failure of the model in this case. These reasons will be discussed qualitatively later in the chapter, along with suggested improvements to the current implementation of the model.

As in the case of the horizontal array, it is of interest to determine if the spatial covariance changes with time. To examine
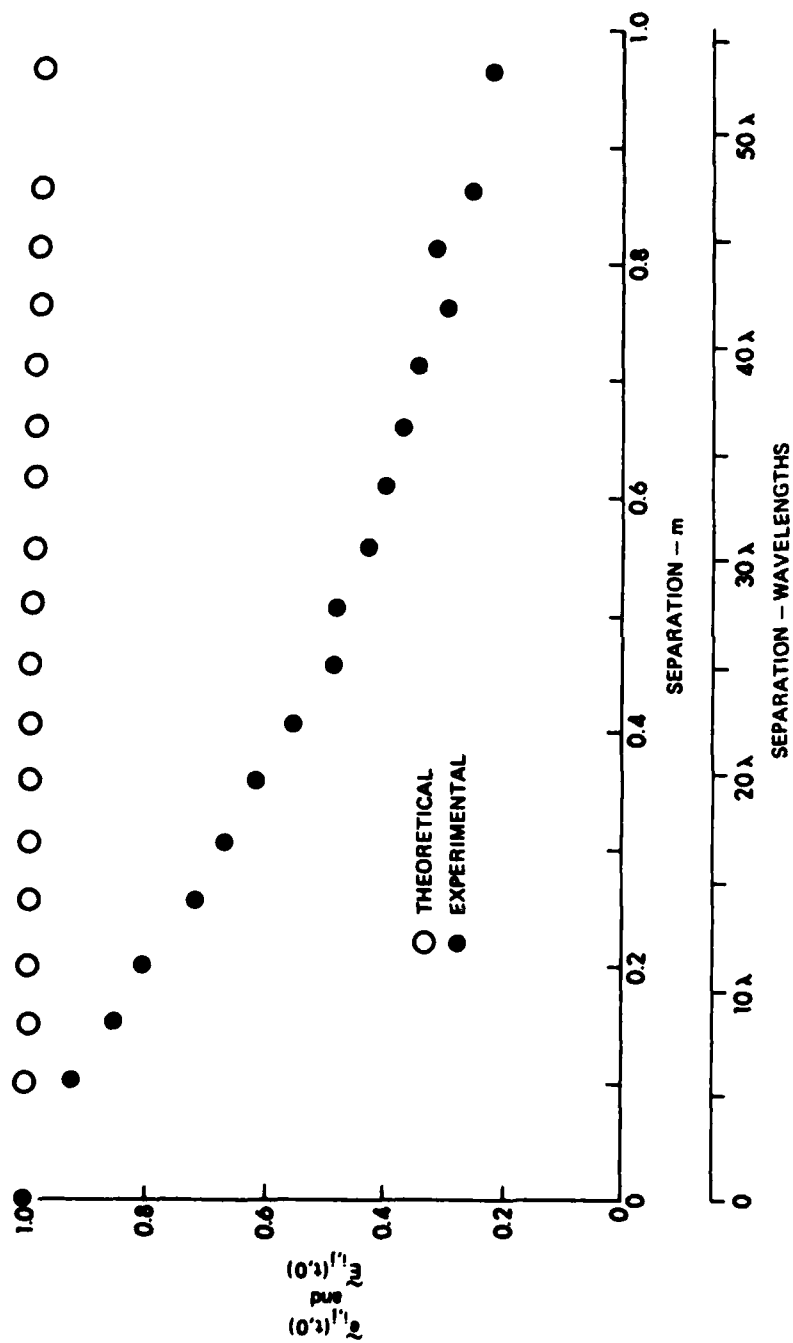
FIGURE V-36

COMPARISON OF THE THEORETICAL AND EXPERIMENTAL DEPENDENCE OF THE ENVELOPES OF THE NORMALIZED COVARIANCE ON SPATIAL SEPARATION FOR A VERTICAL ARRAY

$\tau = 0$

$t = 75.25$ msec

this dependence upon time, the covariance between channel 1 and all the

other channels in the vertical array was calculated at $\tau=0$ for the entire

10 ms interval. Although this does not provide an examination of all of

the possible covariances of the vertical array, nevertheless it should

demonstrate the significant aspects of the dependence of the vertical

covariance upon time. The envelopes of the experimental covariance

are shown in Figs. V-37 and V-38. In like fashion to the horizontal

envelopes of the covariance, the vertical envelope for each separation

does not change significantly with time. The envelope of the normal-

ized auto-covariance, $\tilde{e}_{1,1}(t,0)$, is 1 by definition. As the separation

from the first element increases, the envelope of the covariance

gradually decreases. The fluctuations in the envelopes can be

attributed to the limited ensemble size. Thus it is expected that the

results of Fig. V-33, which show the dependence of the envelopes on

vertical spatial separation at one time $t=75.25$ ms, will be closely

duplicated at all times within the 10 ms interval examined.

The phases of the covariance for the vertical array

are shown in Figs. V-39 and V-40. Unlike the phases of the horizontal

array, the vertical phases change with time even when the envelope

values are not small. The phases change linearly with time, and the

rate of change increases as the separation increases. This effect can

be explained qualitatively by recalling that the covariance at increas-

ing times is due to scattering from the surface at increasing ranges.

The difference in path lengths from the scattering region to two vertical

receivers changes with range, thus resulting in a change in the phase
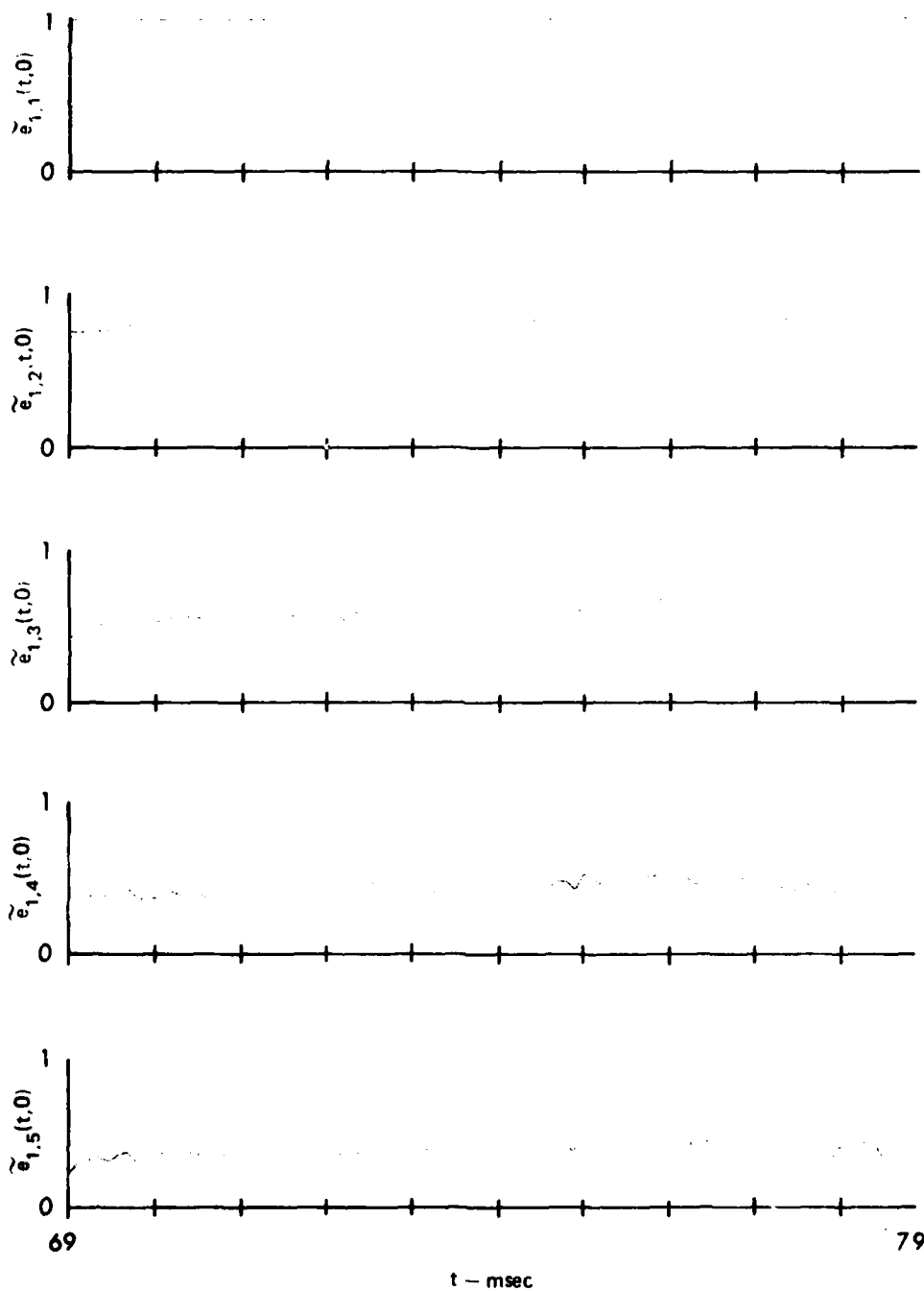
FIGURE V-37
THE DEPENDENCE OF THE EXPERIMENTAL ENVELOPES
OF THE NORMALIZED COVARIANCE ON TIME AT $\tau = 0$
FOR THE VERTICAL ARRAY

ARL:UT
AS-81-300
GRW-GA
3-3-81
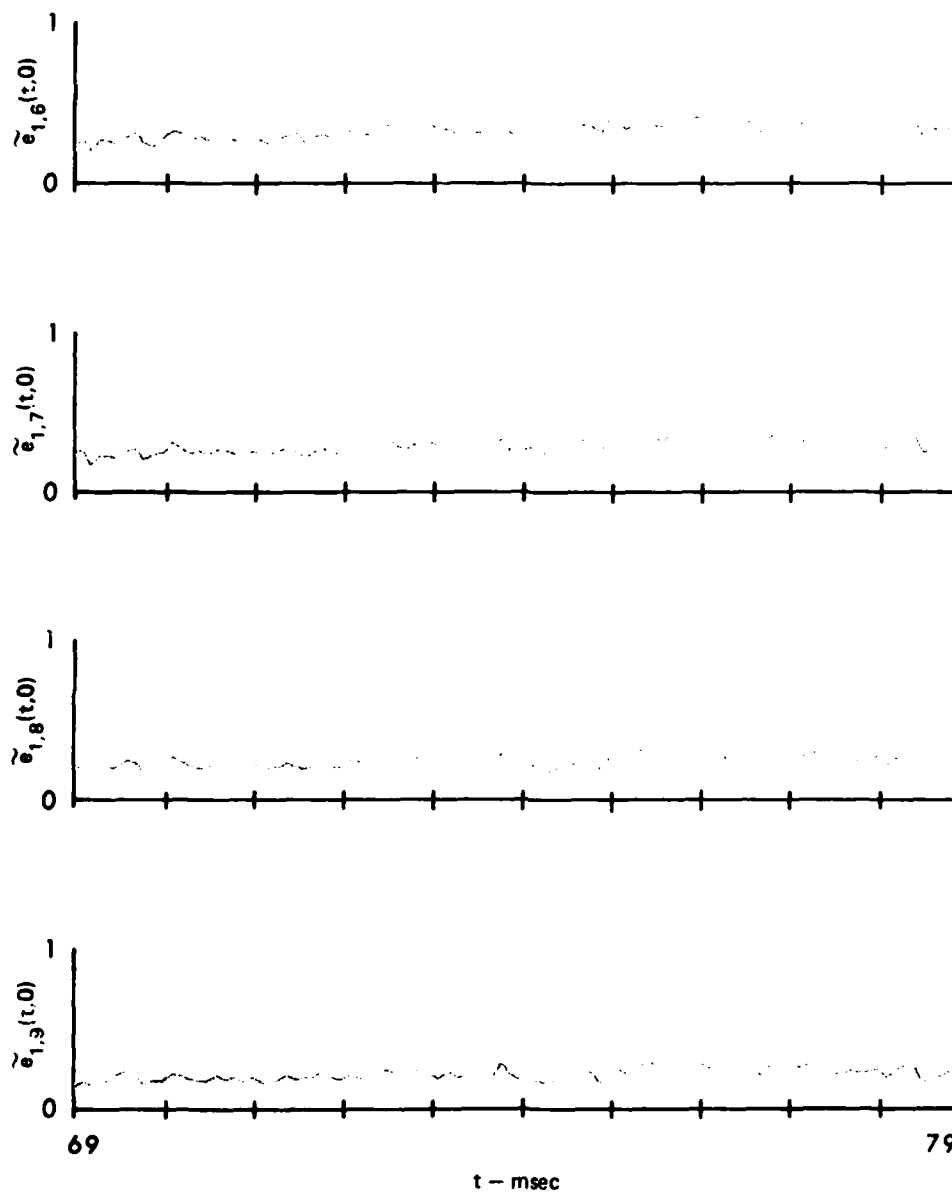
FIGURE V-38
THE DEPENDENCE OF THE EXPERIMENTAL ENVELOPES
OF THE NORMALIZED COVARIANCE ON TIME AT $\tau = 0$
FOR THE VERTICAL ARRAY
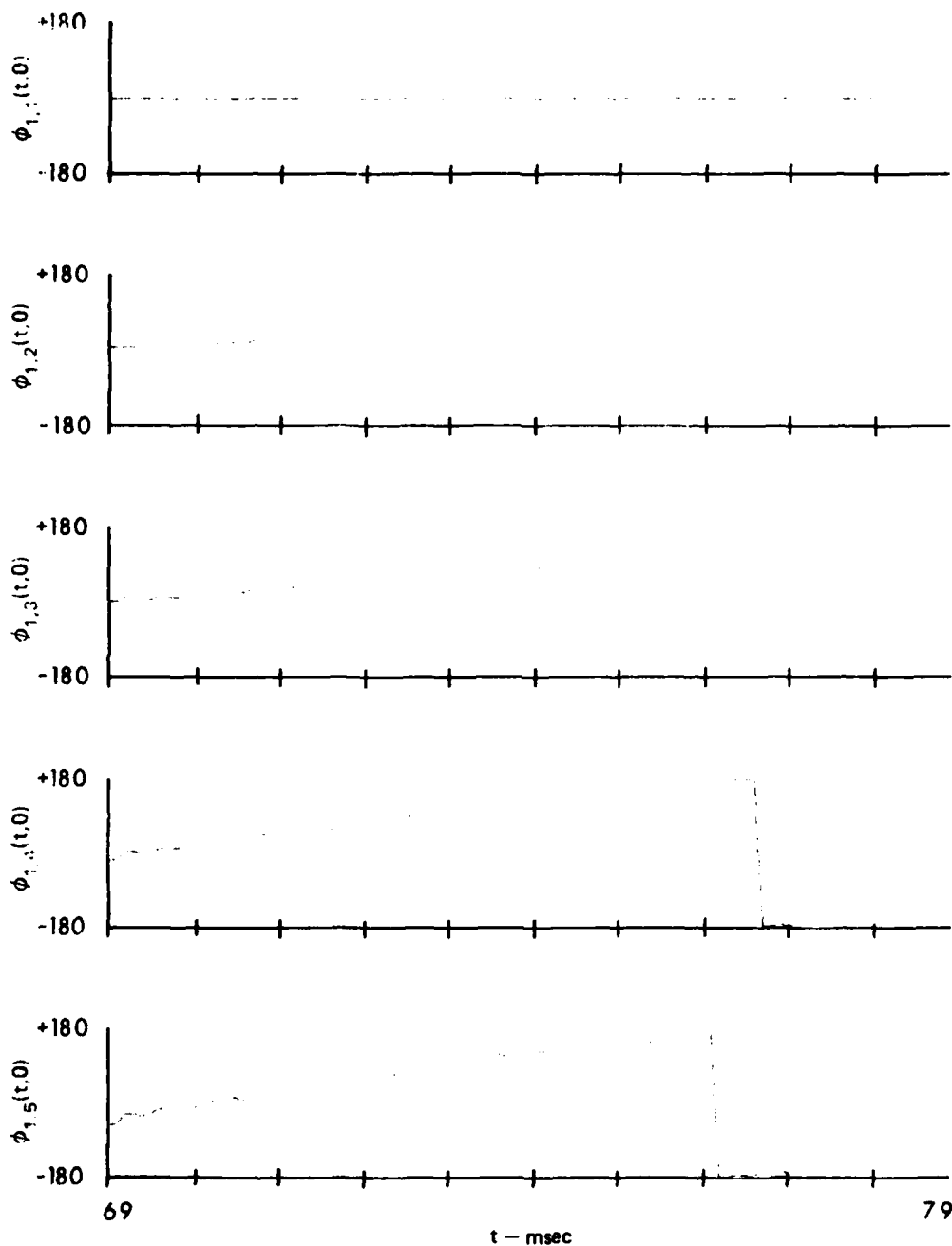
FIGURE V-39
THE DEPENDENCE OF THE EXPERIMENTAL PHASES OF
THE NORMALIZED COVARIANCE ON TIME AT $\tau = 0$
FOR THE VERTICAL ARRAY
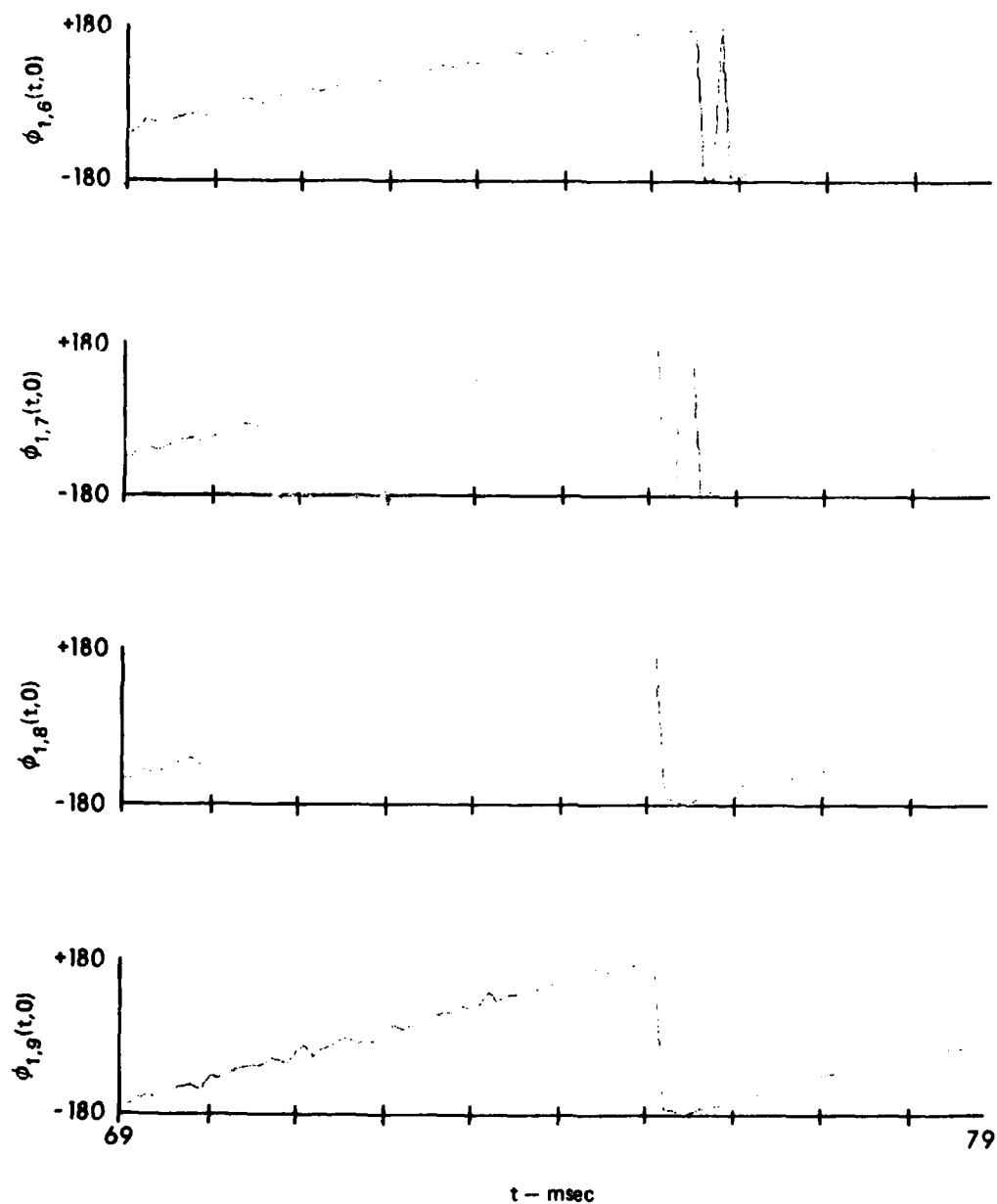
FIGURE V-40
THE DEPENDENCE OF THE EXPERIMENTAL PHASES OF
THE NORMALIZED COVARIANCE ON TIME AT $\tau = 0$
FOR THE VERTICAL ARRAY

of the covariance with time. Receivers which are farther apart have
path length differences to the scattering region which change more
rapidly as the scattering region moves out in range (time); thus the
phase of the covariance changes more rapidly with time for these re-
ceivers. These effects are not seen in the horizontal phases since
the path length differences from the scattering region to two horizontal
receivers does not change appreciably with range.

The significance of the change in phase with time is
that even though the envelope of the covariance does not change with
time, the covariance changes with time in an oscillatory fashion. For
$\tau=0$, the covariance is given by

$$\widetilde{k}_{i,j}(t,0) = \widetilde{e}_{i,j}(t,0)\cos(\phi_{i,j}(t,0)) \qquad .$$

Since the phase changes linearly with time, this can be written as

$$\widetilde{k}_{i,j}(t,0) = \widetilde{e}_{i,j}(t,0)\cos(\omega_{i,j}t)$$

where the term $\omega_{i,j}$ represents the rate of change of the phase with
time, and is dependent upon the separation of the two receivers (as
well as other parameters). Thus the vertical covariance is not constant
with time or equivalently range, but instead oscillates at a frequency
which depends upon various geometrical parameters.

Theoretical estimates of the vertical phase were made
at 1 ms intervals and are compared to the experimental estimates in
Figs. V-41 and V-42. The theoretical estimates also indicate a
linear change in the phase of the covariance with time, and in fact
indicate the same rate of change as was measured experimentally. How-
ever, the theoretical phase has a constant offset from the experimental
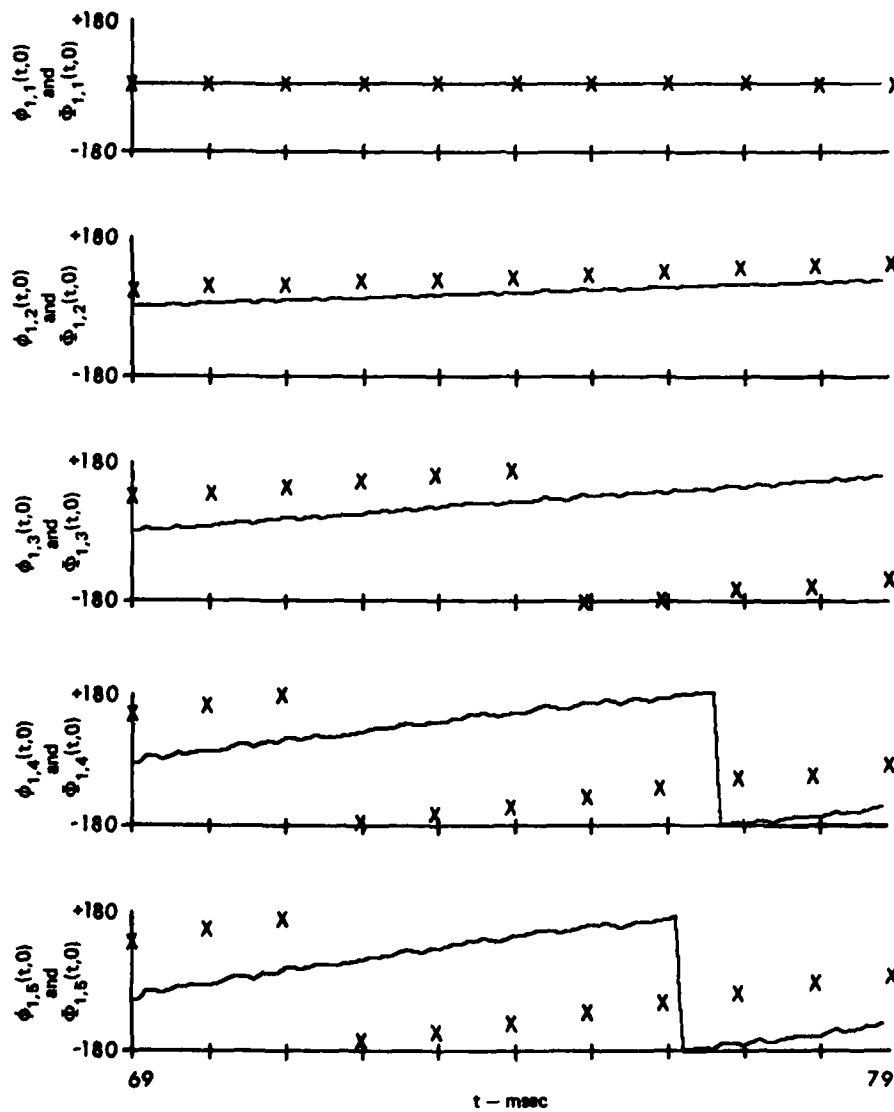
FIGURE V-41
COMPARISON OF THE THEORETICAL AND EXPERIMENTAL DEPENDENCE
OF THE PHASES OF THE NORMALIZED COVARIANCE ON TIME AT $\tau = 0$
FOR THE VERTICAL ARRAY
— EXPERIMENTAL
X THEORETICAL
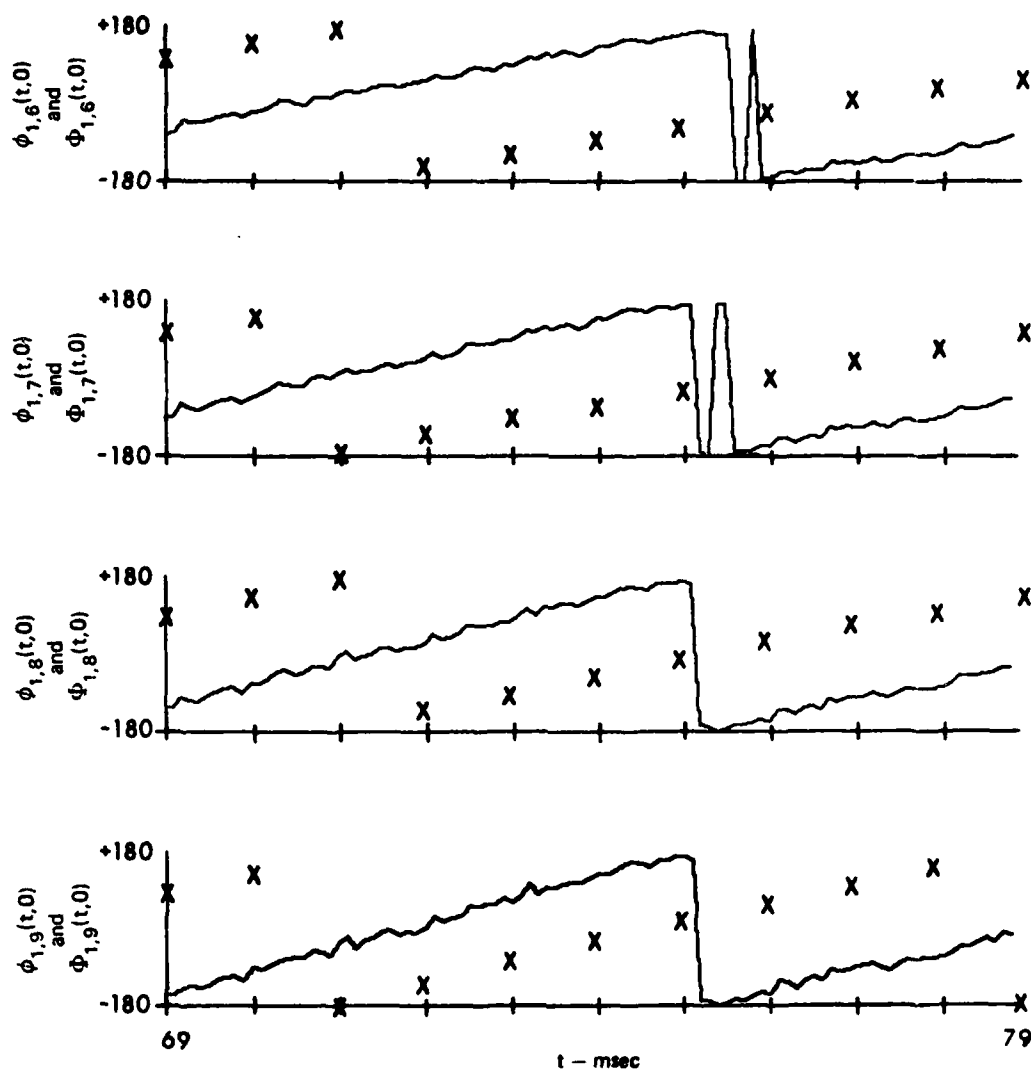
FIGURE V-42
COMPARISON OF THE THEORETICAL AND EXPERIMENTAL DEPENDENCE
OF THE PHASES OF THE NORMALIZED COVARIANCE ON TIME AT $\tau = 0$
FOR THE VERTICAL ARRAY

— EXPERIMENTAL
X THEORETICAL

phase by an amount which depends upon the separation.

One possible explanation for this offset can be found in the orientation of the vertical array with the surface. Any change that the angle of the normal to the planar face of the vertical array makes with the surface will change the path length difference between the scattering region on the surface and two vertical receivers, thus changing the phase of the covariance. The theoretical estimates shown in Figs. V-41 and V-42 were made by considering that the planar faces of the vertical array and projector were parallel, and that their normals intersected the plane of the surface at a 10.5 degree grazing angle. Theoretical estimates were also made with the normal to the face of the vertical array intersecting the surface at a grazing angle of 9.8 degrees, while the projector maintained its 10.5 degree grazing angle. The results are shown in Figs. V-43 and V-44. The offset has been removed and the theoretical phases are in much better agreement with the experimental results. Thus only a 0.7 degree grazing angle difference between the projector and vertical receiving array can make a significant change in the prediction of the phase of the covariance, and thus the covariance itself. It must be pointed out that it cannot be said conclusively that this is the reason for the offset between the experimental and theoretical results. On the other hand, the mechanical mounting of the projector and vertical array in the experiment was such that their angular orientations could certainly not be guaranteed to be the same to an accuracy of less than one degree. Thus it is feasible that this angular difference produced the offset in the theoretical and experimental phases.
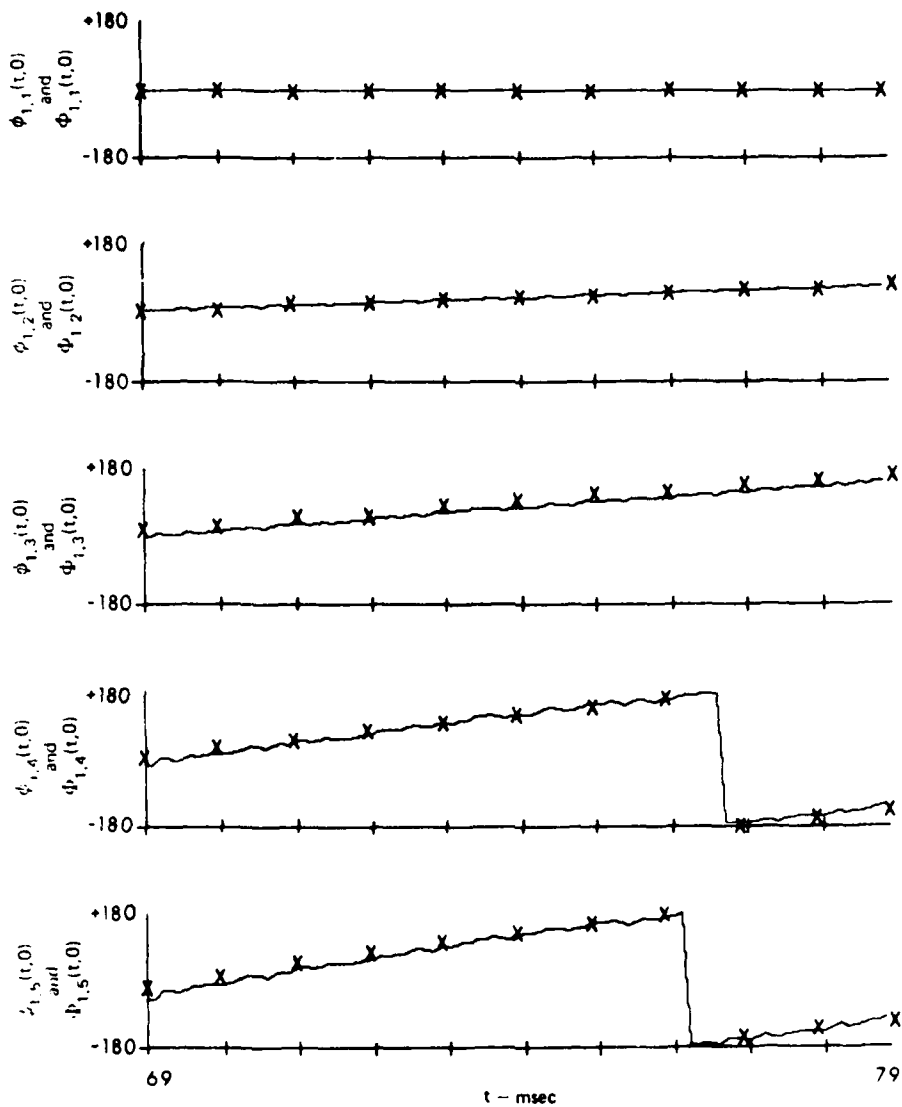
FIGURE V-43
COMPARISON OF THE THEORETICAL AND EXPERIMENTAL DEPENDENCE
OF THE PHASES OF THE NORMALIZED COVARIANCE ON TIME AT $\tau = 0$
FOR THE VERTICAL ARRAY
ORIENTATION OF VERTICAL ARRAY MODIFIED
—— EXPERIMENTAL
X THEORETICAL
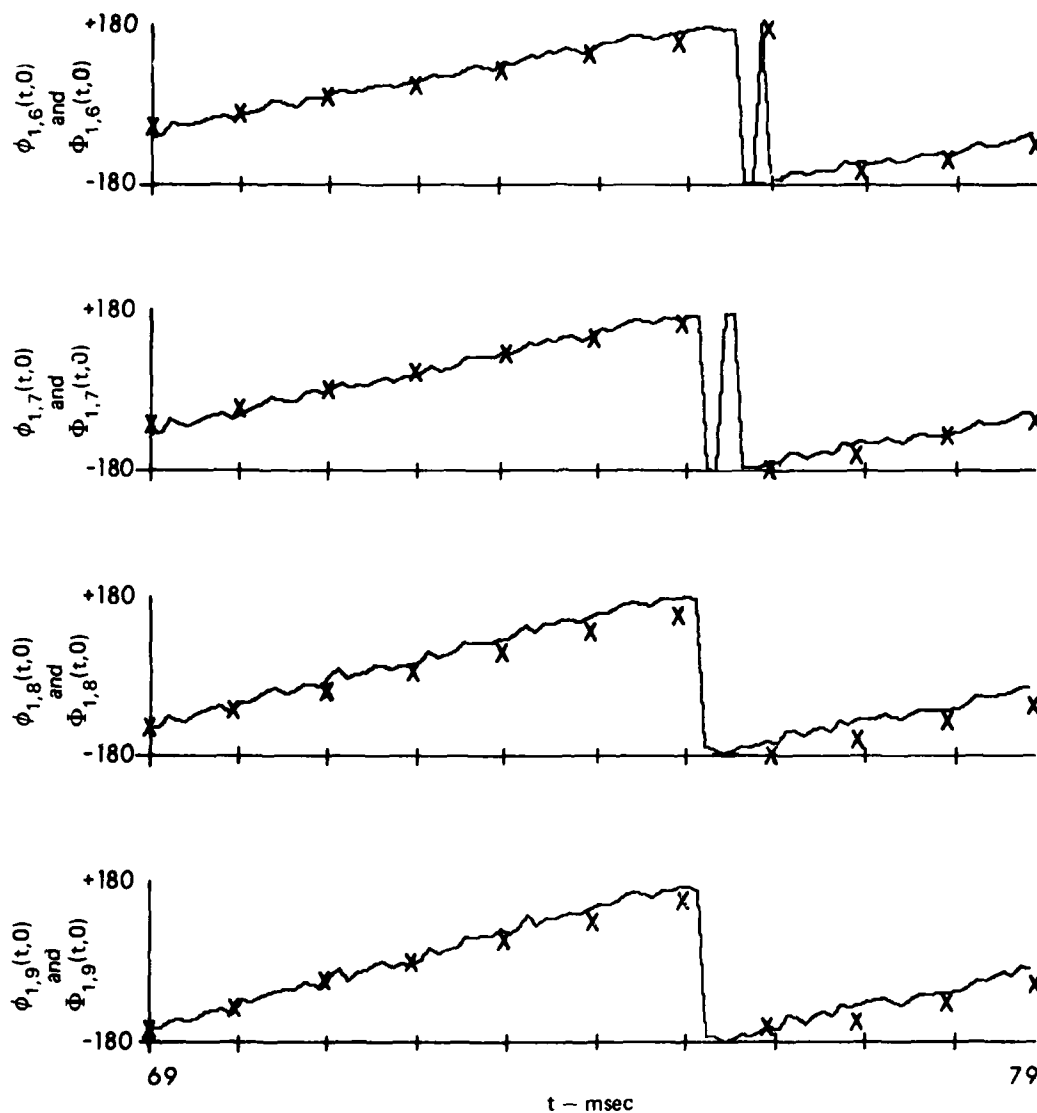
FIGURE V-44
COMPARISON OF THE THEORETICAL AND EXPERIMENTAL DEPENDENCE
OF THE PHASES OF THE NORMALIZED COVARIANCE ON TIME AT $\tau = 0$
FOR THE VERTICAL ARRAY
ORIENTATION OF VERTICAL ARRAY MODIFIED
—— EXPERIMENTAL
X THEORETICAL

V.3.4   The Covariance for $\tau \neq 0$

Thus far, the variance as a function of t, the auto-covariance as a function of τ and t, and the covariance as a function of spatial separation and t for $\tau = 0$ have been examined both experimentally and theoretically for the horizontal and vertical arrays. This section will now present the covariance as a function of spatial separation and τ. The horizontal covariance is presented first, followed by the vertical covariance.

Figure V-45 presents the normalized envelopes of the sample covariance between the various elements of the horizontal array as a function of τ. The diagonal plots in this "matrix" of envelopes are the auto-covariances shown previously. The first row of plots represents the envelopes of the covariance between channel 11 and the other horizontal receiver channels, i.e., the first plot is $\widetilde{e}_{11,11}(t,\tau)$, the next one to the right is $\widetilde{e}_{11,2}(t,\tau)$, etc. Likewise the second row contains the envelopes between channel 12 and the others; the first plot is $\widetilde{e}_{12,11}(t,\tau)$, then $\widetilde{e}_{12,12}(t,\tau)$, and so forth. Because the horizontal elements were unequally spaced, adjacent plots do not represent equal changes in separation. Thus $\widetilde{e}_{11,12}(t,\tau)$ is significantly less than $\widetilde{e}_{11,11}(t,\tau)$ because the separation between the elements changed from zero for $\widetilde{e}_{11,11}(t,\tau)$ (the auto-covariance) to 5.08 cm for $\widetilde{e}_{11,12}(t,\tau)$, whereas $\widetilde{e}_{13,14}(t,\tau)$ has not decreased as much compared to $\widetilde{e}_{13,13}(t,\tau)$, even though they are also adjacent plots in the matrix, because the separation for $\widetilde{e}_{13,14}(t,\tau)$ is only 2.54 cm.

Several observations can be made about the envelopes of the covariance. In general, $\widetilde{e}_{i,j}(t,\tau) = \widetilde{e}_{j,i}(t,\tau)$ only for $\tau = 0$.
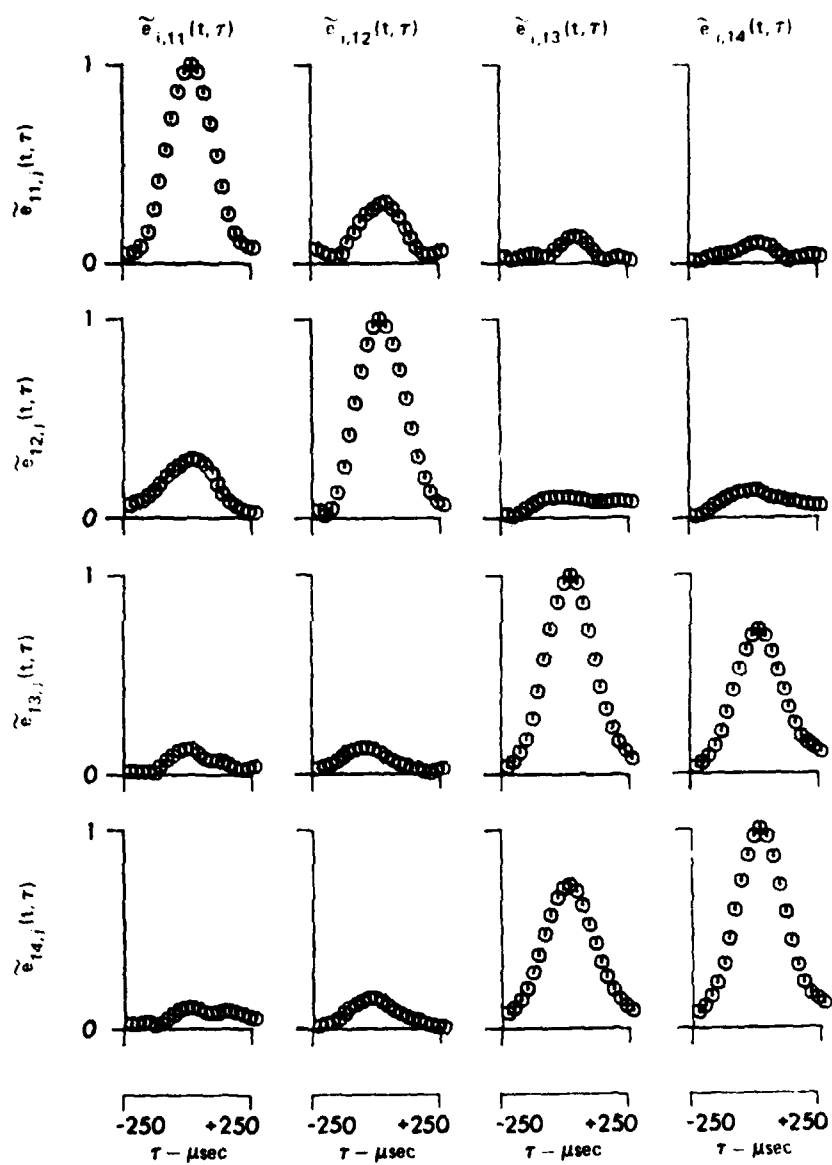
FIGURE V-45
NORMALIZED ENVELOPES OF SAMPLE ESTIMATES OF
THE COVARIANCE OF THE HORIZONTAL RECEIVERS
AS A FUNCTION OF τ FOR t = 75.25 msec

Thus symmetry about the diagonal of the matrix is not required. In this instance, the envelopes are reasonably symmetric about the diagonal plots, but are not exactly symmetric. If two processes are jointly wide-sense stationary, then it can be shown that

$$\widetilde{k}_{i,j}(\tau) = \widetilde{k}_{j,i}(-\tau) \quad .$$

This symmetry can be realized when

$$\widetilde{e}_{i,j}(\tau) = \widetilde{e}_{j,i}(-\tau)$$

and

$$\phi_{i,j}(\tau) = -\phi_{j,i}(-\tau) \quad .$$

Thus some of the symmetry of the envelopes observed would not be un-expected if the reverberation were approximately jointly wide-sense stationary.

It can also be observed that the dependence of the envelope of the covariance on τ is approximately the same for all pairs of receivers. Thus the time extent of the cross-covariance is determined by the duration of the pulse after it has been filtered by the transmit and receive apertures, as was previously shown for the auto-covariance.

The phases of the sample covariance are shown in Fig. V-46 for the various elements of the horizontal array. The phase is not constant over the range of τ shown, indicating that the phase will also make a contribution to changing the covariance as a function of τ. The phases of the auto-covariances are zero at $\tau=0$, and $\phi_{i,j}(t,0) = -\phi_{j,i}(t,0)$, as required for the difference component.

Theoretical estimates of the envelope and phase of the normalized covariance for the horizontal array were calculated for the three
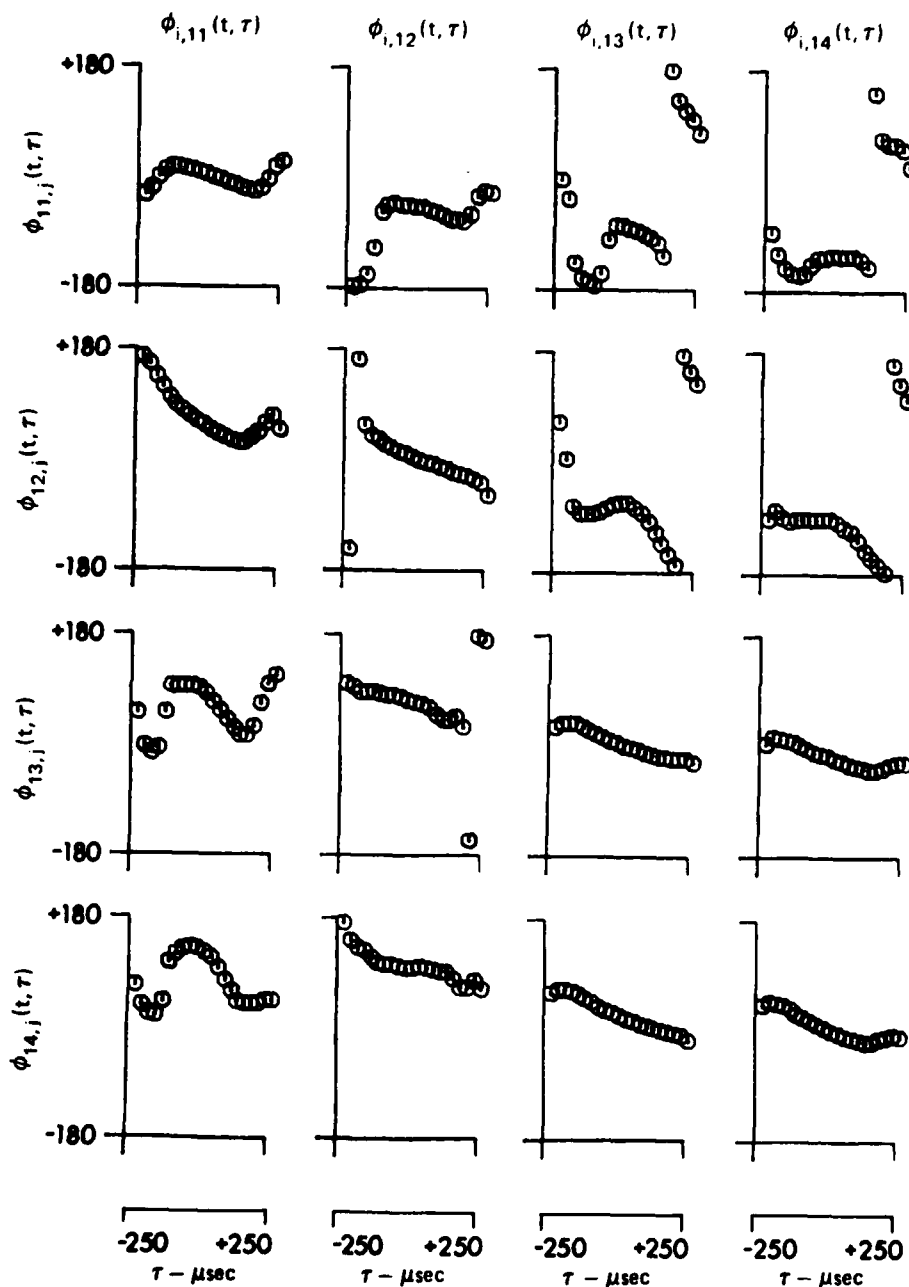
FIGURE V-46
PHASES OF SAMPLE ESTIMATES OF THE COVARIANCE OF THE
HORIZONTAL RECEIVERS AS A FUNCTION OF τ FOR t = 75.25 msec

smallest separations. Figures V-47 and V-48 show the results overlaid
on the sample estimates of the envelope and phase. The theoretical
envelopes show very good agreement with the sample estimates. The
model is correctly predicting the shape of the envelopes as well as
the magnitude.

The theoretical phases, shown in Fig. V-48, indicate
good agreement between closely spaced elements, but poor agreement for
elements spaced farther apart. However, since these elements have
small envelopes, the phase will not make the covariance differ signif-
icantly from zero. It is interesting to note that the theoretical
phases exhibit the symmetry associated with wide-sense stationarity.

It has already been shown that the covariance of the
vertical array is much greater as a function of separation than the
horizontal array. The envelopes of the normalized covariance between
all the possible pairs of nine elements in the vertical array are shown
in Figs. V-49 through V-52. The greater covariance is also obvious
in these plots. It can be seen that all the envelopes have a similar
dependence upon τ. That is, the value of τ for which the envelopes
decrease to zero is the same for all the envelopes.

The corresponding phases are shown in Figs. V-53 through
V-56. It was shown earlier that the phase at any specified separation
changed with time. In these figures the change in phase with separation
at a specified time is more obvious. The change in phase as a function
of τ is also evident. The phases do not exhibit the symmetry demon-
strated by the horizontal phases. Furthermore, the phases change with
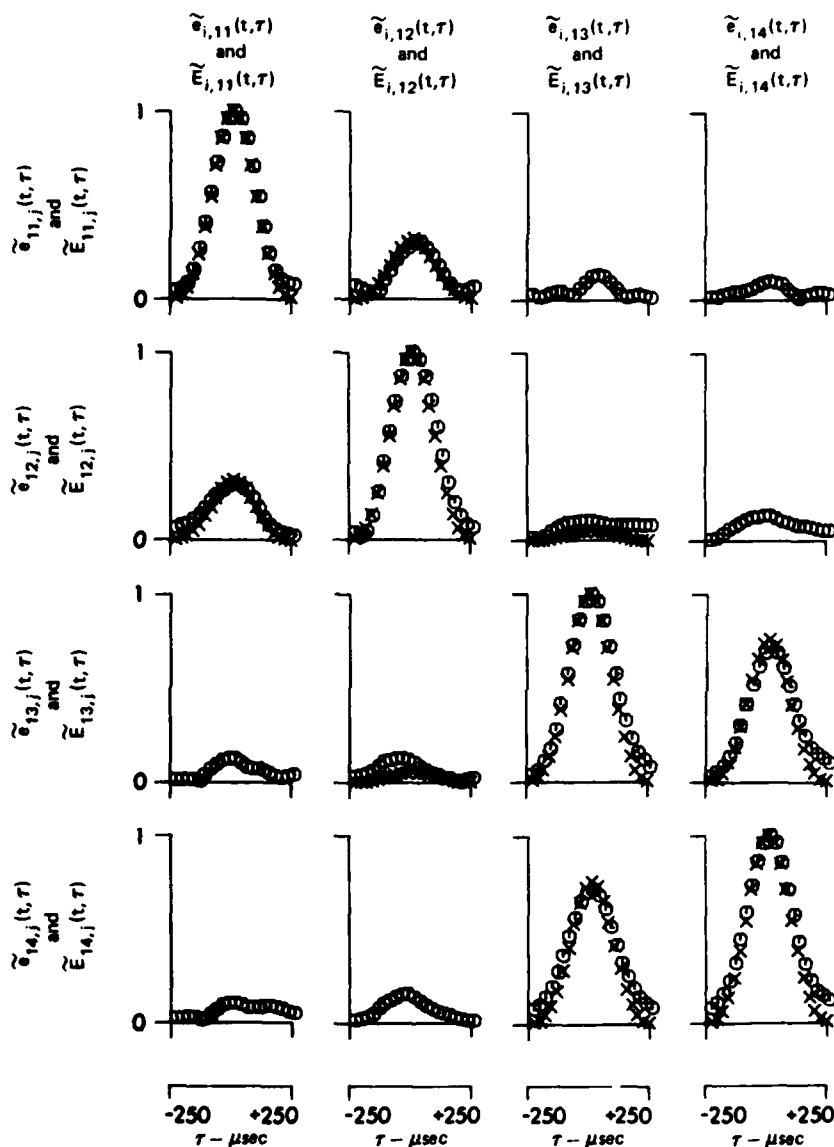
FIGURE V-47
COMPARISONS OF NORMALIZED ENVELOPES OF SAMPLE ESTIMATES AND
THEORETICAL ESTIMATES OF THE COVARIANCE OF THE HORIZONTAL
RECEIVERS AS A FUNCTION OF τ FOR t = 75.25 msec

O – SAMPLE ESTIMATE
X – THEORETICAL ESTIMATE
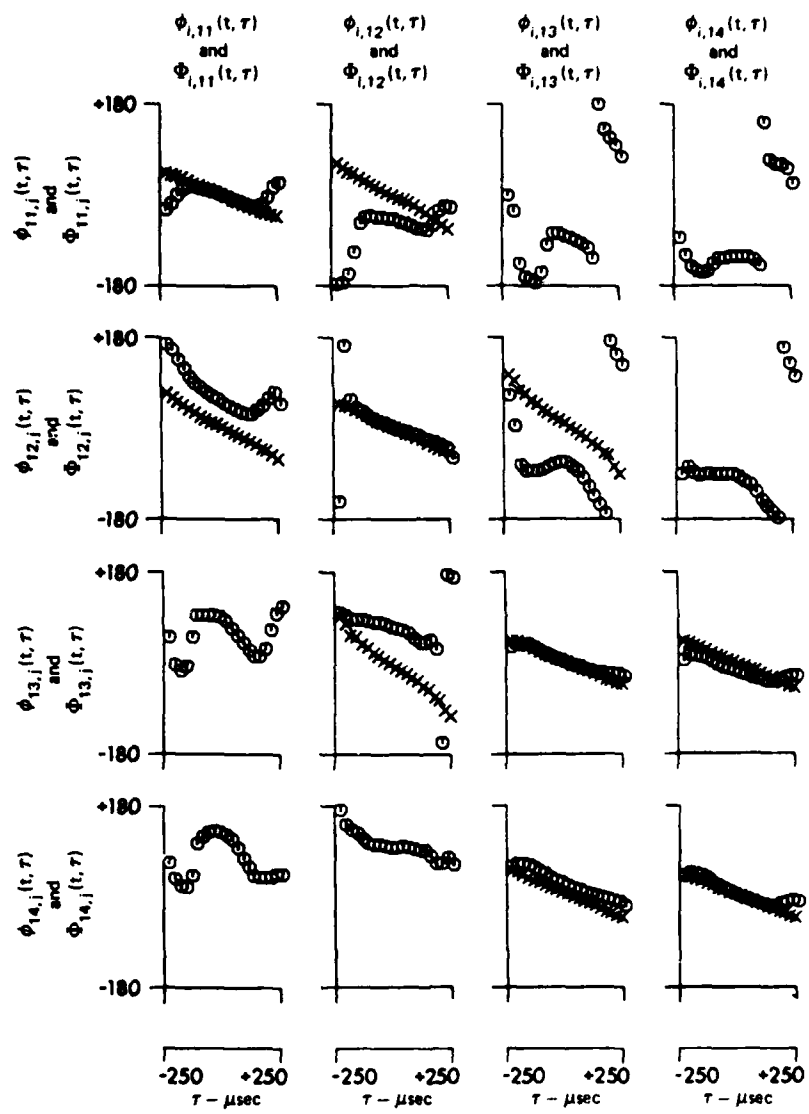
FIGURE V-48
**COMPARISONS OF THE PHASES OF THE SAMPLE ESTIMATES
AND THEORETICAL ESTIMATES OF THE COVARIANCE OF THE
HORIZONTAL RECEIVERS AS A FUNCTION OF τ FOR t = 75.25 msec**

O – SAMPLE ESTIMATE
X – THEORETICAL ESTIMATE
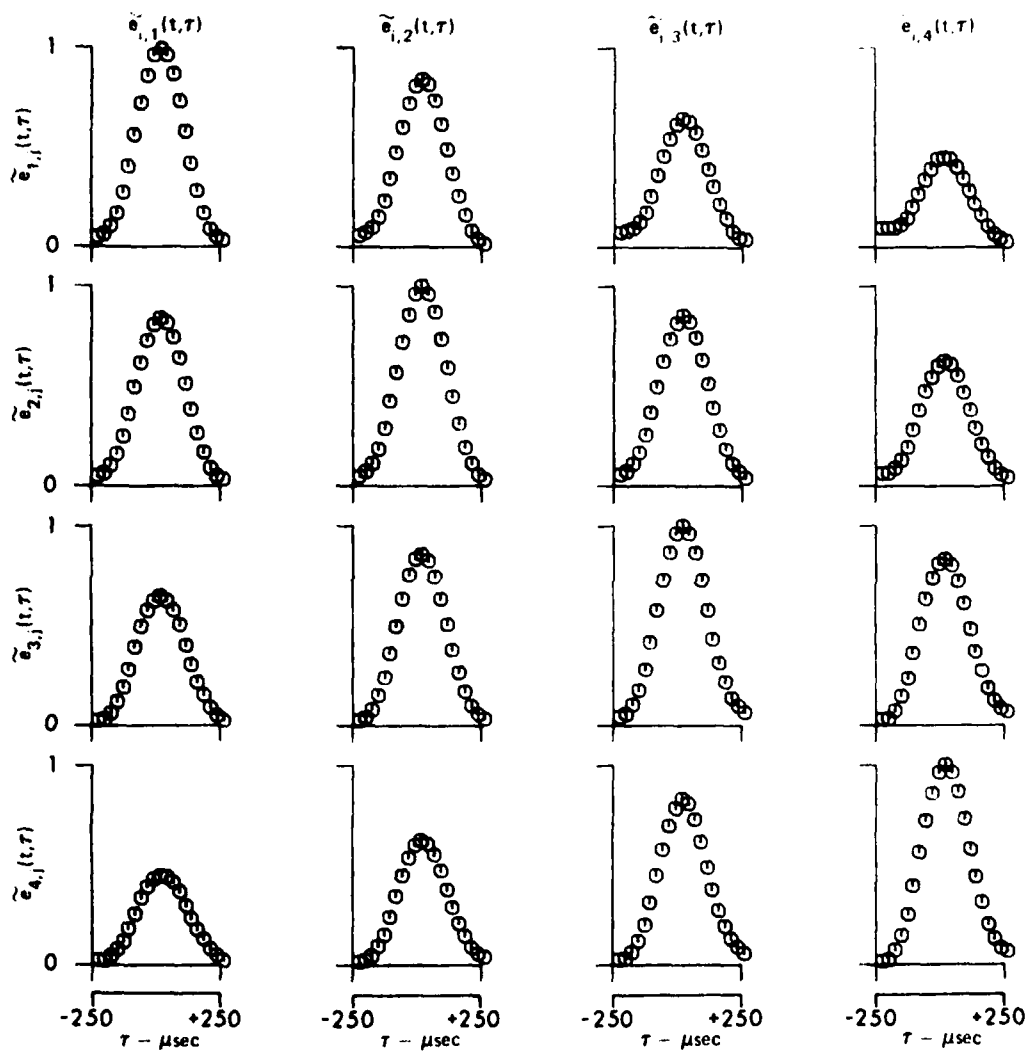
FIGURE V-49
ENVELOPES OF THE SAMPLE ESTIMATE OF THE NORMALIZED COVARIANCE
OF THE VERTICAL ARRAY AS A FUNCTION OF τ FOR $t = 75.25$ msec
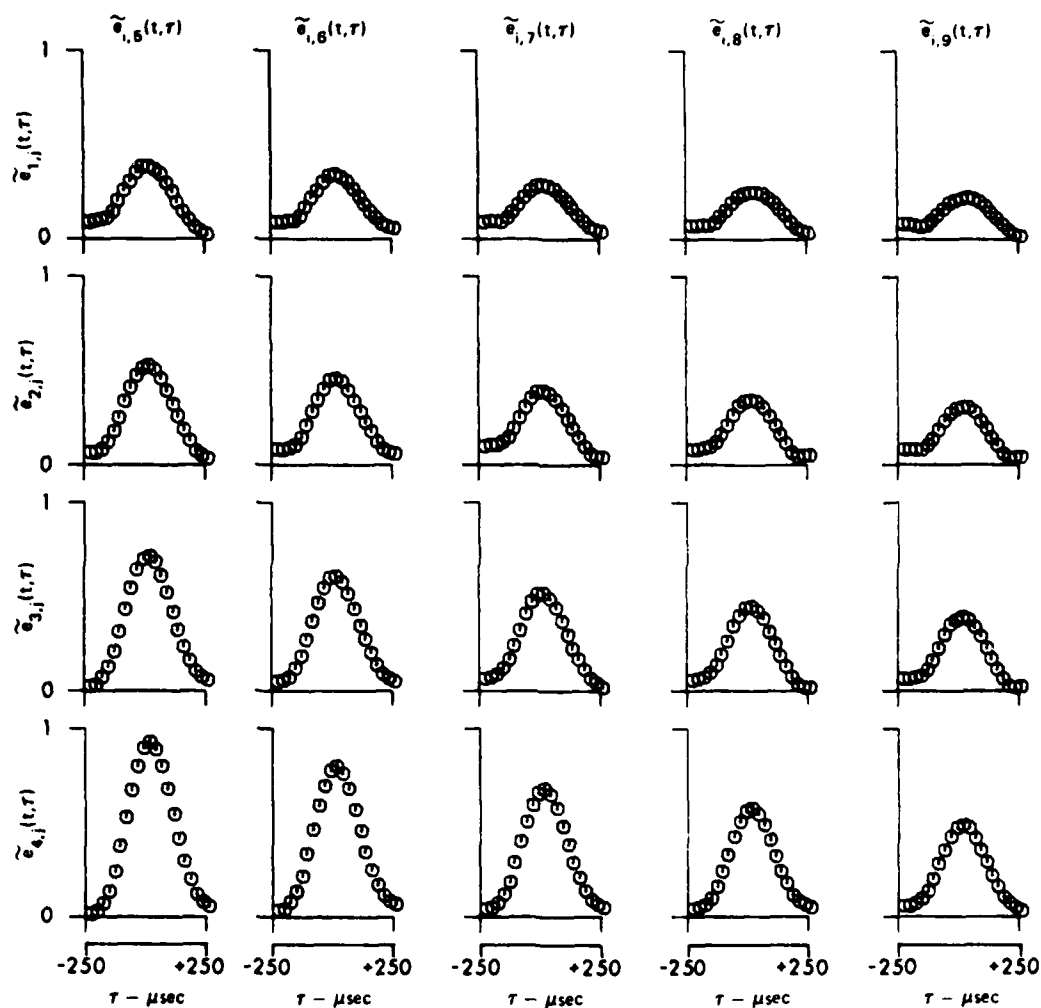
FIGURE V-50
ENVELOPES OF THE SAMPLE ESTIMATE OF THE NORMALIZED COVARIANCE
OF THE VERTICAL ARRAY AS A FUNCTION OF τ FOR t = 75.25 msec
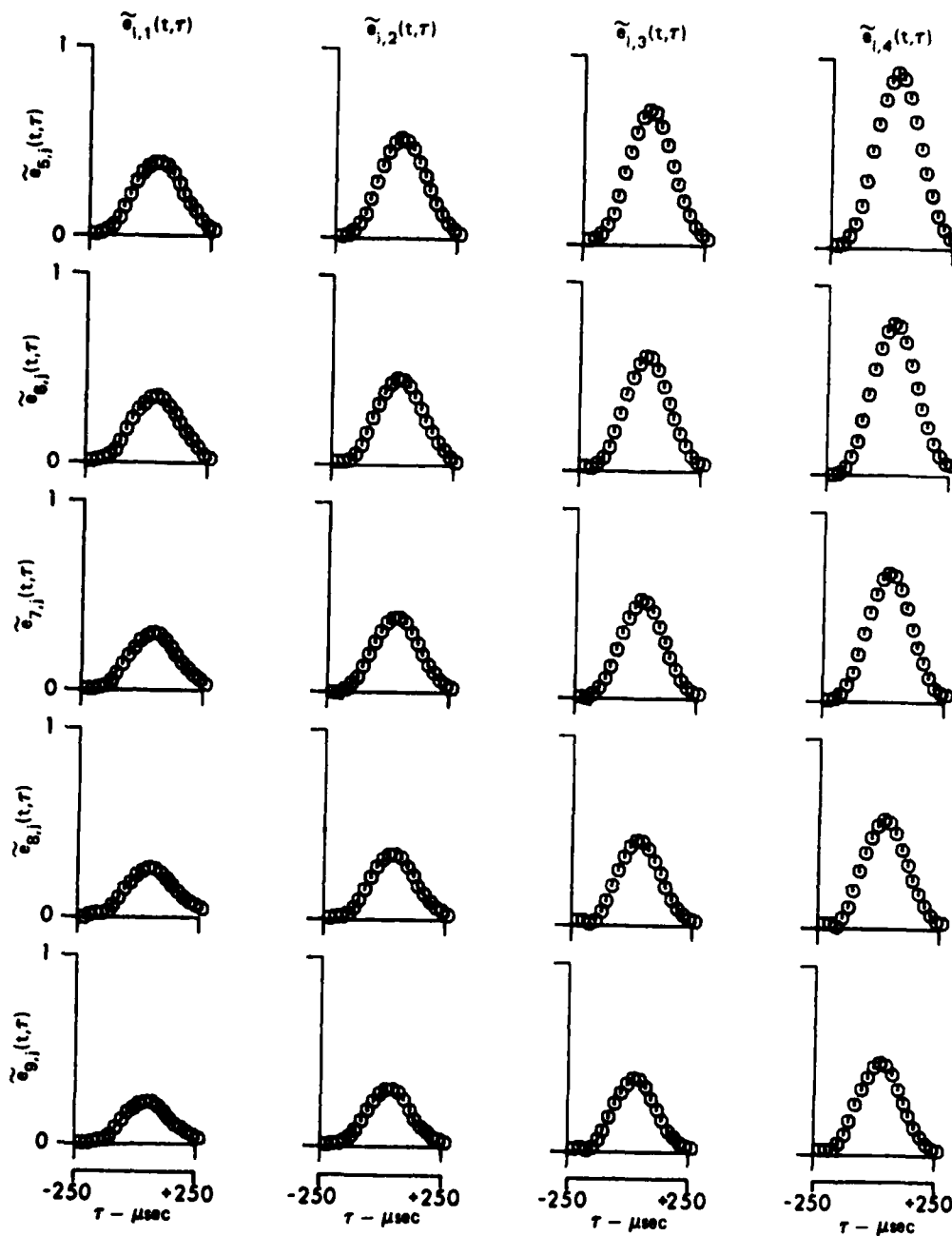
FIGURE V-51
ENVELOPES OF THE SAMPLE ESTIMATE OF THE NORMALIZED COVARIANCE
OF THE VERTICAL ARRAY AS A FUNCTION OF τ FOR t = 75.25 msec
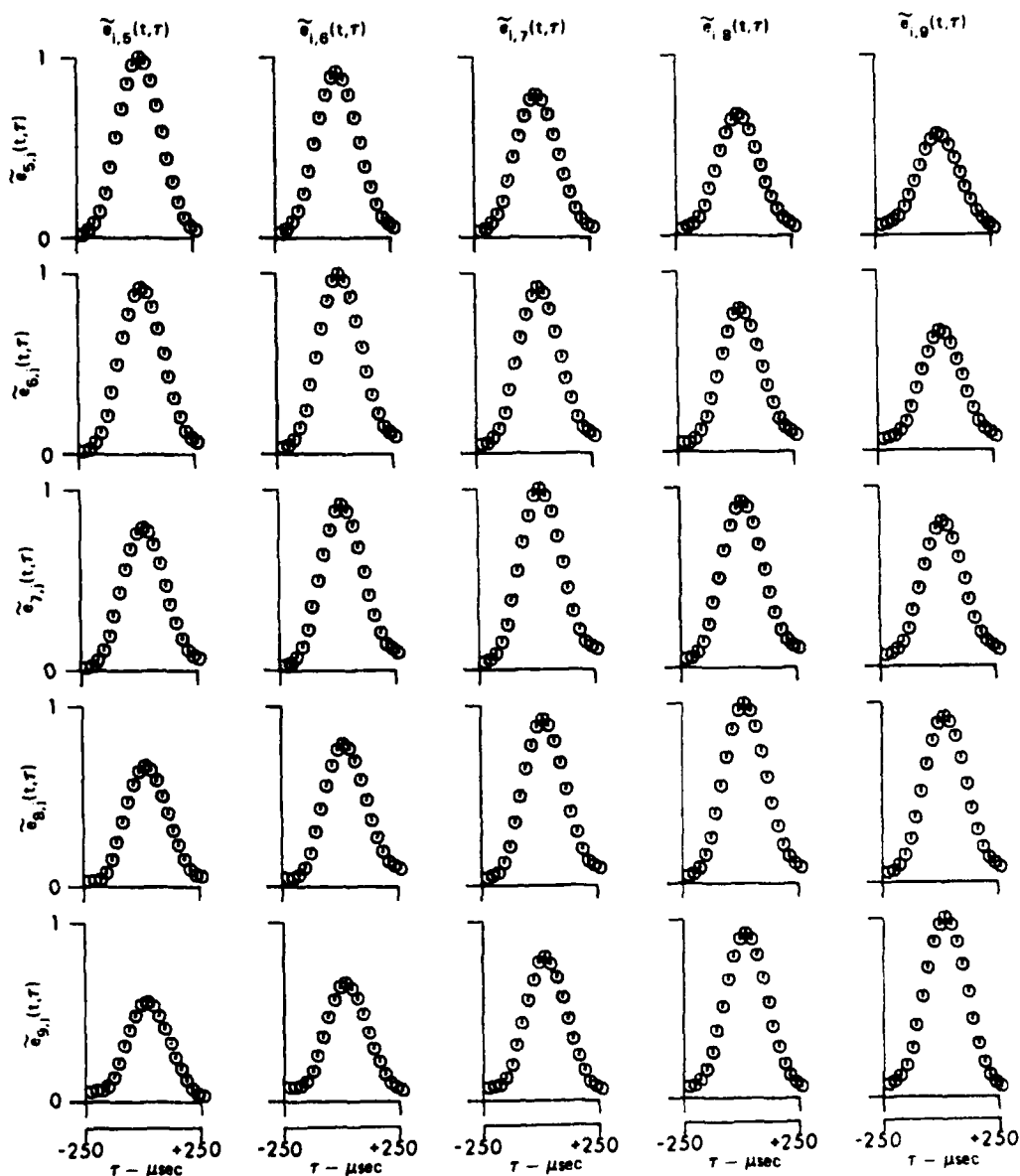
FIGURE V-52
ENVELOPES OF THE SAMPLE ESTIMATE OF THE NORMALIZED COVARIANCE
OF THE VERTICAL ARRAY AS A FUNCTION OF τ FOR t = 75.25 msec
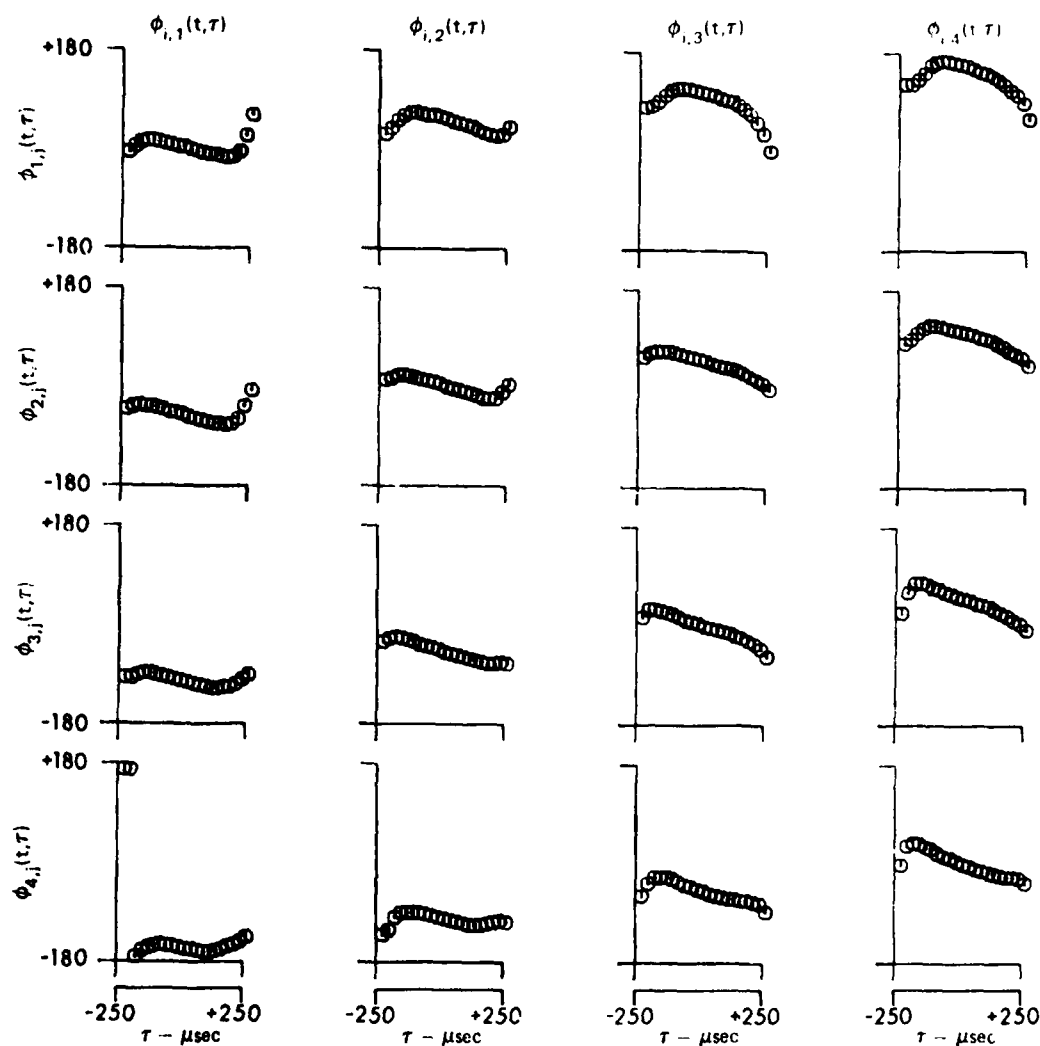
FIGURE V-53
PHASES OF THE SAMPLE ESTIMATE OF THE NORMALIZED COVARIANCE
OF THE VERTICAL ARRAY AS A FUNCTION OF τ FOR t = 75.25 msec
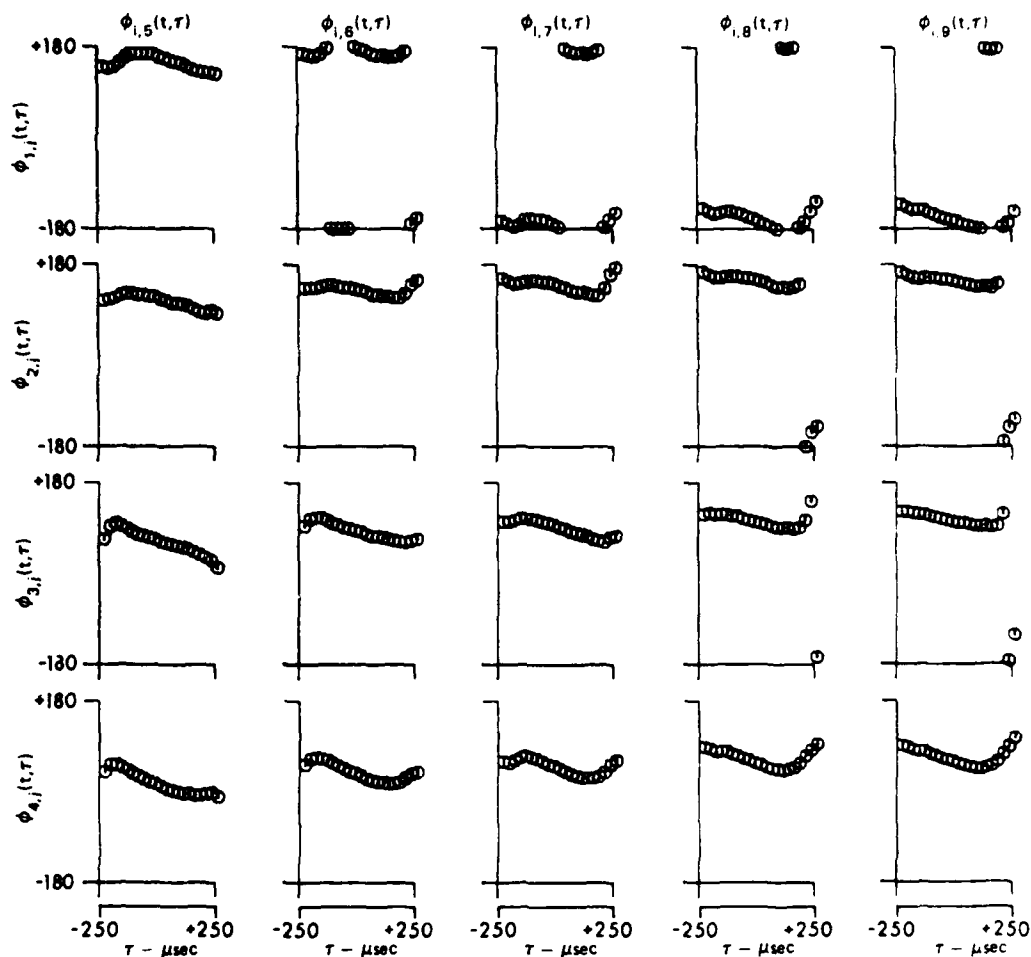
FIGURE V-54
PHASES OF THE SAMPLE ESTIMATE OF THE NORMALIZED COVARIANCE
OF THE VERTICAL ARRAY AS A FUNCTION OF τ FOR t = 75.25 msec
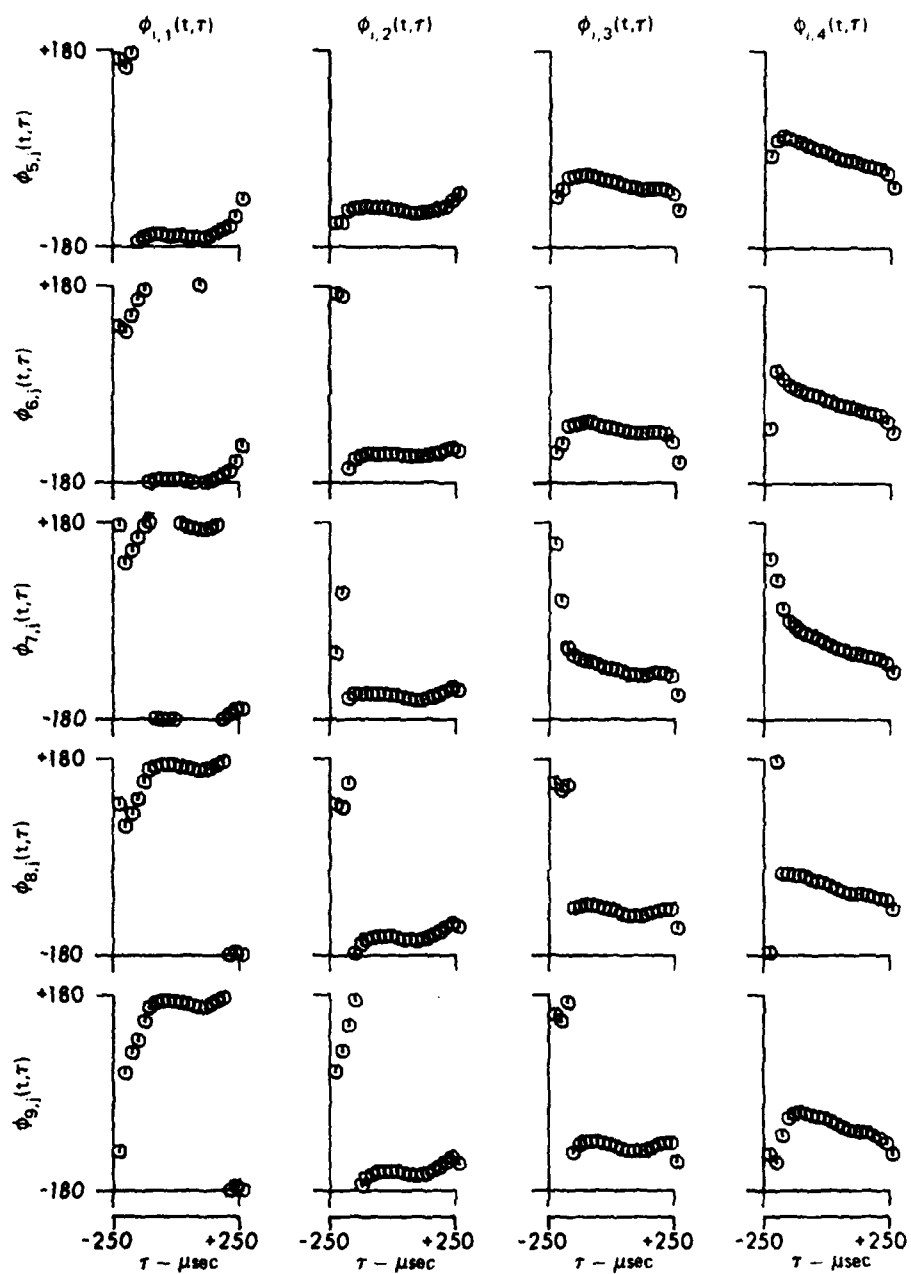
FIGURE V-55
PHASES OF THE SAMPLE ESTIMATE OF THE NORMALIZED COVARIANCE
OF THE VERTICAL ARRAY AS A FUNCTION OF τ FOR t = 75.25 msec
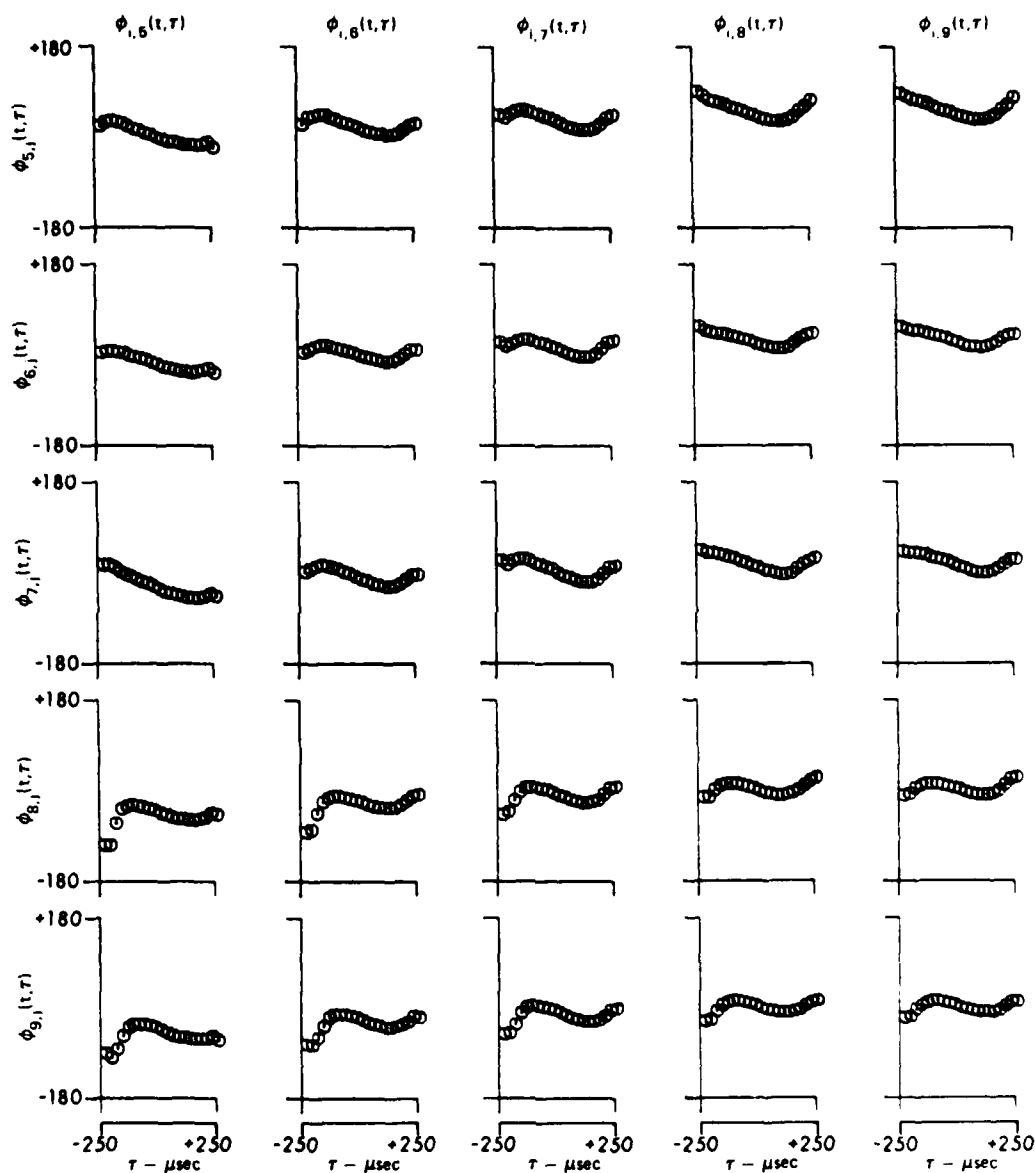
FIGURE V-56
PHASES OF THE SAMPLE ESTIMATE OF THE NORMALIZED COVARIANCE
OF THE VERTICAL ARRAY AS A FUNCTION OF τ FOR $t = 75.25$ msec

time. Thus the vertical covariance does not represent a jointly wide-sense stationary process.

Since the model did not correctly predict the dependence of the envelope of the vertical covariance on spatial separation, computation of the theoretical covariance for all pairs of elements of the vertical array would not provide much additional information. However, the covariance between channel 1 and the other vertical elements was computed and is displayed in Fig. V-57. Even though the model predicted the temporal extent of the envelope correctly, the magnitude of the envelope was overestimated, as was shown previously. The phases were computed with the vertical array and projector at the same grazing angle with the surface. Thus, although the theoretical phase changes with separation as does the sample estimate of the phase, there is an offset between the two estimates.

V.3.5 Examination of the Failure of the Model

In order to gain insights into why the model failed to correctly account for the dependence of the envelope of the covariance on vertical separation, it is important to consider that the model provided good agreement with experiment in many instances. The model correctly predicted the dependence of the variance on time, indicating the grazing angle, directivity patterns, and locations of sensors were being correctly taken into account. It also predicted the temporal extent of the covariance by taking into account the pulse length and frequency response of the projector and receivers. Most importantly, the dependence of the envelope of the covariance on spatial separation
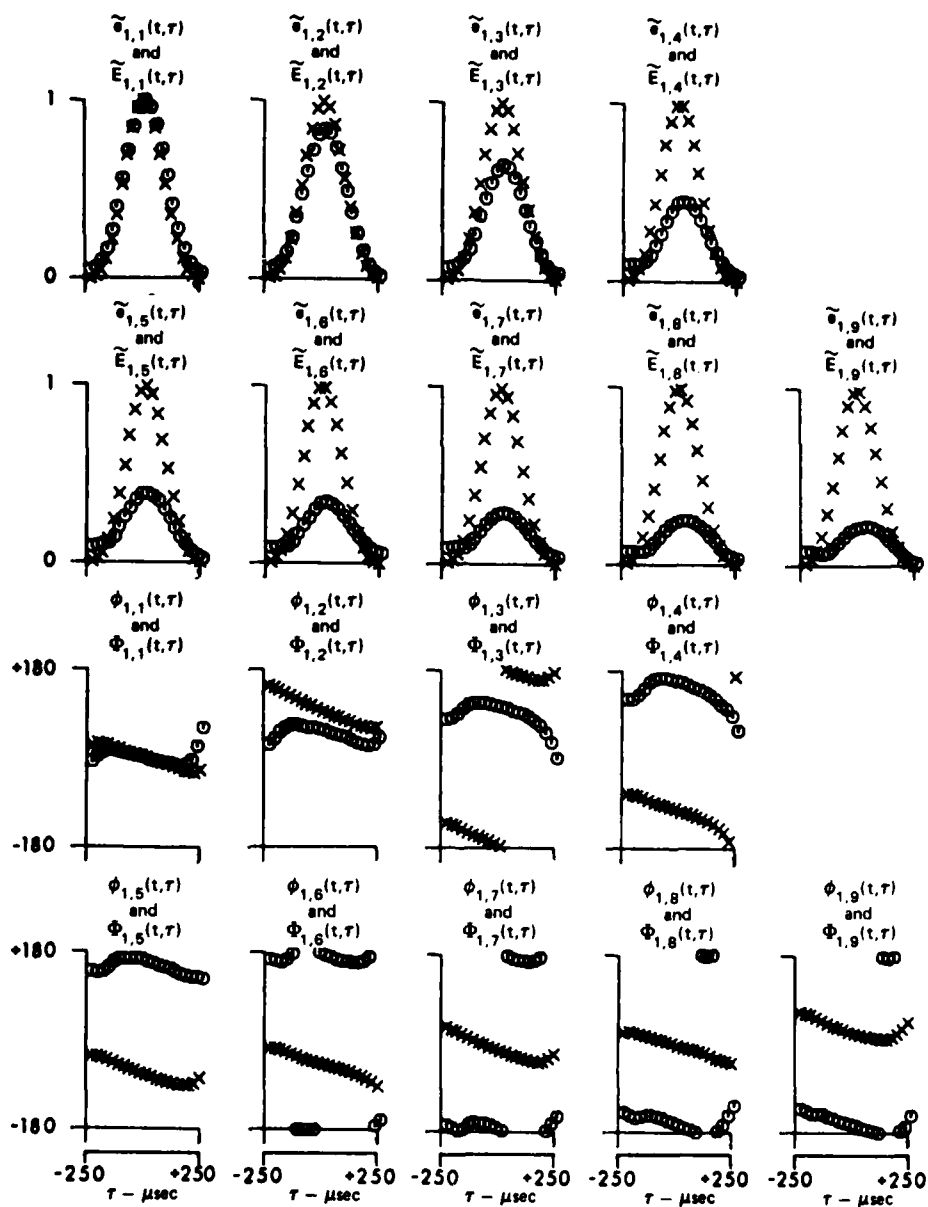
FIGURE V-57
COMPARISON OF THE THEORETICAL AND SAMPLE ESTIMATES OF THE ENVELOPES
AND PHASES OF THE NORMALIZED COVARIANCE FOR CHANNEL 1 OF THE
VERTICAL ARRAY AS A FUNCTION OF τ FOR t = 75.25 msec

X -- THEORETICAL
O -- EXPERIMENTAL

in the horizontal orientation was correctly taken into account. Any

possible explanations of the failure of the model to predict the vertical

covariance, and subsequently any changes to the model, must allow the

model to continue correctly predicting these things. With this guideline

in mind, it is appropriate to examine the model to determine why it

correctly predicted the horizontal covariance.

First of all, it is important to determine why the model

correctly predicted that the horizontal covariance would decrease rapidly

with spatial separation. Determination of the predominant cause of this

decrease in covariance may indicate what additional factors should be

considered which would decrease the covariance in the vertical case. The

basic assumption of the model is that the backscattered return at a

receiver is the result of a linear superposition of returns from point

scatterers imbedded in the surface:

$$X(t) = \sum_{j=1}^{M(t')} U_j(t, \lambda_j) \quad ,$$

where $U_j(t, \lambda_j)$ is the return from the jth scatterer at position λ_j,

$M(t')$ is the number of contributing scatterers at time t', and $X(t)$

is the total return at the receiver at time t. The covariance between

two spatially separated receivers is due to scatterers which are

providing returns to both receivers. If an elementary return is

different at the two receivers, and if all the elementary returns are

contributing differently, then it could be expected that when all the

elementary returns are combined, the returns at the two receivers could

be incoherent. More specifically, the covariance between two returns

$X_1(t_1)$ and $X_2(t_2)$ has been shown in Chapter III to be given by

$$K^{(12)}(t_1,t_2 \mid t') = \int_{\Lambda_{12}} \rho_{12}(\lambda,t') \Big\langle U_1(t_1,\lambda,\theta_1)$$

$$\cdot \; U_2(t_2,\lambda,\theta_2) \Big\rangle_\theta d\lambda \quad ,$$

which in the present study was simplified through the appropriation of several assumptions to

$$K^{(12)}(t_1,t_2 \mid t') = \sigma_s \int_{\Lambda_{12}} U_1(t_1,\lambda) U_2(t_2,\lambda) dS \quad ,$$

where the integration is over the plane of the surface which contains
scatterers distributed uniformly in the region Λ_{12} with a density σ_s.
$U_1(t_1,\lambda)$ is the elementary return at receiver 1 at time t_1 due to the
scatterer at position λ, and $U_2(t_2,\lambda)$ is the return at receiver 2 at
time t_2 due to the same scatterer. If the integration of the product
of U_1 and U_2 over the scattering region is small, then the covariance
will be small. This is the case if the product of U_1 and U_2 is approxi-
mately equally distributed about zero over the range of integration.
It was shown in Chapter III, Section 2, that this product depended upon
terms containing $\cos\omega_0\left(\dfrac{R_{R2}-R_{R1}}{c}\right)$ and $\sin\omega_0\left(\dfrac{R_{R2}-R_{R1}}{c}\right)$ where R_{R1} is the
path length from scatterer to receiver 1, and R_{R2} is the path length
from the same scatterer to receiver 2. Thus if this path length differ-
ence $R_{R2}-R_{R1}$ changed significantly with respect to $\dfrac{\omega_0}{c} = \dfrac{2\pi}{\lambda}$ over the
various contributing scatterers, then the product of U_1 and U_2 would
oscillate and integrate to approximately zero. Therefore it can be
concluded that in a very qualitative sense, if the path length differ-
ence between a scatterer and the two receivers changes significantly

over the region of contributing scatterers, then the covariance between

those two receivers will be small. Conversely, if the path length

difference changes little, then the covariance will be large.

Figure V-58 illustrates the path lengths between two

receivers separated vertically and horizontally for conditions similar

to the present study. The horizontal receivers will be conside   .

The area that the projector illuminates on the surface at any on   ime

has a small downrange extent determined by the pulse length, and a larger

crossrange, or azimuthal, extent determined by the horizontal beamwidth

of the projector. It can be observed that the path length difference

$R_{R2}-R_{R1}$ changes over the region of scatterers. For a scatterer left

of center R_{R2} is greater than R_{R1}, but for a scatterer right of center

the opposite is true. Thus the geometry allows for a small covariance,

depending upon how much the path length differences change over the

scattering region. This in turn is determined by the azimuthal width

of the scattering region and the horizontal separation of the receivers.

For the present study, most of the energy from the projector was confined

horizontally to angles ±15 degrees from center. An approximate calcu-

lation of the change in path length difference over the 30 degree azimuthal

width of the scattering region for the ranges and geometries used was

made. For two elements separated horizontally by 2.54 cm, the closest

horizontal spacing used, the path length differences changed by .7 λ,

where λ is the wavelength of the transmitted sound. This will result

in some oscillation of the integrand of the covariance integral and

result in a decreased, although probably not zero, covariance. This is

AREA ILLUMINATED
BY PROJECTOR

R_{R1} R_{R2}

R_{R1}

R_{R2}

RECEIVER 1 ——— ——— RECEIVER 2
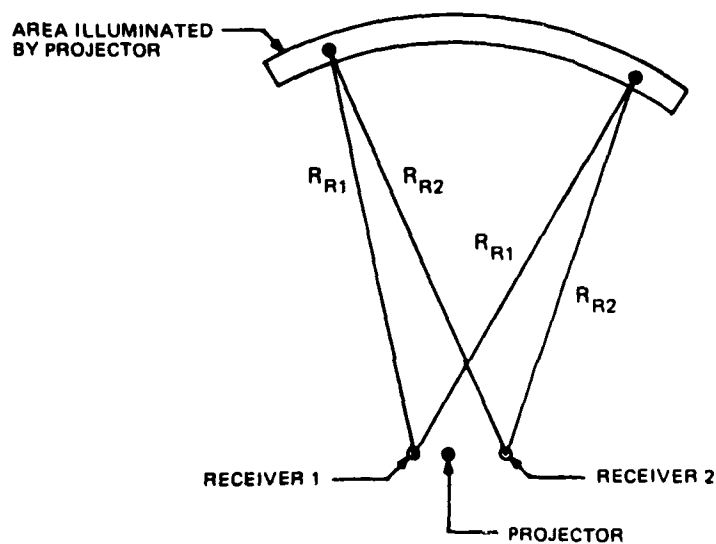
—— PROJECTOR

(a) VIEW FROM ABOVE OF HORIZONTAL RECEIVERS AND PROJECTOR

SURFACE ———

AREA ILLUMINATED
BY PROJECTOR

R_{R1}

R_{R2}

RECEIVER 1 —

PROJECTOR —
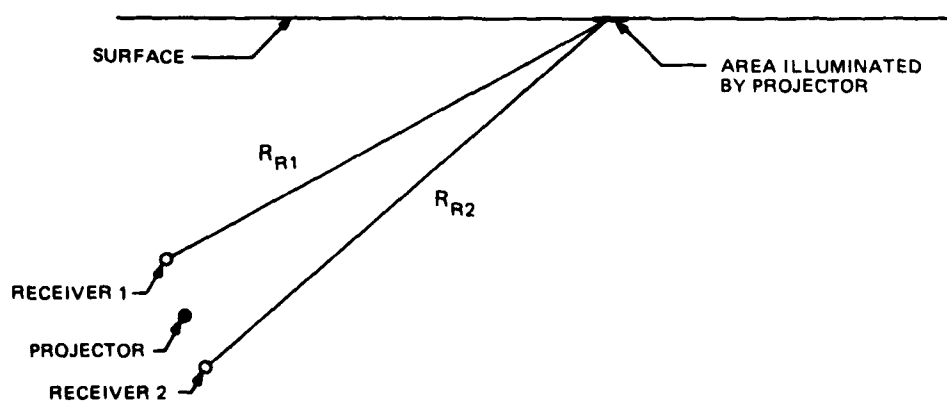
RECEIVER 2 —

(b) VIEW FROM THE SIDE OF VERTICAL RECEIVERS AND PROJECTOR

FIGURE V-58
ILLUSTRATION OF PATH LENGTHS FROM SCATTERER
TO HORIZONTAL AND VERTICAL RECEIVERS

what was observed theoretically and experimentally. For a horizontal

separation of 15 cm, the largest horizontal spacing used, the change

in path length difference was 4 λ, which would produce significant

oscillation of the integrand term and result in very low covariance.

Again, this is what was observed. This agreement indicates that the

qualitative explanation of the covariance is a reasonable one. This

could also explain the larger covariance measured by Frazer, since his

projector was confined horizontally to angles of only ± 10 degrees,

resulting in less change of the path length difference. It was also

found that the path length difference changed negligibly with the small

downrange extent of the scattering region.

The path lengths to the vertical receivers and the

scattering region are indicated in Fig. V-58 from a side view. The

path lengths are different, but it can be seen that the difference

changes little over the region of scatterers. Again, an approximate

calculation indicated that over the 30 degree azimuthal extent, the

path length difference for a 10 cm vertical separation changed only

.03λ. For a vertical separation of 1 m, the change in path length

difference was only .3λ. Thus it can be expected from this qualitative

argument that the model would predict a very large covariance even for

large vertical separations.

Since this reasoning has qualitatively predicted the

performance which has been obtained by the model, then the same reasoning

may indicate possible changes to the model which would bring the vertical

covariance into better agreement with the experimental results. In

particular, it can be observed that in order to change the path length

differences for vertical receivers in the same way in which the horizon-tal path length differences were changed, it would be necessary to consider the scatterers distributed vertically below the surface as well as on the surface and integrate over the depth of the scatterers as well as on the surface. Thus the covariance could be calculated as

$$K^{(12)}(t_1,t_2|t') = \int_{\Lambda_{12}} \rho_v U_1(t_1,\lambda) U_2(t_2,\lambda) dV \quad ,$$

where the integration is now over a volume of scatterers. The scatter density is now a volume scatter density and is a function of the depth below the surface. This implementation would be appropriate if scatter-ing could be physically considered to occur throughout a layer bounded by a flat surface. Although the implementation of the model can pres-ently only perform a surface integration, it was run at several differ-ent depths and the results manually integrated over the depth. It was found that the vertical covariance could be reasonably reduced, depending upon the particular dependence of the density upon depth and the depth of the scattering layer. For example, by considering a con-stant scatter density as a function of depth, the value of the envelope of the covariance at $\tau=0$ between receivers 1 and 2 could be reduced from .99 to .91 by integrating over a 1.2 m depth, and could be further reduced to as little as .24 by an integration over a depth of 3.2 m. The measured value of the envelope was .84.

Although this implementation is conceptually straight-forward, it does have some practical problems. Specifically, it is not obvious how the depth of the scattering layer and the density of scatterers as a function of depth would be determined. Secondly, it is

not known if scattering actually occurs in a layer below the surface
or if it occurs just at the surface. Thus another implementation could
consider scattering at the surface only but allow the surface to vary
randomly in height. The original expression for the covariance contained
an expected value of the product of U_1 and U_2 with respect to random
parameters θ. By retaining one random parameter, the surface wave
height z, and then performing a surface integral over the mean surface
level, the covariance could be expressed as

$$K^{(12)}(t_1,t_2|t') = \sigma_s \int_{\Lambda_{12}} \left\langle U_1(t_1,\bar{\lambda},z)U_2(t_1,\bar{\lambda},z) \right\rangle_z dS \quad ,$$

where $\bar{\lambda}$ is the mean location of the surface and $\langle \rangle_z$ denotes the expected
value with respect to the random surface waveheight z. This implemen-
tation has the advantage of the direct inclusion of the statistical
distribution of the surface wave heights, which is potentially measurable.

It is anticipated that neither of these implementations
would change the results for the horizontal covariance, since the path
length differences to horizontal elements do not change significantly
with depth. It is also anticipated that the temporal results would
be unaffected. Thus it appears that these implementations are reasonable
ones to correct for the vertical covariance.

Finally, it is encouraging to observe that the basic
assumption of a superposition of point scatterers can accurately model
many aspects of the covariance of backscattering, and can at least
qualitatively explain those areas which it cannot presently model well.
Thus it is felt that the basic model itself is still a reasonable model
and that its limitations are due to the simplifications which were

made for the current implementation of the model. It is felt that the present study has further demonstrated the validity and usefulness of the model, and has provided a direction for further improvements to its implementation.

VI. SUMMARY AND CONCLUSIONS

VI.1 Objectives of the Study

The statistical properties of surface reverberation depend upon many varied environmental, geometrical, and sonar parameters. A complete understanding of surface reverberation requires its study under all these conditions. Within this broader context, the present study has attempted to examine a few of the statistical properties under a limited set of these parameters. Four objectives were identified for this study:

1. The primary objective was to simultaneously measure the dependence of the covariance upon spatial separation of the observation points in both the horizontal and vertical orientations. This also involved determining the change of the spatial covariance as a function of time of observation (t) and the difference in the observation times (τ). Although the most closely examined parameter was spatial separation, it was hoped that the dependence upon some other parameters could be inferred as well.

2. The second objective was to compare the measured results to a theoretical model of reverberation. In this way it was hoped that our physical understanding of the acoustic scattering phenomena could be extended. It was of interest to examine a model which included most of the required parameters in a general way, which allowed the computation of various statistical parameters, and which had not been

214

extensively validated experimentally. Thus Middleton's point-scatter model was chosen as the particular model to examine and compare to the measured results. It was also hoped that if the experimental measurements illustrated deficiencies in the model, extensions to the model could be identified which would more accurately predict surface reverberation.

3. A third objective of the study was to experimentally examine the first four univariate moments and perform univariate tests for normality. These measurements would provide some indication of the type of distribution of the reverberation. Although no density estimates were performed, it would be possible to do so with the data presented in this study.

4. Finally, the fourth objective of the study was to refine the techniques for the measurement and validation of reverberation from multiple receivers. A stable platform was desired to minimize possible effects due to platform motion. Larger ensemble sizes were desired in order to reduce the sample error. Statistical tests to efficiently validate these larger ensembles were also needed.

VI.2 Distinctives of the Study

VI.2.1 Experimental Distinctives

1. The measured sound was limited to backscattered sound from the wind-roughened surface of a fresh-water lake.

2. The sound source was pulsed.

3. The receivers were linear arrays oriented horizontally and vertically.

4. A stable platform consisting of a bottom-mounted tower was used.

5. Ensemble estimates were made of the various statistical properties, as opposed to time-average estimates.

6. The possible sources of measurement error were identified and reduced to an acceptable level through the use of specialized data collection/ recording/digitization/processing techniques.

7. Extensive testing of the data was performed to validate the ensembles and to test for normality.

8. The first four moments and the covariance were measured.

VI.2.2 Theoretical Distinctives

1. The model assumed a random surface composed of a collection of independent point scatterers in a homogeneous medium.

2. The model allowed for general geometries, including the spatial distribution of the sensors and the grazing angle.

3. General sources and receivers were allowed: frequency, pulse length, directionality, bandwidth, signal spectrum, and aperture response could be taken

into account.

4. The model was implemented for bandlimited transmissions.

5. The scatterers were modeled as perfect point reflectors distributed uniformly over the surface.

VI.3   Review of the Study

VI.3.1   Chapter I

Chapter I presented an introduction to the study, citing several similar studies and exposing the need for the present study. It was shown that the coherence of forward-scattered sound has been examined for both vertical and horizontal arrays, but that it was expected that backscattered sound would have significantly different statistical properties. It was also shown that explosive sources have been used to measure the coherence of backscattered sound for both horizontal and vertical arrays using time averages. Significant differences were determined between the coherence of horizontal and vertical arrays; thus it was expected that similar differences would be observed using a pulsed source and ensemble averages.

VI.3.2   Chapter II

The second chapter described the experimental measurements. Estimates of the effects of reverberation to ambient noise ratio, crossover between receiver channels, and finite sample size on the accuracy of the calculation of the coherence were made. It was shown that with the measurement system used, the primary limitation was finite sample size. Since the accurate measurement of coherence between re-

ceivers also requires the preservation of the phases of the reverberation
returns at the face of the receivers, the various sources of phase
error which could be introduced into the system were identified. The
techniques for minimizing or correcting these phase errors were described.
The techniques required the proper interaction of special data collection,
analog recording, digitization, and digital processing.

One projector and two line receiving arrays were used
to collect the data. The vertical array consisted of nine elements
with a maximum separation of slightly less than 1 m. The horizontal
array contained four elements with approximately a .15 m maximum separ-
ation. A 100 μs pulsed CW signal at a center frequency of 80.0 kHz
was transmitted at the surface at a 10.5 degree grazing angle. The
center of the array was 10.2 m below the surface in approximately 40 m
of water. The water was isothermal and wave heights in the 35-50 kph
wind were approximately .3-.6 m.

VI.3.3 Chapter III

The theoretical model was described in the third chapter
of this study. Reverberation was modeled as a linear superposition of
the scattered sound from independent point scatterers representing in-
homogeneities at the surface of a homogeneous medium. Special attention
was given to the assumptions inherent in the model, and the additional
assumptions made for its current implementation. The general model
was described first, and an expression for the covariance function
was given. Several simplifying assumptions were then introduced. Among
others, the transmitted signal was assumed to be bandlimited, and the
scatterer was modeled as a perfect point reflector. An expression

for the elementary scattered waveform, representing the waveform from
a single scatterer, was then developed, along with a simplified ex-
pression for the covariance. A quadrature representation of the co-
variance was then developed in order to allow the presentation of the
covariance in terms of its envelope and phase. The specifics of imple-
menting the model on a computer were then discussed. Some of the
details of the development of the model were expanded upon in the three
appendices.

VI.3.4 Chapter IV

Chapter IV began the analysis of the data. The pro-
cedure for sampling the data to form ensembles was described, along
with the assumptions inherent in this sampling process. A 10 ms rever-
beration return was sampled at 320 kHz, resulting in 3200 samples in
time for each of 1084 pings and 13 receivers. Ensembles were formed
at each sample time, resulting in 3200 ensembles of 1084 pings each.
Subsequent analysis of the data was restricted to the last 500 samples
of each ensemble because of a changing reverberation intensity in the
first part of the ensembles.

All 3200 ensembles of each channel were first tested for
statistical validity and then for normality. A general overview of
statistical hypothesis testing was given, and a description of each
test which was employed was provided. Since each sample ensemble is
treated as a random sampling of the reverberation process, then each
ensemble should consist of random variables which are independent and
identically distributed (i.i.d.). To verify the i.i.i. properties of

the ensembles, each ensemble was tested for randomness (independence)
and homogeneity (identical distribution). Independence guarantees that
the generation of one random variable in the ensemble was not affected
by the generation of any others, while homogeneity implies that all
the random variables come from the same parent population, that is,
they all have the same distribution. The runs up and down test was
used for testing for randomness, while the Kolmogorov-Smirnov two-
sample test and the Wilcoxon rank-sum test were used for testing for
homogeneity. Results of the tests were presented for all channels.
After determining the validity of the ensembles, they were then tested
to determine if their underlying distribution was gaussian. Four tests
for normality were applied: Pearson's test of skewness, Pearson's test
of kurtosis, D'Agostino's test, and the Kolmogorov-Smirnov one-sample
test.

VI.3.5 Chapter V

The main objective of the study was finally addressed
in Chapter V. First the techniques for the numerical computation of
the various moments and the covariance were given. It was shown that
the covariance from a bandlimited transmission consists of a time-sum
and a time-difference component. The validity of ignoring the time-sum
component was briefly discussed. The time-difference component of
the covariance was expressed in terms of an envelope function and a
phase function. The technique for normalizing the covariance was
defined. The sample mean, variance, skew, and kurtosis were presented
for a limited section of the 10 ms reverberation return for all 13

channels. The difference component of the variance was also presented and compared to the actual variance.

The last part of Chapter V provided a rather thorough analysis of the covariance. All the analysis was performed with the difference component. The results from the theoretical model were also presented for comparison to the experimental results. First the variance was presented over the entire 10 ms interval. Then the normalized envelopes and phases of the auto-covariance were presented as a function of the time difference τ at a time t=75.25 ms after transmit. The effect of pulse length on the temporal duration of the covariance was discussed, and stationarity was examined. The auto-covariance was then presented over the entire 10 ms interval, both normalized and unnormalized. Secondly, the cross-covariance for $\tau=0$ was also given. The envelope of the covariance as a function of spatial separation for both the horizontal and vertical arrays was presented for one time, and then for the entire 10 ms interval. The phase of the covariance at $\tau=0$ was also given over the 10 ms interval. For the vertical array, the effect of location of the elements on the array was examined for both the envelopes and phases. Thirdly, the covariance envelopes and phases were presented for $\tau\neq0$ at one time as a function of spatial separation. Finally, a qualitative explanation for the failure of the model to correctly predict the dependence of the vertical covariance on spatial separation was presented. Suggested changes to the model were also given.

VI.4   Summary of the Results of the Study

The previous section contained a review of the work which was

performed on this study. The results of the data analysis will now

be summarized. The results will be presented according to the objec-

tives for the study.

VI.4.1 Computation of Vertical and Horizontal Covariance

1. It was found that the normalized envelope of the

    horizontal covariance at $\tau=0$ decreased to a value of

    0.1 at a separation of just over four wavelengths.

    A comparison was made to the horizontal covariance

    measured by Frazer under similar circumstances. It

    was found that the present study obtained smaller

    values of the covariance. The difference was

    attributed to the illumination of more "off-axis"

    scatterers because of the wider transmit horizontal

    beamwidth used in the present study.

2. The horizontal covariance at $\tau=0$ was also determined

    as a function of time after transmit over the 10 ms

    interval from which reverberation samples were taken.

    It was found that the normalized envelopes of the

    horizontal covariance were statistically constant

    throughout the 10 ms interval; any fluctuations

    could be attributed to the finite ensemble size.

    It was also observed that the phases of the co-

    variance were constant for separations which had signif-

    icantly non-zero covariance envelopes, but for

    small values of the covariance envelopes the phases

changed with time. The phases which were constant were non-zero, indicating a non-uniform scatter density and resulting in a covariance which was less than the envelope value.

3. The dependence of the vertical covariance on spatial separation was also examined. The vertical co-variance maintained a significant level at much larger separations than the horizontal covariance. Even at the greatest separation of a little over 50 wavelengths, the normalized envelope of the vertical covariance still had a value greater than 0.2.

4. It was also determined that the normalized envelope of the covariance between vertically separated receivers did not change significantly over the 10 ms interval. However the phase of the vertical co-variance did change with time, and the rate of change increased with increasing vertical separation. The change was approximately linear, indicating that the actual covariance slowly oscillated with time.

5. The vertical array also contained several pairs of elements which had the same separation at different locations on the array. It was determined that the envelope at a specified separation did not change significantly with location on the array, but that the phase did. Thus the covariance was dependent not

only on the separation of the vertical receivers, but also on their position.

6. The horizontal and vertical covariances were also examined as a function of time difference (τ). It was found that the covariance envelopes decreased to zero in a time difference approximately equal to the extent of the transmitted pulse after it was filtered by the projector and receiver. The 100 µs pulse was extended in time to approximately 275 µs, and the envelope of the covariance decreased to zero in approximately 250 µs. The envelopes exhibited an approximate even symmetry about $\tau=0$, and the phases had approximately an odd symmetry.

7. The auto-covariance for one receiver was also shown as a function of t and τ over the 10 ms interval. Non-stationarity was observed in the unnormalized covariance over the 10 ms due to the change of the envelope with time. However much of this non-stationarity was removed from the auto-covariance by normalization.

8. The variance (auto-covariance at $\tau=0$) was also examined as a function of time. It was found to change with time due to the vertical directionality of the projector. The entire 10 ms interval of reverberation resulted from illumination of the surface by the main lobe from the vertical directionality

pattern of the projector.

VI.4.2 <u>Comparison to Theoretical Model</u>

1. The model was found to agree well with the spatial
   dependence of the normalized envelope of the co-
   variance from the horizontal array. This was especially
   significant since the same model also accurately
   predicted the horizontal covariance obtained by
   Frazer, even though the two levels of covariance
   were different.

2. The model also correctly predicted that the envelope
   of the normalized covariance would not change with
   time over the 10 ms interval. The phase was pre-
   dicted to be constant and near zero, as expected,
   since the model assumes a uniform scatter density.
   The measured phase was constant for significant
   levels of covariance but was non-zero; thus the
   actual measured covariance was less than predicted
   because of the non-zero measured phase. The theo-
   retical model did not predict the change in phase
   with time for the low levels of covariance on the
   horizontal array.

3. The envelope of the covariance as a function of
   spatial separation for the vertical array was
   greatly over-estimated by the model. However, the
   model did correctly predict the change in phase

as a function of time for the vertical array, and
the change in phase as a function of vertical separation.

4. The dependence of the covariance on time difference
   was also examined by the model. Very good agreement was obtained between the model and the experimental results. The shapes of the envelopes
   of the auto-covariance and horizontal cross-covariance were predicted very accurately. There was
   also good agreement between the phases as a function
   of τ. The envelopes of the cross-covariance of the
   vertical array were overestimated, as was mentioned
   earlier, but the value of τ for which the envelopes
   went to zero was correctly predicted.

5. The variance was also computed theoretically for
   the entire 10 ms interval on all 13 channels. Good
   agreement was obtained with the experimental results.
   This agreement indicated that the effects of depth,
   grazing angle, and directionality were being correctly taken into account.

6. An explanation for the failure of the model to
   correctly predict the dependence of the envelope
   of the covariance on vertical separation was also
   given. It was shown that better agreement could
   possibly be obtained by considering the scatterers

distributed vertically as well as horizontally in
the plane of the surface. Two methods for including
a vertical distribution of the scatterers were
presented. One method considered the scatterers
to be distributed in a volume layer upper bounded
by the plane of the surface. The other method
considered the scatterers to be distributed only at
the surface but allowed the surface to vary randomly
in height.

VI.4.3 <u>Computation of Moments and Tests for Normality</u>

1. The mean, variance, skew, and kurtosis were examined,
   and all 3200 ensembles of each channel were tested
   for univariate normality. It was shown that the
   moments contained an oscillatory component. The
   fundamental frequency of the oscillation appeared
   to depend upon the order of the moment, that is,
   the rth moment appeared to oscillate fundamentally
   at a frequency of $r \cdot \omega_o$. It was shown that the ampli-
   tude of the mean was not statistically large. It
   was also shown that the oscillation of the variance
   was not statistically large compared to the difference
   component of the variance. The oscillations of
   the skew were shown to be symmetric about zero.
   Since a normal distribution has zero skew, it was
   shown that deviations from normality due to skew
   different from zero were due to the oscillatory

component of the skew. However, this was found not to be the case for the kurtosis. A normal kurtosis has a value of 3, but the measured kurtosis was not symmetric about a value of 3. Rather, it was generally larger than 3. Thus deviations from normality were due to a larger than normal kurtosis.

2. Several tests for normality were performed. The ensembles were generally found to be non-normal due to a slight amount of skew and a significantly large kurtosis. This result is in contrast to other studies which have indicated that surface reverberation was normally distributed.

VI.4.4 Development of Measurement Techniques and Data Validation

1. Tests for randomness and homogeneity were selected for power and computational efficiency. Ensembles of 1000 samples were found to be random (independent) but inhomogeneous. Much of the inhomogeneity was removed by restricting the ensembles to the last 500 samples. The inhomogeneity was attributed to a change in reverberation intensity during the collection of the data. Thus it was possible to generate statistically valid sample ensembles.

2. A technique was demonstrated which reduced the measurement errors to an acceptable level.

VI.5   Conclusions

Now that the work performed in this study has been reviewed and the results summarized, a number of conclusions can be drawn. The conclusions will also be organized according to the objectives of the study.

VI.5.1   Computation of Vertical and Horizontal Covariance

1. Significant levels of covariance can extend out to relatively large separations. It is sometimes assumed that signal processing gain can be achieved by lengthening a receiving array since the noise is incoherent over the extended length while the signal remains coherent. It has been shown here that in some cases this assumption can be very misleading. Thus simplistic assumptions in the design of sonar systems may lead to performance predictions which are not achievable in practice. More accurate designs and performance predictions can be obtained by considering results such as presented in this study.

2. It is also obvious that the covariance between two receivers is greatly affected by the relative orientation of the receivers, and not just by their separation. In particular, the covariance between vertically separated elements is much larger than between horizontally separated elements, at least in

the case examined. The time dependence of the
covariance is also greatly affected by the orienta-
tion of the receivers. The horizontal covariance
was constant with time, while the vertical co-
variance slowly oscillated with time. The vertical
covariance also depended upon the location on the
array. Both these effects, the time dependence
and the location dependence, can be equated to a
dependence upon grazing angle. The normalized
covariance for the horizontal array was unaffected
by grazing angle over the limited range examined,
while the normalized covariance for the vertical
array was greatly affected. Thus geometrical
parameters such as spatial distribution of the
sensors and grazing angle can have a very signifi-
cant effect upon covariance.

3. It can also be concluded from this study that sonar
parameters can determine some of the characteristics
of the covariance. The temporal extent of the
covariance is determined in part by the length of
the transmitted pulse after it has been filtered by
the transmitting and receiving apertures. Thus
the pulse length and the frequency responses of the
transmitter and receivers affect the temporal extent
of the covariance. It has been shown in other

studies[16,19] that the frequency spectrum of the

transmitted signal can also affect the temporal

extent of the covariance. It has been inferred by

a comparison of the results from this study and the

study by Frazer that the level of the covariance

between horizontal receivers can be affected by the

projector's horizontal beamwidth. The projector's

vertical beamwidth certainly affects the level of

the unnormalized covariance. Therefore, sonar

parameters such as pulse length, directionality,

aperture response, and signal spectrum affect the

covariance of surface reverberation.

4. Based on the non-zero phase of the horizontal co-
variance, it was inferred that surface scatter
density was not uniformly distributed. A non-
uniform scatter density is most likely attributable
to a shadowing of scatterers as a function of azi-
muthal angle to the surface. Thus the shadowing
function would depend upon such factors as the angle
between the wind direction and the direction the
array is pointing, the wave height distribution, and
the wave spectrum. It was also shown that the
vertical covariance most likely depends upon wave
height distribution. Thus, although the present
study had very little control over environmental

conditions, several observed phenomena could possibly be explained by environmental effects.

VI.5.2 Comparison to Theoretical Model

1. A realistic model must be able to correctly take into account all these various parameters which affect the covariance of reverberation. It can be concluded that, at least over the range of parameters considered, the model used in this study is correctly taking into account the various sonar and geometrical parameters, but needs to additionally take into account some environmental parameters.

2. In spite of this additional need, a number of properties of the covariance can already be predicted. The horizontal covariance is being modeled reasonably well (with the exception of non-zero phase). The temporal extent of the covariance and the change of the variance and covariance with time is being predicted. Thus many aspects of the covariance can be predicted without environmental information.

3. The present study has also served to reinforce the basic assumptions and approach of the point-scatter model. The many properties of the covariance which could be predicted by the model indicate the reasonableness of its basic approach. In addition, a reasonable explanation of the failure

of the model to predict the vertical covariance

co-ld be made from the model, indicating a failure

not of the basic model, but of its current imple-

mentation. Therefore it can be concluded that this

point-scatter model is a reasonable model of

surface reverberation which has proven to be accurate

under certain conditions.

VI.5.3 <u>Computation of Moments and Tests for Normality</u>

1. From the comparison of the difference component

of the variances and actual variances, it can be

concluded that the sum term of the variance is

measurable. In this case, it was small in

comparison to the difference term of the variance,

but it may not be small in every instance. It is

not known to what extent the sum term of the var-

iance (or covariance) will affect the performance

of signal processing schemes which depend upon

information about the covariance of the noise field.

2. It was also observed that all the moments examined

contained an oscillatory component which had a

varying amplitude. It was shown that although the

mean oscillated, the extent of its amplitude was

not statistically different from zero. Thus from

a statistical viewpoint the mean can be considered

to be zero. That is, the random amplitude of the

oscillation was not significantly different from
zero in comparison to the magnitude of the variance.
In this case it can be concluded that the moments
examined were not con:tant with time, containing
both a random magnitude which changed slowly with
time and a component which oscillated rapidly with
time. However, the magnitudes of these oscillations
were not large.

3. Although density estimates were not made for these
data, the data were tested for normality and found
to be non-gaussian due to a larger than normal
kurtosis. Tests for normality on other surface
reverberation data have shown them to be gaussian.
However, it is not well known under what conditions
gaussian behavior is to be expected. Thus it is
concluded that surface reverberation can exhibit
non-gaussian behavior, although the reasons for
this behavior are unknown.

VI.5.4 Development of Measurement Techniques and Data Validation

1. Considering the validation of the sample ensembles,
one can conclude that random ensembles can be
generated, but that care must be taken to ensure
their homogeneity. In particular, changes in the
reverberation intensity during the generation of the
ensemble data can lead to inhomogeneities. Thus

specific tests for homogeneity should be performed.

VI.6   Accomplishments and Contributions

The summary and conclusions that have just been made for this study lead to the identification of several accomplishments and contributions which have resulted from the study:

1. The covariance of surface reverberation from a pulsed source was measured simultaneously in both the horizontal and vertical orientations and found to be quite different. A detailed analysis of these differences was provided.

2. It was shown that the covariance of surface reverberation depends upon many environmental, geometrical, and sonar parameters.

3. The accuracy of the theoretical model was verified for the horizontal covariance. It was shown that the model is correctly taking into account many of the parameters which affect surface reverberation.

4. A deficiency in the model was identified. The reason for the deficiency was attributed to the failure of the current implementation of the model to take into account certain environmental conditions. The ability of the model to explain the failure of this implementation, along with the ability of the model to correctly predict many aspects of the covariance, has provided additional confidence in the point-scatter approach of the model.

5. Univariate moments of the reverberation were closely

examined. Oscillation of the moments was demonstrated.

6. The sum term of the variance was shown to be measurable, thus bringing into question the indiscriminate application of the difference component approximation of the covariance.

7. It was demonstrated that surface reverberation can be non-gaussian.

8. It was shown that large ensemble sizes (500) could be constructed and validated.

VI.7 Recommendations for Further Study

As is typical of most studies of this type, as many questions have been raised as have been answered. Several directions for further research have become obvious during the course of the study. Thus it seems reasonable to conclude with a list of recommendations for further study:

1. An attempt should be made to extend the theoretical model so that it will correctly predict the dependence of the covariance on vertical separation. It is felt that the greatest potential for doing so lies in the proper inclusion of the statistical distribution of the surface wave heights.

2. The model should also be extended to predict the non-zero phase of the horizontal covariance. The addition of a shadowing function which depends upon the direction of the waves, the wave spectrum, and the wave heights to effectively produce a non-uniform scatter density appears to be a reasonable approach.

3. In order to validate these extensions to the model, additional experimental data, including m ,urements of wind direction, wave heights, and wave spectra, will be necessary,

4. There are several advantages to conducting experiments in a controlled environment such as a tank. The effects of environmental conditions may be studied individually and with better control.

5. It would also be of interest to extend the model to predict other moments in addition to the covariance.

6. Some unexpected effects were observed when the covariance was low. It was speculated that secondary scattering may be their cause. Although these effects appear to have little practical significance, further study of them may be of interest.

7. Additional data at different pulse lengths, grazing angles, and projector horizontal beamwidths would help to confirm some of the tentative conclusions drawn from this study concerning the effects of these parameters.

8. The model has yet to be validated for other than pulsed CW signals. Since experimental results have shown that other transmit types, such as linear frequency modulated transmissions, produce results which differ from the results from pulsed CW transmissions, it would be useful to validate the model under these different conditions.

9. Since it has been shown that reverberation is sometimes gaussian and sometimes non-gaussian, it would be very useful

to determine under what conditions a departure from normality can be expected.

10. Improved criteria for accepting or rejecting an entire set of ensembles for a statistical hypothesis test should be developed.

11. An examination of the power and cross-power spectra in conjunction with the covariance would be useful.

APPENDIX A

DERIVATION OF THE CHARACTERISTIC FUNCTION AND MOMENTS

The following is a derivation of the characteristic function and moments of the reverberation process for one and two receivers. The derivation follows closely Ref. 27, but in abbreviated form.

The receiver output at time t due to a single point scatterer at point λ_j is denoted by $U_j(t,\lambda_j)$. The receiver output from all point scatterers which were illuminated is just the sum of all elementary scattered returns $U_j(t,\lambda_j)$:

$$X(t,t') = \sum_{j=1}^{M(t')} U_j(t,\lambda_j)$$

where $M(t')$ is the number of contributing scatterers at time t'. What needs to be determined here is the covariance of X between two times t_1, t_2. The procedure will be to determine the joint density function of $X(t_1)$ and $X(t_2)$ in terms of the Poisson distribution of the scatterers and then Fourier transform the joint density function to get the joint characteristic function, from which the covariance can be calculated by taking the appropriate derivatives.

The joint density function of the two signals $X(t_1)$ and $X(t_2)$ and the number of contributing scatterers M in the spatial interval Λ at the time t' is

$$W(X_1,t_1,X_2,t_2,M|t',\Lambda)$$

which can be written in terms of the joint conditional density function

$$W(X_1,t_1,X_2,t_2|N,t',\Lambda)$$

as

$$W(X_1,t_1,X_2,t_2,N|t',\Lambda) = P(N|t',\Lambda)W(X_1,t_1,X_2,t_2|N,t',\Lambda)$$

where $P(N|t',\Lambda)$ is the probability function of the discrete random variable N. The joint density function of X_1 and X_2 alone is just

$$W(X_1,t_1,X_2,t_2|t',\Lambda) = \sum_{N=0}^{\infty} W(X_1,t_1,X_2,t_2,N|t',\Lambda)$$

$$= \sum_{N=0}^{\infty} P(N|t',\Lambda)W(X_1,t_1,X_2,t_2|N;t',\Lambda) \quad (A.1)$$

since N is discrete.

$P(N|t',\Lambda)$ is the probability of N events in the interval Λ. The basic assumption is that this probability is Poisson distributed, i.e., for each point λ_j in Λ, the probability that exactly N events occur in a sufficiently small interval $\Delta\lambda_j$ about λ_j is

$$P(N|t',\Delta\lambda_j) = [\rho(t',\lambda_j)\Delta\lambda_j]^N \exp[-\rho\Delta\lambda_j]/N!$$

where $\rho(t',\lambda_j)$ is the density of the process.

By taking the Fourier transform of Eq. (A.1) for the smaller interval $\Delta\lambda_j$, we get

$$F_2(i\xi_1,t_1,i\xi_2,t_2|t',\Delta\lambda_j) =$$

$$\sum_{N=0}^{\infty} P(N|t',\Delta\lambda_j)F_2(i\xi_1,t_1,i\xi_2,t_2|N;t',\Delta\lambda_j) \quad (A.2)$$

where F_2 is the joint characteristic function. From the definition of the characteristic function and the receiver output X:

$$F_2(i\xi_1,t_1,i\xi_2,t_2|N;t',\Delta\lambda_j) = \langle \mathrm{expi}(\xi_1 X_1 + \xi_2 X_2)\rangle$$

$$= \langle \mathrm{expi}(\xi_1 \sum_{j=1}^{N} U_j(t_1,\lambda_j) + \xi_2 \sum_{j=1}^{N} U_j(t_2,\lambda_j))\rangle$$

$$= \langle \prod_{j=1}^{N} \mathrm{expi}(\xi_1 U_j(t_1,\lambda_j) + \xi_2 U_j(t_2,\lambda_j))\rangle$$

$$= \prod_{j=1}^{N} \langle \mathrm{expi}(\xi_1 U_j(t_1,\lambda_j) + \xi_2 U_j(t_2,\lambda_j))\rangle \qquad .$$

This last step is possible since the U_j are independent. By making the assumption that all the U_j are identical, the expression can be written as

$$\langle \mathrm{expi}(\xi_1 U(t_1,\lambda) + \xi_2 U(t_2,\lambda))\rangle^N \qquad .$$

By substituting this into Eq. (A.2), we get

$$F_2(i\xi_1,t_1,i\xi_2,t_2|t',\Delta\lambda) = \sum_{N=0}^{\infty} P(N|t',\Delta\lambda_j) \langle \mathrm{expi}(\xi_1 U_1 + \xi_2 U_2)\rangle^N$$

$$= \sum_{N=0}^{\infty} [\rho\Delta\lambda_j]^N \exp[-\rho\Delta\lambda_j]/N! \langle \mathrm{expi}(\xi_1 U_1 + \xi_2 U_2)\rangle^N$$

$$= \exp[-\rho\Delta\lambda_j] \sum_{N=0}^{\infty} \frac{1}{N!} [\rho\Delta\lambda_j \langle \mathrm{expi}(\xi_1 U_1 + \xi_2 U_2)\rangle]^N$$

$$= \exp[-\rho\Delta\lambda_j] \exp[\rho\Delta\lambda_j \langle \mathrm{expi}(\xi_1 U_1 + \xi_2 U_2)\rangle]$$

$$= \exp[\rho\Delta\lambda_j(\langle \mathrm{expi}(\xi_1 U_1 + \xi_2 U_2)\rangle - 1)]$$

$$= \exp[\rho\Delta\lambda_j \langle \mathrm{expi}(\xi_1 U_1 + \xi_2 U_2) - 1\rangle] \qquad .$$

From the property of this exponential, if Λ is the sum of all indepen-dent, non-overlapping intervals $\Delta\lambda_j$, then

$$F_2(i\xi_1,t_1,i\xi_2,t_2|t^\prime,\Lambda) = \prod_j F_2(i\xi_1,t_1,i\xi_2,t_2|t^\prime,\Delta\lambda_j)$$

$$= \prod_j \exp[\rho\Delta\lambda_j \left\langle \exp i(\xi_1 U_1+\xi_2 U_2)-1\right\rangle]$$

$$= \exp[\sum_j \rho\Delta\lambda_j \left\langle \exp i(\xi_1 U_1+\xi_2 U_2)-1\right\rangle]$$

In the limit as $\Delta\lambda_j \to 0$, this becomes

$$F_2(i\xi_1,t_1,i\xi_2,t_2|t^\prime,\Lambda) =$$

$$\exp[\int_\Lambda \rho(t^\prime,\lambda) \left\langle \exp i(\xi_1 U(t_1,\lambda)+\xi_2 U(t_2,\lambda))-1\right\rangle d\lambda]$$

This is the joint characteristic function of the two receiver outputs $X(t_1)$ and $X(t_2)$. The characteristic function of a single receiver output would just be

$$F_1(i\xi_1,t_1|t^\prime,\Lambda) = \exp[\int_\Lambda \rho(t^\prime,\lambda) \left\langle \exp i(\xi_1 U_1)-1\right\rangle d\lambda]$$

The expected value of $X(t_1)$ is

$$\left\langle X(t_1)\right\rangle = -i \frac{\delta}{\delta\xi_1} F_1(i\xi_1,t_1|t^\prime,\Lambda)|_{\xi=0}$$

$$= -i \int_\Lambda \rho \frac{\delta}{\delta\xi_1} \left\langle \exp i\xi_1 U_1-1\right\rangle d\lambda F_1|_{\xi=0}$$

$$= -i \int_\Lambda \rho \left\langle iU_1 \exp i\xi_1 U_1\right\rangle d\lambda F_1|_{\xi=0}$$

$$= \int_\Lambda \rho \left\langle U_1\right\rangle d\lambda$$

Likewise the expected value of the product of the two receiver outputs $X(t_1)$ and $X(t_2)$ is

$$\left\langle X(t_1)X(t_2)\right\rangle = -\frac{\delta^2}{\delta\xi_1\delta\xi_2} F_2|_{\xi_1=\xi_2=0}$$

which turns out to be

$$\int_\Lambda \rho \left\langle U_1 U_2 \right\rangle d\lambda + \int_\Lambda \rho \left\langle U_1 \right\rangle d\lambda \int_\Lambda \rho \left\langle U_2 \right\rangle d\lambda \quad .$$

Thus, the temporal covariance

$$K_X(t_1, t_2 | t') = \left\langle X(t_1) X(t_2) \right\rangle - \left\langle X(t_1) \right\rangle \left\langle X(t_2) \right\rangle$$

is just

$$\int_\Lambda \rho(t', \lambda) \left\langle U(t_1, \lambda) \, U(t_2, \lambda) \right\rangle d\lambda \quad .$$

This is the temporal covariance of a single receiver. The extension to the joint spatial-temporal covariance of the outputs $X^{(1)}(t_1)$ and $X^{(2)}(t_2)$ of two receivers follows exactly the same argument as above to yield the similar result:

$$K^{(12)}(t_1, t_2 | t') = \int_{\Lambda_{12}} \rho_{12}(t', \lambda) \left\langle U_1(t_1, \lambda) U_2(t_2, \lambda) \right\rangle d\lambda$$

where $X^{(1)}(t_1)$ is the output of receiver 1 at time t_1 and $X^{(2)}(t_2)$ is the output of receiver 2 at time t_2. Λ_{12} is the region of scatterers which contributed to the signal at both receivers and ρ_{12} is the density of these scatterers.

APPENDIX B

THE ELEMENTARY SCATTERED WAVEFORM

Utilizing the assumptions stated in Chapter III, the form for the elementary scattered wave $U(t,\lambda)$ is developed. The procedure amounts to convoluting the transmitting, scattering, and receiving apertures with the appropriate signal and solving the homogeneous wave equation in the medium.

Beginning with the transmitter, the pressure density at the point $\vec{\xi}$ on the surface of the transmitter (Fig. B-1) is just the convolution of the input electrical signal with the response function of the transmitter. In the frequency domain this is

$$G_T(t,\vec{\xi}) = a_T(\vec{\xi}) \int_{-\infty}^{\infty} T_T(f) S_{in}(f) e^{i\omega t} df$$

where

$S_{in}(f)$ is the frequency spectrum of the input electrical signal,

$T_T(f)$ is the frequency response function of the transmitter, and

$a_T(\vec{\xi})$ is the transmitter aperture, and is the spatial Fourier transform of the beam pattern. It is assumed that the aperture is frequency independent and that S_{in} is the same for all points $\vec{\xi}$ on the transmitter.

The incident pressure at any point $\vec{R}_T$ from the transmitter in the homogeneous medium is given by the solution of the wave equation

$$\nabla^2 P_{inc} - \ddot{P}_{inc}/c^2 = -G_T(t,\vec{\xi}) \qquad .$$
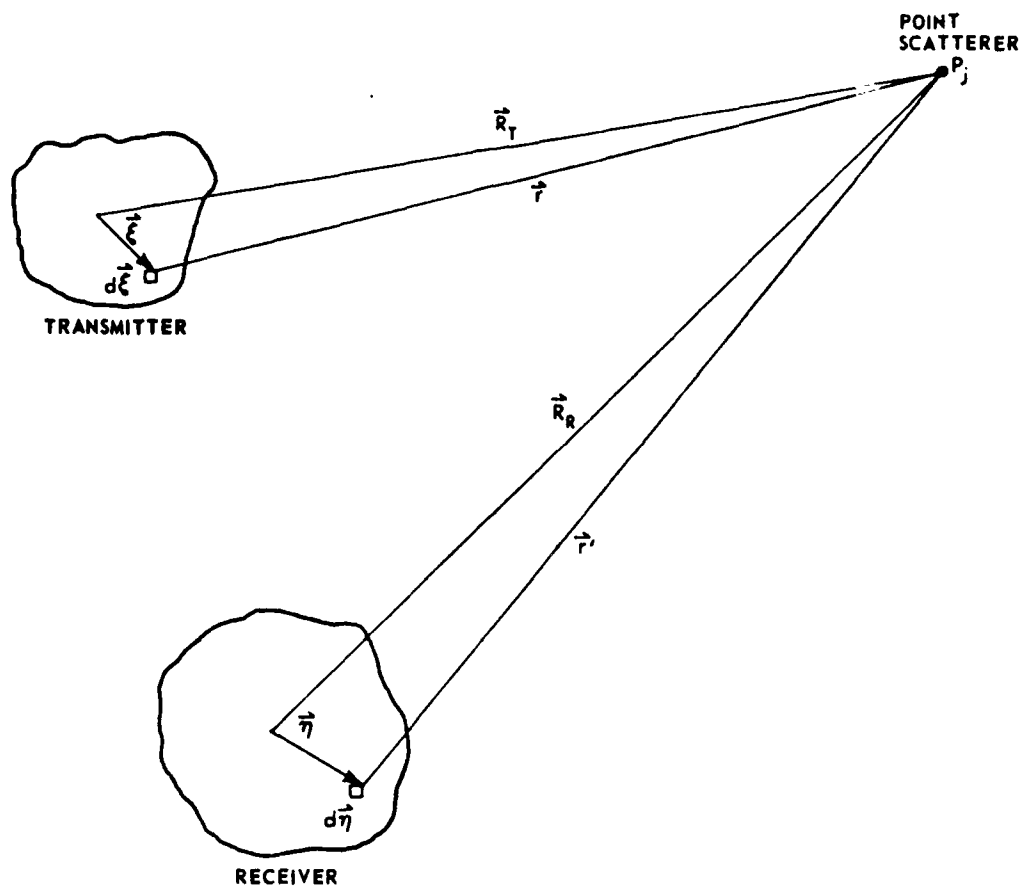
FIGURE B-1
SCATTERING GEOMETRY FOR MIDDLETON'S REVERBERATION MODEL

The solution is

$$P_{inc}(t,R_T) = \int_{V_T} G_T \left(t-\frac{r}{c},\vec{\xi}\right) \frac{d\vec{\xi}}{4\pi r}$$

where G_T is given above and

$$\vec{r} = \vec{R}_T - \vec{\xi} \quad .$$

Applying the farfield assumptions that

$$\frac{1}{r} \simeq \frac{1}{R_T} \qquad \text{and} \qquad \frac{r}{c} \simeq \frac{R_T}{c} - \frac{\vec{\xi}\cdot\vec{R}_T}{c}$$

and substituting G_T in from above gives

$$P_{inc}(t,R_T) = \frac{1}{4\pi R_T} \int_{-\infty}^{\infty} A_T\left(\frac{f}{c}\,\hat{R}_T\right) T_T(f) S_{in}(f) e^{i\omega\left(t-\frac{R_T}{c}\right)} df$$

where the integral over $\vec{\xi}$ has been incorporated into the beam pattern A_T as the inverse Fourier transform of a_T.

To get the scattered pressure, it is first necessary to consider the reradiated pressure density over the scatterer. This pressure density is just the convolution of the incident pressure on the scatterer with the response function of the scatterer, just as was done with the electrical signal and the response function of the transmitter. It is, this time, in the time domain:

$$G_{scat}(t,\vec{R}|\vec{R}_T) = \delta(\vec{R}) \int_{-\infty}^{\infty} h(\tau,t|\vec{R}_T) P_{inc}(t-\tau,R_T) d\tau$$

where $\delta(\vec{R})$ is the delta function and is the spatial aperture of the point scatterer, and $h(\tau,t|\vec{R}_T)$ is the response function of the scatterer. The response function is time varying and thus spreads the incident wave in frequency as well as time delay.

The scattered pressure is again the solution of the homogeneous

scalar wave equation

$$\nabla^2 P_{scat} - \ddot{P}_{scat}/c^2 = -G_{scat}(t,\vec{R}|\vec{R}_T)$$

The solution is

$$P_{scat}(t,\vec{r}') = \int_{V_{scat}} G_{scat}(t-\frac{r}{c},\vec{R}|r_T)\frac{d\vec{R}}{4\pi r}$$

where $\vec{r} = \vec{r}' - \vec{R}$ and $\vec{r}'$ is a vector from the scatterer to receiver.
Substituting in for G_{scat} and integrating over the delta function
$\delta(\vec{R})$ gives

$$P_{scat}(t,r') = \frac{1}{(4\pi)^2 R_T r'} \int_{-\infty}^{\infty} y(f,t-\frac{r'}{c}|R_T)A_T(\frac{t\hat{r}}{c}R_T)T_T(f)$$

$$\times S_{in}(f)e^{i\omega(t-\frac{r'}{c}-\frac{R_T}{c})}df$$

where the impulse response function h has been absorbed into y by
integrating over τ; that is,

$$y(f,t-\frac{r'}{c}|R_T) \equiv \int_{-\infty}^{\infty} h(\tau,t-\frac{r'}{c}|R_T)e^{-i\omega\tau}d\tau$$

All that is left to do now is to convolve this scattered pressure
with the receiving aperture to get the elementary scattered return,
namely:

$$U(t,R_R) = \int_{V_R} d\vec{n}a_R(\vec{n})\int_{-\infty}^{\infty} T_R(f')P_{scat}(f',R_R)e^{i\omega't}df'$$

where $a_R(\vec{n})$ is the receiver aperture, $T_R(f')$ is the receiver frequency
response, and $P_{scat}(f',R_R)$ is the Fourier transform of $P_{scat}(t,R_R)$. It
is assumed that the receiver is in the farfield of the scatterer so

that the farfield assumptions made previously are also applied here. Substituting the equation for $P_{scat}(f',R_R)$ into the equation for the elementary scattered return gives

$$U(t,R_R) = \frac{1}{(4\pi)^2 R_R R_T} \int_{-\infty}^{\infty} df' \int_{-\infty}^{\infty} df T_R(f') A_R(\frac{f'}{c}\hat{R}_R) Y(f,f'-f|\vec{R}_T)$$

$$\times A_T(\frac{f}{c}\hat{R}_T) T_T(f) S_{in}(f) e^{i\omega'(t-\frac{R_R}{c})-i\omega\frac{R_T}{c}}$$

where $Y(f,f'-f|\vec{R}_T)$ is the Fourier transform of y with respect to $f'-f$. It is a measure of the amount a frequency component f is shifted by $f'-f$.

The simplest approximation to make is that the scatterer does not spread the frequencies of the incident wave. In this case

$$Y(f,f'-f|\vec{R}_T) = Y(f|\vec{R}_T)\delta(f'-f)$$

and the elementary scattered return reduces to

$$U(t,R_R) = \frac{1}{(4\pi)^2 R_R R_T} \int_{-\infty}^{\infty} df T_R(f) A_R(\frac{f}{c}\hat{R}_R) Y(f|R_T) A_T(\frac{f}{c}\hat{R}_T) T_T(f)$$

$$\times S_{in}(f) e^{i\omega(t-\frac{R_R+R_T}{c})} \quad .$$

To a good approximation, the beam patterns are independent of frequency for a narrowband signal. If it is also assumed that the point scatterer attenuates all frequencies of a narrowband signal equally, then $Y(f)$ is independent of frequency, $Y(f) = Y$. Thus, the point scatterer is modeled as a perfect point reflector.

With these two assumptions the elementary scattered return is

$$U(t,R_R) = \frac{YA_R(\hat{R}_R)A_T(\hat{R}_T)}{(4\pi)^2 R_R R_T} \int_{-\infty}^{\infty} df T_R(f)T_T(f)S_{in}(f)e^{i\omega(t-\frac{R_R+R_T}{c})}$$

This integral is just a function of the receiver and transmitter frequency response and the spectrum of the input electronic signal. It represents the input signal after it has been filtered by the transmitting and receiving array, and is measured experimentally for the particular transmitter and receiver used. As such, it is a bandlimited signal and can be represented in the form

$$V(t_r) = a(t_r)\cos[\omega_o t_r + \phi(t_r)]$$

where

$$t_r = t - \frac{R_R + R_T}{c}$$

is the retarded time. Thus, the elementary scattered return is

$$U(t,R_R) = \frac{YA_R(\hat{R}_R)A_T(\hat{R}_T)}{(4\pi)^2 R_R R_T} V(t_r)$$

DETAILS OF THE COMPUTATION OF THE DIRECTIVITY

FUNCTIONS AND TRANSFORMATION FACTOR

The directivity functions for the projector and receiver as given in Chapter III need to be expressed in terms of the variables of integration t_T and ϕ. This requires a change of variables from the coordinate system centered on an element to the variables of integration t_T and ϕ. The following is a description of the transformation relationships.

The products $\sin\alpha_T\cos\beta_T$, $\sin\alpha_T\sin\beta_T$, $\sin\alpha_{Ri}\cos\beta_{Ri}$, and $\sin\alpha_{Ri}\sin\beta_{Ri}$ can be related to the vectors $\vec{R}_T$ and $\vec{R}_{Ri}$ by the following:

$$\sin\alpha_T\cos\beta_T = \frac{R_{Tz}}{R_T}$$

$$\sin\alpha_T\sin\beta_T = \frac{R_{Tx}}{R_T}$$

$$\sin\alpha_{Ri}\cos\beta_{Ri} = \frac{R_{Riz}}{R_{Ri}}$$

$$\sin\alpha_{Ri}\sin\beta_{Ri} = \frac{R_{Rix}}{R_{Ri}}$$

where

$$R_T = \sqrt{R_{Tx}^2 + R_{Ty}^2 + R_{Tz}^2}$$

$$R_{Ri} = \sqrt{R_{Rix}^2 + R_{Riy}^2 + R_{Riz}^2}$$

R_{Tx}, R_{Ty}, and R_{Tz} are the Cartesian coordinates of the vector $\vec{R}_T$,

and R_{Rix}, R_{Riy}, R_{Riz} are the Cartesian coordinates of the vector $\vec{R}_{Ri}$, as illustrated in Fig. III-3. Since the coordinates λ of the point scatterer are given in terms of the variables t_T and ϕ, it is necessary to relate $\vec{R}_T$ and $\vec{R}_{Ri}$ to these variables in order to compute these products.

Consider a coordinate system on the surface directly above the center of the array of receivers and projector, as shown in Fig. C-1. The vector $\vec{\lambda}$ is the vector from the origin to the point scatterer, where the components of $\hat{\lambda}$, the unit vector in the direction of $\vec{\lambda}$, are $(\sin\phi, \cos\phi, 0)$. The vector $\vec{R}_{Ri}$ is the vector from the ith receiver to the point scatterer, and $\vec{R}_T$ is the vector from the projector to the point scatterer. The magnitude of $\vec{R}_T$ is

$$|\vec{R}_T| = c \cdot t_T \quad .$$

The coordinate system at the surface can be related to the coordinate system centered at the projector or receivers by a translation to the center of the array representing the depth of the center of the array below the surface, a rotation of the array through an angle ψ to produce the desired grazing angle with the surface, and a translation along the surface of the array to the location of the projector or receivers within the array. Thus the vectors $\vec{R}_T$ and $\vec{R}_{Ri}$ are related to the vector $\vec{\lambda}$ by the following transformations:

$$\vec{R}_T = S(\vec{\lambda} - \vec{u}) - \vec{v}_T$$

$$\vec{R}_{Ri} = S(\vec{\lambda} - \vec{u}) - \vec{v}_{Ri}$$
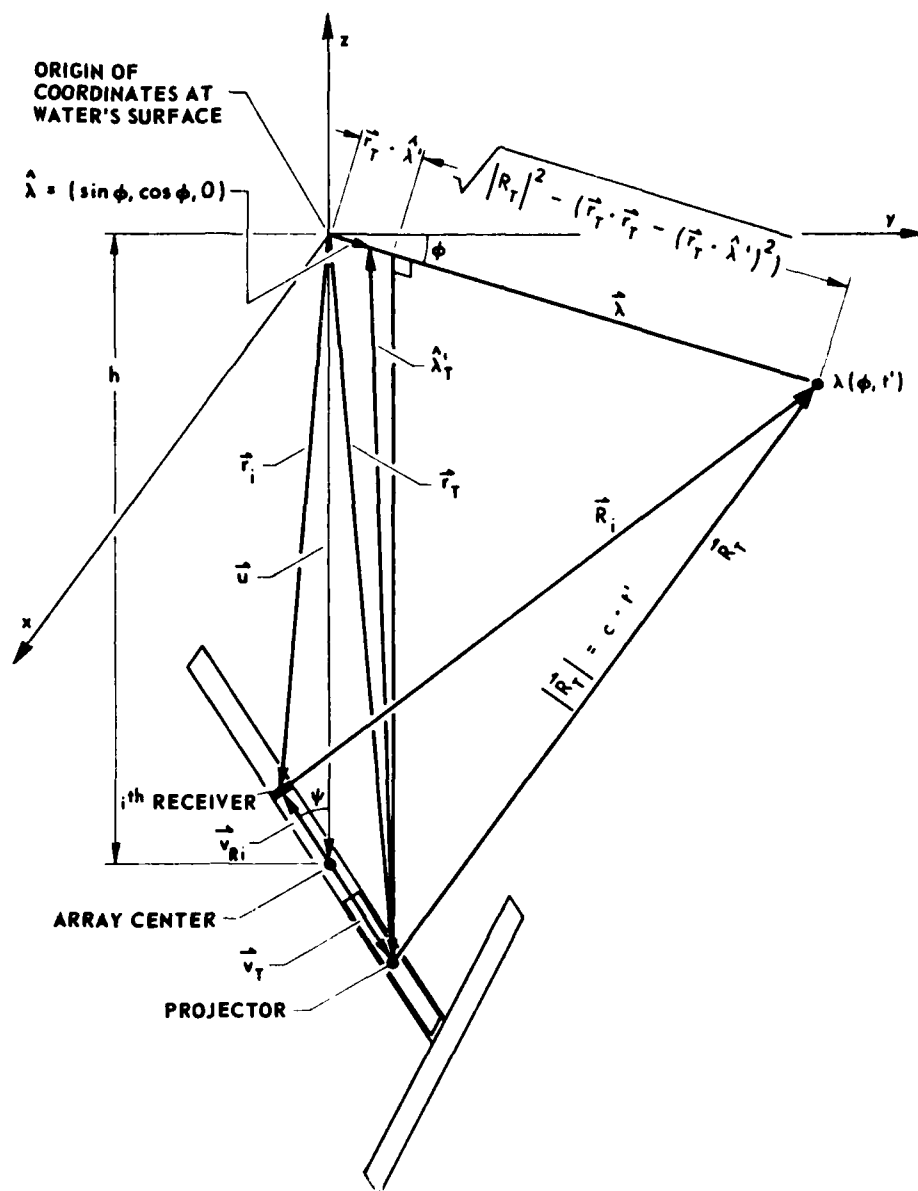
FIGURE C-1
TRANSFORMATION FROM SURFACE COORDINATE SYSTEM
TO COORDINATE SYSTEMS AT PROJECTOR AND RECEIVERS

where

$\vec{u}$ is the vector from the origin on the surface to the center of the array at a depth h below the surface:

$$u = \begin{pmatrix} 0 \\ 0 \\ -h \end{pmatrix} \quad ;$$

$\vec{v}_T$ is the vector from the center of the array to the projector, and depends on the location of the projector on the array;

$\vec{v}_{Ri}$ is the vector from the center of the array to the ith receiver, and depends on the location of the receiver on the array;

and

S is the rotation matrix representing a rotation through the angle ψ:

$$S = \begin{pmatrix} 1 & 0 & 0 \\ 0 & \cos\psi & \sin\psi \\ 0 & -\sin\psi & \cos\psi \end{pmatrix} \quad .$$

Since the unit vector $\hat{\lambda}$ is known, it is only necessary to determine $|\vec{\lambda}|$ in order to determine the vector $\vec{\lambda}$ and thus compute $\vec{R}_T$ and $\vec{R}_{Ri}$. To determine $|\vec{\lambda}|$, consider first the vector $\vec{R}_T$ for $\vec{\lambda} = \vec{0}$. In this case $\vec{R}_T$ points to the origin of the surface coordinates and is given by

$$\vec{R}_T = -(S\vec{u}+\vec{v}_T), \text{ for } \vec{\lambda} = \vec{0} \quad .$$

The negative of this vector is represented in Fig. C-1 by the vector $\vec{r}_T$, i.e.,

$$\vec{r}_T = S\vec{u} + \vec{v}_T \quad .$$

Next, consider the vector $\vec{R}_T$ for $\vec{\lambda} = \hat{\lambda}$. This vector is designated by

$\hat{\lambda}_T$ and is given by

$$\hat{\lambda}_T = S(\hat{\lambda} - \vec{u}) - \vec{v}_T = S\hat{\lambda} - S\vec{u} - \vec{v}_T = S\hat{\lambda} - \vec{r}_{cs} \quad .$$

From Fig. C-1 it can be seen that the vector $\vec{\lambda}$ in the coordinate system centered at the projector, designated by $\hat{\lambda}'$, is just

$$\hat{\lambda}' = \hat{\lambda}_T + \vec{r}_{cs} = S\hat{\lambda} \quad .$$

If a line is drawn from the coordinate origin at the projector to intersect the vector $\vec{\lambda}$ at a right angle, then the distance between the intersection and the coordinate origin at the surface is given by the inner product of $\vec{r}_T$ and $\hat{\lambda}'$. The distance between the intersection and the coordinate origin at the projector is then given by

$$\sqrt{\vec{r}_T \cdot \vec{r}_T - (\vec{r}_T \cdot \hat{\lambda}')^2} \quad .$$

Thus the distance from the intersection to the point scatterer is

$$\sqrt{|R_T|^2 - (\vec{r}_T \cdot \vec{r}_T - (\vec{r}_T \cdot \hat{\lambda}')^2)}$$

and the magnitude of $\vec{\lambda}$ is therefore given by

$$|\vec{\lambda}| = \vec{r}_T \cdot \hat{\lambda}' + \sqrt{|R_T|^2 - (\vec{r}_T \cdot \vec{r}_T - (\vec{r}_T \cdot \hat{\lambda}')^2)} \quad .$$

Since the unit vector $\hat{\lambda}$ is known, then the vector $\vec{\lambda}$ has thus been determined. Knowing $\vec{\lambda}$, the vectors $\vec{R}_T$ and $\vec{R}_{Ri}$ can be calculated from the given coordinate transformations. The components of $\vec{R}_T$ and $\vec{R}_{Ri}$ are then used to compute the products required by the directivity calculations. This thus allows computation of the directivity functions for the projector and receivers in the correct coordinate system.

The transformation factor w can also now be expressed in terms

of t_T and ϕ. The surface integration can be expressed in terms of the surface coordinates $\lambda = |\vec{\lambda}|$ and ϕ by

$$dS = \lambda d\lambda d\phi \qquad .$$

It is now necessary to transform the variable λ to the variable $R_T = ct_T$. From the expression above for λ, it can be seen that

$$\frac{d\lambda}{dR_T} = \frac{R_T}{\sqrt{R_T^2 - (\vec{r}_T \cdot \vec{r}_T - (\vec{r}_T \cdot \hat{\lambda}')^2)}} \qquad .$$

Thus

$$\lambda d\lambda = \frac{\lambda R_T dR_T}{\sqrt{R_T^2 - (\vec{r}_T \cdot \vec{r}_T - (\vec{r}_T \cdot \hat{\lambda}')^2)}}$$

$$= \left[1 + \frac{\vec{r}_T \cdot \hat{\lambda}'}{\sqrt{R_T^2 - (\vec{r}_T \cdot \vec{r}_T - (\vec{r}_T \cdot \hat{\lambda}')^2)}} \right] R_T dR_T$$

$$= w \, R_T dR_T$$

$$= w \, c^2 t_T dt_T \qquad .$$

Therefore

$$dS = w c^2 t_T dt_T d\phi$$

where

$$w = 1 + \frac{\vec{r}_T \cdot \hat{\lambda}'}{\sqrt{R_T^2 - (\vec{r}_T \cdot \vec{r}_T - (\vec{r}_T \cdot \hat{\lambda}')^2)}} \qquad .$$

For the geometry of the present study, w was very close to 1 over the range of t_T and ϕ considered.

REFERENCES

1. E. P. Gulin and K. I. Malyshev, "Spatial Correlation of Amplitude Fluctuations of a Continuous Tone Signal with Reflection from Ocean Surface Waves", Soviet Physics-Acoustics 11, 428-430 (1966).

2. R. J. Urick and T. J. Tulko, "Vertical Coherence of Sound Transmitted over a Twenty-Four Mile Path", J. Acoust. Soc. Am. 46, 1308-1317 (1969).

3. H. Medwin and C. S. Clay, "Dependence of Spatial and Temporal Correlation of Forward-Scattered Underwater Sound on the Surface Statistics. II. Experiment", J. Acoust. Soc. Am. 47, 1419-1429 (1970).

4. R. J. Urick and G. R. Lund, "Low-frequency Coherence of Long Range Explosive Sounds and Ambient Noise in the Deep Sea", U.S. Naval Ordnance Laboratory, White Oak, Maryland, NOLTR 70-111 (July 15, 1970).

5. P. Wille and R. Thiele, "Transverse Horizontal Coherence of Explosive Signals in Shallow Water", J. Acoust. Soc. Am. 50, 348-353 (1971).

6. Willem Wijmans, "An Experimental Study of the Reflection of Underwater Sound from the Sea Surface", Saclant ASW Research Centre, La Spezia, Italy, Saclantcen-SM-51 (1974).

7. A. Wasiljeff, "Spatial Horizontal Coherence of Acoustical Signals in Shallow Water", Saclant ASW Research Centre, La Spezia, Italy, Saclantcen-SM-68 (1975).

8. E. P. Gulin and K. I. Malyshev, "Experiments in the Spatial Correlation of the Amplitude and Phase Fluctuations of Acoustic Signals Reflected from a Rough Ocean Surface", Soviet Physics-Acoustics 10, 365-368 (1965).

9. Robert Charles Spindel, "An Experimental Investigation of a Statistically Distributed Scattering Surface and Acoustic Scattering", Ph.D. Dissertation #71-22, Yale University, New Haven, Connecticut, 713 (1971).

10. V. I. Neklyudov and S. D. Chuprov, "Spatial and Frequency Correlation of the Amplitude Fluctuations of Sound Signals Reflected from the Ocean Surface", Soviet Physics-Acoustics 19, 255-259 (1973).

11. E. Sevaldsen, "Spatial Coherence of Sonar Signals at 7.8 kHz", Norwegian Defense Research Establishment, Kjeller, Norway, NDRE-U-337 (1976).

12. Paul Henry Moose, "On the Detection of Signals in Reverberation", Ph.D. Dissertation #70-19, University of Washington (1970).

13. Terry D. Plemons, "Spectra Covariance Functions and Associated Statistics of Underwater Acoustic Scattering from Lake Surfaces", Ph.D. Dissertation, The University of Texas at Austin (1971).

14. R. L. Swarts, "Covariance Structure of Surface Reverberation", Honeywell Marine Systems Center, Seattle, Washington, Doc. No. 2387 (1972).

15. Terry D. Plemons, Jack A. Shooter, and David Middleton, "Underwater Acoustic Scattering from Lake Surfaces. I. Theory, Experiment and Validation of Data", J. Acoust. Soc. Am. 52, 1487-1502 (1972).

16. Terry D. Plemons, Jack A. Shooter, and David Middleton, "Underwater Acoustic Scattering from Lake Surfaces. II. Covariance Functions and Related Statistics", J. Acoust. Soc. Am. 52, 1503-1515 (1972).

17. Marshall E. Frazer, "A Study of the Properties of the Outputs of a Multielement Sonar Receiving Array Operating in a Reverberant Environment", Ph.D. Dissertation, The University of Texas at Austin (1974). Also published as Applied Research Laboratories Technical Report No. 74-16 (ARL-TR-74-16), Applied Research Laboratories, The University of Texas at Austin (May 1974).

18. Terry D. Plemons, "Experimental Studies of the Covariance Functions of the Envelope of Narrow-Band Reverberation Processes", J. Acoust. Soc. Am. 56, 1422-1425 (1974).

19. Yoshitsugu Omichi, "An Experimental Study of Covariance Functions of Reverberation from a Lake Surface", Applied Research Laboratories Technical Report No. 75-25 (ARL-TR-75-25), Applied Research Laboratories, The University of Texas at Austin (20 May 1975).

20. R. J. Urich and G. R. Lund, "Vertical Coherence of Explosive Reverberation", J. Acoust. Soc. Am. 36, 2164-2170 (1964).

21. R. J. Urich and G. R. Lund, "Vertical Coherence of Shallow-Water Reverberation", J. Acoust. Soc. Am. 47, 342-349 (1970).

22. R. J. Urich and G. R. Lund, "Horizontal Coherence of Explosive Reverberation", J. Acoust. Soc. Am. 47, 909-911 (1970).

23. J. W. Strutt (Lord Rayleigh) Theory of Sound (Dover, New York 1945).

24. J. L. Uretsky, "The Scattering of Plane Waves from Periodic Surfaces", Ann. Phys. 33, 400-427 (1965).

1.0

1.1

1.25   1.4   1.6

2.8   2.5

2.2

2.0

1.8
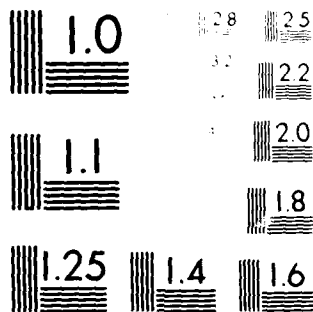
MICROCOPY RESOLUTION TEST CHART

25. C. Eckhart, "The Scattering of Sound from the Sea Surface", J. Acoust. Soc. Am. 25, 566-570 (1953).

26. H. W. Marsh, "Exact Solution of Wave Scattering by Irregular Surfaces", J. Acoust. Soc. Am. 33, 330-333 (1961).

27. D. Middleton, "A Statistical Theory of Reverberation and Similar First-Order Scattered Fields. Part I: Waveform and the General Process", IEEE Trans. Inf. Theory 13, 372-392 (1967).

28. D. Middleton, "A Statistical Theory of Reverberation and Similar First-Order Scattered Fields. Part II: Moments, Spectra, and Spacial Distributions", IEEE Trans. Inf. Theory 13, 393-414 (1967).

29. D. Middleton, "A Statistical Theory of Reverberation and Similar First-Order Scattered Fields. Part III: Waveforms and Fields", IEEE Trans. Inf. Theory 18, 35-67 (1972).

30. D. Middleton, "A Statistical Theory of Reverberation and Similar First-Order Scattered Fields. Part IV: Statistical Models", IEEE Trans. Inf. Theory 18, 68-90 (1972).

31. L. Fortuin, "Survey of Literature on Reflection and Scattering of Sound Waves at the Sea Surface", J. Acoust. Soc. Am. 47, 1209-1228 (1970).

32. H. Cramér, Mathematical Methods of Statistics (Princeton University Press, Princeton, New Jersey, 1971).

33. R. H. Barker, "Group Synchronization of Binary Digital Systems", Communications Theory, W. Jackson (ed.) (Academic Press, New York and London, 273-287, 1953).

34. A. J. Estes, "An Experimental Investigation of a Neyman-Pearson Detector for a Multichannel Active Sonar Operating in a Reverberant Environment", M.S. Thesis in Engineering, The University of Texas at Austin (1980).

35. O. D. Grace and S. P. Pitt, "Sampling and Interpolation of Bandlimited Signals by Quadrature Methods," J. Acoust. Soc. Am. 48, 1311-1318 (1970).

36. Barry M. Marks and E. Eugene Mikeska, "Reflection from Focused Liquid-Filled Spherical Reflectors", J. Acoust. Soc. Am 59, 813-817 (1976).

37. R. Batey and B. Korts, "Lake Travis Test Station", Applied Research Laboratories, The University of Texas at Austin, Austin, Texas, (1973).

38. D. Middleton, "Acoustic Modeling, Simulation, and Analysis of Complex Underwater Targets, II. Statistical Evaluation of Experimental Data", Applied Research Laboratories Technical Report No. 69-22 (ARL-TR-69-22), Applied Research Laboratories, The University of Texas at Austin (1969).

39. Charles R. Baker, "Some Statistical Tests for the Analysis of Sonar Data", Department of Statistics, University of North Carolina, Chapel Hill, Report No. B-74-3 (June 1974).

40. James V. Bradley, Distribution-Free Statistical Tests (Prentice-Hall, Englewood Cliffs, New Jersey, 1968).

41. Marshall E. Frazer, "Some Statistical Properties of Lake Surface Reverberation", J. Acoust. Soc. Am. 64, 858-868 (1978).

42. Athanasios Papoulis, Probability, Random Variables, and Stochastic Processes (McGraw-Hill, New York, 1965).

43. P. J. Kim and R. I. Jennrich, "Tables of the Exact Sampling Distribution of the Two-Sample Kolmogorov-Smirnov Criterion, D_{mn}, $m \leq n$", Selected Tables in Mathematical Statistics, Vol. I, ed. Institute of Mathematical Statistics (1970).

44. P. J. Kim, "On the Exact and Approximate Sampling Distribution of the Two-Sample Kolmogorov-Smirnov Criterion D_{mn}, $m \leq n$", J. Amer. Stat. Assoc. 64, 1625-1637 (1969).

45. L. R. Verdooren, "Extended Tables of Critical Values for Wilcoxon's Test Statistic", Biometrika 50, 177-186 (1963).

46. E. S. Pearson, "A Further Development of Tests for Normality", Biometrika 22, 239-249 (1930).

47. E. S. Pearson, "Note on Tests for Normality", Biometrika 22, 423-424 (1930).

48. S. S. Shapiro, M. B. Wilk, and H. J. Chen, "A Comparative Study of Various Tests for Normality", J. Amer. Stat. Assoc. 63, 1343-1372 (1968).

49. E. S. Pearson, "Some Problems Arising in Approximating to Probability Distributions, Using Moments", Biometrika 50, 95-112 (1963).

50. Ralph B. D'Agostino, "An Omnibus Test of Normality for Moderate and Large Size Samples", Biometrika 58, 341-348 (1971).

51. M. G. Kendall and A. Stuart, <u>The Advanced Theory of Statistics,</u>
     Vol. 1 (Hafner Publishing Co., New York, 1958).

52. Z. W. Birnbaum, "Numerical Tabulation of the Distribution of
     Kolmogorov's Statistic for Finite Sample Size", J. Amer. Stat.
     Assoc. <u>47</u>, 425-441 (1952).

53. F. J. Massey, Jr., "A Note on the Estimation of a Distribution
     Function by Confidence Limits", Annals of Mathematical Statistics
     <u>21</u>, 116-119 (1950).

54. Gordon E. Martin and John S. Hickman, "Directional Properties of
     Continuous Plane Radiators with Bizonal Amplitude Shading",
     J. Acoust. Soc. Am. <u>27</u>, 1120-1127 (1955).

55. R. Clark Jones, "On the Theory of the Directional Patterns of Con-
     tinuous Source Distributions on a Plane Surface", J. Acoust. Soc.
     Am. <u>16</u>, 147-171 (1945).

56. G. I. Bourianoff and C. W. Horton, Sr., "Ensemble and Time Averages
     of Reverberation from a Sea Surface: A Computer Study", J. Acoust.
     Soc. Am. <u>49</u>, 237-245 (1971).

57. Hubert W. Lilliefors, "On the Kolmogorov-Smirnov Test for Normality
     with Mean and Variance Unknown," J. Amer. Stat. Assoc. <u>62</u>, 399-402
     (1967).

58. J. Durbin, <u>Distribution Theory for Tests Based on the Sample
     Distribution Function</u> (Society for Industrial and Applied
     Mathematics, Philadelphia, 1973).

59. J. Durbin, "Kolmogorov-Smirnov Tests when Parameters are
     Estimated," <u>Empirical Distributions and Processes</u> (Selected Papers,
     Meeting on Mathematical Stochastics, Oberwolfach, 1976), pp. 33-44.

60. J. Durbin, "Weak Convergence of the Sample Distribution Function
     when Parameters are Estimated," Annals of Statistics <u>1</u>,
     279-290 (1973).

61. J. Durbin, "Kolmogorov-Smirnov Tests when Parameters are Estimated
     with Applications to Tests of Exponentiality and Tests on Spacings,"
     Biometrika <u>62</u>, 5-22 (1975).

62. M. A. Stephens, "Asymptotic Results for Goodness-of-Fit
     Statistics with Unknown Parameters," Annals of Statistics <u>4</u>,
     357-369 (1976).

63. Constance L. Wood, "On Null-hypothesis Limiting Distributions of
     Kolmogorov-Smirnov Type Statistics with Estimated Location and
     Scale Parameters," Communications in Statistics-Theory and Methods
     <u>A7</u>, 1181-1198 (1978).

DISTRIBUTION LIST FOR
ARL-TR-81-23
UNDER CONTRACT N00014-80-C-0490
UNCLASSIFIED

Copy No.

	Commanding Officer
	Office of Naval Research
	Arlington, VA 22217
1	Attn: R. Ryan (Code 400R)
2	E. Wegman (Code 436)
3	R. Obrochta (Code 230)
4	CAPT A. Gilmore (Code 200)
5	Office of Naval Research
	Branch Office Chicago
	Room 286, 536 South Clark St.
	Chicago, IL 60605
	Commander
	Naval Sea Systems Command
	Department of the Navy
	Washington, DC 20362
6	Attn: C. Smith (Code 63R)
7	D. Baird (Code 63X3B)
8	E. Liszka (Code 63R1)
9	F. Romano (Code 63R3)
	Commanding Officer
	Naval Ocean Research and Development Activity
	NSTL Station, MS 39529
10	Attn: E. Chaika (Code 530)
11	L. Solomon (Code 500)
12	S. Stanic (Code 340)
13	B. Blumenthal (Code 530)
14	A. Anderson

Distribution List for ARL-TR-81-23 under Contract N00014-80-C-0490 (Cont'd)

Commander
New London Laboratory
Naval Underwater Systems Center
Department of the Navy
New London, CT 06320
15   Attn: D. Walters
16   J. Kyle
17   W. I. Roderick
18   L. King
19   R. Dwyer
20   A. A. Filippini
21   N. L. Owsley
22   W. Schumacher
23   R. Deavenport

Marine Physical Laboratory
The Scripps Institution of Oceanography
The University of California/San Diego
San Diego, CA 92152
24   Attn: V. C. Anderson
25   F. Fisher

Naval Research Laboratory
Underwater Sound Reference Division
Orlando, FL 32800
26   Attn: J. Blue

Commanding Officer
Naval Oceanographic Office
NSTL Station, Bay St. Louis, MS 39522
27   Attn: W. Jobst
28   R. Winokur
29   G. Lewis

Commanding Officer
Naval Coastal Systems Center
Panama City, FL 32401
30   Attn: S. Richardson
31   D. Folds
32   E. Moritz
33   J. Hammond
34   C. Loggins

Commander
Naval Ocean Systems Center
Department of the Navy
San Diego, CA 92132
35   Attn: J. Stewart
36   S. I. Chou
37   H. Bucker

Distribution List for ARL-TR-81-23 under Contract N00014-80-C-0490 (Cont'd)

Copy No.

38 - 49   Commanding Officer and Director
Defense Technical Information Center
Cameron Station, Building 5
5010 Duke Street
Alexandria, VA 22314

Applied Physics Laboratory
University of Washington
Seattle, WA 98105
50   Attn: S. Murphy, Director
51   C. Sienkiewicz
52   D. Princehouse
53   C. Eggen

Applied Research Laboratory
The Pennsylvania State University
P. O. Box 30
State College, PA 16801
54   Attn: S. T. McDaniel
55   L. H. Sibul

Commander
Naval Surface Weapons Center
White Oak Laboratory
Silver Spring, MD 20910
56   Attn: Library

Superintendent
Naval Postgraduate School
Monterey, CA 93940
57   Attn: H. Medwin
58   Library

Admirality Underwater Weapons Establishment
Portland, DORSET DT522JJ
UNITED KINGDOM
59   Attn: H. Pearson

Director
SACLANT ASW Research Centre
La Spezia, ITALY
60   Attn: R. Goodman
61   Library

Bendix Corporation
11600 Sherman Way
North Hollywood, CA 91606
62   Attn: R. Cunningham

Distribution List for APL TR-81-23 under Contract N00014-80-C-0490 (Cont'd)

Copy No.

	Raytheon Company
	Submarine Signal Division
	West Main Road
	Portsmouth, RI 02871
63	Attn: R. Pridham
64	D. Viccione

Tracor, Inc.
6500 Tracor Lane
Austin, TX 78701
65 Attn: T. Plemons
66 J. Wilkinson

Honeywell, Inc.
Marine Systems Center
5303 Shilshole Ave., N.W.
Seattle, WA 98107
67 Attn: R. L. Swarts

Laboratoire de Detection Sous Marine
DCAN
Toulon, FRANCE
68 Attn: H. Mermoz

Universitat Bremen
B F Electrotechnik
Bremen, GERMANY
69 Attn: A. Wasiljeff

Faculty of Engineering
Memorial University of Newfoundland
St. Johns, NEWFOUNDLAND
CANADA
70 Attn: D. Dunsiger

Norwegian Defense Research Establishment
P. O. Box 115
N-2191 Horton, NORWAY
71 Attn: Library

Forschungsanstalt der Bundeswehr
für Wasserschall-und Geophysik
Klausdorfer Weg 2-24
2300 Kiel 14
GERMANY
72 Attn: G. Ziehm

Copy No.

Acoustics Laboratory
Technical University of Denmark
Building 352 Lundtoftevej 100
DK-2800 Lyngby
DENMARK
73   Attn: L. Bjorno

School of Phsyics
University of Bath
Claverton Down
BATH BA2 7AY
UNITED KINGDOM
74   Attn: H. O. Berktay

Department of Physics
The University of Texas at Austin
Austin, TX 78712
75   Attn: A. W. Nolle
76   T. Griffy

Department of Electrical Engineering
The University of Texas at Austin
Austin, TX 78712
77   Attn: T. Wagner

Department of Business
The University of Texas at Austin
Austin, TX 78712
78   Attn: T. Sager

Department of Electrical Engineering
Texas A&M University
College Station, TX
79   Attn: D. Halverson

Department of Physics
The University of Auckland
Auckland, NEW ZEALAND
80   Attn: A. Kibblewhite

Department of Physics
The Catholic University
6220 Michigan Ave., N.E.
Washington, DC 20017
81   Attn: H. M. Überall

	Department of Business Finance
	The University of Texas at Austin
	Austin, TX 78712
82	Attn: P. Brockett
	Chinhae Machine Depot
	Box 18, Chinhae
	Kyungnam, KOREA
83	Attn: Jungyul Na
	Tracor, Inc.
	1601 Research Blvd.
	Rockville, MD 20850
84	Attn: R. J. Urick
	Hughes Aircraft Co.
	1901 West Malvern
	Fullerton, CA 92634
85	Attn: S. Autrey
86	David Middleton
	127 E. 91st Street
	New York, NY 10028
87	Office of Naval Research
	Resident Representative
	Room 582, Federal Building
	Austin, TX 78701
88	Signal Physics Division, ARL:UT
89	Signal Physics Group, ARL:UT
90	Charles Baker, ARL:UT
91	Garland R. Barnard, ARL:UT
92	Raymond M. Bohls, ARL:UT
93	George P. Coble, ARL:UT
94	Marshall E. Frazer, ARL:UT
95	Loyd Hampton, ARL:UT
96	Robert Hollingsworth, ARL:UT
97	Claude Horton, SR., ARL:UT

Distribution List for ARL-TR-81-23 under Contract N000124-80-C-0490 (Cont'd)

<u>Copy No.</u>

98	John M. Huckabay, ARL:UT
99	Chester McKinney, ARL:UT
100	Tom Muir, ARL:UT
101	Clark S. Penrod, ARL:UT
102	Dennis Powell, ARL:UT
103	Jack A. Shooter, ARL:UT
104	Reuben H. Wallace, ARL:UT
105	Joseph F. Willman, ARL:UT
106	Joseph Woods, ARL:UT
107	Library, ARL:UT
108 - 150	Reserve, ARL:UT